DISSERTATION

OPTIMIZING THE SCAVENGING SYSTEM FOR HIGH EFFICIENCY AND LOW EMISSIONS: A COMPUTATIONAL APPROACH

Submitted by

S. Scott Goldsborough

Department of Mechanical Engineering

In partial fulfillment of the requirements

for the Degree of Doctor of Philosophy

Colorado State University

Fort Collins, Colorado

Fall 2002

COLORADO STATE UNIVERISTY

October 24, 2002

WE HEREBY RECOMMEND THAT THE DISSERTATION PREPARED UNDER OUR SUPERVISION BY S. SCOTT GOLDSBOROUGH ENTITLED **OPTIMIZING THE SCAVENGING SYSTEM FOR HIGH EFFICIENCY AND LOW EMISSIONS: A COMPUTATIONAL APPROACH** BE ACCEPTED AS FULFILLING IN PART, REQUIREMENTS FOR THE DEGREE OF DOCTOR OF PHILOSOPHY

Committee on Graduate Work

Advisor

Department Head

ABSTRACT OF DISSERTATION

OPTIMIZING THE SCAVENGING SYSTEM FOR HIGH EFFICIENCY AND LOW EMISSIONS: A COMPUTATIONAL APPROACH

A free piston internal combustion engine operating on high compression ratio, HCCI combustion is being developed to significantly improve the thermal efficiency and exhaust emissions relative to conventional crankshaft-driven SI and Diesel engines. A two-stroke scavenging process recharges the engine and is key to realizing the efficiency and emissions potential of the device. To ensure that the engine's performance goals can be achieved the scavenging system was configured using Computational Fluid Dynamics, zero-dimensional and one-dimensional modeling, along with single step parametric variations. Visualization of the in-cylinder and port dynamics allowed the flow through the engine to be more completely understood and better controlled.

Through a comprehensive study a wide range of design options were investigated including the use of loop, hybrid-loop and uniflow scavenging methods, different charge delivery options, and various operating schemes. Parameters such as the intake/exhaust port arrangement, valve lift/timing, charging pressure and piston frequency were varied. Operating schemes including a standard uniflow configuration, a low charging pressure option, a stratified scavenging geometry, and an over-expansion (Atkinson) cycle were studied. High scavenging and trapping efficiencies (~0.85, >0.99, respectively), as well as overall thermal efficiency and exhaust emissions were metrics by which the designs were evaluated.

The computational results indicated that the loop and hybrid-loop arrangements are inadequate, however, the uniflow geometry can produce both high scavenging and high trapping

efficiencies. The delivery tank pressure and temperature histories are important to enabling steady charging, high operating compression ratio and low pumping power consumption.

Stratified scavenging and over-expansion operating schemes can significantly improve the efficiency of the engine cycle, through increased compression ratio (~24:1) (by more complete flushing) and additional blowdown recovery, respectively. However, the over-expansion arrangement was calculated to result in large cycle-to-cycle variability for slightly altered operating conditions.

It was found that the in-cylinder flows are important to both NOx and short-circuiting emissions with inadequate mixing (and resulting temperature stratification) the predominant driver of NO production, and fuel penetration to the valve region the main cause of short-circuiting emissions. In addition, early auto-ignition of the charge by the hot residual gases can lead to reduced efficiency potential.

S. Scott Goldsborough
Department of Mechanical Engineering
Colorado State University
Fort Collins, Colorado
Fall 2002

ACKNOWLEDGEMENTS

Several individuals were of great assistance during the completion of this dissertation. First and foremost, Dr. Peter Van Blarigan of Sandia National Laboratories, California was extremely encouraging with both his intellectual guidance and financial support. He provided a unique and stimulating atmosphere in which to work. Professor Charlie Mitchell of Colorado State University was always helpful in our numerous discussions, both concerning academic as well as non-academic topics. I appreciate his openness and sincerity, along with his continual encouragement. Dr. Norman Johnson of Los Alamos National Laboratory was often times invaluable in his assistance with the KIVA software. Our discussions of multi-dimensional modeling in general were extremely useful. Tony Amsden of Los Alamos National Laboratory was very helpful with the programming aspects of the KIVA code. His instruction provided a great start to utilizing the software. Anders Grimsrud and the team at Computational Engineering International supplied a good deal of assistance with the Ensight visualization software.

Finally, my wife, Laura was remarkably patient, supportive, and understanding through the duration of this project. I will always be indebted to her for this.

The work performed for this dissertation was supported by the U.S. Department of Energy, Office of Solar Thermal, Biomass Power and Hydrogen Technologies.

DEDICATION

This dissertation is dedicated to our son, Nathen Clay Goldsborough.

TABLE OF CONTENTS

CHAPTER I INTRODUCTION

Fuel economy and output emissions have become important factors in the design of advanced electric power generators. Fuel cells, microturbines and free piston internal combustion (IC) engines are examples of devices expected to achieve higher conversion efficiencies and lower pollutant emissions, relative to conventional crankshaft-driven engine-generators. But while fuel cells and microturbines still require significant advances in fuel compatibility, material properties, and heat losses before these devices can become viable options, free piston engine-generators have the advantage of utilizing existing IC engine technology, and should therefore be able to realize considerable fuel and pollutant mitigation savings in the near future.

Free piston IC engines have been around for over 50 years, but it is only recently that they have been considered viable for high efficiency electrical generation. This is a result of improvements in magnet materials, electronic controls, and the use of homogeneous charge compression ignition (HCCI) combustion to achieve near Otto cycle performance. The fundamental components of combustion, and electrical conversion have been established for the free piston engine, however, the design of a highly efficient gas charging system still remains a considerable challenge. The topic of this dissertation considers the optimization of the gas transfer system to ensure high cycle thermal efficiency and low output emissions.

What follows next is a brief description of the free piston engine-generator, and of the two-stroke cycle scavenging process used to recharge the engine. The approach to optimizing the design, as well as the objective and scope of this thesis are presented after that.

Free Piston Engine-Generator

The free piston engine-generator illustrated in Figure 1.1 is configured with a double ended piston, a double ended cylinder and a linear alternator [1]. The linear alternator component is integrated into the center of the device so that the dynamics of the piston can be directly harnessed - the varying magnetic flux of permanent magnets attached to the piston is efficiently converted into electric power. Within the engine, combustion occurs alternately at each end of the cylinder driving the piston motion. The operating compression ratio (CR) is controlled by the alternator as it precisely manages the piston's kinetic energy through each stroke. HCCI combustion is employed where the cylinder's premixed air-fuel charges are compressed to the point of autoignition. Compression is achieved quickly, and rapid combustion occurs at nearly top dead center (TDC). Two-stroke cycle scavenging is used to recharge the engine.

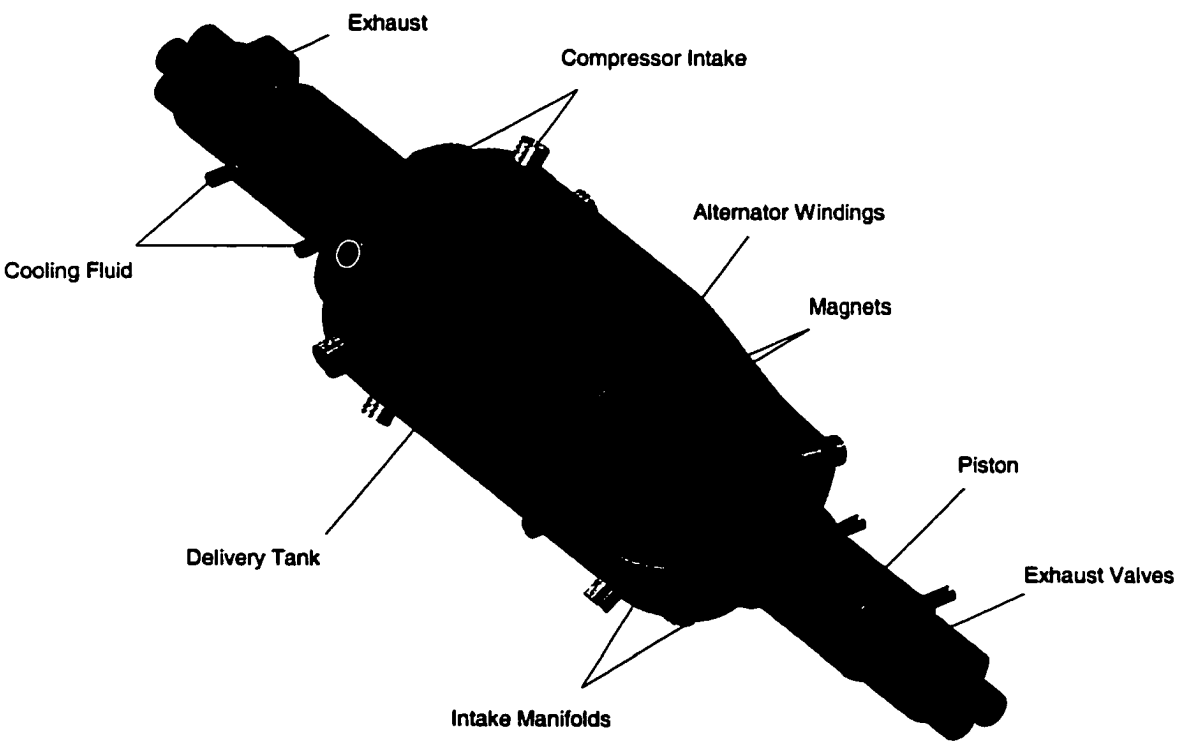

Figure 1.1 – Free Piston Engine-Generator

Several advantages ensue from this unconventional engine design. First, the free piston driven HCCI combustion process is extremely fast, ensuring that most of the fuel energy is converted to heat at maximum compression. The Otto cycle's constant-volume combustion condition is more closely approached in this configuration. As a result, the achievable thermal efficiency is not restricted by finite combustion processes (e.g. burn duration, mixing/diffusion) as it is in conventional IC engines.

A second important attribute of the engine is that the free piston's compression ratio is variable, and potentially greater than crankshaft-driven configurations. This characteristic allows very lean air-fuel mixtures to be successfully ignited at high compression ratios using the HCCI process. It also enables operation on a variety of different fuels without significant hardware modifications, since the compression can be adjusted to match the fuel's autoignition characteristics. Lean operation dramatically reduces the formation of NOx, and improves the engine's thermal efficiency, through decreased energy losses by heat transfer, and the utilization of more favorable specific heat ratios. High compression ratios (greater than 25:1) may further increase the efficiency of the engine cycle.

A third factor is that the unique dynamics of the free piston help to minimize the time that the cylinder gases spend at elevated combustion temperatures. Heat losses from the cylinder charge are reduced, and NOx emissions are better controlled.

Integration of the linear alternator directly into the free piston geometry leads to additional benefits. In this compact arrangement mechanical losses in the engine are decreased, since there is essentially one moving part. This allows the engine to utilize a longer stroke-to-bore ratio (~2:1), relative to conventional crankshaft-driven geometries, without sacrificing significant power to increased frictional losses. The long stroke-to-bore ratio is important because of the need to provide adequate clearance at TDC for high compression ratios.

In addition, the engine can be configured to operate at a single optimal speed, and thus reduce the losses associated with varying the engine speed. These characteristics enhance the overall fuel-to-electricity generation efficiency of the device.

Scavenging

Two-stroke cycle scavenging is a necessary component of the advanced engine-generator. Scavenging is the process where the cylinder's burned gases are replaced with a fresh charge (air or air-fuel mixture), using both the high blowdown pressure of the expanded combustion gases and the fluid dynamics of the incoming charge. This process requires only a fraction of the piston's stroke to complete, with the exhausting and recharging events occurring simultaneously, and is critical to ensuring that the cylinder gases are adequately prepared for the next combustion cycle.

Two-stroke cycle engines have obvious advantages over four-stroke cycle counterparts in terms of power output and reduced engine friction. Lower loss compressors can be used to pump fresh air into the cylinder, and power can be generated on each oscillation of the piston. However, important engineering challenges must be overcome with regard to cylinder charging, and fuel short-circuiting. The efficiency and emissions potential of the engine-generator can be severely restricted by inadequate charge preparation and unchecked fuel loss through the exhaust port. Additionally, this process, unlike the four-stroke pumping process, is fully fluid dynamic in nature, and therefore can be quite difficult to control.

The free piston configuration, in conjunction with the HCCI combustion system, however, presents certain advantages over conventional two-stroke cycle engines. First, the generator is configured to operate at a near constant piston oscillation rate, based on the engine's optimal performance. As a result, the scavenging arrangement can be designed for a specific operating point, and constructed to maximize the efficiency of the cylinder charging process for this speed.

A second important characteristic is that, since the combustion process is capable of igniting and sufficiently burning nearly any equivalence ratio mixture, the final charge composition should not be critical to successful engine operation, as long as it is adequately mixed. As such, it may be possible that a significant fraction of burned charge (~30%) could remain in the cylinder at the end of each scavenging cycle.

Finally, the ability to utilize long stroke-to-bore ratios allows unique schemes to be employed to achieve desirable characteristics for the scavenging process - schemes that would not operate adequately, or efficiently under short stroke / variable speed conditions. Such options include over-expanding the combusted gases before scavenging begins, and utilizing additional piston travel below the port bottom.

Approach

The approach used to optimize the design of the scavenging system for high efficiency and low emissions was to computationally analyze the engine flow behavior over various design spaces. Single step parametric variations were used to narrow the design possibilities and arrange the scavenging design for optimal overall performance. The primary tool for this was computational fluid dynamics (CFD) modeling.

CFD modeling has been widely employed to describe and predict the processes that occur within IC engines. Combustion, heat transfer and in-cylinder gas flow have all been studied in this manner. However, due to the complexity of engine phenomena, and the limitations of computer and model capabilities, the accuracy of the calculations has been a limitation in applying CFD to engine design. On the other hand, recent advances in meshing techniques, boundary treatments, and computer hardware have enabled more accurate computations of the gas flow process to be completed. Utilizing the advantages of CFD codes - especially the ability to visualize the in-cylinder flow behavior, and to determine trends in engine operation – has provided valuable insight into the means of optimizing the scavenging system.

To maximize the engine's overall efficiency, the losses associated with blowdown, short-circuiting, pumping and friction have been included in the analysis, as well as the issue of adequate charge preparation (for quick, high CR, TDC HCCI combustion). For sufficient emissions control the issue of fuel short-circuiting was addressed, along with NOx generation from fuel-rich or hot regions in the cylinder.

Objective

The objective of this research was to optimize the scavenging system for the free piston engine-generator, to enable the device to achieve high thermal efficiency and minimal output emissions, and to ensure that the engine's potential is not degraded through the recharging event. The design of the two-stroke process, including the geometrical arrangement, the air-fuel delivery method, and the operating conditions, is expected to greatly affect the overall performance of the engine cycle. The best combination of these scavenging parameters was investigated.

Scope

The means to accomplishing this objective was to use CFD modeling to study and understand the free piston engine's scavenging system. Single step parametric variations were used to narrow the range of design options and configure the system for optimal thermal efficiency and emissions performance. To facilitate this optimization process, an established multi-dimensional code (KIVA-3V) was employed where the code's accuracy and capabilities have been documented through previous studies. The major system losses of blowdown, short-circuiting, pumping and friction were considered, along with the issue of adequate cylinder charge preparation. The use of one-dimensional gas dynamics modeling to configure the intake/exhaust manifolds was not included in this study. In addition, experimental verification of the computational results is expected to be completed at a later time, however some of the calculations are compared to experimental results.

Outline

In the following chapters the background, method of analysis, computational results, and conclusions of this investigation are presented. Included in the background chapter (Chapter II) are discussions of conventional two-stroke engine designs and the design considerations for the free-piston engine-generator. Empirical, experimental and computational approaches to design are also reviewed. In Chapter III, the method of analysis for this thesis is detailed with the computational approach presented. The initial simulations, and simulations with four unique

operating schemes are also described. Chapter IV presents the results of the simulations, and illustrates how these were used to configure the scavenging system. In the final chapter (Chapter V) the study is summarized and conclusions are presented with recommendations for future work.

CHAPTER II BACKGROUND

Two-stroke cycle scavenging has been utilized since the development of the first IC engines as the easiest way of recharging the cylinder [2]. Today both the largest (~30,000MW) and smallest (~15W) IC engines use this means of gas transfer [2]. The two-stroke design results in a compact, lightweight and mechanically simple configuration.

Over the years many attempts have been made to modify the scavenging process to improve the engine's operational characteristics (power/torque output) and to minimize fuel consumption. Recently emissions control has become equally important. However, the main objective of the process still remains the same - adequately prepare the cylinder charge for the combustion cycle by removing the burned gases from the cylinder, and replacing them with a charge of fresh air (in direct injection (DI) schemes) or an air/fuel mixture (in port injection or carbureted schemes). In-cylinder gas flow patterns, as well as fuel concentration and distribution are important results of the process.

In this chapter some background is presented regarding the methods used thus far to scavenge the engine. Experimental and computational tools employed to understand and design the gas transfer system are also described. Finally, an explanation is given for the tools chosen to facilitate the optimization of the free piston engine's scavenging system.

Definitions

The following definitions are useful for understanding this text. Scavenging efficiency (η_{sc}) is the ratio of trapped fresh charge to the total trapped mass of the cylinder. Trapping efficiency (η_{tr}) is the ratio of trapped fresh charge to the total delivered fresh charge. Delivery ratio (Λ_{dr}) is the ratio of actual delivered mass to the mass of fresh charge that would occupy the

displaced volume at ambient conditions. Equivalence ratio (ϕ) is the ratio of the actual air-fuel ratio to the stoichiometric air-fuel ratio. Dilution ratio (ϕ_{eff}) is the ratio of the actual fuel-diluent ratio to the stoichiometric fuel-air ratio; this can be considered an effective equivalence ratio, taking into account the residual gases in the cylinder.

Scavenging Methods

In general three types of scavenging methods have been used, with variations of each employed. These are cross-flow, loop, and uniflow configurations where the major features of each are illustrated in Figure 2.1. The significant difference between these methods is the in-cylinder flow patterns that result. A brief description of these methods follows.

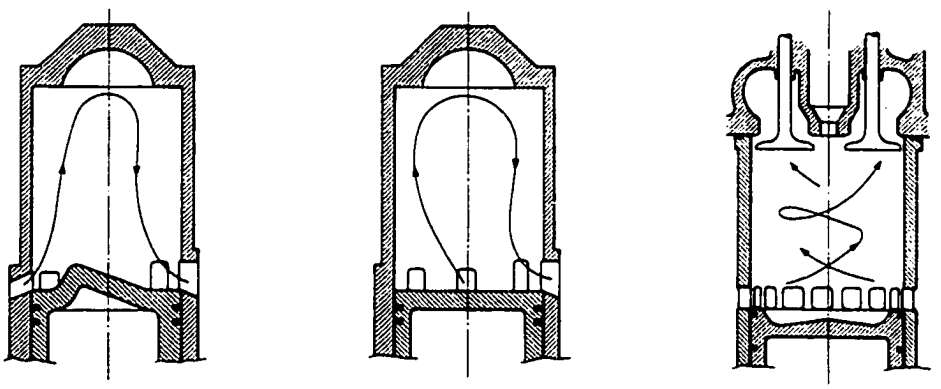

(a) Cross-flow (b) Loop (c) Uniflow

Figure 2.1 – Scavenging Methods

Cross-flow scavenging utilizes a contoured piston to direct the incoming charge towards the top of the cylinder. The combusted gases are displaced by the fresh charge and pushed toward the exhaust port, located directly across from the intake port (in the bottom of the cylinder wall). Cross-flow scavenging is the simplest and most compact means of arranging the gas transfer ports and was the earliest scavenging method used [2]. Complications with this arrangement can arise, however, if the piston develops hot spots and preignition of the air/fuel mixture follows (the operating compression ratio of cross-flow scavenged engines is limited by this problem). In DI schemes the fuel injection and mixing is hindered by the piston's profile.

Loop scavenging, in contrast to cross-flow scavenging, uses the geometry of the intake manifolds to direct the incoming charge toward the top of the cylinder, displacing the burned gases. The intake and exhaust ports are located at the bottom of the cylinder and are arranged so that a looping flow results from the momentum of the incoming charge. In this configuration a contoured piston is not used, but complicated manifold configurations are required.

Both cross-flow and loop designs rely on a long scavenging path (the fresh charge travels the length of the cylinder twice) to displace the combusted gases. Because of this there is ample opportunity for the burned and unburned gases to interact and mix, especially in long stroke-to-bore ratio geometries. This can cause problems when large fractions of the burned charge are entrained; the combustion process is degraded if too much residual gas is trapped in the cylinder, while high delivery ratios are required to achieve adequate scavenging efficiencies. Additionally, there is a tendency for the fuel to be short-circuited (in premixed operation) since the intake and exhaust ports are located very close to one another.

Uniflow scavenging, in contrast to both cross-flow and loop scavenging, expels the burned gases from one end of the cylinder and introduces the fresh charge at the other. Either wall ports or valves are used at the top of the cylinder, with wall ports at the bottom. In this configuration a shorter scavenging path is realized since the incoming gases only travel the length of the cylinder once. Less charge interaction results and better control of the scavenging process can be achieved. Conversely, complexity is introduced since the ports/valves at the top of the cylinder must be controlled.

Charge Delivery

For each of the scavenging methods the fresh charge is delivered to the cylinder after the cylinder pressure is reduced below the intake manifold pressure. This is accomplished through both the blowdown of the combusted gases out the exhaust ports/valves, and sometimes additional piston expansion. The fresh charge is usually supplied at a pressure higher than the exhaust manifold pressure and requires some sort of compressing system.

Two configurations are generally used to pressurize the incoming gas; one utilizes the dynamics of the working piston, while the other employs a separate mechanism. Incorporating the motion of the working piston, an internal pump can be constructed that is very compact. In this configuration the fresh charge is compressed either by the underside of the working piston, or by a stepped arrangement. These two schemes are shown in Figure 2.2.

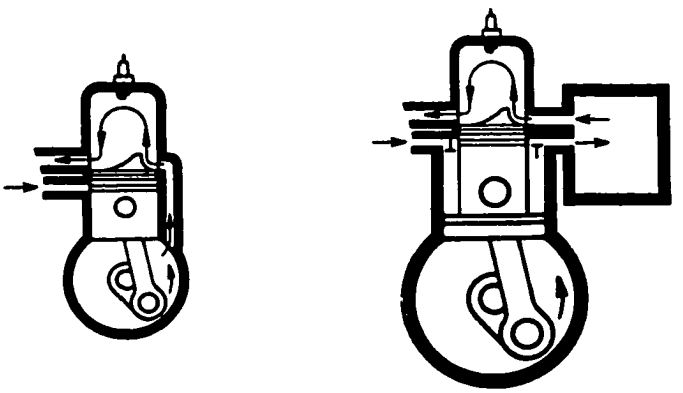

(a) Crankcase (b) Stepped Piston

Figure 2.2 – Internal Compressors [3]

In the crankcase design the incoming charge is retained within the crankcase volume until the intake ports open. In the stepped piston arrangement the compressed charge is delivered to a separate receiver tank before being introduced to the cylinder (in single-cylinder engines), or directly into another cylinder (in multicylinder engines). In both of these configurations the delivery process is affected by intake and exhaust pressure fluctuations, though the influence can be much greater in the crankcase arrangement. With the stepped piston option the mechanical complexity of the system is increased, however, the compressor can then be isolated from the pressurized charge. This allows the delivery ratio to be increased since the effectiveness of the pump is improved, and this results in enhanced performance at high altitude.

Several types of external pumps are commonly used in engine applications; these include centrifugal, reciprocating and roots-type compressors. Figure 2.3 illustrates these three options. External devices require a separate driving mechanism and increase the size of the engine;

however, certain advantages can be realized. Centrifugal blowers are simple, efficient and lightweight, but they are influenced by pressure fluctuations within the intake/exhaust systems. Reciprocating and roots-type compressors on the other hand, add bulk to the design but are able to deliver a fixed amount of fresh charge to the cylinder, independent of the upstream/downstream conditions. These devices can be used effectively over a wide range of operating conditions.

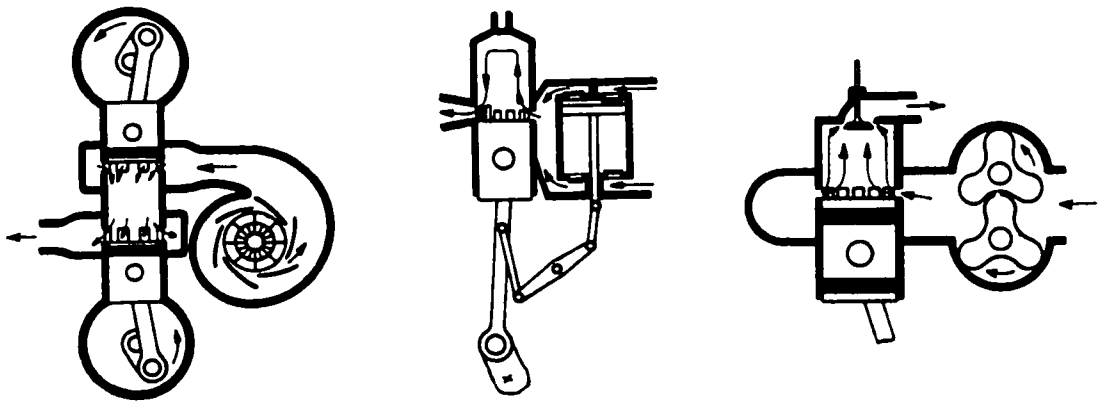

(a) Centrifugal (b) Reciprocating (c) Roots-type

Figure 2.3 – External Compressors [3]

Design Constraints

While each scavenging system must satisfy the design goals and operating characteristics of the individual engine, they are bound by similar constraints. One of the main design parameters, and often the most challenging for conventional scavenging systems, is the need to operate over a wide range of engine speeds. The ability to perform adequately under this constraint is significant, since the fluid and gas dynamics that dominate the process vary quite dramatically over typical engine speeds. Without compensation, mass flow through the engine will change with piston speed, and the intake and exhaust wave characteristics will be altered depending on the port/valve opening and closing times. These points are illustrated clearly in Figures 2.4 and 2.5. The result of such variations can be excessive short-circuiting, insufficient charging, as well as changes in the in-cylinder flow patterns.

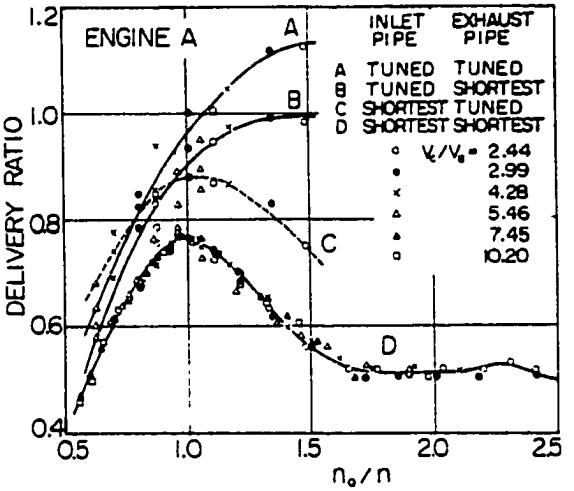

Figure 2.4 – Delivery Ratio vs. Engine Speed Ratio (speed at which maximum delivery ratio is achieved in untuned engine to actual engine speed) [4]

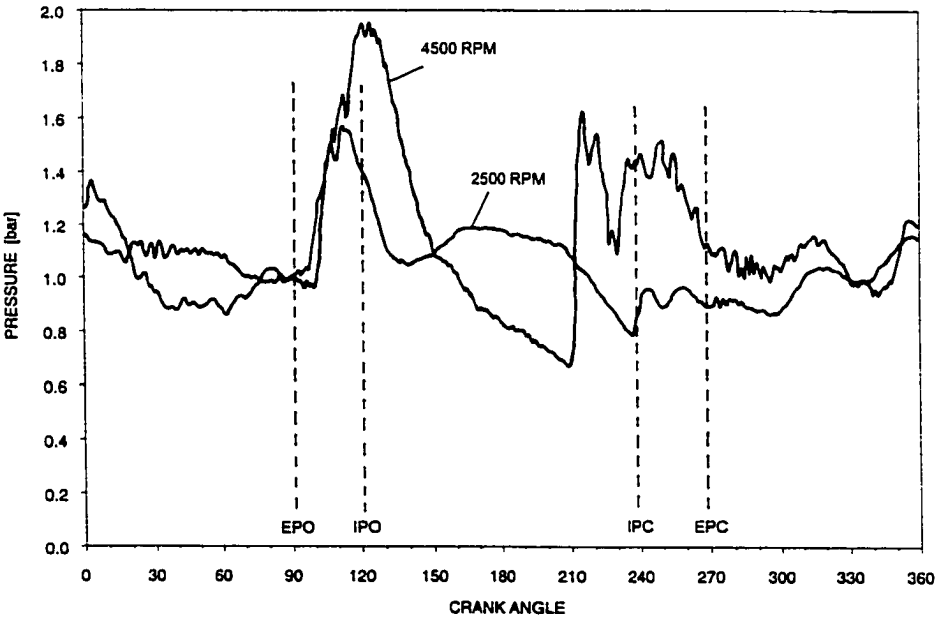

Figure 2.5 – Exhaust Pressure vs. Crank Angle [5]

Another common constraint for the gas transfer system is the need for adequate charging at light load, or throttled conditions (in premixed schemes). When the mass flow to the engine is restricted to decrease the power output, excessive amounts of previously combusted gas can become trapped in the cylinder at port/valve closure. This greatly affects the stability and

completeness of spark-ignited combustion, and therefore must be controlled. Figure 2.6 illustrates this problem.

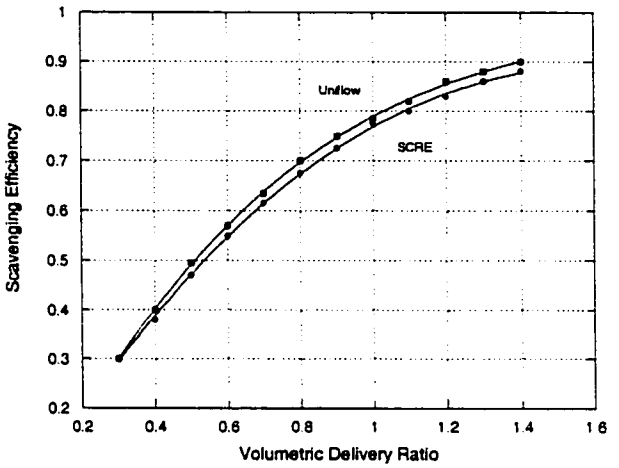

Figure 2.6 – Scavenging Efficiency vs. Volumetric Delivery Ratio [6]

Recent attempts to address these issues have included variable port/valve timing [7,8], exhaust manifold throttling [9-11], stratified scavenging [12-14], direct injection of the fuel after port/valve closure [15-19], and HCCI combustion at light load [20-21]. While these solutions are promising, however, implementing them effectively can be challenging. Further, complications in the combustion cycle can result if the fuel concentration and distribution are not adequate, or if the in-cylinder flow patterns are insufficient for ignition and flame diffusion/propagation.

Free Piston Engine Considerations

When designing the scavenging system for the free piston engine-generator the unique operating requirements of this IC engine must be considered. Most significant of these is the incorporation of the engine into a high conversion efficiency, low emissions device. This is important because the potential of the free piston HCCI process can be degraded by inadequate charge preparation or fuel short-circuiting. For efficient HCCI combustion the in-cylinder gases (air/fuel/residual) must be mixed sufficiently by TDC so that combustion is uniform throughout the bulk of the cylinder and proceeds with a very rapid pressure rise (almost constant volume).

Further, the local equivalence ratios and gas temperatures must be low enough so that NOx formation is inhibited. Since the scavenging process directly affects combustion and pollutant formation, and therefore the overall performance of the engine, it must be configured to achieve the engine's efficiency and emissions goals.

Low equivalence ratio operation requires that the losses in the engine be minimized. This must occur so that a high fraction of the work output can be converted into useful electrical power. Because of this, restrictions on the scavenging scheme (e.g. low pumping power, no high pressure, in-cylinder fuel injection mechanism, low blowdown losses, etc.) are imposed.

Of benefit to the design is the limited operating regime over which the engine-generator is expected to function. Because this device will be used for continuous electrical generation, performance over a wide range of speeds is not needed. This significantly simplifies the design process.

Two more considerations for the free piston configuration are the desire for a long stroke-to-bore ratio (for adequate TDC clearance, and an advantageous surface area to volume ratio) and mechanical simplicity (since there is no crankshaft to operate valves, pump, etc.).

The combination of the engine's design goals, its unique configuration, and the operating characteristics enable a number of interesting options to be investigated.

Design Tools

Over the years many tools have been developed to aid the understanding and design of two-stroke cycle scavenging. Both experimental and computational methods have been used with some success [2], however the bulk of the design work remains based on empirically determined knowledge [22]. The means to configuring an effective scavenging system is surely not yet complete, with the application of most methods limited. On the other hand, as various design tools are improved and refined, and better detail of the scavenging process is learned, non-empirical methods are expected to see more use. A description of the tools currently available is presented next.

Empirical

Empirically determined knowledge (mainly through trial and error) has led to the development of a number of decent scavenging designs. Both good and bad two-stroke configurations have been constructed, and from this basis, guides for the scavenging layout have emerged. Parameters including the port timing, port configuration (specific open-area times, number of ports and their incoming angles), exhaust manifold tuning, and induction system configuration have all been quantified. In addition, items such as maximum allowable port width to avoid piston ring breakage have also been detailed. A good description of these can be found in [22]. Empirical methods, for all of their extensive use, are restricted of course in the development of advanced designs and the implementation of unique scavenging concepts. They can, however, provide a good starting point for the design.

Experimental

Experimental tools currently in use include steady flow measurements, single stroke similarity tests, motored and fired engine measurements, and laser-based velocity and fuel distribution assessments. Steady flow measurements are most often used to study the direction and distribution of the incoming charge, without including the influence of unsteady gas dynamic effects or the piston motion. These tests have been used for over 40 years and have provided some of the earliest experimental insight into the in-cylinder gas motion [23-25].

In steady flow tests the cylinder head is usually removed and the piston set to the bottom dead center (BDC) position; though the piston can be motored. An upstream pressure is imposed to force gas through the intake ports. Figure 2.7 depicts the engine setup for a typical steady flow test. Analysis of the pressure distribution across the cylinder (at the top of the cylinder), along with viewing the movement of indicator strips placed within the cylinder, or the flow of dyed gases helps illustrate how the engine is scavenged. A qualitative judgment can be made about the effectiveness of the process. Steady flow experiments have been successfully used to compare 'good' and 'bad' scavenging arrangements, however, they are limited in their analysis to studying

cross-flow and loop configurations. Additionally, they cannot truly represent the dynamic parameters (e.g. blowdown, pressure waves, etc.) that dominate the scavenging process.

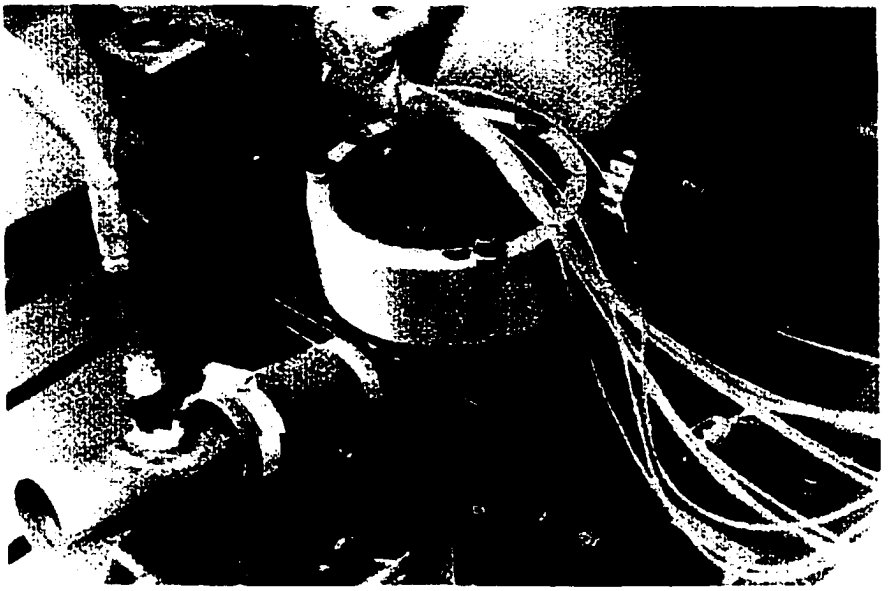

Figure 2.7 – Steady Flow Test Apparatus [22]

Single stroke/cycle similarity tests are frequently used to modify port geometries in order to improve the engine's scavenging characteristics. These tests are simple and inexpensive, and allow the incoming flow behavior to be characterized under dynamic conditions [26-28]. For these analyses the flow into and out of the engine is usually modeled using two different liquids, instead of gases, since the flow is much slower and more easily recorded visually. In configuring these tests similar geometric ratios, as well as Reynolds and Euler numbers are generally used. Here, a model of the piston and cylinder, and intake/exhaust manifolds are constructed where the piston's motion is set to closely resemble the actual piston's motion. The tests are run through a single scavenging cycle (exhaust port opening to exhaust port closing) with measurements made both during and after the cycle. A schematic of a typical single cycle test is shown in Figure 2.8 with some results presented in Figure 2.9.

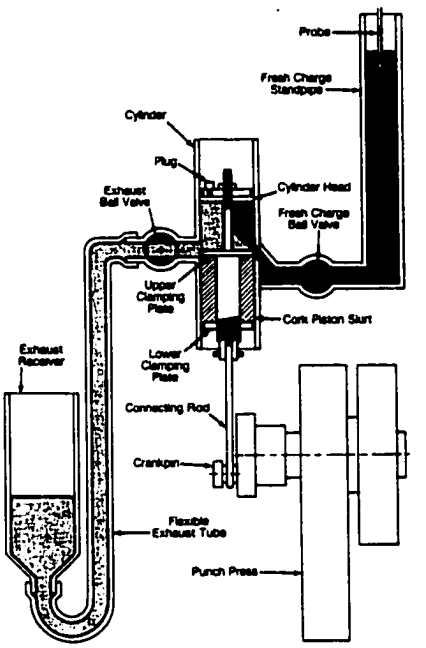

Figure 2.8 – Single Cycle Test Apparatus [26]

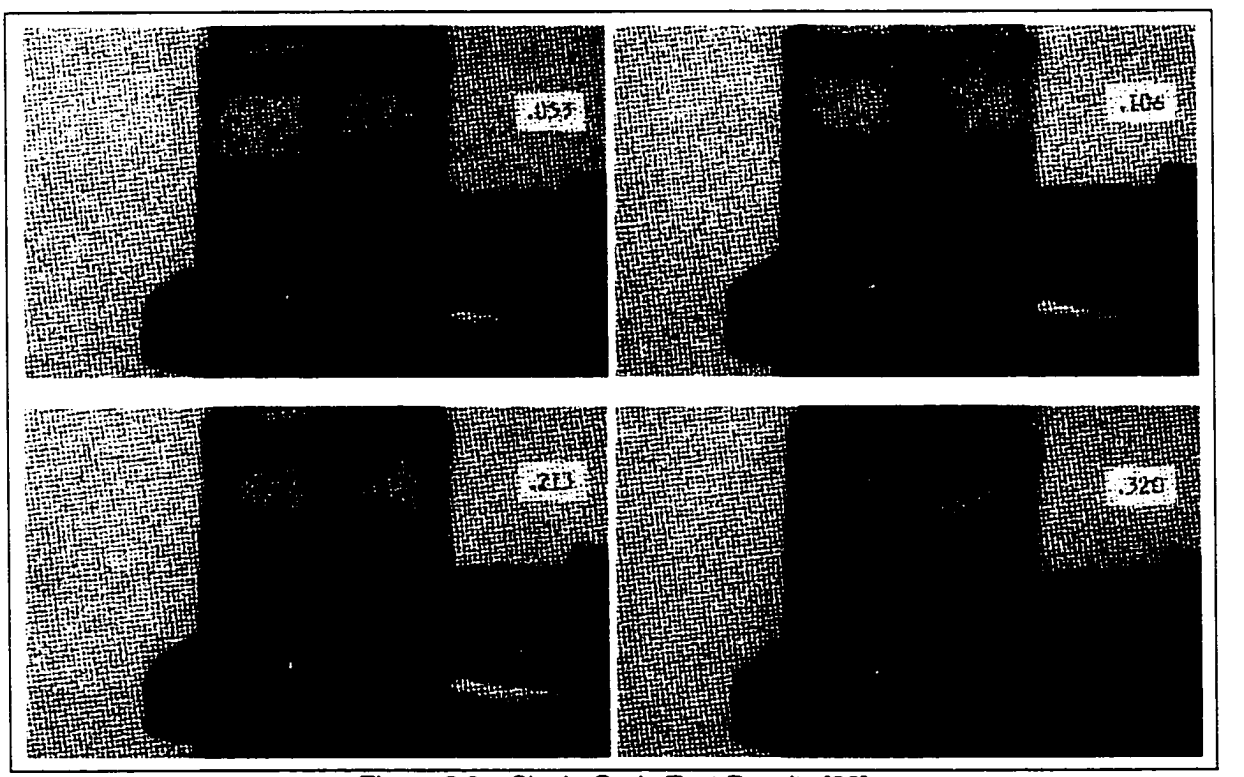

Figure 2.9 – Single Cycle Test Results [26]

Through single cycle experiments the incoming charge can be suitably visualized with poorly scavenged regions, and rates of mixing and short-circuiting determined qualitatively. Additionally, quantitative measurements of the exhaust purity and overall scavenging efficiency can help measure the effectiveness of the process (especially comparing different scavenging configurations). Conversely, the compression, expansion and blowdown processes are usually not included, and the effects of heat transfer, diffusion, compressibility, and intake/exhaust pressure variations not taken into account.

Operating (motored or fired) engine measurements are an effective way of characterizing the scavenging performance under actual operation [29-31]. Any configuration can be used with a full range of parameters investigated. In these tests the in-cylinder and/or exhaust gases are sampled during the scavenging period, along with in-cylinder and manifold pressure data, to create an illustrative picture of how the process progresses. Gases representing the burned (e.g. CO, CO_2) or unburned (e.g. O_2, CH_3NH_2) charges are generally used in the analyses, where the measurement and analyses techniques have been well developed. A detailed description can be found in [29].

Gas concentration sampling provides a convenient and reliable way of determining the scavenging and trapping efficiencies of the operating engine. Though the details of the in-cylinder flows are not available, many of the dominant parameters missing from steady flow and single stroke tests are included. The downside to this technique is that it can only be performed on scavenging systems that have been designed and constructed, and therefore provides little direction during the design process.

Laser-based measurements have recently improved the understanding of many in-cylinder processes and have enabled some computational analyses to be verified [32-37]. In these experiments, laser beams or sheets are used to optically quantify various in-cylinder quantities during the gas transfer process. Laser Induce Photochemical Anemometry (LIPA) [32] and Laser Doppler Velocimetry (LDV) [35] accurately measure gas velocities (from seeded

particles) at points within the cylinder, and help illustrate how the in-cylinder gas motion is affected by the incoming charge. Laser Induced Fluorescence (LIF) [36] and Mie-scattering [37] help determine how injected fuel disperses within the cylinder as it mixes and burns. (Light scattering and fluorescence techniques are used to produce images dependent on local fuel concentrations.) Even though these experimental tools provide a great deal of information (both qualitative and quantitative) regarding the in-cylinder processes, they are complicated, costly, and very time consuming to perform. As a result they have had limited application in two-stroke engine designs.

Computational

Computational tools have gained increasing popularity in recent years due to advancements in computer capabilities and to model improvements. Often these analyses are used to complement empirical and experimental results. However, with the increased accuracy possible for gas flow calculations, many now have significant roles in the design process.

Mathematical models for the scavenging process can be classified as either zero-, one- or multi-dimensional. Zero-dimensional (0D) models are generally used in the context of full cycle engine models as a means of approximating how the burned and unburned charges interact within the cylinder. These analyses are often used to determine the influence of the gas exchange process on the rest of the engine cycle, with respect to speed, load, spark/injection timing, and super/turbo charging.

Zero-dimensional models reduce the complex in-cylinder features of the scavenging process to single/multi-zone, single/multi-phase events [38-40]. Throughout the scavenging period, flows into and out of the zones within the cylinder are prescribed based on the amount of mixing/displacement assumed. An illustration of a 0D model is presented in Figure 2.10. In this Figure the cylinder volume is divided into three zones: a burned, unburned and mixed zone. Flow enters and exits each zone depending on the time within the scavenging period, while the overall mass flow through the cylinder is calculated based on quasi-steady or unsteady calculations.

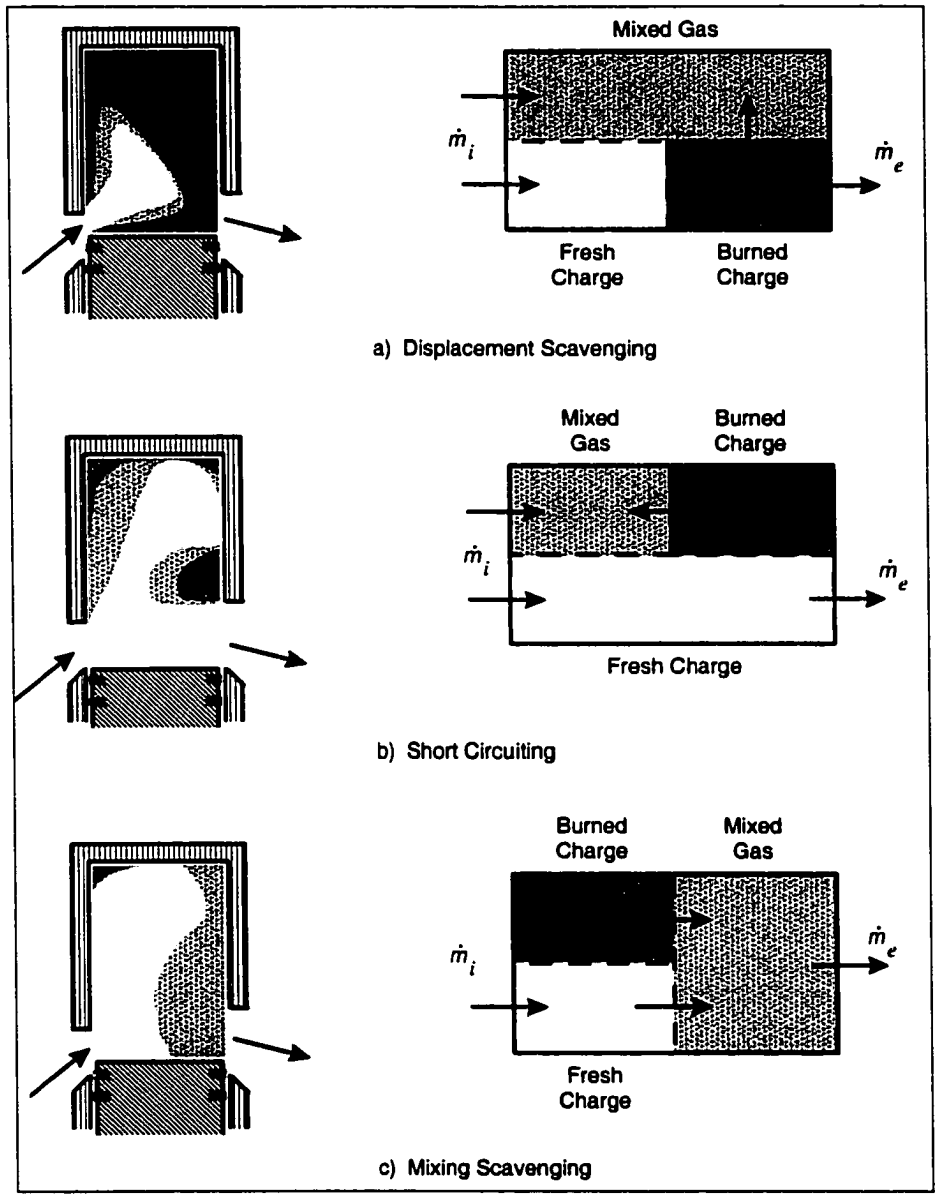

Figure 2.10 – Scavenging Process as Defined by a 0D Model [38]

Zero-dimensional models are generally correlated to specific scavenging schemes and must be re-correlated for different configurations. As such detailed designs cannot be accomplished using these reduced analyses [2].

One-dimensional (1D), or gas dynamic models are often used to describe the effect of compression/expansion waves within the intake/exhaust manifolds on the filling/emptying of the cylinder during scavenging [41,42]. These models attempt to compute the pressure fluctuations

throughout the engine flow system using 1D compressible flow equations. The unsteady mass, momentum and energy conservation equations are solved during the scavenging period, where a thermodynamic analysis within the cylinder links the intake and exhaust flows. Variations with engine speed, intake/exhaust design, and port dimensions and timing are adequately predicted with these calculations. Figure 2.11 shows an example of such a calculation where the exhaust pressure history is compared to experimental results. Figure 2.12 illustrates the computational and experimental results with regard to variations in engine speed.

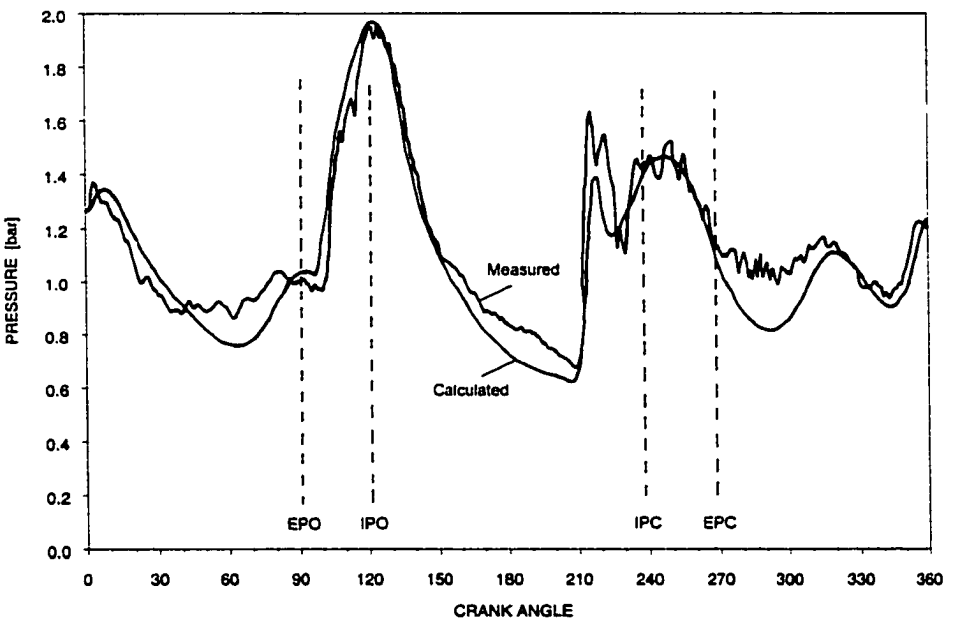

Figure 2.11 – Exhaust Pressure vs. Crank Angle [5]

Often 1D analyses are useful for tuning the intake and exhaust systems to maximize the engine's throughput while minimizing short-circuiting during the later part of the scavenging period. These models cannot, however, describe the in-cylinder gas flows (including burned/unburned charge interaction), and therefore must be used in conjunction with either 0D approximations or multi-dimensional models.

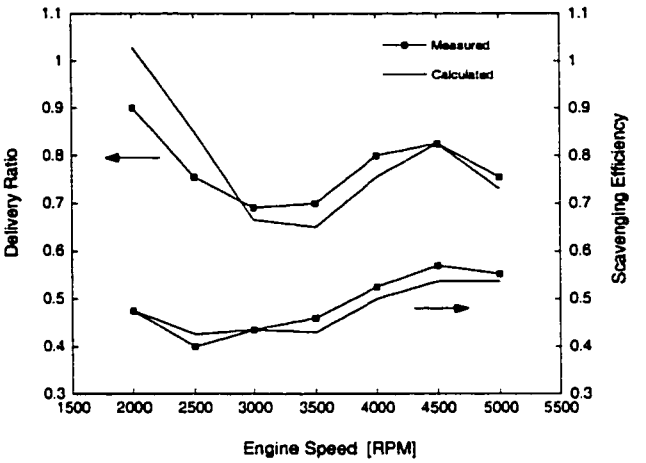

Figure 2.12 Delivery Ratio and Scavenging Efficiency vs. Engine Speed [5]

Multi-dimensional models, in contrast to 0D and 1D analyses, are able to describe the full flow field within the engine cylinder, and have been used to help understand the detailed interactions of the incoming and burned charges [43-56]. Multi-dimensional models solve the differential equations for mass, momentum, energy and species concentration conservation while incorporating models for transport, turbulent flow phenomena, and boundary conditions. The equations are applied to a multi-dimensional computational grid that closely resembles the topography of the combustion chamber, scavenge ports/ducts, and the moving piston. An illustration of a sample mesh is given in Figure 2.13.

These models have been used to determine the effect of complex cylinder and port geometries, valve arrangements, and operating conditions on the in-cylinder flow, and the complex mixing and short-circuiting phenomena. With multidimensional models unique scavenging arrangements can be investigated where the charge interaction is easily viewed through particle tracing techniques. However, they require extensive computer resources and are limited by the incompleteness of the sub-models incorporated into the codes, and the complexity of the in-cylinder processes. Further, insufficient application of the boundary conditions can significantly alter the results computed by these codes.

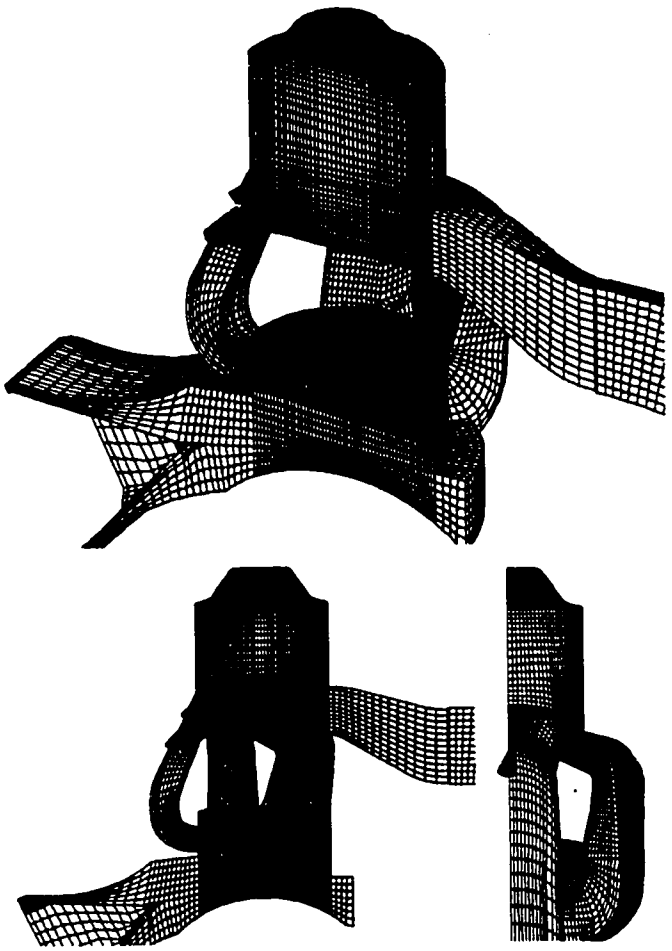

Figure 2.13 – Sample CFD mesh [50]

Free Piston Engine Design

The design constraints and unique considerations for the free piston engine-generator led to the conclusion that employing multi-dimensional computational modeling as the main design tool would yield the most useful information for the design objectives. Incorporating component models to account for the intake charge delivery system and friction losses will allow the effects of these processes to be investigated. Using these tools a comprehensive study of the design, investigating a wide range of parameters and configurations was undertaken. The following chapter presents some details regarding the computational tools employed as well as the methods used to converge on an optimal configuration.

CHAPTER III METHOD OF ANALYSIS

To optimize the scavenging system for high thermal efficiency and low output emissions a single step parametric analysis was conducted with CFD modeling used as the primary design tool. A large design space was explored where various parameters (both geometric and operating) affecting the two-stroke process were investigated. A series of initial simulations was first conducted to narrow the design possibilities, then the overall performance of the engine was optimized by comparing a few select operating schemes. The details of this analysis are described below.

Computational Tools

The bases for optimizing the scavenging system are the efficiency of the engine cycle and the degree of NOx and short-circuiting emissions. Charge preparation and trapping capabilities are critical to the engine's combustion process and emissions generation. To best represent these features, a multi-dimensional fluid dynamics model was used which could capture the dynamics of the gas flow through the cylinder. In addition, a 0D model was used to simulate the intake charge compression process, while a 1D model calculated frictional losses from the piston-cylinder motion. The overall efficiency could be analyzed in this way.

Intake and exhaust wave dynamics were not included in this analysis; it was assumed that manifold tuning could be performed later to manage the pressure variations for the engine's single speed operation. The computational tools used in this dissertation are described next.

Computational Fluid Dynamics

The CFD code KIVA-3V was employed for this study. KIVA-3V was chosen due to its versatility and long history of application to IC engine studies [57-69], and because its source code

is completely accessible for modification. The KIVA family of 3D codes solves the unsteady equations of motion for turbulent, chemically reacting flows on finite-volume grids. Coupled, implicit differencing techniques are used, with sub-models implemented to describe sub-scale phenomena such as heat transfer, spray formation and turbulence.

The KIVA-3V version allows for complicated geometries through its use of block-structured grids and an efficient grid snapping routine. Complex piston-head configurations, intake/exhaust ports and valves, and intake/exhaust manifolds can be modeled quite well. The ports and valves are able to open and close realistically according to defined piston motion and valve lift curves. Continued improvement to KIVA's various sub-models has progressively increased the accuracy of the computational results. The full details of this code can be found in Refs. [70-73].

The validity of KIVA-3V, and its predecessors has been demonstrated through numerous studies where experimental engine data have been reasonably matched to the code's calculations [74-79]. These studies have shown that overall engine variables like power output and delivery ratio can be predicted with decent accuracy by the code, while calculated flow quantities are close to actual measured values. In addition, predictions in trends based on changes to operating parameters and geometrical configurations have shown great value. On the other hand however, significant discrepancies still exist in calculating sub-scale values (e.g. turbulence), and in treating complex combustion phenomena such as spray impingement and emissions formation.

The basis of this dissertation is dependent on the capability to accurately analyze the two-stroke flow phenomena that define the scavenging process (e.g. port/valve flows, in-cylinder mixing, etc.). The use of parametric studies to determine trends in scavenging performance is also key to achieving an optimal design. As stated earlier, in-cylinder fuel injection schemes are not considered practical for the engine-generator, and combustion is accomplished through an HCCI process. These factors significantly decreased the computational demands of the simulations. Based on these considerations, it was expected that KIVA-3V could adequately meet the requirements for this study.

The KIVA-3V code was modified slightly for this investigation. Changes included the calculation of pertinent scavenging parameters (e.g. scavenging and trapping efficiencies, flow rates, etc.), the definition of the free piston motion, modification to allow various time dependent intake boundary conditions, and the incorporation of the intake charge compression model.

Visualization

An important aspect of analyzing the CFD results is developing an understanding of the gas motion through the cylinder, especially the interaction of the burned/unburned charges. To achieve this the 3D visualization software Ensight was used [www.ceintl.com]. Ensight's particle tracing routine provided a means of tracking the fresh and burned charge motion through the cylinder, and added a good deal more insight than merely studying velocity vector plots or instantaneous streamline calculations. Additionally, the capability to illustrate dynamically the fuel concentration gradients throughout the cylinder enabled a determination to be made of fuel short-circuiting and charge uniformity at TDC. A fundamental understanding of the gas exchange process was gained through visualizing of the CFD results.

Intake Charge Compression

The compressor model used for this study calculates the work required for the incoming gases to be compressed to the desired charging pressure, and also provides temperature and pressure inputs to the KIVA-3V code. The process is modeled assuming that the compressor is integrated into the engine design in a stepped piston arrangement, as depicted in Figure 3.1. Here the alternator's magnets function as the stepped piston. The compressor receives premixed fresh charge at atmospheric conditions, assumed steady, and feeds it to a delivery tank at an elevated pressure. The delivery tank then supplies the intake manifold of the KIVA-3V mesh.

The gas in the compressor is modeled using a 0D representation of the energy and mass conservation equations, as given by

$$\frac{dU}{dt} = \frac{dQ}{dt} - P\frac{d\forall}{dt} + \sum_i \dot{H}_i - \sum_e \dot{H}_e \qquad (3.1)$$

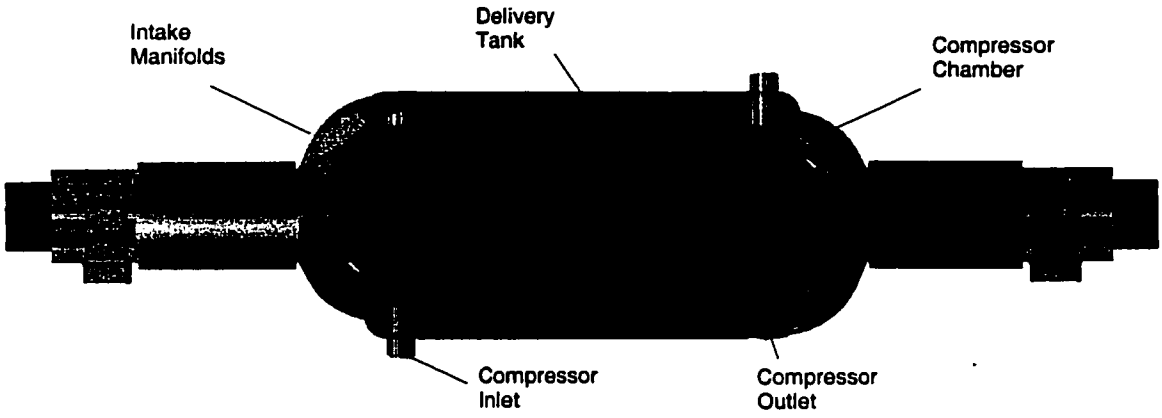

Figure 3.1 – Stepped Piston Compressor Configuration

and

$$\frac{dm_j}{dt} = \sum_i x_{j,i}\,\dot{m}_i - \sum_e x_{j,e}\,\dot{m}_e \,. \tag{3.2}$$

In Eq. (3.1) $\frac{dU}{dt}$ is the time rate of change of the internal energy of the compressor gases, $\frac{dQ}{dt}$ the rate of heat transfer to the gases, $P\frac{d\forall}{dt}$ the rate of work done by the stepped piston, and $\dot{H}_i$ and $\dot{H}_e$ the rates of enthalpy flows into and out of the compressor, respectively.

The heat transfer to the gases is assumed to be defined using a spatially averaged correlation, as given by [80]

$$h_c = c_1\, D_{eff}^{-0.2}\, P^{0.8}\, T^{-0.546}\, \bar{s}_p^{\,0.8}\,, \tag{3.3}$$

where the overall rate of heat transfer is

$$\frac{dQ}{dt} = h_c\, SA\,(T_w - T)\,. \tag{3.4}$$

In these equations h_c is the heat transfer coefficient, c_1 the correlation constant, D_{eff} the effective bore, P the gas pressure, T the gas temperature, and $\bar{s}_p$ the average piston speed. SA is the surface area of the compressor, T_w the wall temperature. Equation (3.3) was derived for typical piston-cylinder configurations, but it was assumed to be useful in this study's concentric design.

Spring-loaded check valves are used for the intake and exhaust openings where once a defined flow restriction (ΔP) is reached, the valve instantaneously opens to a fixed cross-sectional area. There is no lag time included to account for spring dynamics. (Reed valves were considered for this study but were found to be difficult to configure for the system, and therefore not used in the parametric analysis.)

Flow through the check valves is assumed to be one-directional and quasi-steady where the mass flow rate is calculated by

$$\dot{m}_{i,e} = \left[C_D A_v \frac{P_o}{\sqrt{RT_o}} \left(\frac{P_T}{P_o} \right)^{1/\gamma} \left\{ \frac{2\gamma}{(\gamma-1)} \left[1 - \left(\frac{P_T}{P_o} \right)^{(\gamma-1)/\gamma} \right] \right\}^{1/2} \right]_{i,e} \tag{3.5}$$

for unchoked conditions, and

$$\dot{m}_{i,e} = \left[C_D A_v \frac{P_o}{\sqrt{RT_o}} \gamma^{1/2} \left(\frac{2}{\gamma+1} \right)^{(\gamma+1)/2(\gamma-1)} \right]_{i,e} \tag{3.6}$$

for choked conditions. Choking occurs when the pressure ratio (P_T/P_o) falls below $(2/\gamma+1)^{\gamma/(\gamma-1)}$. In these equations C_D represents the discharge coefficient and A_v the effective valve area. P_o and T_o are the stagnation pressure and temperature, respectively, and R the gas constant. P_T represents the downstream pressure and γ the ratio of specific heats.

For this study the discharge coefficients are assumed to be constant, based on the assumption of fully open valves and one-directional flow [80]. A value of 0.7 was chosen to facilitate the calculations.

The enthalpy flows through the compressor are calculated by

$$\dot{H}_{i,e} = \sum_{i,e} \dot{m}_{i,e} h_{i,e}, \tag{3.7}$$

where the subscript i denotes flow entering, and e flow exiting the compressor. The molar specific enthalpy is determined using

$$h_{i,e} = \sum_{j} x_j h_j^*, \tag{3.8}$$

where x_j is the mass fraction of species j, and the species specific enthalpy, h_j^* is given by

$$h_j^* = \Delta H_j^0 + \int_{T^\circ}^{T} c_{p,j}\, dT\,. \tag{3.9}$$

Here ΔH_j^0 represents the heat of formation of specie j at reference temperature T°, while $c_{p,j}$ is the species specific heat at constant pressure.

The delivery tank was modeled similar to the compressor so that Eqs. (3.1) and (3.2) are applicable. For the tank the piston work is zero, and the heat transfer is calculated based on either an adiabatic or isothermal assumption, which represents operating limits for the device (insulated or cooled). The enthalpy/mass flows into the tank are determined from the compressor flow calculations, while the flow from the delivery tank is calculated by the KIVA-3V code, using the tank as KIVA's inlet boundary conditions. Mass is free to move between the tank and the intake manifold mesh boundary, allowing for some oscillation. Outflow from the computational mesh into the tank is assumed to mix instantaneously with the entire tank volume, and therefore the tank presents a uniform condition for KIVA's boundary.

Friction

The friction model determines the friction work between the piston rings and cylinder liner. This is the dominant form of friction within the free piston engine-generator, since there is no crankshaft or other significant moving parts. The ring friction is calculated assuming that a thin oil film lubricates the walls of the cylinder [82]. The Reynold's equation is used to compute the pressure distribution within the oil film and the instantaneous friction force.

The 1D Reynold's equation is expressed as

$$\frac{d}{dx}\left(th^3 \frac{dP_{oil}}{dx} \right) = 6\,\mu \left(2\frac{dth}{dt} - v_p \frac{dth}{dx} \right), \tag{3.10}$$

where x is the direction along the piston ring's axis. Figure 3.2 illustrates the geometry used in this calculation. In Eq. (3.10) th is the oil film thickness, P_{oil} the oil film pressure, μ the viscosity of the oil and v_p the piston/ring velocity. The oil film thickness is given by

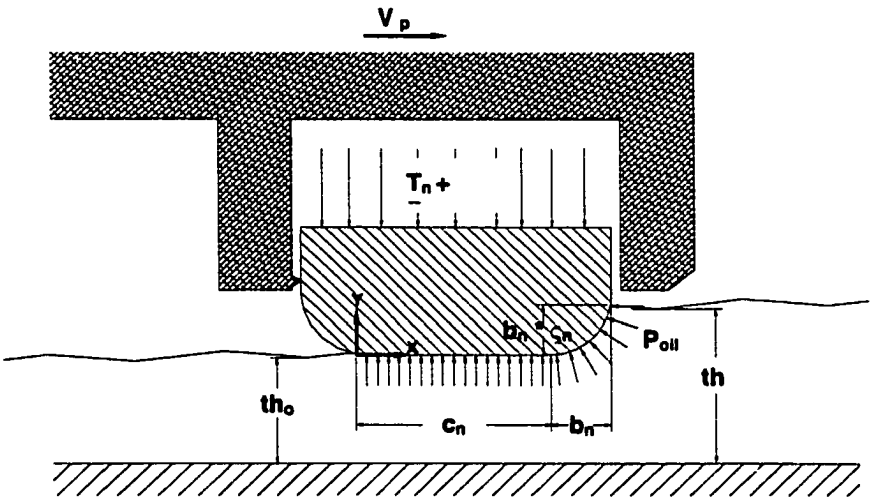

Figure 3.2 – Piston Ring Diagram

$$th = th_o \qquad x < c_n \qquad (3.11)$$

$$th = th_o + (b_n \varsigma_n)\left[\frac{x - c_n}{b_n}\right]^2 \qquad x > c_n, \qquad (3.12)$$

where ς_n, b_n, and c_n are parameters for the ring geometry that are labeled in Figure 3.2.

The friction force, F_f, is then calculated using

$$F_f = \pi D\left[\int_0^{c_n+b_n} \frac{th}{2}\frac{dP_{oil}}{dx}\,dx + \mu v_p \int_0^{c_n+b_n} \frac{1}{th}\,dx\right], \qquad (3.13)$$

where this is integrated over the piston's travel to compute the total friction work. In Eq. (3.13) D is the cylinder bore and $c_n + b_n$ represents the limit of oil contact with the ring.

Assumed in this model is that the rings are fully immersed in oil (no cavitation) and that the film thickness varies only in the direction of ring motion. The rings are assumed not to twist, and thermal and elastic deformations are negligible. An incompressible Newtonian lubricant is used where friction effects are from oil shearing only.

Optimization Method

The free piston engine's scavenging system was optimized so that the overall engine cycle can achieve maximum thermal efficiency with low output emissions. The scavenging system's contribution to the engine's performance is characterized by the effectiveness of the charge preparation (for HCCI combustion), the extent of fuel short-circuiting, and losses associated with recharging the cylinder. For this dissertation a series of initial simulations were conducted to assess the capabilities and limitations of various scavenging methods, as well as options for the charge delivery system. Single step parametric investigations allowed the effects of different geometric and operating parameters to be determined. Based on the results, more narrowly defined computations were performed using four different operating schemes. An optimal system was then identified. The details of the procedure are described in the following sections.

Initial Simulations

The objectives of the initial simulations were to determine the key factors affecting the performance of the scavenging process in the free piston configuration, and to gain an understanding of the in-cylinder dynamics necessary to optimize the process. In addition, it was important to determine which scavenging method should be used in the final optimization runs. Establishing the impact of the intake charge compression process on the overall cycle was also essential.

SCAVENGING METHODS - Three different scavenging methods were investigated including a classic loop, a hybrid-loop, and a uniflow configuration. These arrangements are illustrated in Figure 3.3. Cross-flow scavenging was not considered due to its associated preignition problems and the difficulties of controlling the orientation of a contoured free piston.

A goal of the initial runs was to achieve high scavenging efficiencies (necessary for high compression ratio HCCI combustion (desired to maximize the cycle efficiency potential)) and low

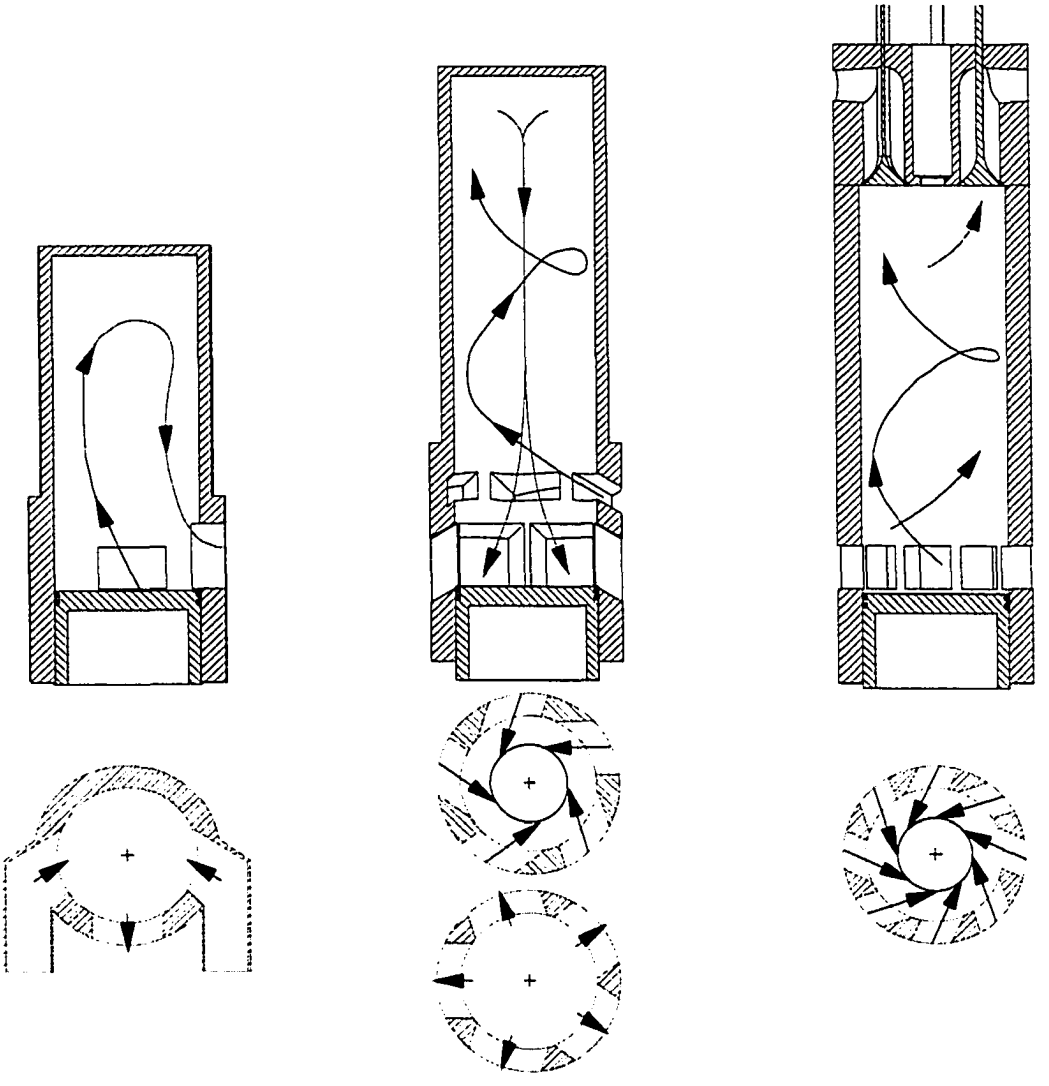

(a) Loop (b) Hybrid-loop (c) Uniflow

Figure 3.3 – Loop, Hybrid, Uniflow Scavenging Configurations

trapping losses, in a mechanically simple configuration – the best option for the engine (see [83]). As such, a classic loop design was investigated first. Here the performance of the system is based on steady inflow/outflow pressure boundaries with the incoming charge premixed (used to decrease the computational demands of the runs; the possibility of port-injection was not include in this study, though it's use may be important in the final engine design). Simulations were conducted to determine the influence of intake charge pressure, intake equivalence ratio (ϕ), exhaust/intake timings and port areas, and piston frequency on the overall scavenging process.

A hybrid-loop configuration was investigated next. In this arrangement, as can be seen in Figure 3.3b, the intake ports are located circumferentially around the cylinder wall above the exhaust ports. The intake manifolds are angled so that swirling flow is directed toward the top of the cylinder with the intent of flushing the burned charge down the core of the cylinder and out the exhaust ports. The motivation for this unique arrangement was to enhance scavenging at the top of the cylinder (a challenge in the long stroke-to-bore design with bottom located ports), while maintaining high trapping capabilities (since the exhaust ports close before the intake ports). Simulations were conducted to determine the influence of the number of intake/exhaust ports, intake charge pressure, exhaust timing and port area, and piston frequency.

Based on the poor performance of the loop and hybrid-loop arrangements, a uniflow configuration was investigated, with the hope that the burned/unburned charge interaction could be minimized relative to the previous geometries. This would lead to both high scavenging efficiency and low trapping losses. Simulations were conducted to study the effects of exhaust valve lift/timing, intake port configuration (number of ports, incoming swirl angles, and area/timing), piston frequency, and piston travel past the bottom of the intake port.

CHARGE DELIVERY – Variations of several different parameters for the stepped piston compressor were investigated in the initial simulations. These included changes to the volumetric compression ratio, delivery tank volume, inlet/outlet valve areas, and adiabatic/isothermal tank conditions. The effect on the in-cylinder flows, overall engine cycle, and required pumping power were determined.

Final Simulations – Optimal Configuration

Using the initial simulations as a baseline, an optimal scavenging arrangement was configured. The uniflow arrangement was adopted due to its superior performance, even though this results in a more mechanically complicated system.

The objective of the final simulations was to select an operating scheme that would maximize the overall thermal efficiency of the cycle while minimizing the output emissions. The means to achieving high scavenging and trapping efficiencies in the uniflow arrangement had been determined from the initial simulations. For evaluation purposes the cycle thermal efficiency was assumed to include work output from the combustion gases, as well as losses resulting from short-circuiting, pumping, and friction; emissions were in the form of NO and short-circuited fuel.

For the final runs, the scavenging system was configured with regard to a nominal output power level. This means that for the four schemes analyzed each arrangement was configured to achieve similar power outputs. The efficiency and emissions performance were calculated based on this. A low dilution ratio (~0.38) ensured that NO formation was minimized.

The following operating schemes were investigated:

1. A low charging pressure (1.2bar) and sufficient port/valve timing was used to achieve a moderate scavenging efficiency (0.8) with low trapping losses (1%). A moderate piston frequency (45Hz) was employed. This is the nominal power configuration.
2. The charging pressure was decreased to reduce the pumping work. In this option, the operating frequency was also decreased to allow for sufficient scavenging; the cylinder volume had to be increased to achieve the nominal power output. The resulting change in friction losses however, may offset the decrease in pumping work.
3. A stratified scavenging arrangement was used to improve the scavenging efficiency (0.9) without increased short-circuiting losses. (Stratified scavenging is an arrangement where the cylinder is initially flushed with air only, with a rich fuel/air mixture introduced late in the scavenging cycle.) Higher pumping power was expected since more air is delivered to the cylinder; this may negate the improvements in cycle thermal efficiency.
4. An over-expanded (Atkinson) cycle was used to recover additional work from the charge and decrease the blowdown losses. In this cycle the combusted gases

are expanded to reduce the cylinder pressure to the level of the intake charging pressure before the exhaust valves or intake ports open. The friction was expected to increase due to the longer stroke, and the altered in-cylinder flows may negate the increased piston work.

These four arrangements were configured to achieve the operating goals (η_{sc}, η_{tr}, Power) based on the parametric studies from the initial simulations.

After comparing the performance of these operating schemes an analysis was also conducted to investigate the 'robustness' of these options when the equivalence ratio and piston frequency were adjusted by ±10%. These trials were run to determine how the scavenging system's and the engine's performance are affected by slight changes in the operating conditions – a useful analysis for actual engine operation. An optimal arrangement was concluded based on these computational analyses.

The use of KIVA-3V, in conjunction with the compressor and friction models was expected to yield significant information towards optimizing the scavenging system for the free piston engine. Using these computational tools and single step parametric variations a comprehensive study was undertaken analyzing a variety of different operating configurations. It was expected that the first steps towards optimizing the scavenging cycle could be achieved based on the modeling results. Presented in the next chapter are the results of this computational study.

CHAPTER IV RESULTS

The goal of this computational study was to achieve an optimal scavenging design for the free piston engine-generator, based on the engine's overall efficiency and output emissions. The CFD simulations and the compressor and friction modeling provided the basis for understanding the in-cylinder flow dynamics, and allowed the key parameters affecting the overall gas transfer process to be determined. The knowledge gained from a series of initial simulations was used to converge on an optimal configuration for the system.

The purpose of this chapter is to detail some of the computations conducted and to illustrate how the final scavenging arrangement was determined. The outline of this chapter is as follows. First some specifics regarding the computational analysis are discussed, then the details and results of the initial simulations for the loop, hybrid-loop and uniflow scavenging arrangements are presented. This is followed by the analysis of the charge delivery system. Finally, simulation results for the four options listed in Chapter III are presented with a discussion of the optimal configuration for the scavenging system.

Computational Analysis

As stated earlier, the CFD code KIVA-3V was used to model the dynamics of the two-stroke scavenging flow. Detailed here are a few specifics regarding the code's application to the free piston engine analysis.

CFD Initialization

Two-stroke engines are extremely dynamic devices where the performance of each engine cycle greatly influences the succeeding cycle. For example, the blowdown of the burned charge through the exhaust ports/valves is dependent on the pressure of the expanded in-cylinder

gas when the ports/valves open. This pressure is dependent on the efficiency of combustion and the overall dilution ratio, which is in turn dependent on the in-cylinder flows, means of fuel introduction, and local ratios of trapped residual and fresh gases. These variables result from the previous scavenging cycle, which depends on the effectiveness of the blowdown of the expanded charge. Emissions formation is also influenced by the in-cylinder flows generated over the previous cycle.

Because of this interdependency, the simulations needed to be initialized over a number of engine cycles (typically 3-10, depending mainly on the quality of the initial conditions) to stabilize the computational results. Cycle-to-cycle stability was assessed based on the amount of delivered charge, and the amount of mass in the cylinder at port/valve closure. Convergence was reached when changes in these variables were less than 2%.

Combustion Calculations

Calculations of the full engine cycle (including the HCCI combustion process) were important for the initialization routine, and the evaluation of the efficiency and NO emissions. Since the engine operates on HCCI, no spark timing or injection parameters were utilized; chemical equations controlled the start, duration and completeness of combustion. For this study propane was used as the fuel. The chemical kinetic mechanism and associated equilibrium reactions used for these simulations are given in Tables 4.01 and 4.02. These equations have been used previously to model SI combustion in an IC engine [83], and were chosen to reduce the computational demands, while sufficiently simulating HCCI combustion and emissions generation.

Table 4.1 lists the parameters for the kinetic reactions where the reaction rate, $\dot{\omega}$, is expressed as $\dot{\omega} = k\prod_i [C_i]^{a'_i}$, with k, the rate constant defined as $k = AT^m \exp[-E/T]$, $[C_i]$ the species concentration and a'_i the reaction order, which is not necessarily the stoichiometric coefficient and can account for empirical correlation. Table 4.2 lists the parameters for the partial equilibrium reactions where the equilibrium constant, K_{eq}, is expressed as $K_{eq} = \exp\left[a\ln(T_A) + b/T_A + c + dT_A + eT_A^2\right]$, with $T_A = T/1000K$.

	Reaction	*A*	m	*E*		
	$C_3H_8 + 5O_2 \rightarrow 3CO_2 + 4H_2O$	1.4956e+11	0	1.5780e+04	$[C_3H_8]^{0.1}$	$[O_2]^{1.65}$
1	$C_3H_8 + 5O_2 \leftarrow 3CO_2 + 4H_2O$	0	0	0	$[CO_2]^0$	$[H_2O]^0$
	$O_2 + 2N_2 \rightarrow 2N + 2NO$	1.5587e+14	0	6.7627e+04	$[O_2]^{0.5}$	$[N_2]^{1.0}$
2	$O_2 + 2N_2 \leftarrow 2N + 2NO$	7.5000e+12	0	0	$[N]^{1.0}$	$[NO]^{1.0}$
	$2O_2 + N_2 \rightarrow 2O + 2NO$	2.6484e+14	1.0	5.9418e+04	$[O_2]^{1.0}$	$[N_2]^{0.5}$
3	$2O_2 + N_2 \leftarrow 2O + 2NO$	1.6900e+09	1.0	1.9678e+04	$[O]^{1.0}$	$[NO]^{1.0}$
	$N_2 + 2OH \rightarrow 2H + 2NO$	2.1230e+14	0	5.7020e+04	$[N_2]^{0.5}$	$[OH]^{1.0}$
4	$N_2 + 2OH \leftarrow 2H + 2NO$	0	0	0	$[H]^{1.0}$	$[NO]^{1.0}$

Table 4.1 – Kinetic Reactions

	Reaction	*a*	*b*	*c*	*d*	*e*
1	$H_2 \leftrightarrow 2H$	0.990207	-51.7916	0.993074	-0.343428	0.0111668
2	$O_2 \leftrightarrow 2O$	0.431310	-59.6554	3.503350	-0.340016	0.0158715
3	$N_2 \leftrightarrow 2N$	0.794709	-113.2080	3.168370	-0.443814	0.0269699
4	$O_2 + H_2 \leftrightarrow 2OH$	-0.652939	-9.8232	3.930330	0.163490	-0.0142865
5	$O_2 + 2H_2O \leftrightarrow 4OH$	1.158882	-76.8472	8.532155	-0.868320	0.0463471
6	$O_2 + 2CO \leftrightarrow 2CO_2$	0.980875	68.4453	-10.5938	0.574260	-0.0414570

Table 4.2 – Partial Equilibrium Reactions

Comparison to Experiment

The reliability of the combustion calculations was determined by comparing the code's results to experimentally obtained HCCI data. For this comparison KIVA-3V was used to simulate HCCI in a single shot, free piston Rapid Compression Expansion Machine (RCEM). The RCEM device has been used to evaluate HCCI characteristics of a number of different fuels, the details of which can be found in Ref [1].

Figure 4.1 illustrates the experimental and KIVA-3V computed compression, combustion and expansion pressures for the single shot device. A Cartesian cylindrical mesh was used with no crevice volume or allowed ring blowby. The differences in peak and expansion pressures, as well as the points of combustion initiation, and burning rates are evident in this figure. These are most likely due to the inadequacies of the heat transfer and kinetic modeling. However, reasonable agreement between the two traces was established. This was important with regard

to calculating the efficiency of the cycle and the output NO, and to determining the blowdown pressure. The measured and calculated emissions are also noted in this figure for reference.

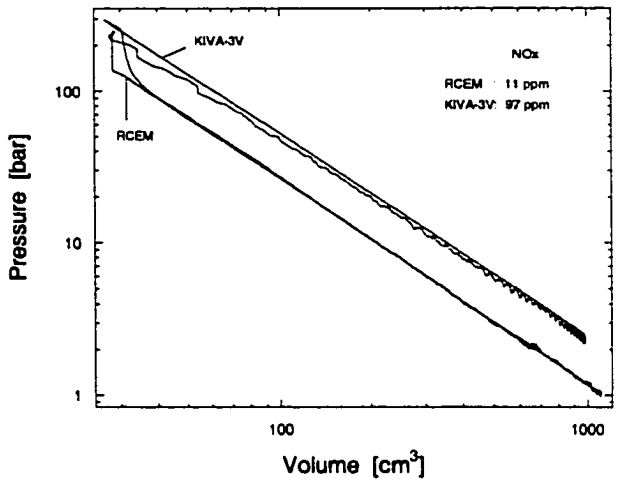

Figure 4.1 – KIVA-3V and RCEM HCCI Pressures vs. Cylinder Volumes

Turbulence

The RNG k-ε turbulence model was used for these .

Computational Meshes and Simplifications

For the engine simulations the computational mesh included the cylinder, intake and exhaust ports and valves, and some intake/exhaust manifolding. The meshes were constructed using the mesh generating program K3PREP, which was included with the KIVA distribution. For these runs, the cylinder and head were assumed to have a pancake geometry with no crevice volume, and the ports and ducting were assumed to have rectangular cross-sections, with some curvature along the length of the manifold. The use of only sufficiently fine and simplified grid arrangements enabled a large number of configurations to be meshed and computed in a reasonable amount of time.

A few additional simplifications were employed to reduce the computational demands of some of the CFD calculations, and to speed up the study. These included using steady

intake/exhaust boundary pressures, geometric symmetry in the hybrid-loop configuration, and a premixed fuel/air input to the intake boundary.

Free Piston Dynamics

The dynamics of the free piston were incorporated into the KIVA-3V code in place of the standard crankshaft-driven motion generally used. The dynamics were defined based on the results of a 0D free piston engine code [84] that calculates the free piston's motion as a function of engine operating cycle, electromagnetic force, and piston mass. For the CFD simulations the position/velocity profile was input using a Fourier series approximation of the 0D output. The profile was adjusted depending on the desired operating frequency (f) and the stroke of the piston. There was no coupling however, between the KIVA-3V output and the free piston's motion.

Initial Simulations

As stated earlier the purpose of the initial simulations was to parametrically analyze the capabilities and limitations of three scavenging methods (loop, hybrid, and uniflow) with regard to the engine's efficiency and emissions goals. Key factors affecting the scavenging process were determined. For these initial runs the simulation results were evaluated based on the calculated scavenging and trapping efficiencies; high η_{sc} (~0.9) and η_{tr} (~0.99) will best meet the operating requirements of the engine-generator. The arrangement of the charge delivery system is also important. Power consumption and the effects on the in-cylinder flows were the metrics by which these parameters were judged.

In an interest of saving space, and not overwhelming the reader with exhaustive details of each simulation performed, only the essential results of the trials will be presented here. A more complete description can be found in Appendices A-D.

Loop Scavenging

The loop scavenging option was investigated first based on its mechanically simple configuration. A typical mesh for the combustion chamber and intake/exhaust manifolds is illustrated in Figure 4.2. This arrangement utilized two rear-facing side intake ports, with the manifolds angled toward the top of the cylinder. The exhaust port was located along the 'front' of the cylinder. This arrangement was employed throughout the runs. (Preliminary simulations with a geometry that included three additional intake ports along the rear face indicated that a good deal of fresh charge from these ports is lost to short-circuiting.) The two intake port geometry was expected to minimize the trapping losses.

Evident in Figure 4.2 is the long stroke-to-bore ratio utilized. For these runs a ratio of 2:1 (compression stroke-to-bore) was prescribed; typical loop scavenged IC engines are constructed with a geometric ratio of 1:1. The meshes here contained approximately 15,000 cells and required, on average, about 20 hours to run (~6 cycles). The resolution of the computational meshes was minimized through a series of simulations, rerunning a test problem until the results diverged significantly.

Table 4.3 presents the geometric parameters for this mesh for reference. Here, CAD (Crank Angle Degree) is used to note the port timings for exhaust opening and closing (EPO,

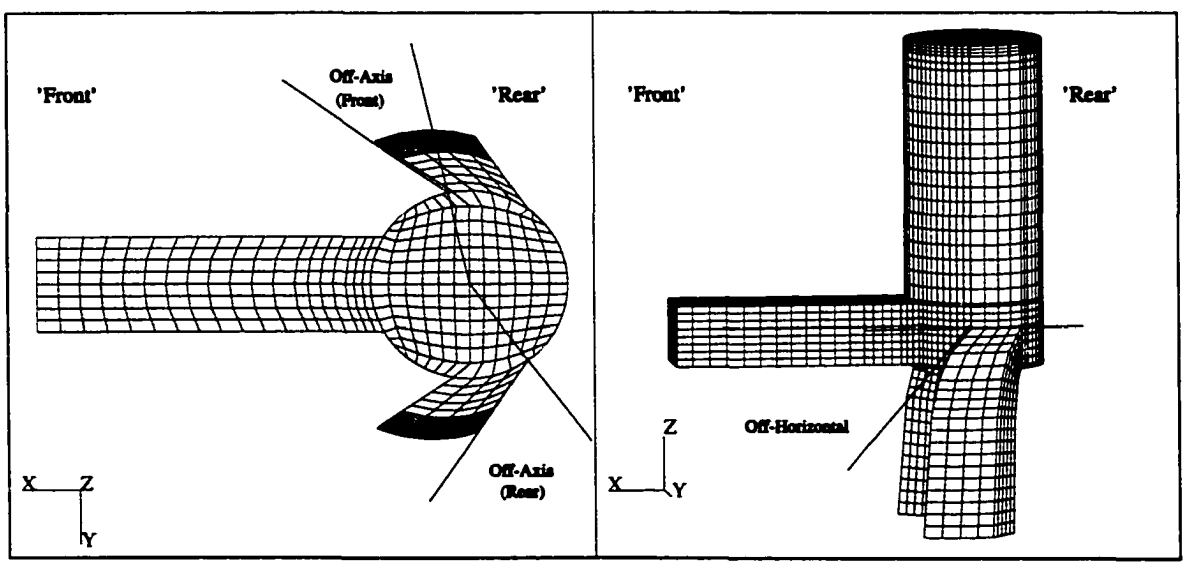

FIGURE 4.2 – Loop Scavenging Mesh [2 Intake / 1 Exhaust Arrangement]

Bore [cm]	7.62
Stroke [cm]	18.03
Compression Ratio	18:1
EPO [CAD]	131
IPO [CAD]	144
IPC [CAD]	210
EPC [CAD]	222
Ex Port Width [cm]	3.81
Ex Port Height [cm]	3.50
In Port Width [cm]	3.04
In Port Height [cm]	2.25
In Incline Angle	40°
In Off-Axis Angle (rear)	72°
In Off-Axis Angle (front)	45°

Table 4.3 – Loop Scavenging Geometric Parameters

EPC) and intake opening and closing (IPO, IPC). However it is used only as a notation since the free piston engine does not have a crankshaft to define the piston's motion. (This time notation refers to the fraction of the cycle devoted to scavenging, where CAD = $(t\text{-}t_{TDC}) \cdot f \cdot 360$.)

Using geometries similar to that described above, variations in a number of parameters were simulated in order to understand the loop flow behavior, and to maximize the scavenging and trapping efficiencies for this configuration.

Typical flow behavior for the loop scavenging arrangement is presented first followed by the results of the parametric variations. Figure 4.3 illustrates the flow visualization calculations using Ensight's particle tracing method. The incoming fresh charge is represented by small dark spheres, and the burned charge by small lighter spheres. Trailing lines indicate velocity. For better viewing, half of the computational mesh is made transparent. (These Ensight computations took about 40 minutes to complete using a 1.2 MHz Athelon PC.)

The series of pictures in this figure is for a charging pressure of 1.2 bar, an operating frequency of 50 Hz, and an intake ϕ of 0.8. As can be seen in these pictures, the fresh charge is

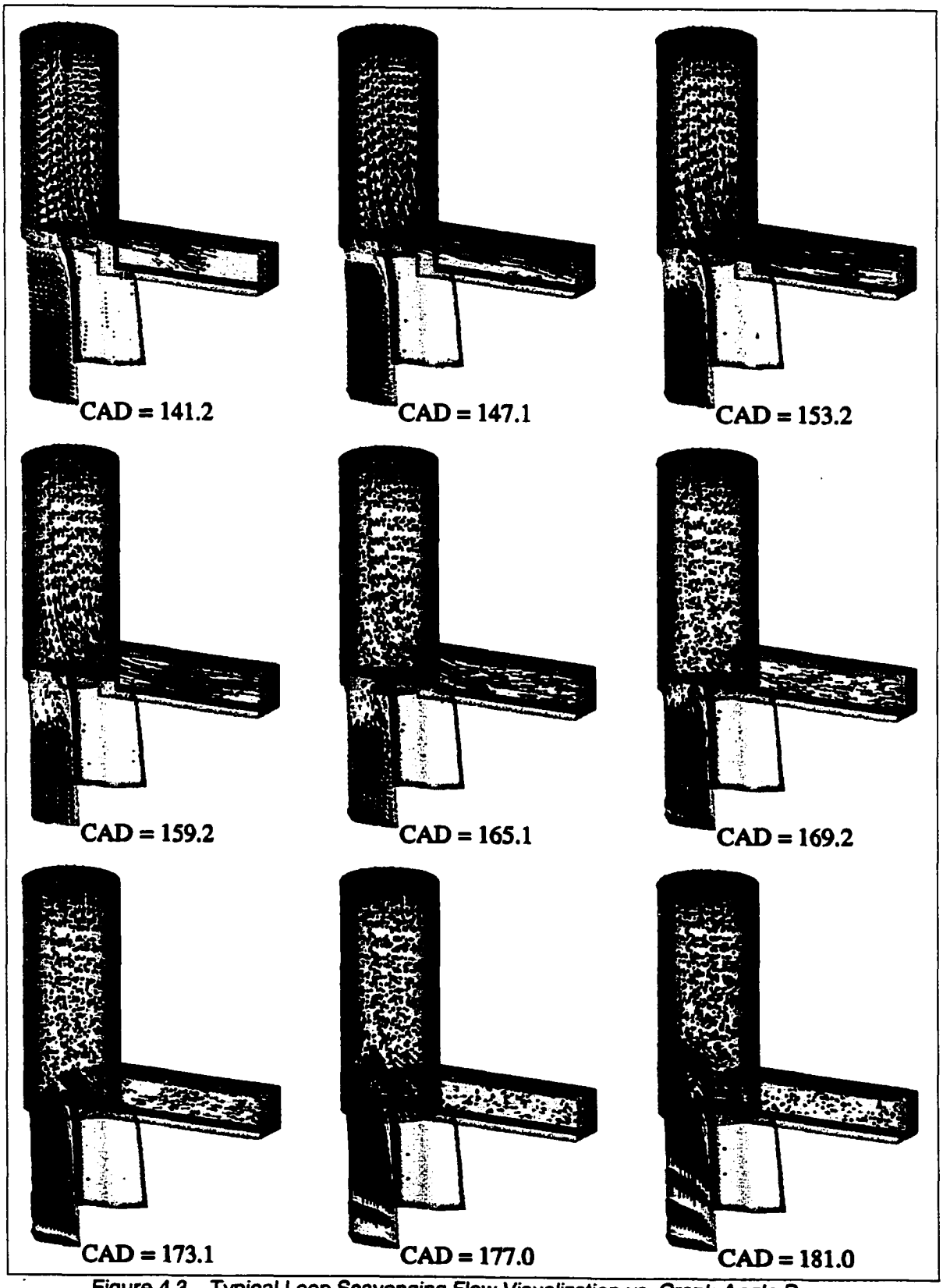

Figure 4.3 – Typical Loop Scavenging Flow Visualization vs. Crank Angle Degree

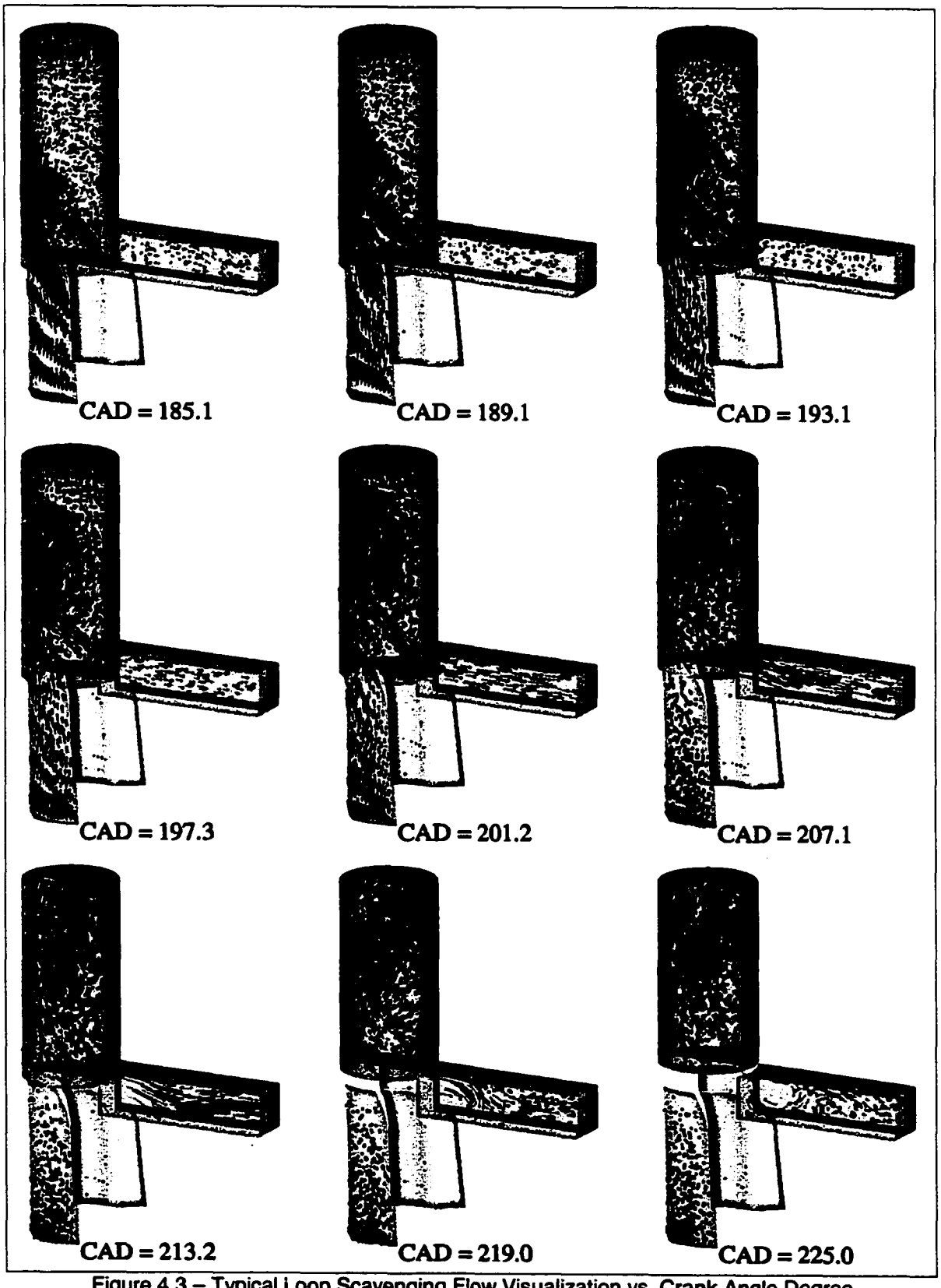

Figure 4.3 – Typical Loop Scavenging Flow Visualization vs. Crank Angle Degree

directed along the back wall of the cylinder towards the top of the combustion chamber to flush the burned charge from this region.

For these operating conditions backflow into the intake manifold can be seen through 165 CAD. This is due to the high cylinder pressure at IPO where the configuration did not allow the burned charge to sufficiently discharge from the cylinder before the intake ports opened. The fresh charge enters the cylinder around 171 CAD and at about the same point some backflow into the cylinder from the exhaust manifold is induced. This is due to the dropping cylinder pressure caused by the continually expanding piston. The reverse flow prevents the combusted gases from being more completely removed from the cylinder.

Another observation from these pictures is that it takes a long time (to 207 CAD) for the fresh charge to reach the top of the cylinder. Because of this the cylinder cannot be fully flushed by EPC. These factors contribute to the low scavenging efficiency calculated for this operating arrangement.

An additional visualization of the flow is presented in Figure 4.4. Here the flow paths of a few select points from within the intake manifold are illustrated. Flat 'ribbons' indicate twisting, or rotation as the gas moves through the cylinder.

Observable in this figure is that the angled intake manifolds generate a helical motion within the cylinder, as the opposed incoming charges collide with each other and the back wall of the cylinder. A result of this helical motion is that a good portion of the burned charge becomes entrained within the fresh charge. This feature is present throughout most of the loop scavenged simulations and prevents more complete replacement of the combusted gases without sacrificing significant amounts of fresh charge. This mixing motion, however detrimental to the trapping capabilities leads to good uniformity at TDC, which is beneficial for efficient HCCI combustion.

The case presented in Figures 4.3-4 achieved a scavenging efficiency of approximately 0.45. This is quite low compared to the desired levels and will significantly affect the performance

Figure 4.4 – Loop Scavenging Flow Visualization Illustrating Path Lines from Select Points within the Intake Manifold

of the engine. (For this run combustion was calculated to occur at a compression ratio of about 12:1 – not nearly the 25:1 desired.) The trapping efficiency was 0.95.

In an effort to improve the performance of this arrangement, variations in the intake charge pressure, intake equivalence ratio, exhaust/intake port areas and timings, and piston dynamics were simulated. The highlights of these results are presented next. Again, a more detailed account can be found in Appendix A.

INTAKE CHARGE PRESSURE – For this series of simulations the charging pressure was increased from 1.1 to 1.8 bar in an attempt to generate better penetration to the top of the cylinder and greater flushing of the burned charge from this region – a challenge seen for the long stroke arrangement. The exhaust pressure for these runs was set at 1.0 bar. The same configuration was used as in Table 4.3.

The results for this simulation series are presented in Figure 4.5. Here the scavenging and trapping efficiencies are plotted versus the charge pressure. As can be seen, as the pressure

is increased the scavenging efficiency increases significantly however the trapping efficiency also declines substantially. The improvement in η_{sc} is due to slightly better penetration of the fresh charge (though not as much as expected), however, a more significant factor is the improvement of the blowdown process. The exhaust blowdown is better because the cylinder pressure at EPO (P_b) is much higher (P_b = 2.0 bar @ P_{in} = 1.2 bar; P_b = 3.3 bar @ P_{in} = 1.8 bar). The higher pressure is due to the greater amount of gas in the cylinder, and the higher dilution ratios that resulted from the higher scavenging efficiency, since the intake ϕ was fixed. The improved blowdown process leads to a greater fraction of the charge removed from the cylinder by the time the intake ports open.

Another factor which improves the scavenging efficiency at higher charging pressures is a higher rate of mass flow through the cylinder. This leads to better flushing of the burned gas from the cylinder.

The change in trapping efficiency can be explained as follows. As the incoming flow rates increase there is greater mixing between the fresh and burned charges within the cylinder. The helical flow patterns as seen earlier become more pronounced and as a result more of the fresh charge is forced from the cylinder with the burned gases.

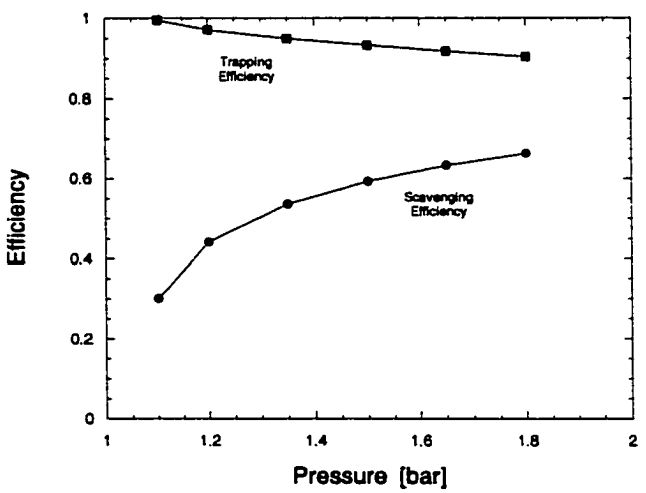

Figure 4.5 – Scavenging and Trapping Efficiencies vs. Intake Charge Pressure

Based on these findings the thrust of the next two sections was to improve the discharge of the combusted gases so that the incoming charge was not required to 'push' such a large fraction of the combusted charge from the cylinder.

INTAKE EQUIVALENCE RATIO – Two simulations were conducted to investigate the extent to which the intake equivalence ratio affects the blowdown process and thus the overall scavenging performance. Adjusting the intake ϕ provided a means of altering the blowdown pressure, while at the same time maintaining the delivery potential of the incoming charge.

Figure 4.6 illustrates the results of these simulations, where the intake equivalence ratio was decreased to 0.5 and increased to 0.95. The charging pressure for these runs was fixed at 1.35 bar. Labeled in this figure are the resulting blowdown pressures. From this figure it can be seen that the equivalence ratio has only a small effect on the overall process.

Through the output of the CFD code and the visualization software it was determined that the change in η_{sc} is indeed due to better discharging the burned gases before IPO. However, the change in η_{tr} results from changes in the in-cylinder flow field. For the lower ϕ case there is less backflow into the intake manifold due to the lower P_b. This allows the fresh charge to enter the cylinder earlier in the cycle and because of this there is more mixing between the burned and unburned charges. This results in more short-circuiting.

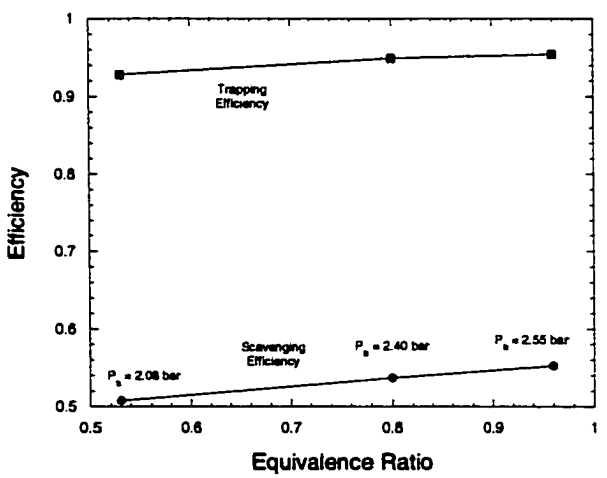

Figure 4.6 – Scavenging and Trapping Efficiencies vs. Intake Equivalence Ratio

At the higher intake ϕ, P_b is increased and this leads to more backflow into the intake manifold. The introduction of fresh charge is delayed since a greater amount of burned charge must be redelivered to the cylinder. Because of this the direction of the incoming gas flow seems to be better established (up along the 'back' wall) by the time the fuel/air mixture enters the cylinder. This leads to a slight drop in short-circuiting losses. From these runs it can be inferred that for trapping purposes it may be beneficial in the loop configuration to allow some backflow into the intake manifold.

EXHAUST PORT AREA / TIMING – These simulations were run determine how the exhaust port flow area and timing affects the blowdown process. Here the port area was altered by increasing the port width (keeping the timing the same) and by increasing the port height (adjusting the timing in the cycle). For the height modifications, the stroke of the piston was increased to maintain a compression stroke-to-bore ratio of 2:1. In addition, the piston frequency was adjusted to keep the intake port open time ($\Delta t_{IPO-IPC}$) constant at 3.6 ms. The intake equivalence ratio was modified for each case so that an overall dilution ratio was fixed at about 0.35.

Figure 4.7 plots the scavenging and trapping efficiencies results for these runs; here the total cross-sectional area is used as the basis. As can be seen the scavenging efficiency increases slightly for both width and height modifications, however there is a drop off for the tallest exhaust port. The trapping efficiency is not significantly affected by the width increases, however the taller ports substantially increased the trapping losses.

From an examination of the in-cylinder dynamics it was concluded that increases in η_{sc} resulted from improvements to the blowdown process as more burned gas can be discharged through the larger port. However as the port becomes too large and the timing too early the exhaust flow tends to oscillate across the port, initially discharging quickly and then reentering the cylinder. As the fresh charge is delivered the burned gases are expelled again from the cylinder. The drop off in scavenging efficiency for the tallest port is due to the mismatch between the port timing and the oscillating flow, with more of the burned charge becoming trapped in the cylinder.

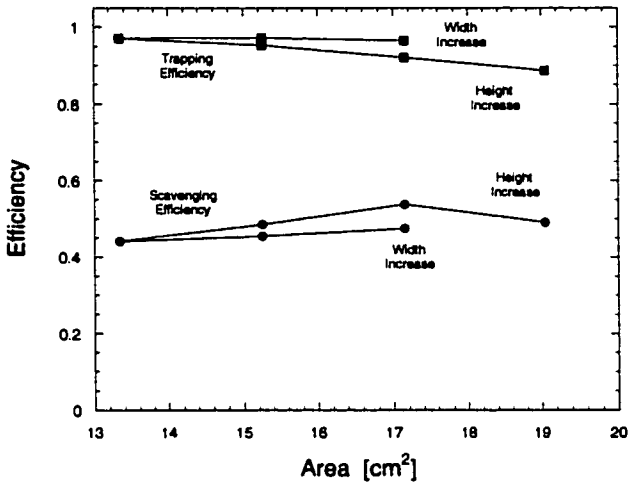

Figure 4.7 – Scavenging and Trapping Efficiencies vs. Exhaust Port Area

This oscillating behavior helps to explain the drop in trapping efficiency as the reentering burned gas tend to mix to a greater degree with the fresh charge, and thus can disrupt the looping behavior characterized in Figure 4.3.

Realizing that changes to affect the blowdown process had only limited improvement to the scavenging performance, issues affecting the fresh charge delivery were investigated next.

INTAKE PORT AREA / TIMING – In an attempt to improve the effectiveness of the fresh charge delivery, the configuration of the intake ports was modified. For this investigation the incoming angles were not modified, however the area available for the charging flow was increased using both width and height changes. As with the previous series increases to the port heights affected the opening and closing times. With this series the intake equivalence ratio was modified for each case so that the overall dilution ratio was set to about 0.35.

Figure 4.8 plots the results of this simulation series with respect to total intake area. As can be seen, for the port width increases the scavenging efficiency increases, but the trapping efficiency also declines. This will be discussed first.

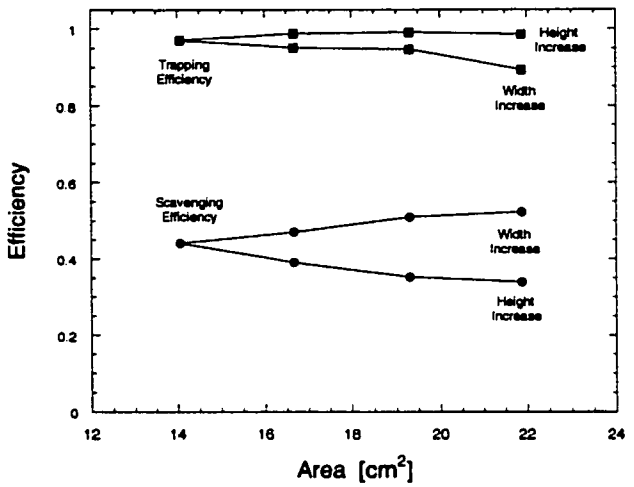

Figure 4.8 – Scavenging and Trapping Efficiencies vs. Intake Port Area

As the ports become wider there is more fresh charge flow through the cylinder (in fact the delivery ratio increases 60% for the widest port). This enhances the flushing of the burned charge. However, as the port becomes too wide the in-cylinder flow patterns change with the fresh charge entering over a wider circumference of the cylinder. The incoming gas begins to trap a good portion of the residual charge at the top of the cylinder. The looping path is dramatically shortened, and as a result a greater fraction of fresh gas is short-circuited.

With regard to the port height changes it can be seen that as the intake port height is increased the scavenging efficiency decreases. This is mainly due to increased backflow into the intake manifold. This delays the introduction of fresh charge and restricts the scavenging capability of this orientation. The change in η_{tr} is a result of the delayed charging.

As the intake flow area/timing had limited impact on improving the scavenging performance, changes to the scavenging time were investigated. It was expected that just as increased charging pressures could improve the scavenging efficiency, changes in the time available for scavenging could improve the engine's performance.

PISTON FREQUENCY – For this series of simulations adjusted piston frequencies were used to change the scavenging times. Oscillation rates of 16.7, 33.3 and 66.7 Hz were simulated, this time with the intake ϕ fixed at 0.8. The scavenging times ranged from 15.0 to 7.6 to 3.8 ms, respectively.

The results from the frequency variation runs are shown in Figure 4.9. As can be seen, the scavenging efficiency increased significantly (even more than with the changes in charging pressure). The trapping efficiency however, decreased to unacceptable levels. On the other hand, as the frequency is reduced the in-cylinder mixing is improved and the charge is quite uniform at TDC. The frequency decreases also reduce the power output of the engine.

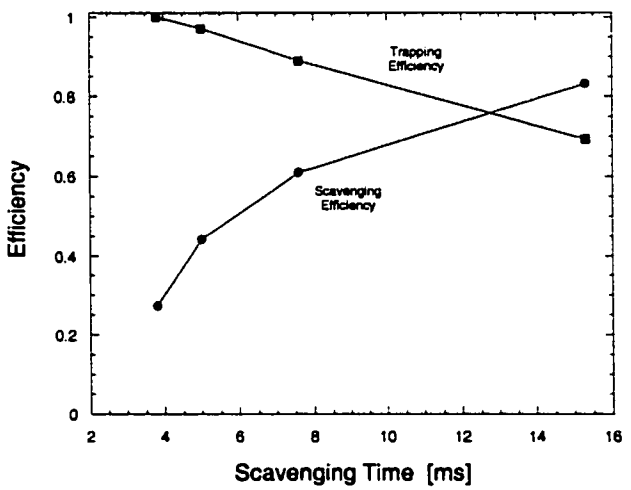

Figure 4.9 – Scavenging and Trapping Efficiencies vs. Scavenging Time

SUMMARY OF LOOP SCAVENGING SIMULATIONS – The loop scavenging configuration (2 intake / 1 exhaust) represented a mechanically simple option for the free piston engine. However, due to the cylinder's long stroke to bore ratio, problems arose with regard to both adequate charging and short-circuiting losses. In an attempt to improve the scavenging efficiency, variations in intake charge pressure, intake ϕ, exhaust and intake port area/timing, and piston frequency were investigated.

The computations revealed that only the intake charge pressure and the piston's frequency could significantly impact the engine's charging performance. On the other hand, as the scavenging efficiency was substantially increased, the trapping losses became unacceptable. In addition, either high charging pressure or low power output must be sacrificed in order to achieve sufficient charging.

Hybrid-Loop Scavenging

In an attempt to improve the trapping characteristics of the engine and to achieve adequate flushing at the top of the cylinder, the hybrid-loop scavenging option was devised. In this arrangement the intake ports are located above the exhaust ports with the incoming charge directed in a swirling motion toward the top of the cylinder, away from the exhaust ports. (See Figure 3.3.) It was expected that the burned charge could be flushed down the core of the cylinder and out the exhaust ports. With this geometry it was hoped that the scavenging efficiency could be increased, while early closure of the exhaust ports could control short-circuiting.

A typical mesh for the combustion chamber and intake/exhaust manifolds is illustrated in Figure 4.10. In this arrangement 5 intake ports are located circumferentially around the cylinder and angled to generate swirling motion toward the top of the combustion chamber. Five exhaust ports are located directly below the intake ports with the manifolds constructed underneath the

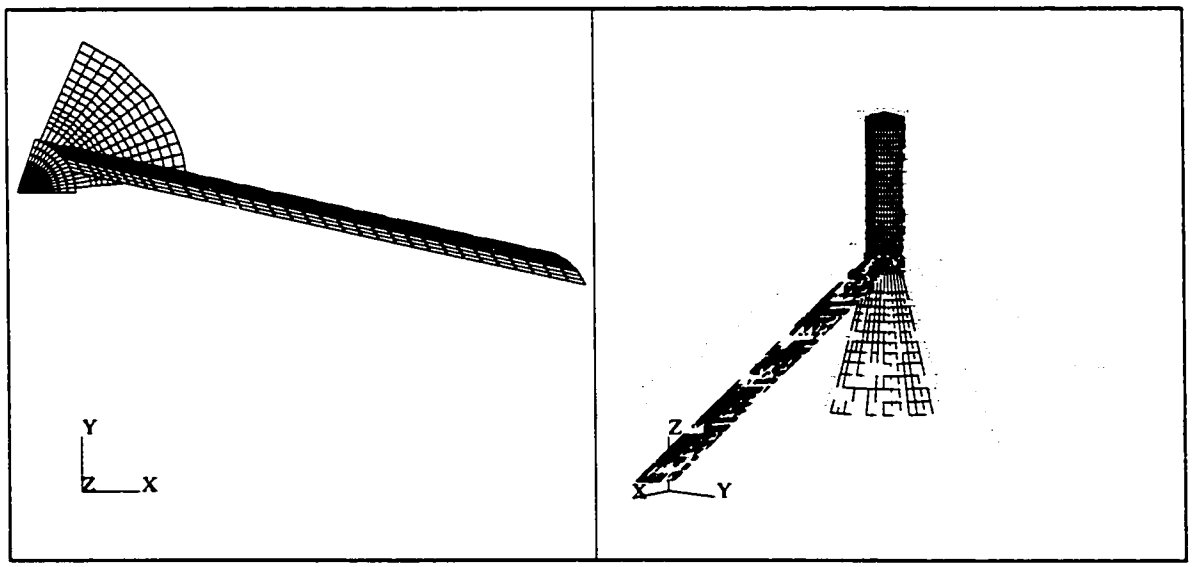

Figure 4.10 – Hybrid-loop Scavenging Mesh [5-port Arrangement]

Number of Ports	5
Bore [cm]	7.62
Stroke [cm]	20.58
Compression Ratio	25:1
IPO [CAD]	115
EPO [CAD]	141
EPC [CAD]	213
IPC [CAD]	235
Ex Port Width [cm]	4.20
Ex Port Height [cm]	3.00
In Port Width [cm]	2.92
In Port Height [cm]	1.25
Ex Decline Angle	65°
In Incline Angle	35°
In Swirl Angle	57.5°

Table 4.3 – Hybrid-Loop Scavenging Geometric Parameters

intake ducts. For the simulation runs, only one sector of the cylinder was computed, with periodic boundary conditions applied to the angular faces. Complex 3D interactions are captured in this mesh arrangement. The sector included 1 intake port and 1 exhaust port and dramatically decreased the computational time.

Evident in Figure 4.10 is the very long intake manifold used for these runs. This was required to 'capture' the residual gases blown into the intake port at IPO. (Problems with the implementation of KIVA-3V's reed valve option necessitated this orientation.)

The meshes for the hybrid simulations contained approximately 9000 cells and required, on average, about 50 hours to run (~9 cycles). This was dramatically reduced from the computation of the full geometry (~300hrs), but was increased relative to the conventional loop runs due to the additional number of cycles necessary to stabilize the computations. As with the conventional loop scavenging runs, the resolution of the hybrid-loop meshes was minimized through a series of simulations, rerunning a test problem until the results diverged.

Of concern with the hybrid geometry was the ability to direct the incoming flow to generate enough momentum so that the burned/unburned charge mixing during the scavenging period was

minimal. The swirl angle determined the degree to which the incoming flow hugged the cylinder wall, while the incline angle controlled the extent of penetration to the top of the cylinder, as well as the interaction between the incoming charges.

The geometric parameters for the case in Figure 4.10 are listed in Table 4.4. (For the hybrid series runs the compression ratio was increased to 25:1 to ensure combustion during the initialization routine.) Using geometries similar to that above, variations in a number of parameters were simulated in order to understand and optimize the scavenging behavior for this configuration

Figure 4.11 shows the typical flow patterns for the 5-port geometry. This was calculated using Ensight's particle tracing method. Again the incoming fresh charge is represented by small dark spheres and the burned charge by small lighter spheres. Trailing lines indicate velocity. For these pictures flow from only one intake port is illustrated in order to better visualize the fresh charge behavior in the cylinder. The computational time required to create this figure was about one hour using a 1.2 MHz Athelon PC.

This series of pictures is for an charging pressure of 1.5 bar, an operating frequency of 50 Hz, and an intake ϕ of 0.52. Through 166CAD the backflow into the intake manifold can be seen. As the exhaust ports open and the cylinder pressure drops, forward flow from the intake manifolds is induced. The fresh charge enters the cylinder and is directed up around the walls toward the top of the chamber. Interaction between the fresh and burned charges, along with significant reverse flow across the exhaust ports prevents the desired swirling-loop from forming. Because of this the cylinder is not adequately flushed and the charge is quite stratified at port closure, with little mixing seen during the compression process. Most of the fresh charge remains near the cylinder walls, with a region of combusted gas in the core (center) of the cylinder. This, certainly, is not optimal for efficient HCCI combustion.

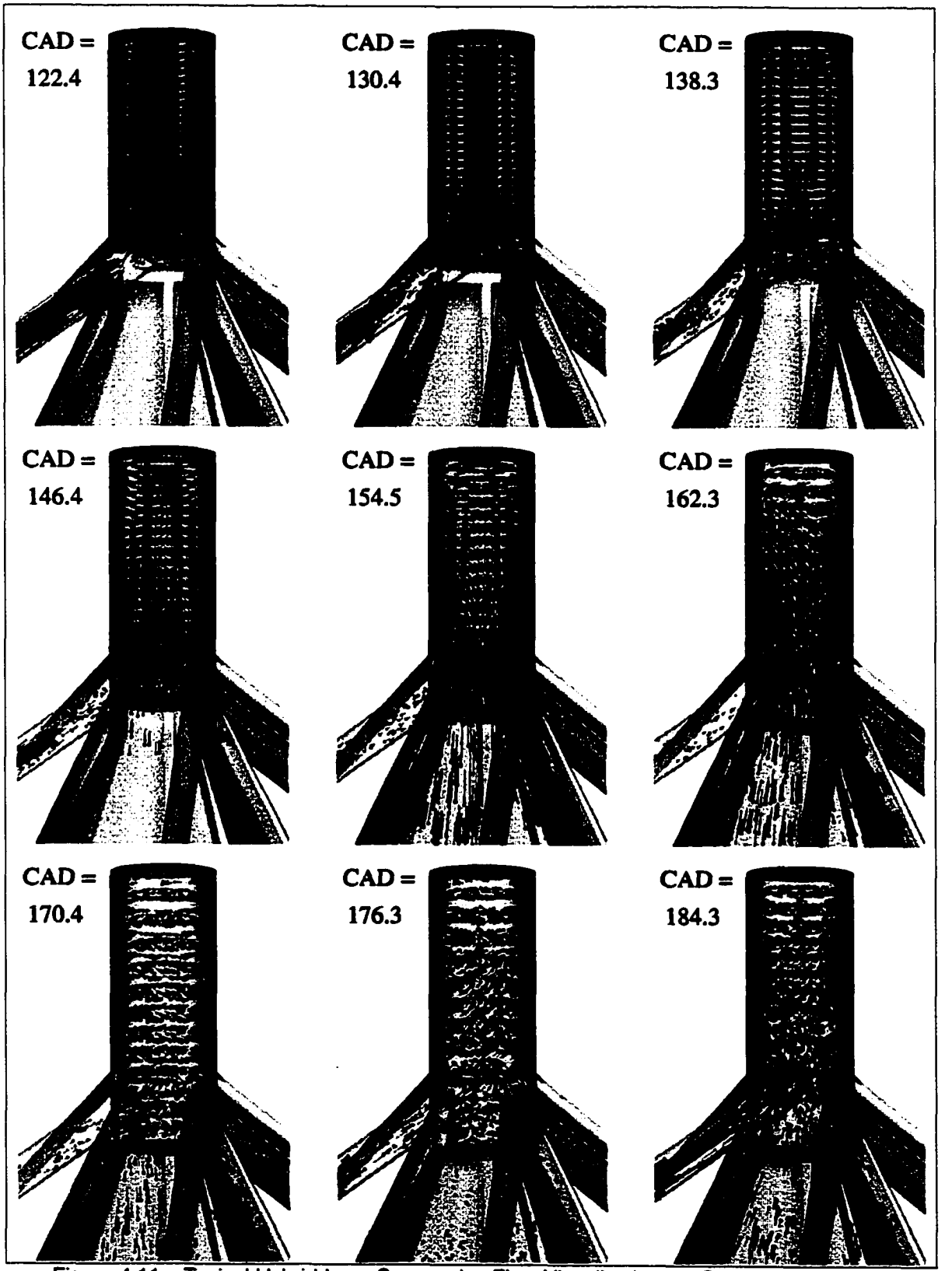

Figure 4.11 – Typical Hybrid-Loop Scavenging Flow Visualization vs. Crank Angle Degree

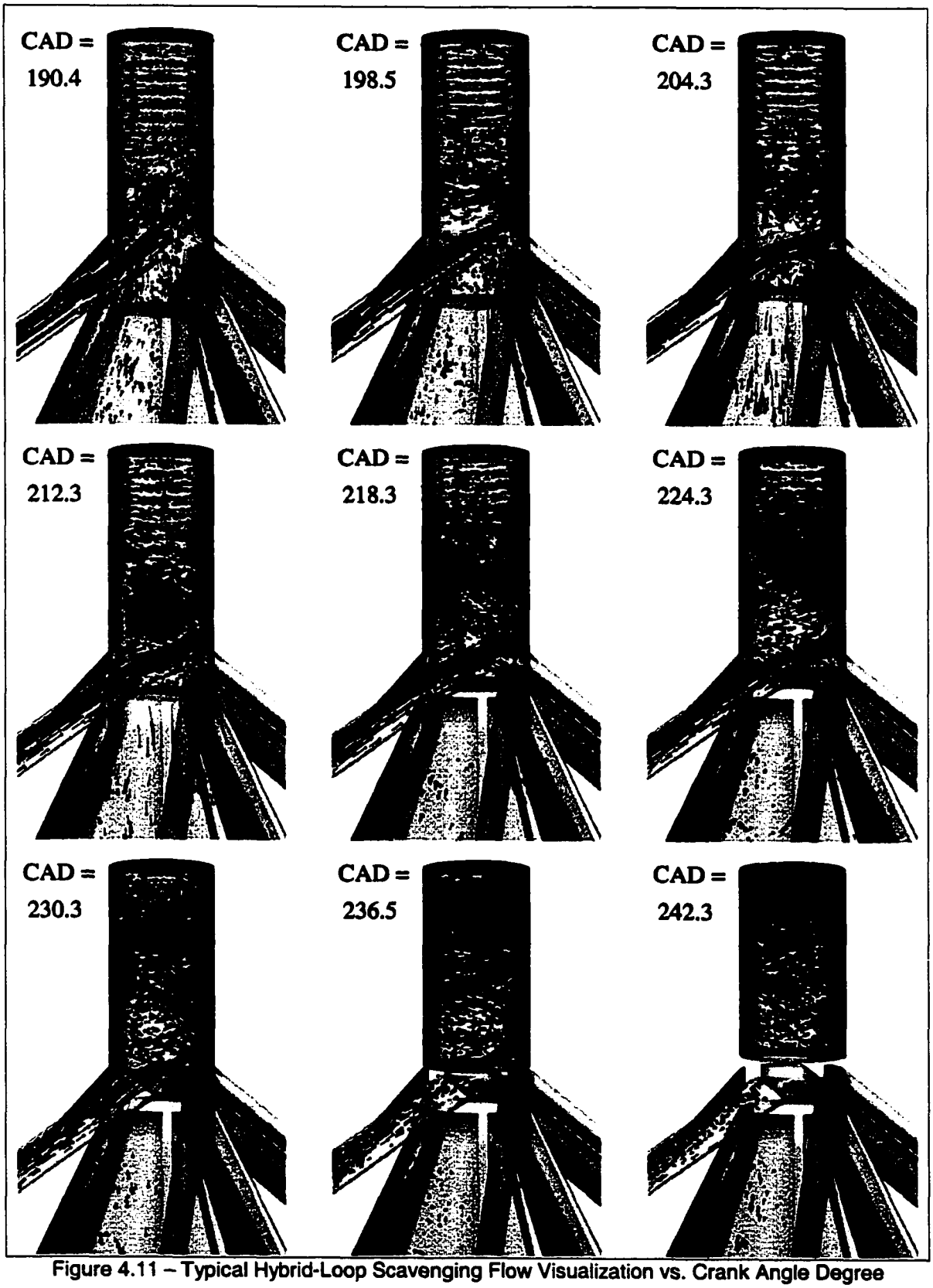

Figure 4.11 – Typical Hybrid-Loop Scavenging Flow Visualization vs. Crank Angle Degree

Because of the uniqueness of this scavenging scheme a few specifics regarding its operation will be discussed. Figures 4.12 and 4.13 presents the cylinder pressure, and intake and exhaust flow rates over the scavenging cycle. Here the exhaust port timings are labeled with the limits of the plot representing the intake port opening and closing times.

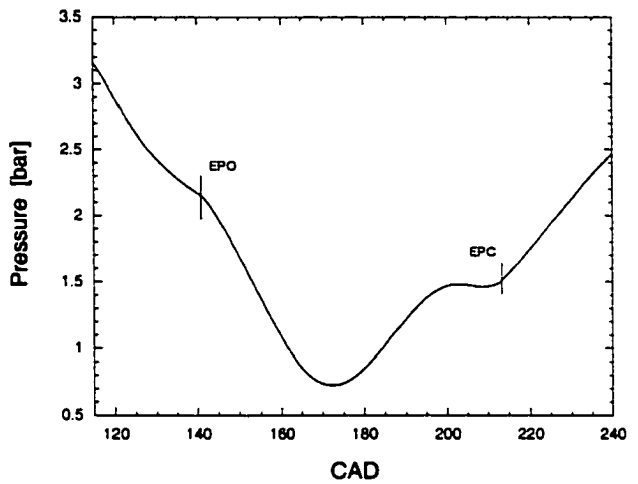

Figure 4.12 – Cylinder Pressure vs. CAD

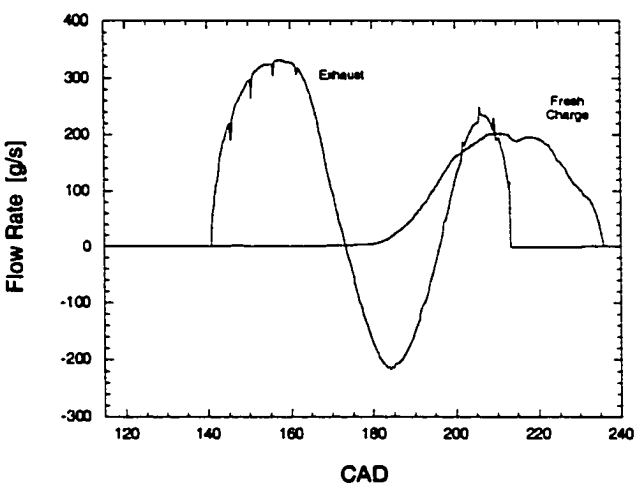

Figure 4.13 – Fresh Charge and Exhaust Flow Rates vs. CAD

These plots give some insight into the in-cylinder dynamics, and the resulting flow behavior for these runs. As can be seen the cylinder pressure drops as the intake ports are uncovered, with the combusted charge forced into the intake manifolds. As the exhaust ports open the pressure decreases even more with burned charge flowing into the exhaust manifold. In this manner the cylinder pressure drops very rapidly, and below the exhaust boundary pressure of 1.0 bar. As a result, reverse flow across the exhaust port is induced midway through the scavenging period, after which the cylinder pressure begins to increase.

In Figure 4.13 it can be seen that reverse flow across the exhaust port is significant, and this flow oscillates as the scavenging process progresses. This behavior dramatically affects the in-cylinder motion with the incoming fresh charge 'sucked' down toward the exhaust ports as the burned charge flows back and forth. This 'sucking' flow pattern is somewhat visible in Figure 4.11 above.

Evident in the plots above is that the fresh charge continues to enter the cylinder even after the in-cylinder gas is compressed above the intake boundary pressure of 1.5 bar. This behavior is due to the unsteady nature of the intake manifold pressure, which varies significantly through the scavenging period. This is illustrated in Figure 4.14 where the average manifold pressure is plotted. This behavior is different than was seen with the conventional loop simulations, and is a result of the intensity of the intake blowdown process, and the use of long manifolds in the intake configuration.

The scavenging efficiency for this run was calculated to be low (η_{sc}~0.4) with the trapping losses are near 5%. As with the loop scavenged runs this low scavenging efficiency causes the combustion to initiate earlier than desired, at a compression ratio of about 8:1.

In an effort to improve the performance of the hybrid-loop scavenging arrangement variations in the number of intake/exhaust ports, the intake charge pressure, exhaust port timing and area, and the piston's frequency were simulated. The highlights of these results are presented next, with more detail given in Appendix B.

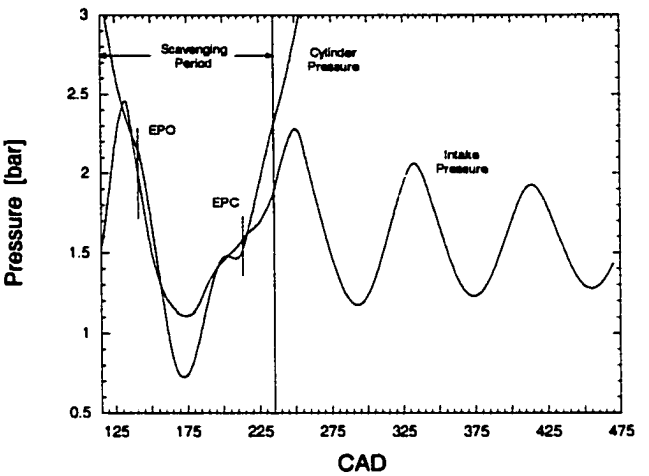

Figure 4.14 – Average Intake Manifold Pressures vs. CAD

NUMBER OF INTAKE/EXHAUST PORTS – To better control the flow behavior of the incoming charge configurations with 8 and 10 intake/exhaust ports were constructed in addition to the original 5-port geometry. For the 8-port arrangement the total intake cross-sectional area was kept constant (8 cm^2), while the 10-port arrangement used the same circumferential area as the 5-port geometry (19 cm^2). The swirl and incline angles were increased slightly for these geometries to direct the charge away from the core and towards the top of the cylinder.

The results for these three geometries are presented in Figure 4.15 where the scavenging and trapping efficiencies are plotted. It can be seen here that the scavenging efficiency is nearly the same for the 5- and 8-port configurations but drops significantly for the 10-port geometry. This drop is due to the reduced flow area available for this arrangement. The trapping efficiency is improved for the 10-port geometry, but this is also because of the drop in delivery ratio. For the 8-port geometry the increased trapping losses are a result of the slight changes in flow behavior that follow from the change in intake port configuration.

Overall, the flow within the cylinder is quite similar for all three cases; the number and orientation of the ports seems insignificant to improving the scavenging of the hybrid-loop

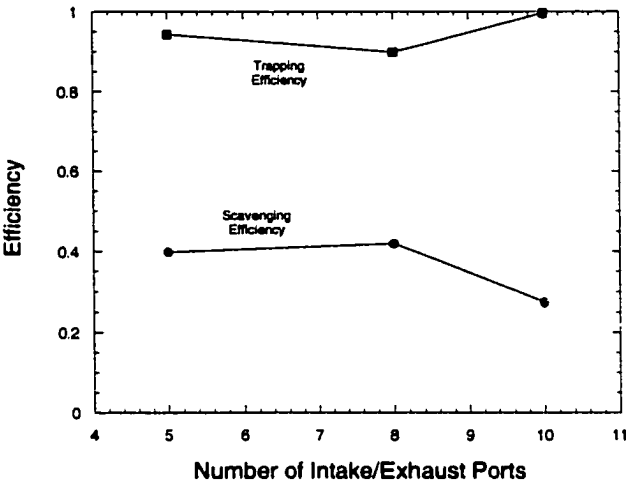

Figure 4.15 – Scavenging and Trapping Efficiencies vs. Number of Intake/Exhaust Ports

geometry. The main drivers seem to be the intake manifold fluctuations and the exhaust flow oscillations. Controlling these was the thrust of the next three parametric series.

INTAKE CHARGE PRESSURE – To reduce the influence of the intake backflow process on the rest of the scavenging cycle higher charging pressures were investigated. Both the 8- and 10-port configurations were used for these simulations. It was hoped that by increasing the resistance to the blowdown flow, the manifold pressure oscillations could be reduced, and the gas transfer process better controlled. Constant boundary pressures of 1.8 and 2.1 bar were used.

Figure 4.16 plots the scavenging results for these runs. From this figure it can be seen that the higher charging pressure leads to somewhat improved scavenging efficiency with slightly altered trapping efficiencies. These changes are due mainly to the increased mass flow through the engine, as seen with the conventional loop configuration.

However, the intake manifolds are still plagued by pressure oscillations. This is caused by the higher blowdown pressures which result at IPO. The pressure fluctuations in the manifolds are only offset by the increased charging potential, with the intensity unchanged. The dynamics of the scavenging process, and the in-cylinder flows that result are changed little by increases to the charging pressure.

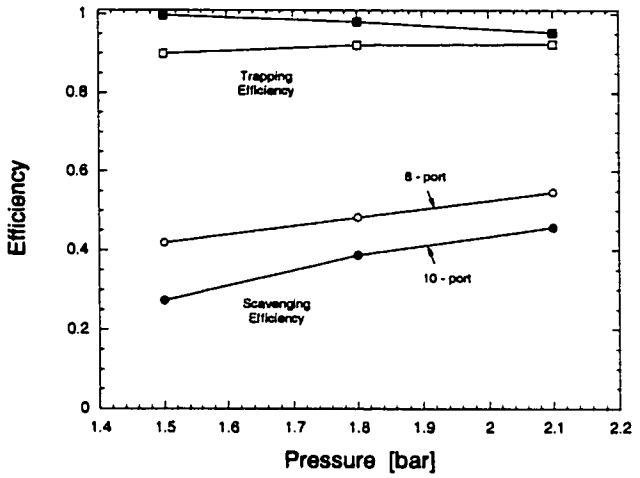

Figure 4.16 – Scavenging and Trapping Efficiencies vs. Intake Charge Pressure

EXHAUST PORT TIMING / AREA – To address the other significant feature in the scavenging design (exhaust flow oscillations), variations in the scavenging time were investigated. The goal was to increase the scavenging time to reduce the significance of the exhaust flow oscillations, and thus allow the forward pressure to dominate the flow.

The first trial increased the scavenging time (from 6.57 to 9.26ms) by increasing the exhaust port height (from 3.0 to 5.4 cm). To address the issue of intake manifold backflow the frequency was adjusted slightly so that the time between port openings ($\Delta t_{IPO-EPO}$) remained constant at 1.38ms. For these simulations the 10-port arrangement was used and the charging pressure was set at 1.8 bar.

Figure 4.17 plots the results for this series where the scavenging and trapping efficiencies are again illustrated. As can be seen, the effect of a taller exhaust port is not consistent, with the scavenging efficiency initially increasing, but then decreasing. The trapping efficiency initially declines then increases and declines again.

The reason for these results is that the exhaust flow dynamics are changed little by the increased exhaust port height; the increased scavenging time only allows more flow oscillation over the scavenging period, with the magnitude of these oscillations generally unaffected. Depending on the direction of the flow at the time of port closure the scavenging and trapping

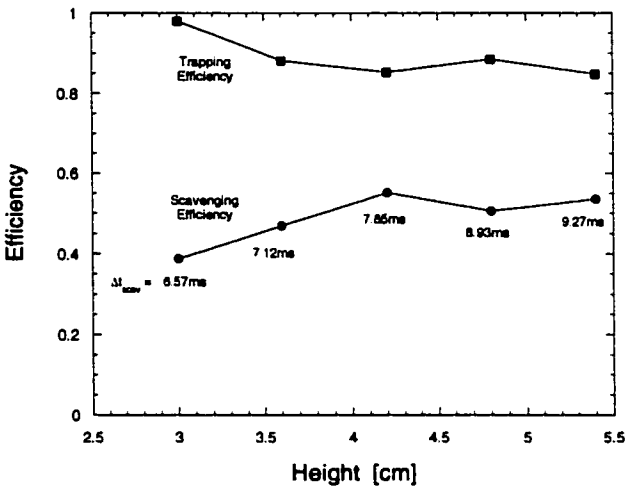

Figure 4.17 – Scavenging and Trapping Efficiencies vs. Exhaust Port Height

efficiencies will either be improved or degraded. Again, the swirling-loop is not formed and the cylinder charge is stratified at TDC. It was apparent that the scavenging time was not long enough for the forward pressure differential to dominate, and the flow to be effectively controlled.

PISTON FREQUENCY – In a final attempt to configure the hybrid geometry and minimize the detrimental effects of the exhaust flow dynamics, the piston frequency was reduced. For this run, the 5-port geometry was used with f = 16.7 Hz; the overall scavenging time increased to 19.1 ms, with the intake blowdown time ($\Delta t_{IPO-EPO}$) now increased to 3.8 ms. The intake manifold length had to be increased (to 90 cm) in order to 'capture' the additional backflow. An intake pressure boundary of 1.5 bar was used.

Figures 4.18 and 4.19 plot the results for this run. As can be seen, the exhaust flow still oscillates, however the reverse motion occurs before the fresh charge is introduced to the cylinder. In addition, the intake manifold pressure fluctuations are dramatically reduced during the scavenging period. These changes allow the fresh charge to be more consistently directed toward the top of the cylinder.

However, even in this case the desired swirling-loop cannot be generated and the fresh charge does not displace the burned gas at the top and in the core of the cylinder. A scavenging

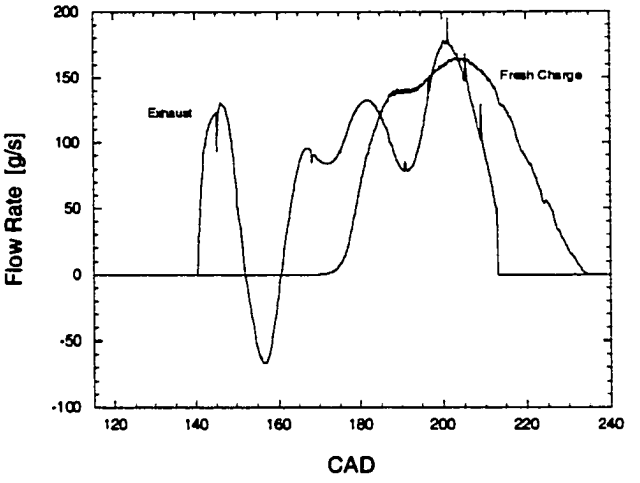

Figure 4.18 – Exhaust and Fresh Charge Flow Rates vs. CAD

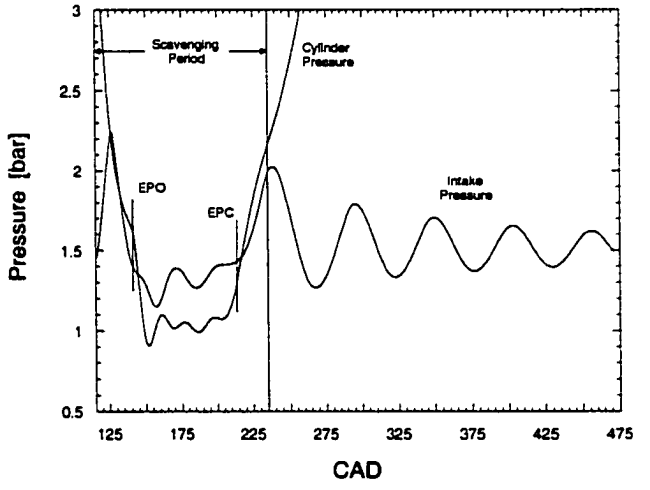

Figure 4.19 – Cylinder and Average Intake Manifold Pressures vs. CAD

efficiency of 0.6 results and a good deal of unburned gas is lost to short-circuiting (~40%). Again, the bulk of the fresh gas remains trapped along the cylinder walls during compression and combustion.

SUMMARY OF HYBRID-LOOP SCAVENGING SIMUATIONS – The hybrid-loop scavenging configuration represented a mechanically simple option for the free piston engine, with the possibility of controlling short-circuiting losses while achieving better scavenging at the top of the

cylinder. However, due to pressure fluctuations in the intake manifold and flow oscillations across the exhaust port, the desired flow patterns could not be established. Low scavenging efficiency and high charge stratification resulted, along with the possibility of significant trapping losses.

To improve the cylinder flushing, trapping characteristics and charge uniformity, variations in the number of intake/exhaust ports, intake charge pressure, exhaust port area/timing, and piston frequency were investigated. The computations revealed that only a decrease in piston frequency could significantly alter the in-cylinder dynamics, however, this was at the cost of substantial trapping losses. In none of these runs could the desired swirling-loop be created, and the resulting charge was extremely stratified at TDC with the fresh gas concentrated at the cylinder walls.

Uniflow Scavenging

Because neither the conventional loop nor the hybrid-loop options could be configured to achieve the desired scavenging and trapping efficiencies, the uniflow option was investigated next. Though this arrangement increases the mechanical complexity of the engine, it was expected to achieve much better scavenging performance. In addition, the use of exhaust valves at the top of the cylinder ensures the flushing of this region and improves the control capabilities of the system, allowing unique operating schemes (over-expanded cycle) to be employed.

A typical mesh for the combustion chamber and intake/exhaust manifolds is illustrated in Figure 4.20; the parameters for this are listed in Table 4.5. In this arrangement 8 intake ports were located circumferentially around the bottom of the cylinder and angled, in some cases, to generate swirling motion toward the top of the combustion chamber. Four exhaust valves were located in the cylinder head. The goal of this arrangement was to generate plug-type flow within the cylinder from the intake ports to the exhaust valves, keeping the burned and unburned gases essentially separate. In this manner, it was hoped that high scavenging efficiency could be achieved with minimal trapping losses.

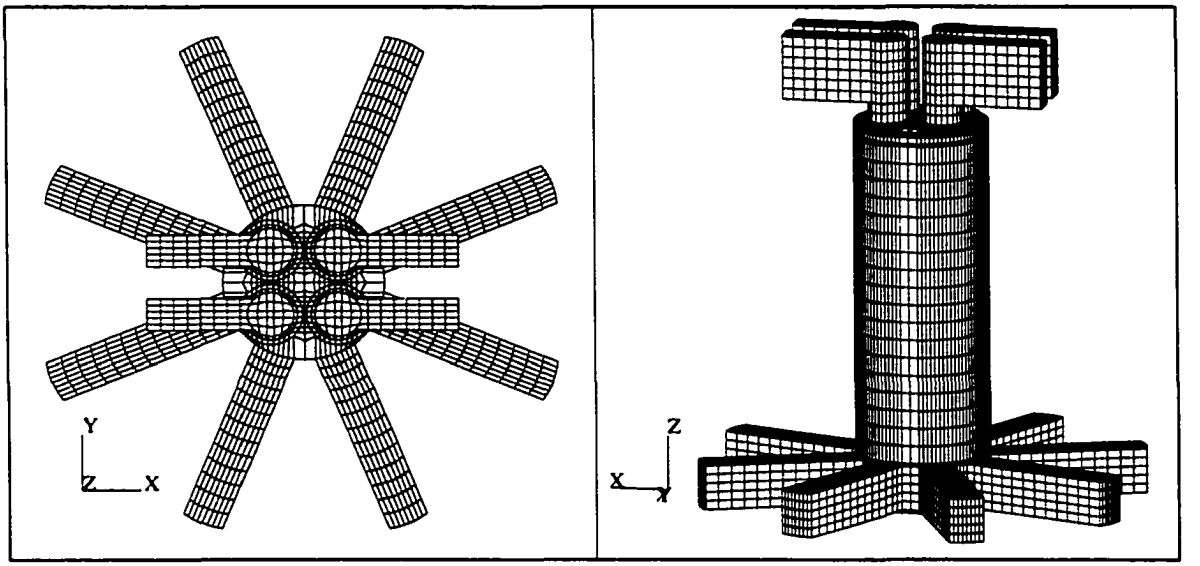

Figure 4.20 – Uniflow Scavenging Mesh

Bore [cm]	7.62
Stroke [cm]	22.26
Compression Ratio	45:1
EVO [CAD]	116
IPO [CAD]	144
IPC [CAD]	210
EVC [CAD]	232
Valve Diameter [cm]	2.54
Valve Lift [cm]	0.85
Port Width [cm]	2.00
Port Height [cm]	2.60
Swirl Angle	0°

Table 4.5 – Uniflow Scavenging Geometric Parameters

For these simulations the full geometry was modeled in order to investigate non-uniform flow behavior in the cylinder. This, and the addition of valve movement, significantly increased the computational times relative to the previous two configurations. On average the simulations took 60 hours to compute (~4 cycles) using meshes of approximately 30,000 cells. On the other hand though, these calculations tended to stabilize more quickly than either the loop or hybrid-loop

runs. As with the previous configurations the resolution of the computational meshes was minimized through a series of simulations, rerunning a test problem until the results diverged.

A large determinant for the amount of computing time required was the number of cells through which the exhaust valve moved. This was due to KIVA-3V's snapping subroutine. Another factor was the resolution of the valve and valve pocket. The mesh density in this region was propagated throughout the entire grid, including into the intake manifolds, and this affected the computational loads. However, lower resolution in the valve region substantially reduced the computing time (~50-65%) while having little impact on the results of the overall gas transfer computations. This option was possible because HCCI is used as the combustion mode. (Direct, or spark ignited operation would require much better resolution at TDC to adequately simulate combustion.)

The typical flow patterns for the uniflow geometry are illustrated in Figure 4.21. Again the particle tracing method is used where the fresh charge is represented by small dark spheres and the burned charge by small lighter spheres. Trailing lines indicate velocity. In this series of pictures flow from only one intake port is depicted in order to better visualize the fresh charge behavior. The computational time required to create this figure was about one hour using a 1.2 MHz Athelon PC.

Through 144 CAD blowdown through the exhaust valves can be seen. As the intake port opens at this point fresh charge begins to enter the cylinder. In this simulation backflow into the intake manifold is minimal since the timing between EVO and IPO is better matched to the operating conditions of the engine. As the flow enters the cylinder swirling motion is generated and the fresh charge displaces the combusted gases. Here mixing between the burned and unburned charges is significantly decreased relative to the loop and hybrid loop configurations, with this resulting in much better scavenging performance.

For preliminary simulations with this geometry reasonably high scavenging efficiencies (η_{sc} ~ 0.7) were achieved with virtually no trapping losses. However, issues arose concerning the

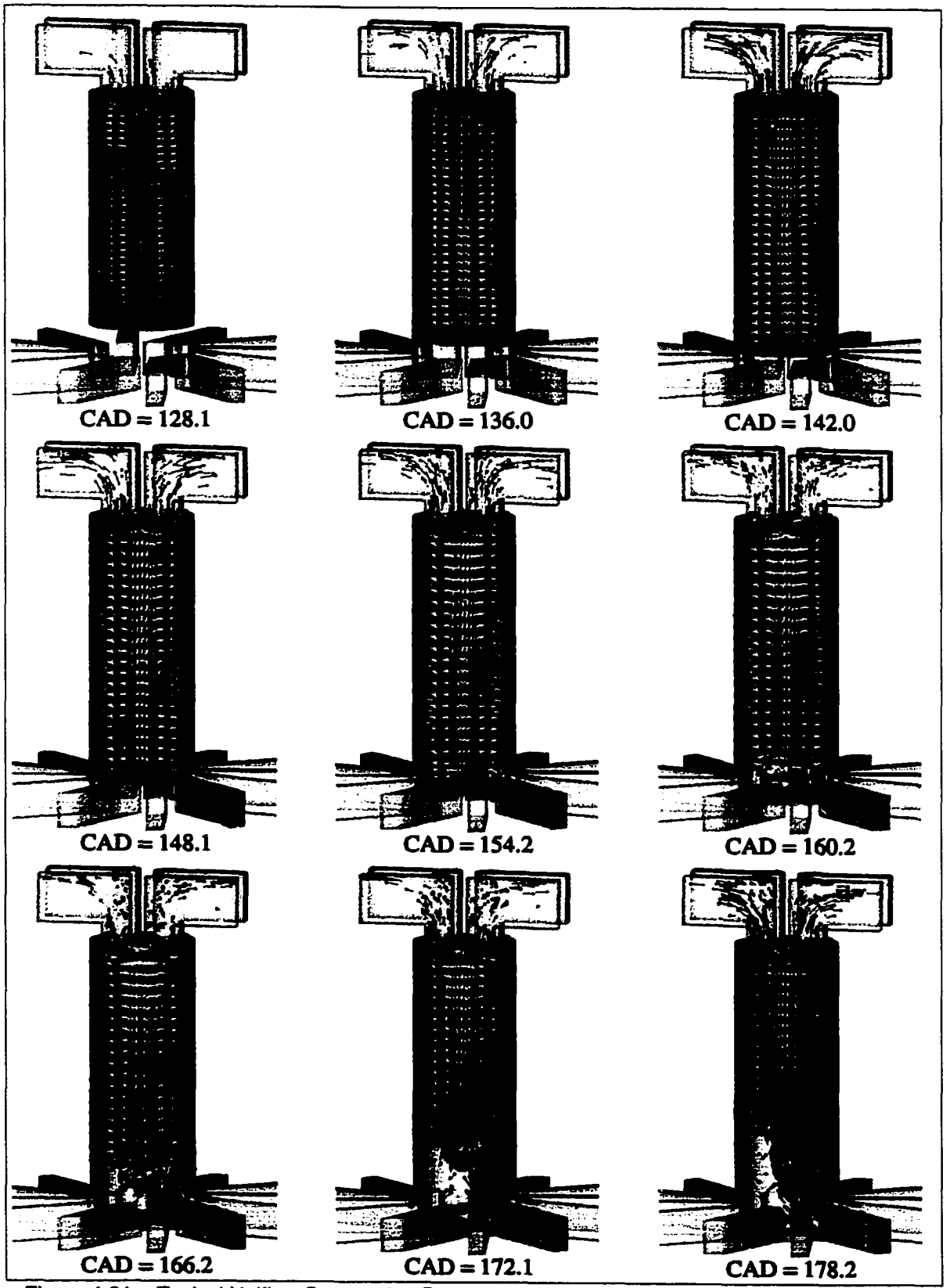

Figure 4.21 – Typical Uniflow Scavenging Flow Visualization vs. Crank Angle Degree [20° swirl]

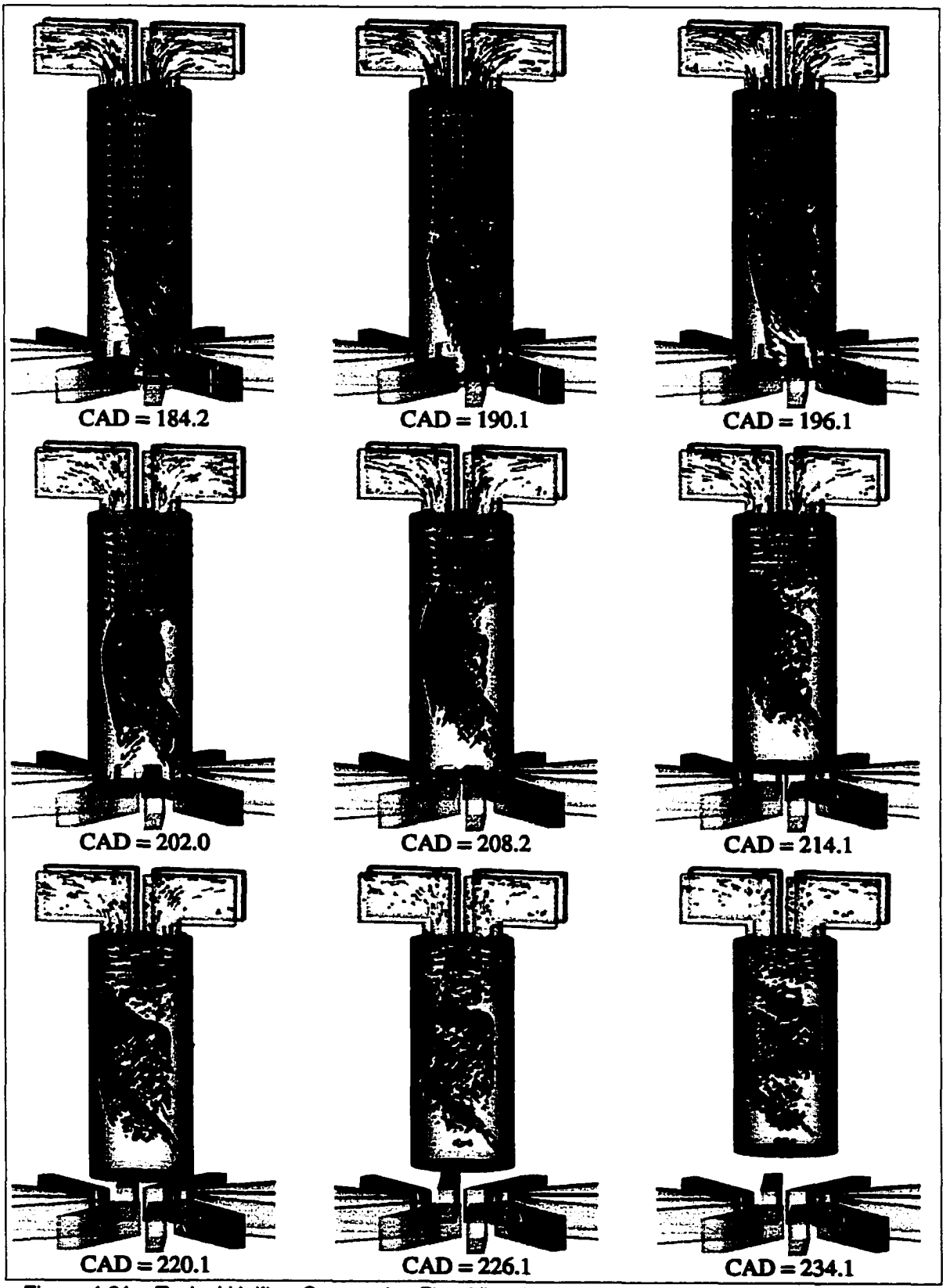

Figure 4.21 – Typical Uniflow Scavenging Flow Visualization vs. Crank Angle Degree [20° swirl]

ability of the fresh charge to sweep both the core of the cylinder and the regions near the walls, as well as the uniformity of the charge at TDC, due to the decreased in-cylinder mixing.

In an effort to address these concerns, and optimize the flow regime for this configuration, simulations were conducted varying the parameters of exhaust valve lift and timing, intake port configuration (swirl angles, number of ports, port flow area), piston frequency, and travel past the port bottom. More detail will be given here regarding these results since the uniflow configuration was adopted for the free piston engine design. However, a full description can be found in Appendix C.

EXHAUST VALVE LIFT / TIMING – The first simulation series investigated the relationship between valve lift and valve timing on the scavenging process. It was expected that both extended scavenging times and longer lifts could improve the cylinder's flushing, however it was unclear which was more important.

For these runs the exhaust valve lift was increased from 0.7 to 1.0 cm, while at the same time the timing was decreased from 158 to 70CAD. The total integrated 7valve area-time was kept constant at 0.093 $cm^2 \cdot s$. (The integrated area-time was defined as $\int_0^{\Delta t_{scav}} A_{port}\, dt$.) The intake height was adjusted (from 2.77 to 2.5 cm) in order to keep the integrated intake port area-time constant. A relatively low charging pressure of 1.2 bar was used, and the piston frequency set to 50 Hz. The intake ϕ was fixed at 0.42. For these first trials swirl angles of 0° were used and the compression ratio increased to 45:1 to ensure HCCI combustion during initialization procedure.

Figure 4.22 presents the results from these runs where the scavenging and trapping efficiencies are plotted. Here it can be seen that there is an optimal lift/timing arrangement for which the scavenging efficiency is maximized. This result is due mainly to the timing of the intake port opening relative to EVO; the optimal arrangement is when the intake port opens just as the cylinder pressure has blown down to the intake charging pressure. In this case the fresh charge enters the cylinder as soon as the ports are uncovered.

For the cases where the ports open before the pressures have equalized there is some backflow into the manifold. This delays the delivery of the fresh charge, and as a result the charging is not as effective. As well, the amount of delivered mass is lower and the pressure at EVC is reduced. For the cases where the ports open after the cylinder pressure has dropped below the charging pressure, the delivery of the fresh charge into the cylinder is more intense with more mixing and greater penetration to the top of the cylinder. This accounts for the drop in trapping efficiency, as more of the fresh charge escapes through the exhaust valve.

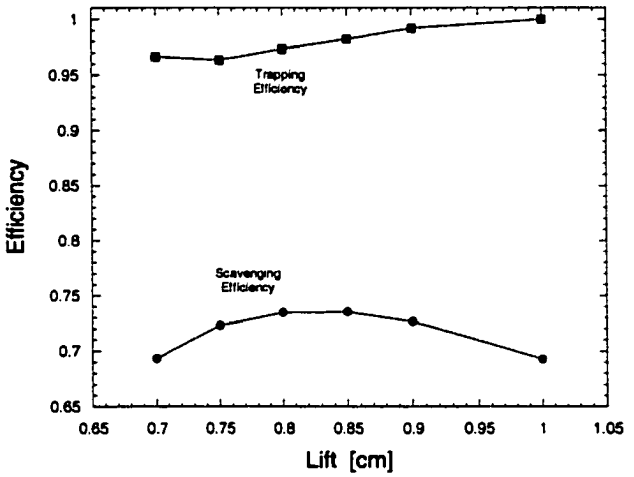

Figure 4.22 – Scavenging and Trapping Efficiencies vs. Valve Lift

In order to determine how the intake port configuration affects the scavenging process, the next three simulation series were conduced.

UNIFORM SWIRL ANGLES – A classic feature of the uniflow arrangement is its ability to flush the burned charge from the cylinder by generating plug-type flow. However, this process is not ideal and some burned charge can become trapped along the cylinder walls or in the core of the cylinder. This can degrade the operation of the free piston engine by limiting the scavenging efficiency, or by leaving hot spots within the cylinder, which can result in preignition of the mixture.

On the other hand, some trapped residuals may prove beneficial in insulating the fresh mixture from the cylinder surfaces during combustion, and thereby reduce heat transfer losses,

ring blowby, and oxidation of the piston's lubricating fluid. Since a determination of these effects on the combustion cycle was beyond the scope of these computations, the objective for the KIVA-3V simulations was to generate as uniform a plug-type flow as possible, while recognizing that core displacement is more important than wall flushing.

For this series of simulations a 12-port geometry was used where the incoming swirl angles were uniformly set at 0°, 10°, 20° and 40°. (It was thought that better flow control might be achieved using a 12-port arrangement, relative to a 4- or 8-port configuration. However, an 8-port geometry will be compared to these results later in this chapter.) The total cross-sectional area of the intake ports was kept constant for these runs by adjusting the widths of the ports. The operating conditions were similar to those listed in Table 4.5, where the optimal port timing from the previous series was utilized.

Figures 4.23-4.26 present the results for these runs. In these figures the in-cylinder flow is visualized through contour plots of the residual gas fraction, presented at various points in the scavenging cycle. In this manner the ability to generate uniform plug flow can be assessed. For these illustrations the contours are plotted on a plane parallel to the cylinder's axis. (The valves are clearly visible at the top of the cylinder.) Contours representing fractions of 0.76, 0.69, 0.61, 0.53, 0.46, 0.38, 0.31, 0.23, 0.15, 0.08, respectively from the top of the cylinder, are shown.

Through this visualization the differences in in-cylinder composition, and thus flow patterns can be seen. Clearly the 0° case (Fig. 4.23) flushes the burned charge from the center of the cylinder leaving a region of residual gas near the wall. The 40° case (Fig. 4.26) on the other hand, sweeps the cylinder walls leaving a residual core in the center of the cylinder. The 10° and 20° cases (Fig. 4.24, Fig. 4.25) result in graduations between these two extremes.

Through these examples it is apparent that the 0° case results in some fuel short-circuiting (1% calculated), while the 10° and 20° cases have room for improvement in scavenging efficiency without the loss of fresh charge (η_{sc}~0.75, η_{tr}~1.0). In addition, it seems that neither the 10° nor 20° cases actually generates plug flow, and as such some residual charge entrainment is unavoidable.

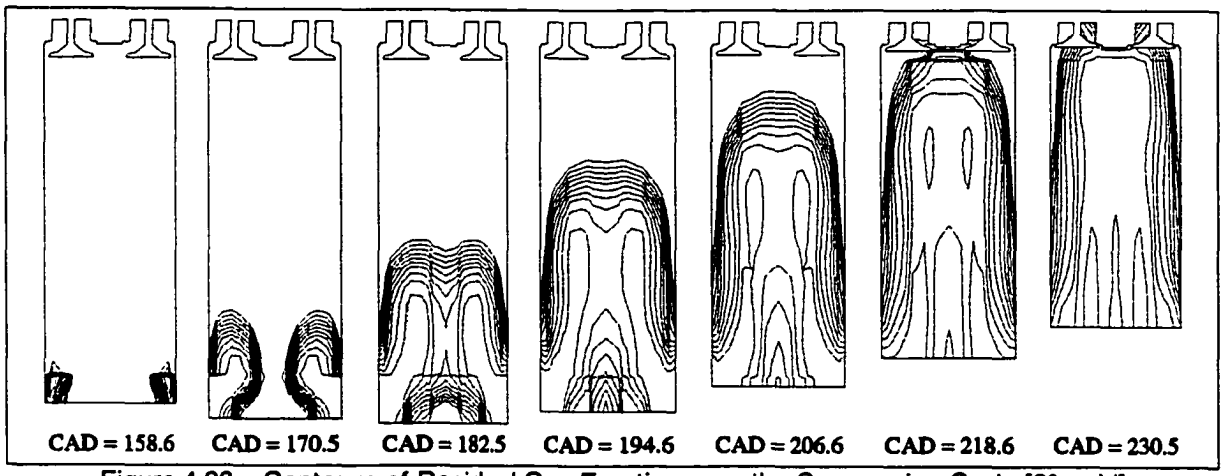

Figure 4.23 – Contours of Residual Gas Fraction over the Scavenging Cycle [0° swirl]

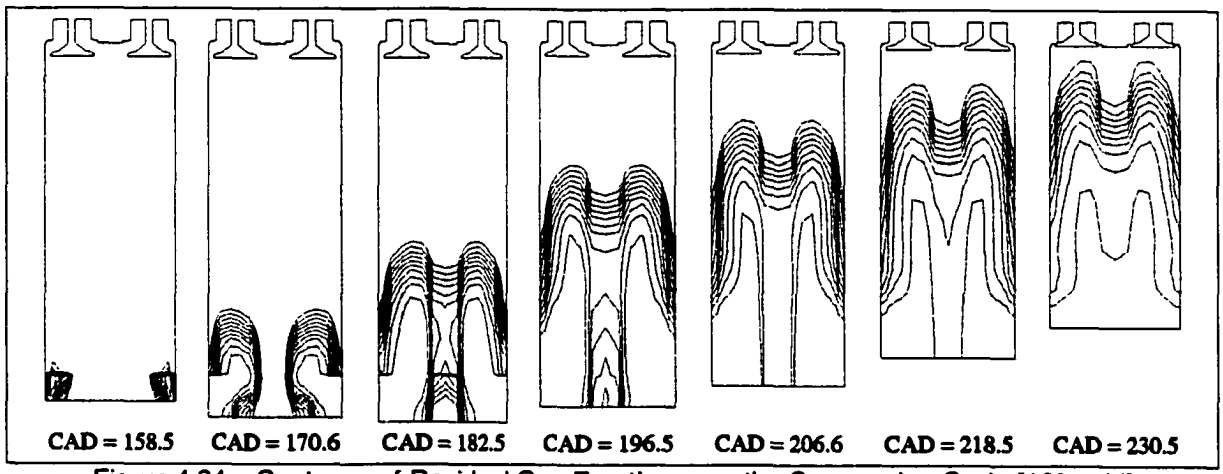

Figure 4.24 – Contours of Residual Gas Fraction over the Scavenging Cycle [10° swirl]

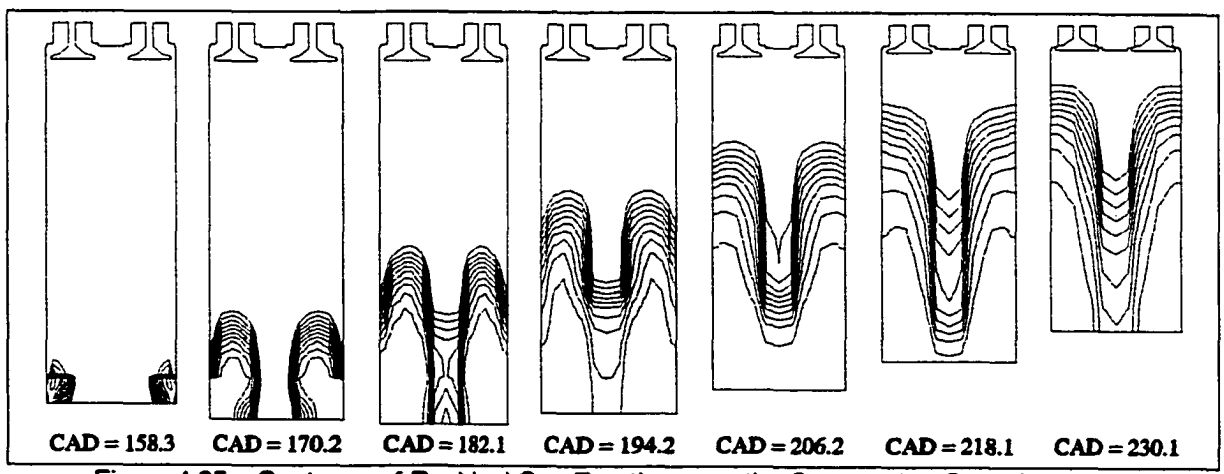

Figure 4.25 – Contours of Residual Gas Fraction over the Scavenging Cycle [20° swirl]

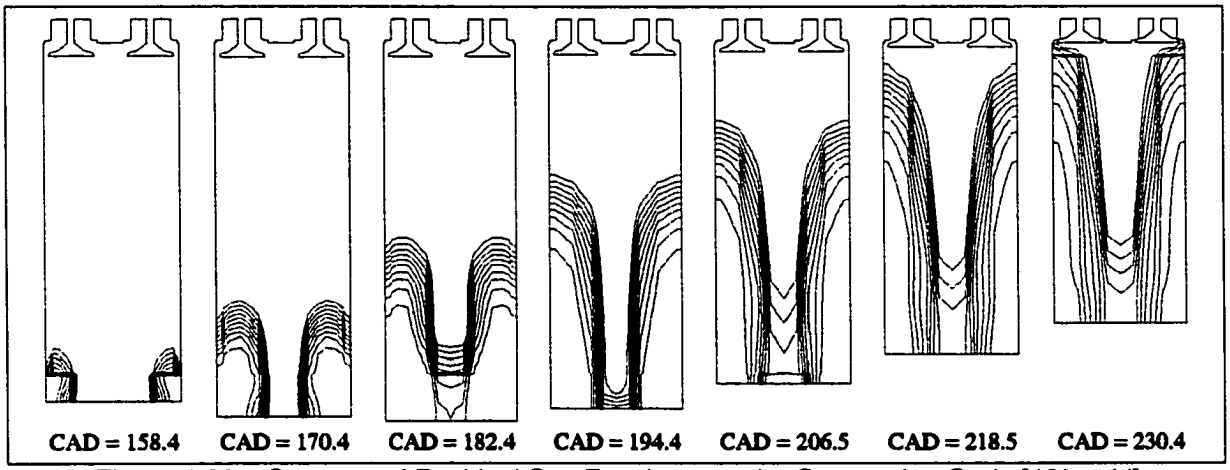

Figure 4.26 – Contours of Residual Gas Fraction over the Scavenging Cycle [40° swirl]

Another result of these runs is that there seems to be little mixing after EVC. This is quite different than in the conventional loop design and may be significant with regards to charge uniformity by TDC. On the other hand, since the cylinder can be recharged much more effectively with a high percent of burned charge removed, the effect of this may be small.

NON-UNIFORM SWIRL ANGLES – In an attempt to improve the characteristics of the in-cylinder flow (making it more plug-type), configurations with non-uniform swirl angles were investigated. The objective of these was to sweep the core of the cylinder while at the same time generating enough swirl to flush the cylinder walls. Figure 4.27 presents an example of the type of arrangement used for this series. Here some ports are directed toward the center of the cylinder, while others are angled to sweep the walls. In all, 5 designs were considered with the total intake cross-sectional area again fixed by adjusting the individual port widths. The valve lift/timing, and port heights were the same as before.

The results of these runs indicated that no improvement can be made through using non-uniform swirl angles. An example of some of the resulting flow behavior is presented in Figure 4.28. In this figure the flow patterns are illustrated by plotting two iso-surfaces through the scavenging period. The iso-surfaces differentiate three gas regions that exist in the cylinder – burned, unburned and mixed gas. The gas composition at the boundaries is the same as the maximum and minimum contours presented in Figures 4.23-4.26 – residual fractions of 0.76 and

0.08, respectively. For reference, the flow through the 20° uniform swirl cylinder is presented in Figure 4.29.

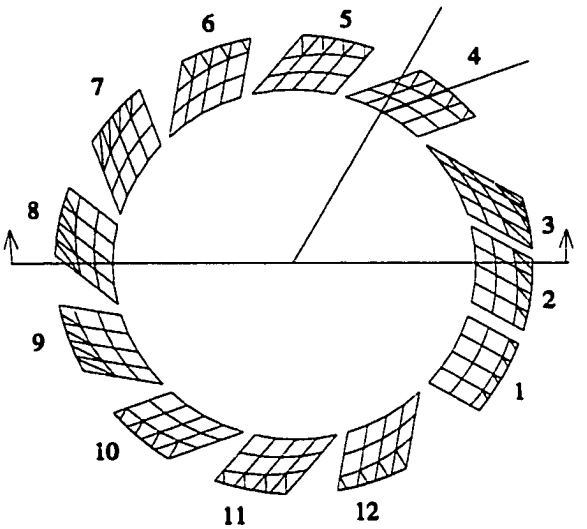

Figure 4.27 – Intake Port Arrangement [CASE 1]

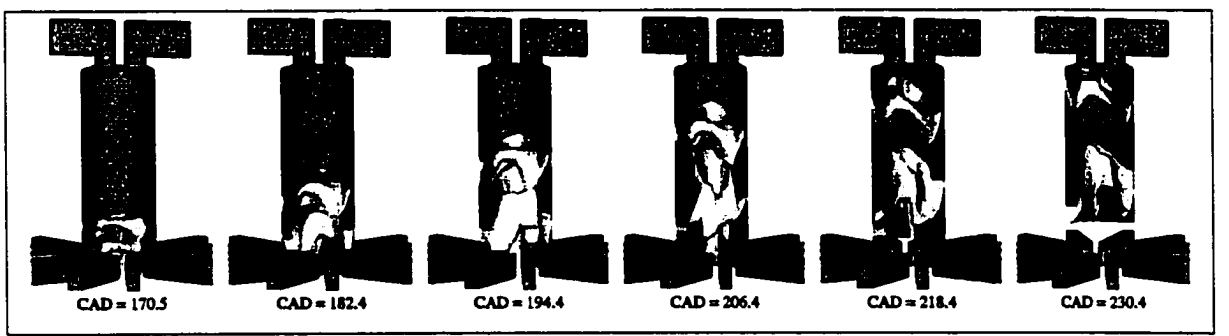

Figure 4.28 – Iso-surfaces of Residual Gas Fraction over the Scavenging Cycle [CASE 4]

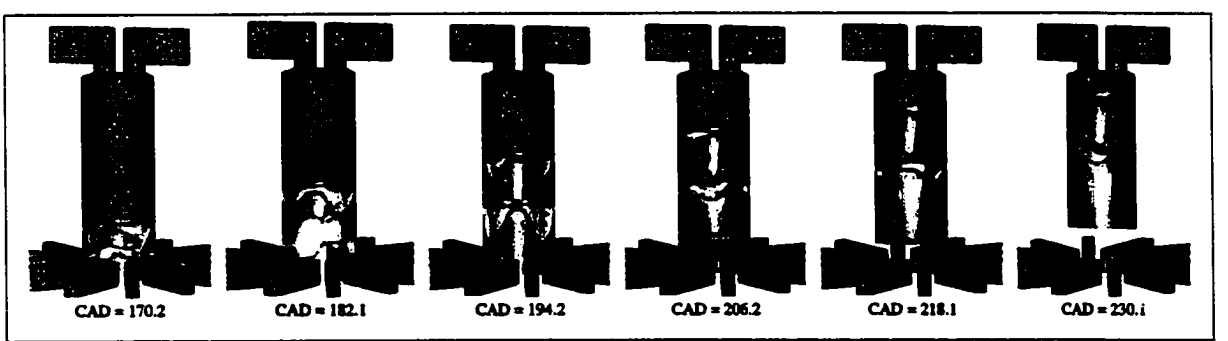

Figure 4.29 – Iso-surfaces of Residual Gas Fraction over the Scavenging Cycle [20° CASE]

It is clear in these figures that the non-uniform port arrangement leads to non-uniform flow behavior in the cylinder. Uniform plug flow is not generated and there is greater likelihood of short-circuiting in these arrangements as the fuel can reach the valve region.

After analyzing these two series of simulations, it appears that a uniform angle of 10° to 20° will best meet the desired flow characteristics for the scavenging system.

NUMBER OF INTAKE PORTS – In order to determine the significance of the number of intake ports on the in-cylinder flow, simulations were conducted using an 8-port arrangement with uniform swirl angles of 0° and 40°: the limits of the 12-port configuration studied.

Overall, the scavenging results were quite similar, in terms of cylinder pressure, mass flow rates, and scavenging/trapping efficiencies. In addition, visualization of the residual contours suggested that the in-cylinder flow patterns are also similar. With no apparent benefit to using a 12-port design, an 8-port arrangement was chosen for the design.

INTAKE PORT AREA – In an attempt to increase the scavenging efficiency relative to the previous runs the intake port heights were increased. This was done to increase the area for the incoming flow, and at the same time allow more time for scavenging. Heights of 3.0, 3.5, 4.0 and 4.5 cm were used. Although the stroke of the piston increased, f was maintained at 50 Hz. Swirl angles of 15° were utilized, and the valve timing was adjusted, based on earlier results, so that 1.9 ms was available for blowdown through the exhaust valve. The overall scavenging time increased from 6.65 ms to 7.52 ms (+13%).

The results of these runs indicated that there was almost no change in scavenging performance for the increased port heights (η_{sc} ~ 0.75; η_{tr} ~ 0.999). There were two reasons for this. First, there is still the issue of timing the blowdown so that the cylinder and manifold pressures are equalized by IPO. As the intake flow area and scavenging time were increased, the amount of mass delivered to the cylinder increased (+6.9%, for the tallest case). This led to higher pressures at EVC/O requiring more time to discharge this gas through the valves. As a

result the cylinder pressure at IPO was higher than expected, and this led to greater backflow (0.4% → 2.8%). An attempt was not made to match the valve/port timings for these runs.

The second factor, and more significant though, is that the valve flow represents the major restriction in the uniflow configuration. Substantially more time is required for the burned charge to be flushed through the valves.

PISTON FREQUENCY – In an effort to address the valve flow issue the piston frequency was decreased. The scavenging time was increased to 8.5, 9.4 and 10.8 ms using frequencies of 43.3, 36.7, and 30 Hz. For these runs a longer valve lift was used (0.925 cm – this was expected to be the maximum realistic lift useable) and the port heights set to 3.5 cm. Again, no attempt was made to match the blowdown timing to the operating conditions; however, by varying the valve timing it was fixed at 2.03ms. The intake ϕ was set to 0.42 for these runs.

Figure 4.30 plots the scavenging and trapping efficiencies versus the scavenging time for these runs. It is clear how the increased scavenging time can dramatically affect the scavenging performance, substantially improving the cylinder flushing. However, the issue of trapping efficiency becomes more significant as the time increases too much. On the other hand though, the overall performance is substantially improved relative to both loop and hybrid-loop arrangements.

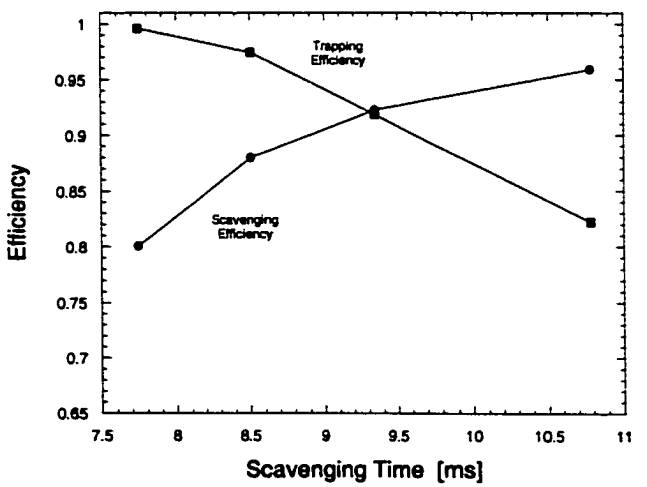

Figure 4.30 – Scavenging and Trapping Efficiencies vs. Scavenging Time

PISTON TRAVEL PAST PORT BOTTOM – The final simulations for the uniflow configuration investigated the effect of using piston travel past the intake port bottom to increase the scavenging time instead of changes to the piston frequency. The previous runs demonstrated that a substantial improvement in scavenging efficiency could result from increases to the scavenging time; however, as f is decreased, the power output of the engine is reduced. In order to maintain the frequency, and thus the power level, the stroke of the piston was increased past the bottom of the intake port, increasing the fraction of the stroke devoted to scavenging. This was seen as a reasonable option for the free piston since friction is reduced relative to conventional crankshaft-driven configurations, and this change may not lead to significant losses.

For these runs the piston travel past intake port bottom was increased from 0.15 to 1.65 and 4.0 cm, increasing the scavenging time to 8.48 and 9.43 ms, respectively (the same change as with the piston frequency modifications). The intake port height was maintained at 3.5 cm and the valve timing was adjusted so that the blowdown time was again 2.03 ms.

Figure 4.31 presents the scavenging and trapping results for these runs. The results from the previous section are included for reference. It can be seen that the scavenging efficiency improvement is not as substantial as with the decrease in f, and there is little change between the 1.65 cm and 4.0 cm configurations.

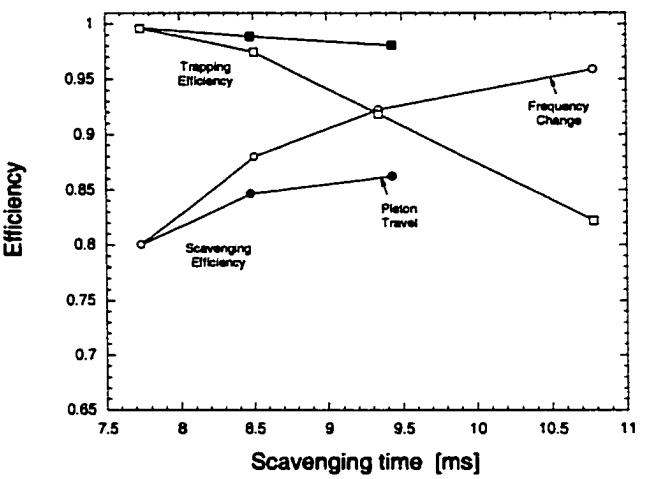

Figure 4.31 – Scavenging and Trapping Efficiencies vs. Scavenging Time

These results can be explained by the change in in-cylinder flow behavior. As the travel past the port bottom is increased the piston's downward motion tends to trap some residual charge between the incoming fresh gas and the piston crown. This burned gas cannot be flushed from the cylinder and as a result the scavenging efficiency is degraded. Additionally, some of this residual gas is forced into the intake manifold as the piston begins its upward stroke. (This is greatest in the 4.0 cm travel case with 2% of residual charge in the manifold at IPC.) This burned charge must be redelivered to the cylinder during the next scavenging cycle.

An interesting result of the increased piston travel simulations however, is that more mass can be delivered to the cylinder (15 and 30%, respectively) due to the increased scavenging time. This results in increased power output for the engine. Thus, without changing f, the power is improved. (The increases in mass delivery were seen with the frequency simulation series, however the decreased piston frequency offset the gains there.)

On the other hand, the changes in piston stroke significantly increased the piston's velocity profile where the average speed was increased from 2580 cm/s to 3250 cm/s, for the longest stroke case.

SUMMARY OF UNIFLOW SCAVENGING SIMUALTIONS – The uniflow scavenging configuration represented the best means of flushing the cylinder with respect to the engine's high efficiency and low emissions goals. Adequate charge replacement and low trapping losses seem possible with this arrangement. This represents a substantial improvement over both loop and hybrid-loop configurations.

Based on the KIVA-3V calculations, this design can be optimized if: the exhaust/intake timings are matched so that the cylinder has blown down to the charging pressure before IPO; the intake ports have sufficient flow area to adequately charge the cylinder; the ports are oriented with a uniform swirl angle of about 15°; the valve lift and flow area are maximized and the piston frequency is adjusted to allow adequate discharge of the burned gases through the exhaust valves.

Charge Delivery

The purpose of analyzing the charge delivery system was to determine the key factors affecting power consumption and the influence on the in-cylinder flows. The major components of the charge delivery system for the free piston engine are the stepped piston compressor, the delivery tank, and valves into and out of the compressor. The purpose of the delivery system is to supply the KIVA-3V mesh with fresh charge at an elevated pressure.

The arrangement of this system assumed for this analysis is shown in Figure 4.32. In this configuration the alternator's magnets function as a 'stepped piston' where fresh gas is inducted into one side of the compressor during the compression stroke of the other side's combustion chamber. As the piston changes direction, the fresh charge is pressurized and sent to the delivery tank through the compressor's outlet valves. In this arrangement the tank will have maximum pressure at IPO. (This assumes the delivery tank can be divided so as to not interact with both sides of the engine. That the tank is divided may be important regarding cylinder coupling in a combined configuration, but this was not included in the analysis.)

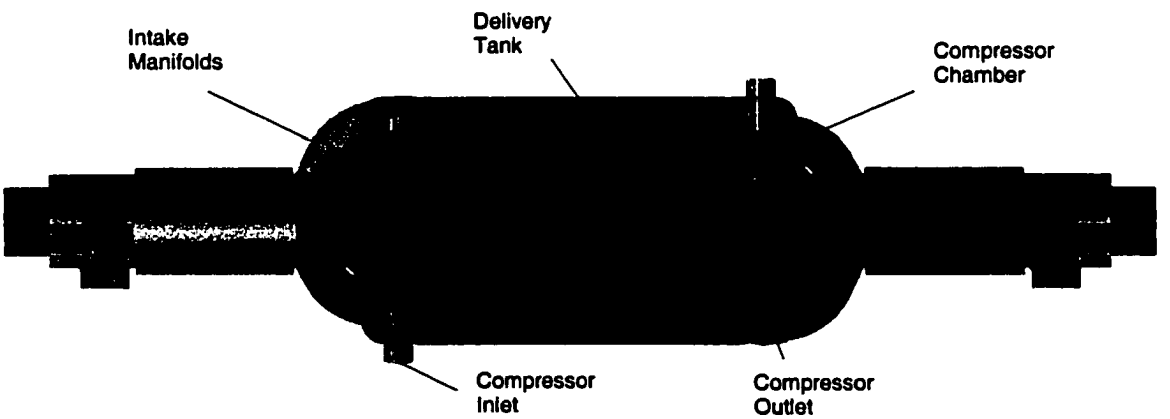

Figure 4.32 – Charge Delivery System

For the initial simulations the effects of the compressor's volumetric compression ratio, the delivery tank volume, flow area of the compressor's valves, and the tank temperature on the performance of the system were determined. The uniflow arrangement from the frequency

variation section was used with the frequency set to 43.3 Hz. A summary of the parametric simulations is presented next with more detail given in Appendix D.

COMPRESSION RATIO – The volumetric compression ratio of the compressor was set at 3.5:1 and 30:1. For the low CR_{comp} case the inner and outer diameters were 8.0 and 13.0 cm, respectively. For the high CR_{comp} case the diameters were 8.0 and 10.9 cm. (The low CR_{comp} compressor was substantially larger, as this was necessary to deliver the same amount of charge at the lower compression ratio.) A large tank (20L) was used for these runs to achieve a near-constant charging pressure (similar to the scavenging simulations with the loop, hybrid-loop and uniflow configurations). The flow areas were set to 4.5 cm^2 for both the inlet and outlet check valves. A constant tank temperature of 300K was used.

The results from these simulations indicated that there is little difference in the maximum/minimum compressor pressures, and this leads to little difference in the delivery tank conditions. As such the resulting scavenging performance was essentially the same for the two cases. The overall compressor work for these two runs was also similar, with the work fraction (W_{comp}/W_{cycle}) about 0.210. [W_{cycle} is the integrated net work for the engine's thermodynamic cycle, and W_{comp} the work of the compressor.]

TANK VOLUME – A smaller delivery tank (0.1L) was used next to simulate crankcase-type delivery, with high initial pressure followed by near-atmospheric conditions toward the end of the scavenging cycle. Including the intake manifold volume (in the KIVA-3V mesh), the small tank option represented 55% of the swept cylinder volume. On the other hand, the large tank and manifold represented 18.4 times the cylinder volume. The larger tank size tended to stabilize the charging pressure. For this and the following runs CR_{comp} was set to 30:1 in order to reduce the compressor's size. The other parameters were the same as before.

The results of these simulations indicated that as the maximum charging pressure is increased (1.2 bar to 2.3 bar) the compressor work fraction is increased (15% to 0.243). This results from the higher pressure to which the charge must be compressed, even though the total

mass delivered is the same. Figure 4.33 plots the delivery tank pressures over the engine cycle to illustrate how the charging pressure changes with tank size.

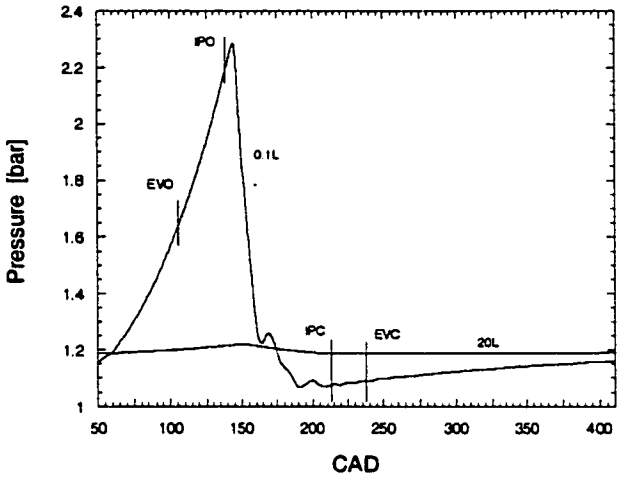

Figure 4.33 – Tank Pressure vs. CAD

A significant result of this increased pressure is the change in charge delivery. Initially the incoming flow rates are high, but then they drop to near-zero for almost ⅓ of the intake port open time. The effect of this on the in-cylinder dynamics is detrimental, with increased swirl, more mixing between the fresh and burned charges and greater penetration of the fresh charge to the valve region (leading to more short-circuiting).

INLET/OUTLET FLOW AREAS – The next simulation investigated the effect of the compressor flow area on the compressor work. The flow areas were somewhat arbitrary for this model so it was beneficial to review the magnitude of error introduced by the choice of these values. For this run the flow areas were increased to 8.0 cm^2 (almost double the initial values).

The result of this run is presented in Figure 4.34 where the compressor pressure is plotted versus the compressor volume. It is evident how much the driving pressure is reduced in order to deliver the same amount of charge. This dramatically affects the power consumption of the device, decreasing the work fraction by 40% (to 0.124). On the other hand, the scavenging performance was virtually unchanged by the increased flow areas.

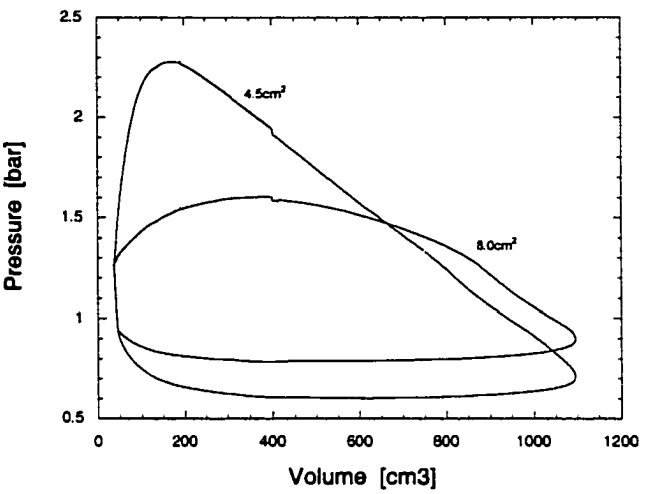

Figure 4.34 – Compressor Pressure vs. Compressor Volume

ADIABATIC TANK - The final simulation for the charge delivery system compared an adiabatic tank to the isothermal condition previously assumed. This simulation was conducted to indicate the limit of performance with respect to the tank's heat transfer characteristics. In the absence of a tank cooling system, an adiabatic assumption might be more representative of actual engine operation.

For the configuration assumed the large tank equilibrated to a temperature of about 400K, with little change through the cycle. (Three initial tank temperatures were used (300, 380 and 400K) with a 300K tank requiring a good deal of computing time to stabilize (~50 cycles).) Flow areas of 4.5 cm^2 were used for this run.

The results for this simulation indicated that the adiabatic/isothermal condition has a significant effect on the charge delivery process and in-cylinder dynamics. For the higher tank temperature, the cylinder is charged with a hotter gas mixture. This results in two things that significantly affect the engine's performance. First, the engine operates at a lower compression ratio due to earlier HCCI combustion (15:1, compared to 23:1); this decreases the efficiency potential.

Second, the trapped mass at EVC is much lower for the same charging pressure. This reduces the power output of the engine, while the compressor work remains constant. As such,

the work fraction is increased 70% (to 0.353). Further, the trapping losses are increased significantly (285%) as the trapped cylinder mass is reduced relative to the delivered charge.

SUMMARY OF CHARGE DELIVERY SIMUATIONS – The charge delivery simulations provided a means of analyzing the system with regard to the free piston engine's efficiency and emissions goals. It was determined from the calculations that the tank size, inlet/outlet valve areas, and operating temperature of the tank are significant factors impacting the performance of the engine. To best configure the system for optimal scavenging performance a large tank, sufficient valve area, and low tank temperature should be used.

Summary of Initial Simulations

The objectives of the initial simulations were to determine the key factors affecting the performance of the scavenging process in the free piston engine configuration, and to gain an understanding of the in-cylinder dynamics necessary to optimize the process. These objectives were achieved through the use of the KIVA-3V code, a 0D compressor model, and single step parametric variations. It was determined that neither the conventional loop, nor the hybrid-loop configurations can achieve the scavenging and trapping efficiency goals of the engine, and as such, the more mechanically complex uniflow arrangement must be used.

However, the calculations suggested that an orientation can be configured to achieve acceptable performance while the design allows some unique operating schemes to be implemented. One such scheme is the over-expanded cycle, and this will be discussed in the next section.

The initial simulations with the charge delivery system suggested that the tank size, tank temperature, and compressor flow areas are important parameters affecting the performance of the engine.

Final Simulations - Optimal Configuration

The objective of the final simulations was to select an operating configuration that will best achieve the design goals of the engine: maximum thermal efficiency and low exhaust emissions. To achieve this four different operating schemes were investigated. The results of these simulations will be presented here.

This section is organized as follows. First the metrics by which the operating schemes were judged will be presented then a description of the four options is given, along with the motivation for each. After this the operating results for these schemes are presented and discussed. A study of the 'robustness' of each design is then described. Finally, a summary for the final simulations is stated with the implications for the optimal design.

Metrics

For this section the operating results are compared based on the calculated thermal efficiency and exhaust emissions. The thermal efficiency was defined as

$$\eta_{TH} = \frac{W_{cycle} - W_{comp} - W_{fric}}{\left(m_f\right)_{del} * LHV_f} \tag{4.1}$$

where W_{cycle} is the integrated net work for the engine's thermodynamic cycle, W_{comp} the work of the compressor, and W_{fric} the friction work. The total mass of delivered fuel including that lost to short-circuiting, $\left(m_f\right)_{del}$, is used in this calculation. LHV_f is the heating value of the fuel.

The exhaust emissions included short-circuited fuel and NO. The KIVA-3V combustion calculations were not sophisticated enough to determine partially burned hydrocarbon fractions or CO emissions; however, the NO calculations seemed adequate to indicate fuel-rich, or hot regions in the cylinder, so these were included.

COMPRESSOR WORK – The compressor work was calculated using the compressor model (as explained previously) where the flow areas into and out of the compressor were chosen based on the ratio of total area to the amount of delivered mass per cycle. This ratio was set to 6.7 cm^2/g.

(It was hoped that this could account for variations in the cases due to the power output goal, while still providing a comparison for the compressor work fraction.)

FRICTION WORK – The fiction work was calculated using the friction model detailed in Chapter III (Eqs. 3.12-3.13). The parameters used for this model are listed in Table 4.6. For the friction simulations a 2-ring configuration was used where the pressure drop across the top ring was assumed to be 35%. Oil starvation was not included. (It should be noted here that the Reynold's equation used to approximate the lubrication process required a limit on the curvature of the piston rings (noted in Fig. 3.2). This was calculated to be 0.001; values higher than this produced erroneous results for the friction work.)

Ring Parameters	
ς_1	0.001
b_1 [cm]	0.11
c_1 [cm]	0.02
T_1 [N]	80
ς_2	0.001
b_2 [cm]	0.11
c_2 [cm]	0.02
T_2 [N]	80
Oil Parameters	
μ (5W-20, 80C) [dyne-s/cm]	0.253

Table 4.6 – Friction Model Parameters

An example of the calculated instantaneous friction force is given in Figure 4.35. Here the force is plotted as a function of piston position, and this shows that the maximum values occur near TDC, where the effect of the high cylinder pressure is significant. Through the stroke of the piston though, the friction force more or less resembles the velocity profile of the free piston (as seen in Figure A.10).

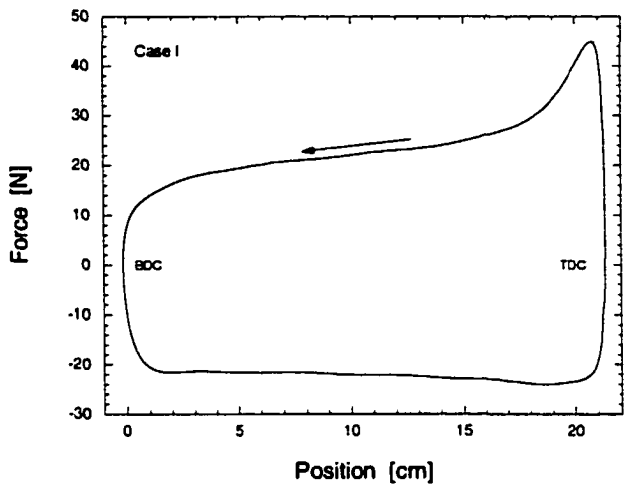

Figure 4.35 – Friction Force through Stroke of Piston

Operating Schemes

Four different operating schemes were investigated in this section. These were a standard configuration (Case I), a very low charging pressure / low frequency option (Case II), a stratified scavenging configuration (Case III), and an over-expansion arrangement (Case IV). To review, the stratified scavenging configuration is an arrangement where the cylinder is initially flushed with air only, and then a rich fuel/air mixture is introduced late in the scavenging cycle. The over-expanded arrangement expands the combusted gases to a pressure similar to the charging pressure before the exhaust valves or intake ports open.

As stated in Chapter III the expected benefits of these schemes, relative to the standard configuration, were:

Case II – Decreased pumping power, with the operating frequency reduced to ensure adequate charging.

Case III – Increased scavenging efficiency, with short-circuiting controlled by late fuel introduction. The higher operating compression ratio leads to improved cycle thermal efficiency.

Case IV – Increased work output through recovered blowdown potential.

CASE	I	II	III	IV
Bore [cm]	7.62	8.85	7.24	7.62
Stroke [cm]	21.46	29.63	25.56	44.05
Effective Compression Ratio	19:1	19:1	26:1	19:1
EVO [CAD]	116	102	99	142
IPO (Air) [CAD]	NA	NA	132	NA
IPO (Fuel/Air) [CAD]	146	130	148	139
IPC (Fuel/Air) [CAD]	208	222	207	214
IPC (Air) [CAD]	NA	NA	220	NA
EVC [CAD]	232	245	248	285
Valve Diameter [cm]	2.54	2.86	2.38	2.54
Valve Lift [cm]	0.925	0.925	0.925	0.925
Fuel/Air Port Width [cm]	2.00	2.27	2.20	1.93
Air Port Width [cm]	NA	NA	1.63	NA
Fuel/Air Port Height [cm]	2.30	5.80	2.70	6.50
Air Port Height [cm]	NA	NA	4.70	NA
Swirl Angle	15°	15°	15°	15°
Operating Frequency [Hz]	45	33	45	45
Charging Pressure [bar]	1.2	1.1	1.2	1.2
Intake ϕ	0.475	0.475	2.70	0.475

Table 4.7 – Geometric and Operating Parameters

For each of these cases a uniflow geometry was used with 4 vertical valves and 8 intake ports. The orientations and timings were configured based on the findings of the initial simulations. Operating goals for these schemes were scavenging efficiencies of 80% (except for Case III where the desired η_{sc} was 90%), and trapping losses of around 1%. Relatively constant power output (~20kW) was also a goal.

A series of iterations was used to achieve the desired performance for each scheme. For the standard configuration 11 trials were needed to converge on these values; for Case II 6 trials were used; for Case III 13 trials were necessary; and for Case IV 8 trials were required. The results of the final designs are presented in Table 4.7 where the geometric and operating parameters of each case are listed. (Due to the setup and computing times required for each iteration however, only an approximation of the power goal was achieved.)

The meshes for each case in this series are illustrated in Figures 4.36-4.39. The differences relative to the standard configuration are apparent. Case II requires a larger swept

volume to account for the decrease in frequency and taller intake ports to allow sufficient time and flow area for scavenging at the lower pressure. Case III utilizes a smaller swept volume, to account for better charging, with four tall ports to deliver the initial flushing charge, and four short ports to deliver the fuel-rich mixture later in the scavenging cycle. Case IV uses a very long stroke, and tall intake ports to achieve the desired scavenging/operating performance.

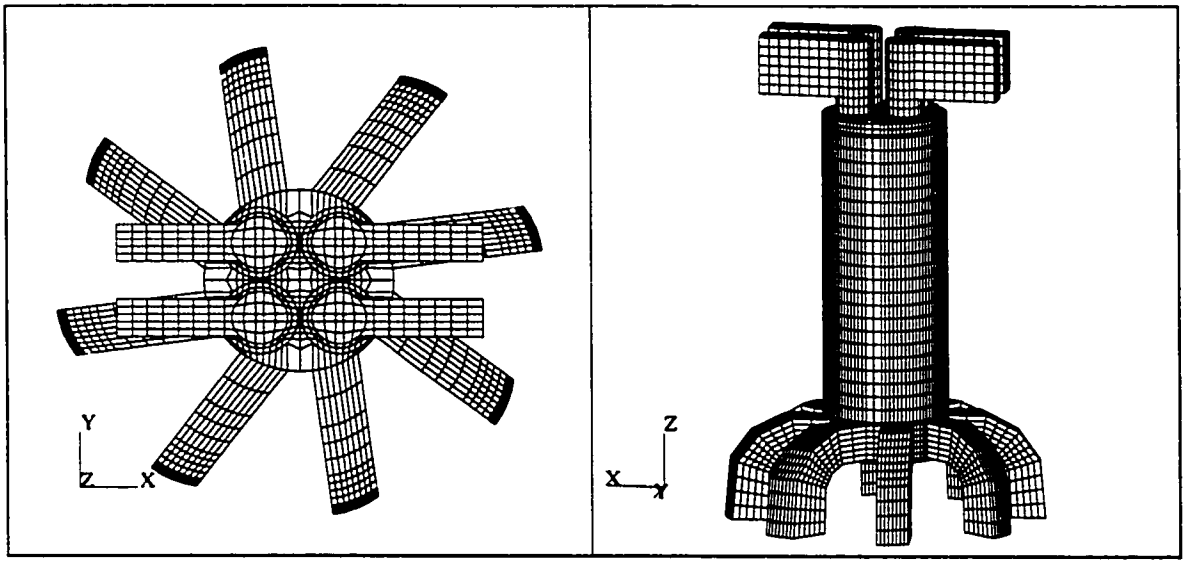

Figure 4.36 – Mesh for Case I - Nominal Configuration [35,200 cells]

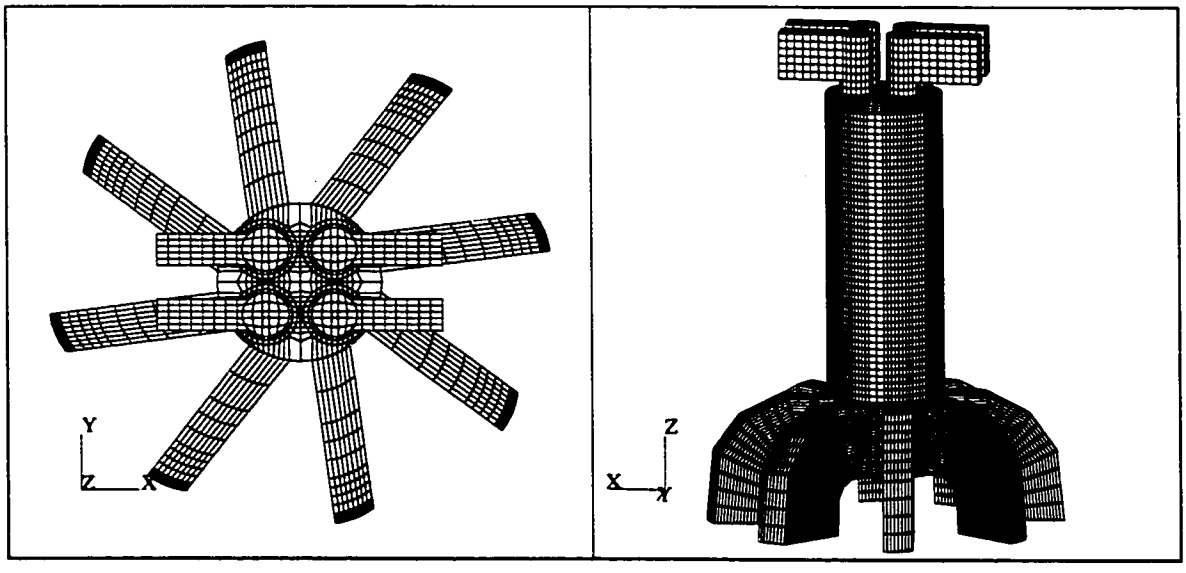

Figure 4.37 – Mesh for Case II - Low Pressure / Low Frequency Configuration [76,200 cells]

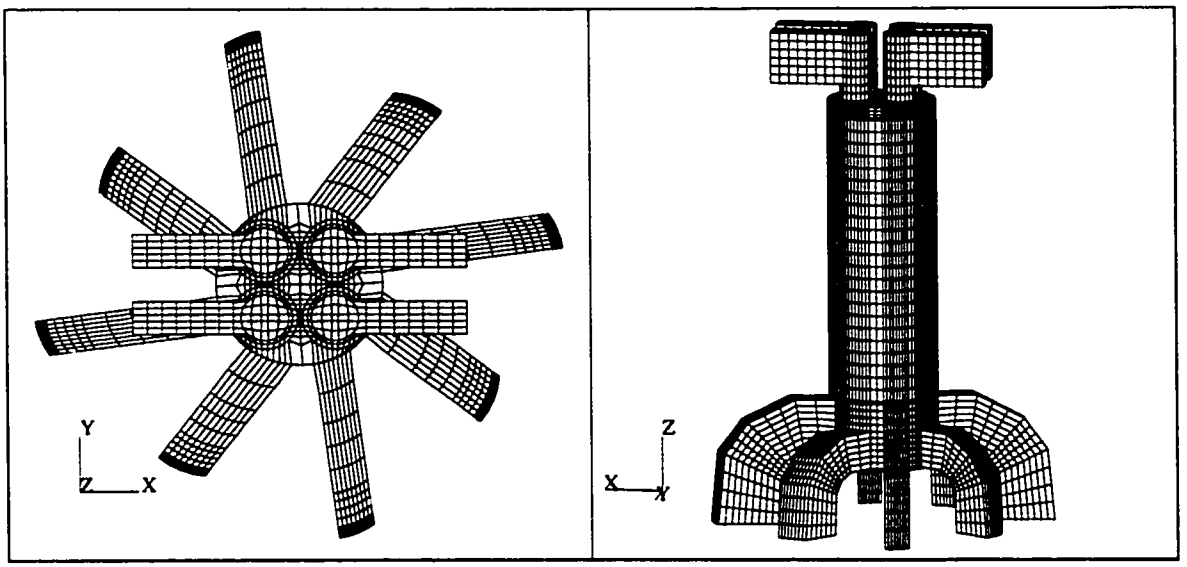

Figure 4.38 – Mesh for Case III - Stratified Scavenging Configuration [40,300 cells]

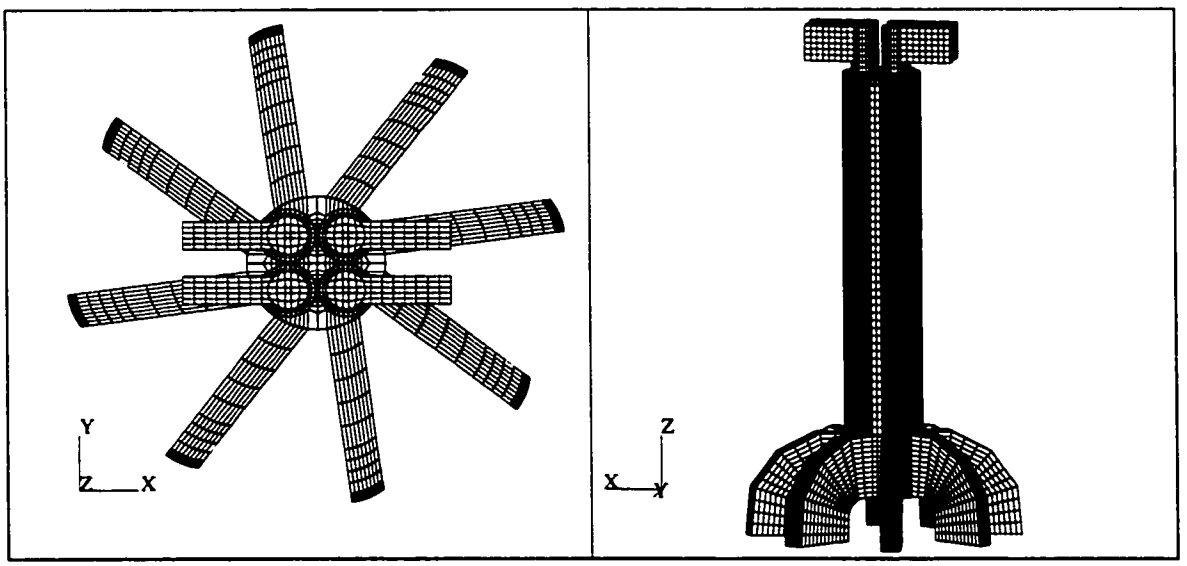

Figure 4.39 – Mesh for Case IV - Over-expansion Arrangement [59,200 cells]

Operating Results

The results of the simulations for the four cases are discussed next. Table 4.8 presents the output for the four schemes. In this table the differences in scavenging performance, as well as the changes in the cycle efficiencies and output emissions are noted. For Cases I, II and IV the scavenging performance is similar (η_{sc}~0.83, η_{tr}>0.994), while the stratified scavenging option has a scavenging efficiency of 0.93 and fuel trapping losses less than 1.3% (the air-only trapping

	η_{sc}	η_{tr}	m_{del} [g]	W_{cycle} [J]	W_{comp} [J]	W_{fric} [J]	η_{th}	C_3H_8 [ppm]	NO [ppm]	Power [kW]
CASE I (nominal)	0.83	0.997	0.69	480	24.6	19.2	0.475	67	281	18.7
CASE II (low P_{ch})	0.83	0.995	1.15	790	29.7	31.2	0.475	133	707	23.1
CASE III (stratified)	0.93	0.928 (A) 0.988 (F/A)	1.03 0.16	644	45.1	24.3	0.525	206	94	24.6
CASE IV (over-expanded)	0.84	0.994	0.92	697	35.6	59.9	0.491	136	560	25.7

Table 4.8 – Operating Results

losses were ~7%). These were the operating goals for the arrangements. (The lower η_{tr} for Case III can be attributed to the tediousness of the iteration process where it was difficult to achieve both η_{sc} and η_{tr} goals, as well as the dilution ratio and power output goals for the configuration chosen. This explains the increased short-circuiting emissions for this case, as seen in the table below.)

Table 4.8 shows that the overall thermal efficiency for Case II is the same as for the standard configuration; however, the short-circuiting and NO emissions are increased (+200% and +250%, respectively). On the other hand, Case III has an increased thermal efficiency (+10%), with higher short-circuiting losses (+300%) and lower NO (-70%). Case IV also operates with a higher thermal efficiency (+3%) than the nominal run, but greater short-circuiting and NO emissions (+200%) result.

The differences in these results are explained by studying the operating cycle and cylinder/port flows for the four arrangements. The effects of the compressor and friction work on the overall cycle, as calculated by the 0D and 1D models, are also important, and will be discussed below.

Figure 4.40 presents the thermodynamic cycles for the four configurations; in this figure the cylinder pressures are plotted against the respective cylinder volumes. The valve and port timings are included for reference. Comparing these runs, it can be seen that for Case II the

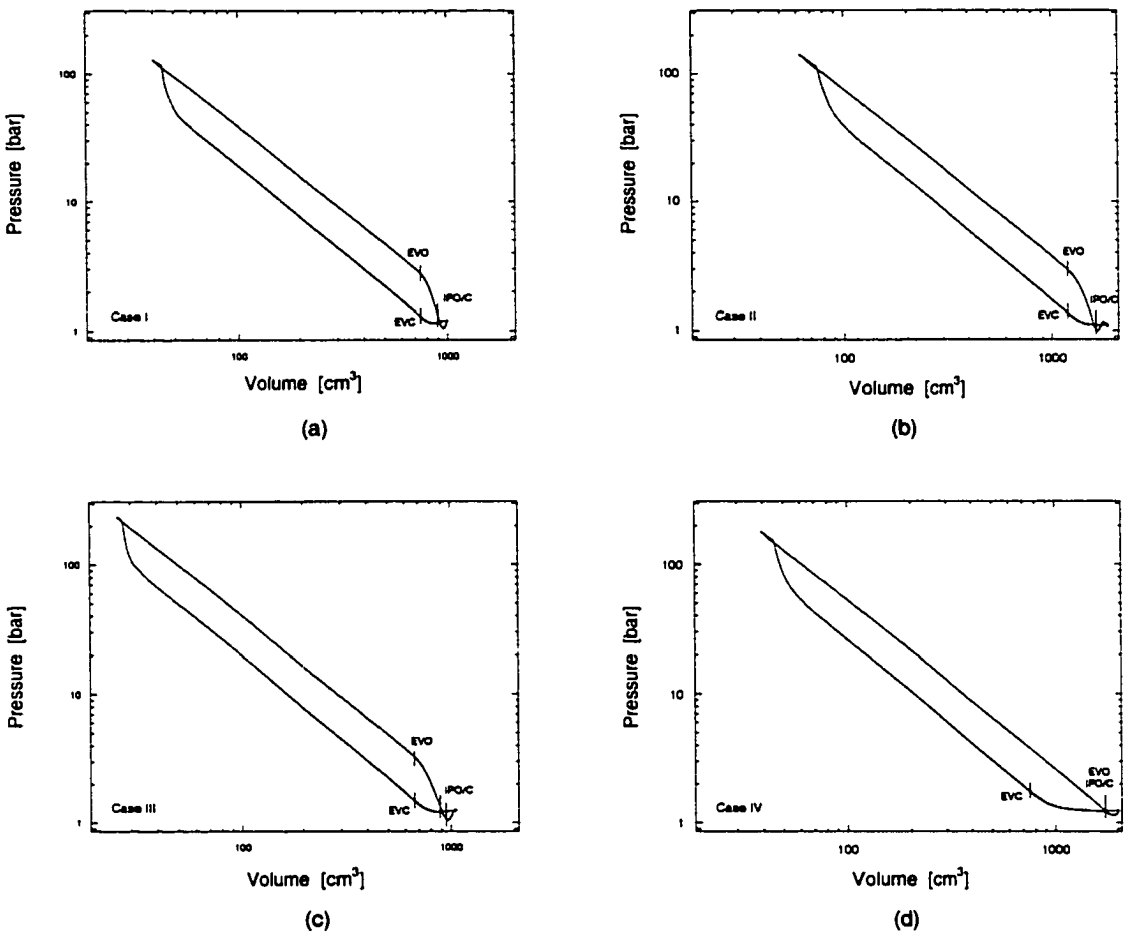

Figure 4.40 – Average Cylinder Pressure vs. Volume

operating cycle is shifted (to the right in the plot) with the increased cylinder volume. Also apparent is that the initiation of HCCI combustion occurs somewhat earlier in the stroke, with over-compression of the burned charge after combustion. This leads to the higher NO emissions noted in Table 4.8, and will be discussed in greater detail below. Regarding the scavenging period it can be seen that the cylinder pressure is not as stable after the blowdown process with some fluctuation as the fresh charge is delivered.

The thermodynamic cycle for Case III is quite similar to the standard case, however, the increase in compression ratio before combustion is apparent. This is due to the lower bulk temperature at EVC, achieved through more complete replacement of the burned charge.

For Case IV the change in the scavenging cycle is significant with no blowdown present (though there is some pressure drop after EVO/IPO due to continued piston expansion). The cycle for this case is also shifted relative to the nominal arrangement, due to the higher pressure that results at EVC. This higher pressure is mainly caused by the valve timing, and the difficulty of discharging the cylinder gases rapidly enough for the faster moving piston. (V_{avg}= 3960 cm/s, compared to V_{avg}= 1930 cm/s for the nominal case.) In this case, there is also significant compression after combustion, as was seen in Case II.

The exhaust and intake flow rates for these four runs are shown in Figure 4.41; here the flow rates are plotted versus CAD. In this figure the differences in the scavenging dynamics are apparent. Figure 4.41(a) presents the results for the standard case. Here the initial blowdown across the valves is observed, with secondary flow due to the incoming charge. This pattern is repeated for Case II however, the valve open time (EVO-EVC) is much longer, in terms of CAD and time (11.96 ms compared to 7.19 ms), due to the requirements of the low charging pressure operation. This arrangement leads to some fluctuation in the cylinder pressure (seen above) and the resulting intake/exhaust flow rates.

For the stratified scavenging case (4.41(c)) the flow rates through both the air and fuel-air ports are shown. It can be seen that the rates are significantly different for the two types of ports, with some reverse flow into the fuel ports as the piston begins its compression stroke. However, the overall exhaust flow is similar to the nominal case.

The flow rates for the over-expanded cycle are illustrated in Figure 4.41(d). The change in exhaust flow behavior is apparent with a nearly constant discharge rate during the scavenging process. On the other hand, the incoming flow rate looks quite similar to that for Case I.

To further explain the operating results, flow visualizations for the four cases are presented next. Here again particle tracing is used with the fresh charge represented by dark spheres and the burned charge by lighter spheres. (For the stratified scavenging run the air-only charge is represented by very light spheres.) Trailing lines indicate velocity. Half of the cylinder is

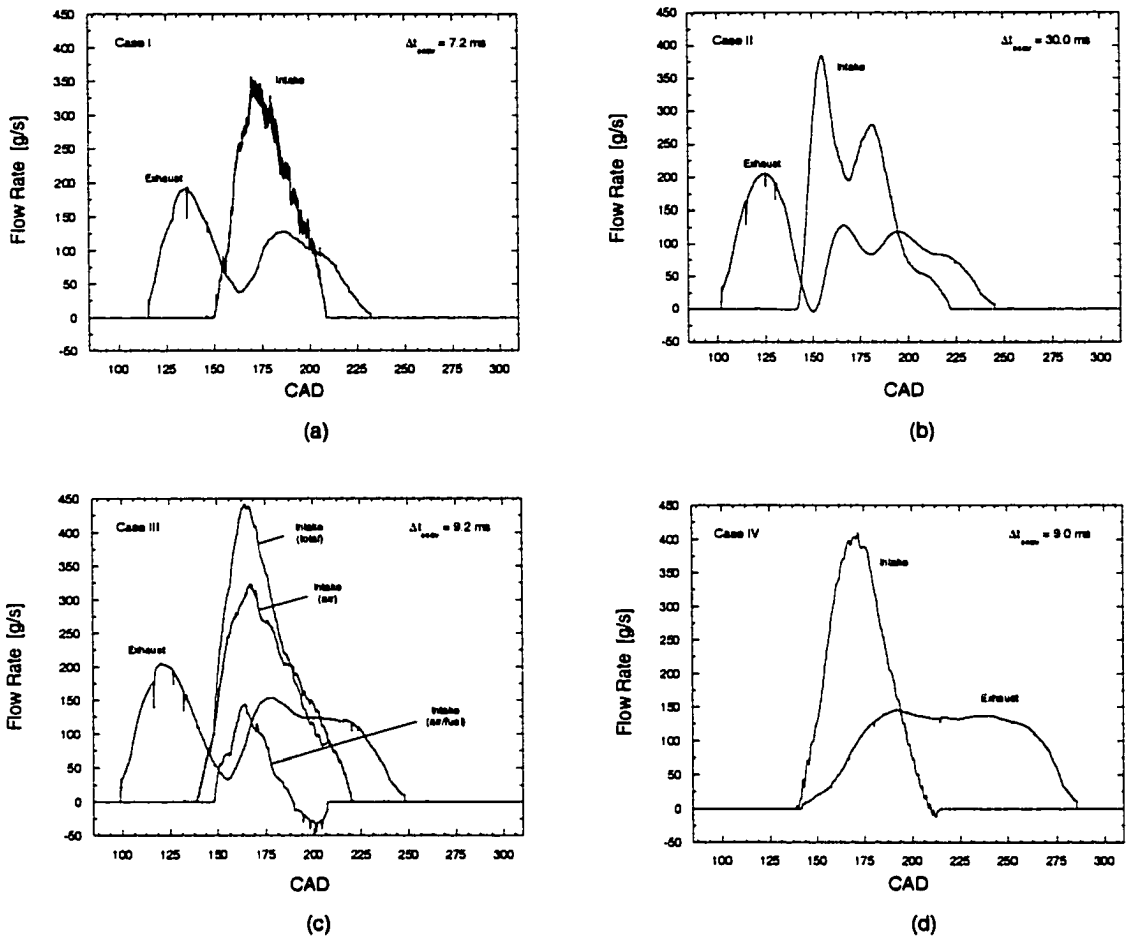

Figure 4.41 – Exhaust and Intake Flow Rates vs. CAD

transparent, and only flow from one intake port is illustrated. (The computational times for these illustrations ranged from 1.5 to 2.5 hours, again using a 1.2 MHz Athelon PC.) Using these figures the differences in in-cylinder and port flow behavior are described.

As can be seen throughout all of these figures, typical uniflow-type behavior is observed, with the incoming charge generating swirling flow toward the top of the cylinder. Two notable changes result however, as the port heights are increased for Cases II, III and IV. First, it can be seen that some of the burned charge becomes trapped just above the piston, and some of this is forced into the intake manifold as the piston begins its compression stroke. (This is similar to that observed in the studies of the piston travel past the intake port bottom.) For the short fuel-rich port in Case III this reverse flow is substantial, as evidenced in Figure 4.41(c).

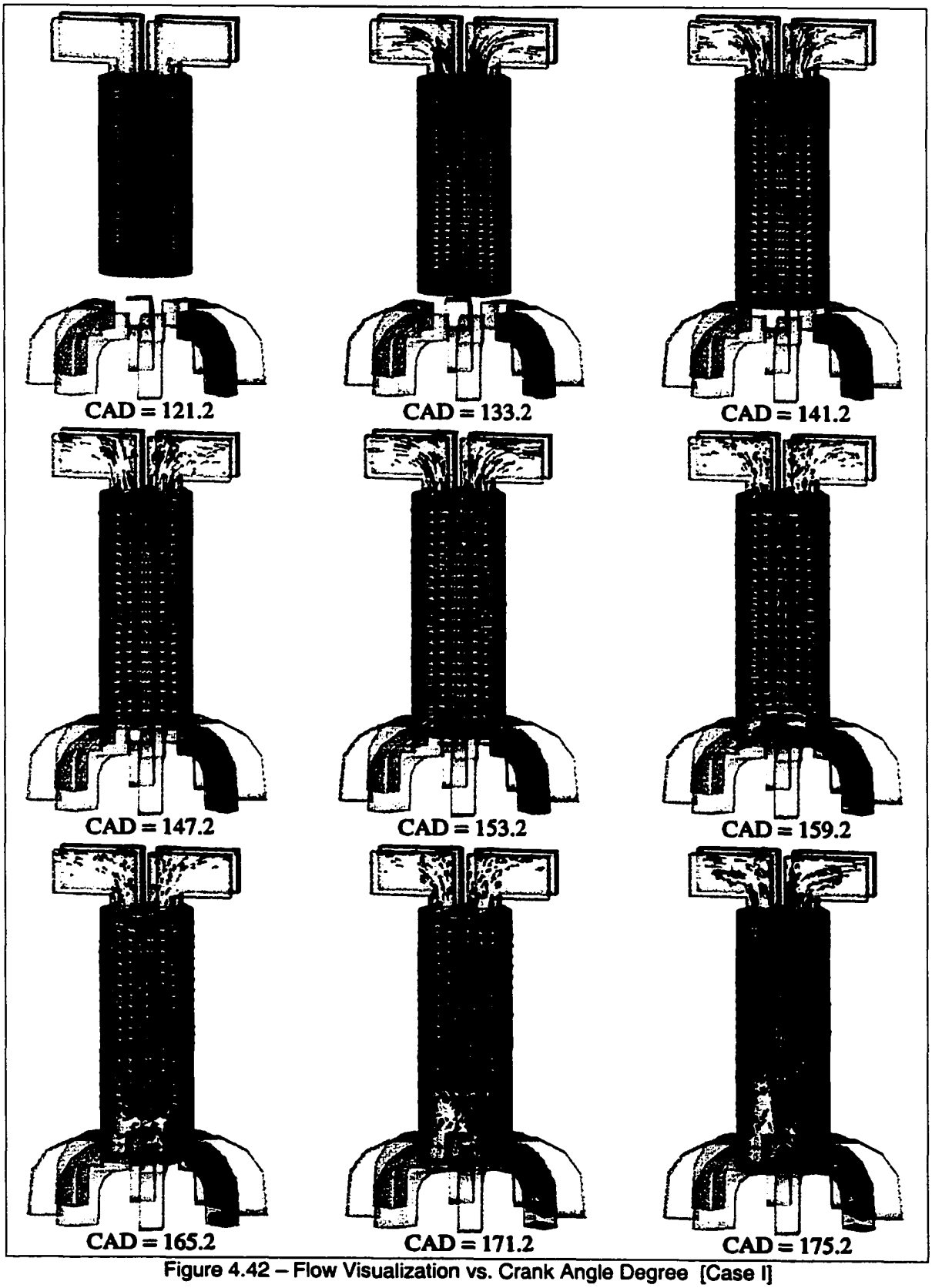

Figure 4.42 – Flow Visualization vs. Crank Angle Degree [Case I]

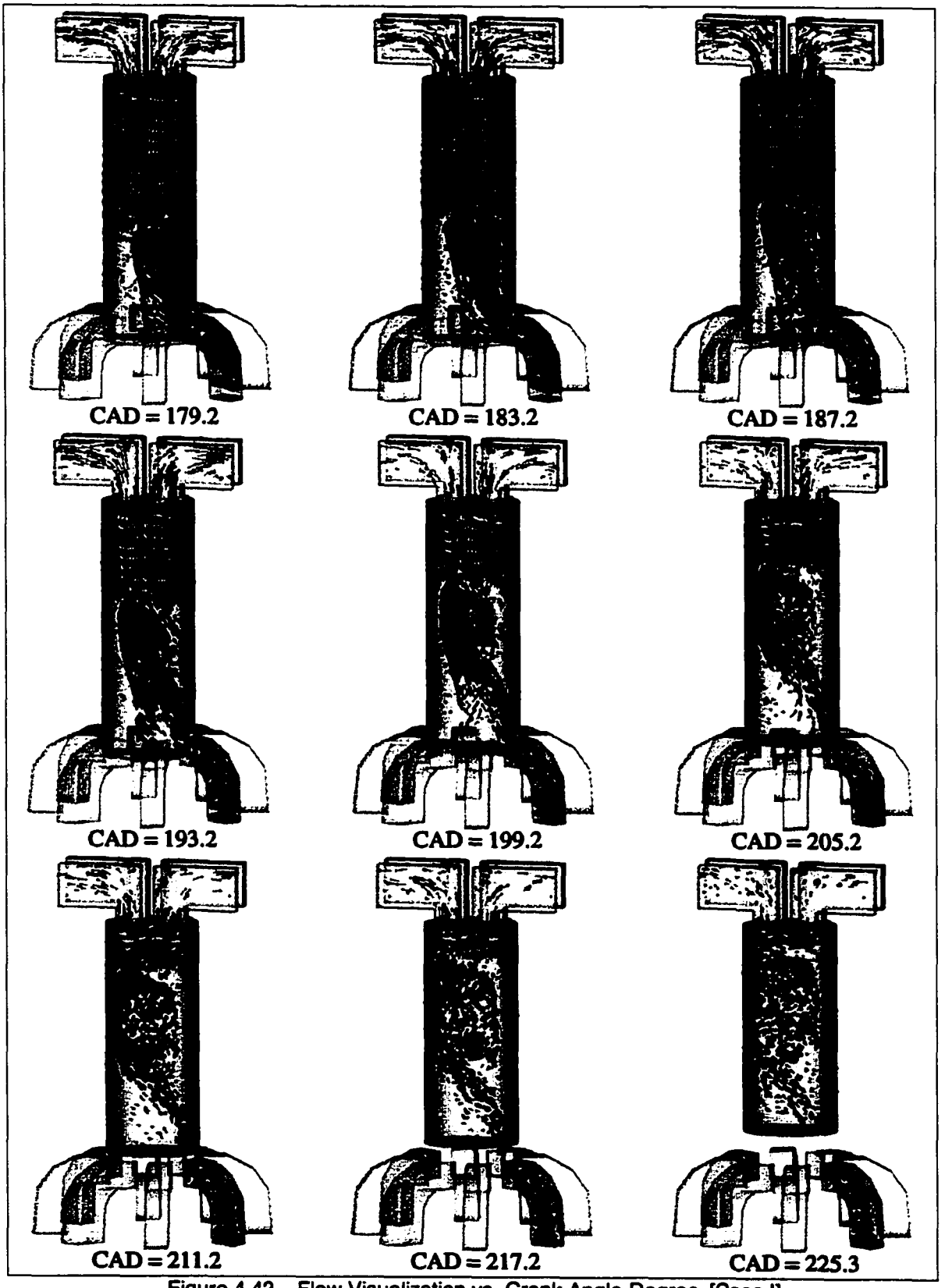

Figure 4.42 – Flow Visualization vs. Crank Angle Degree [Case I]

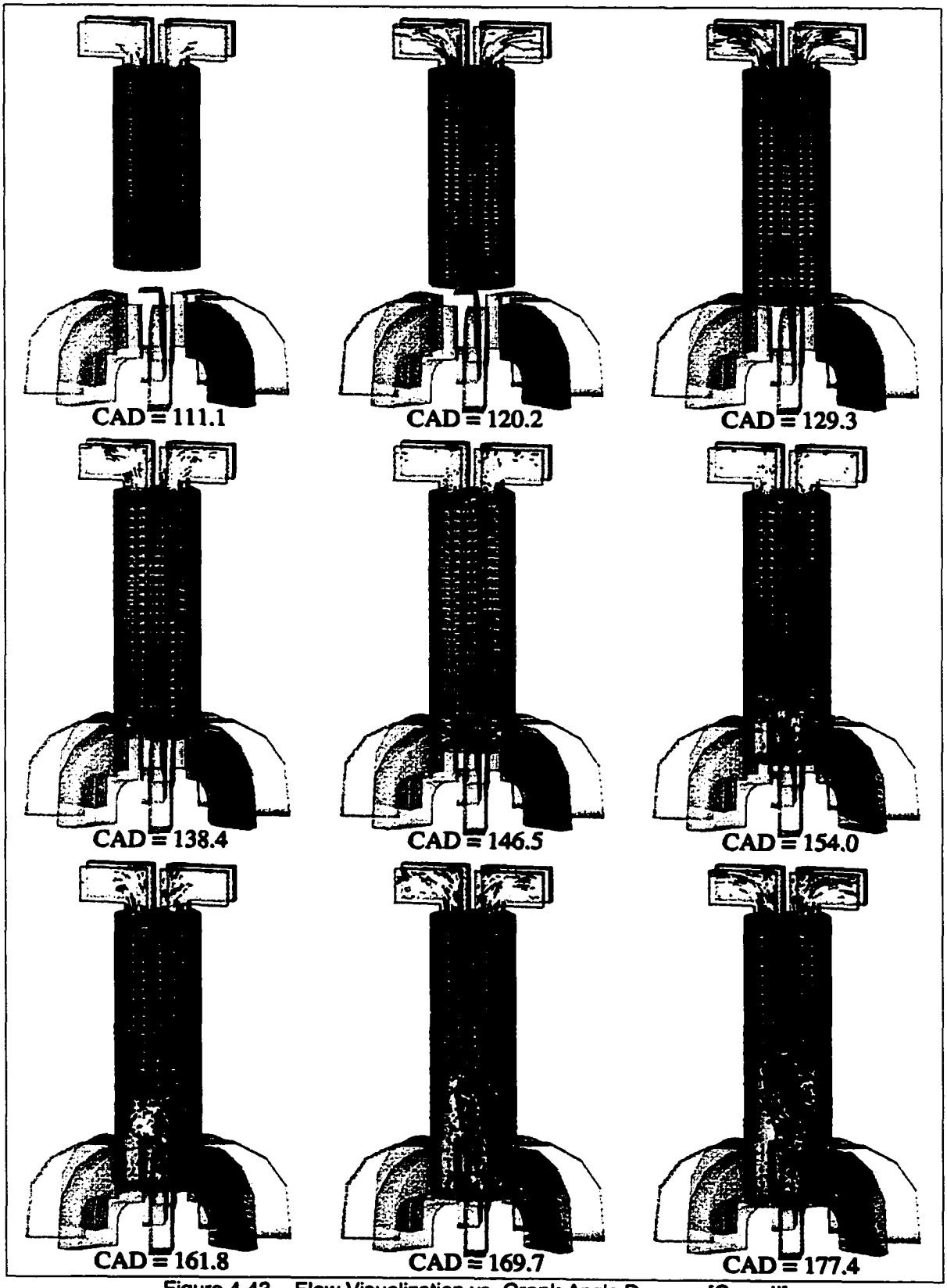

Figure 4.43 – Flow Visualization vs. Crank Angle Degree [Case II]

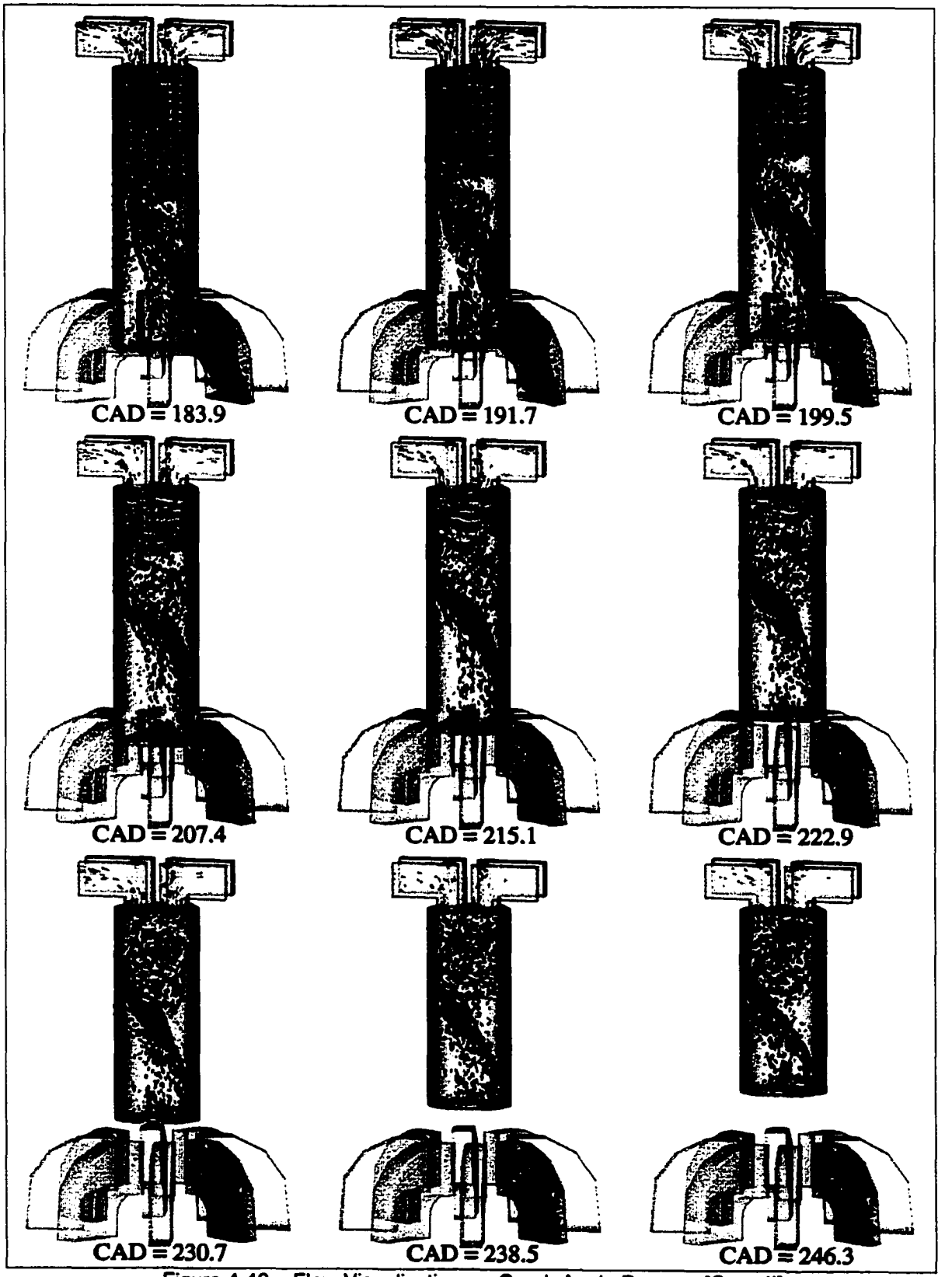

Figure 4.43 – Flow Visualization vs. Crank Angle Degree [Case II]

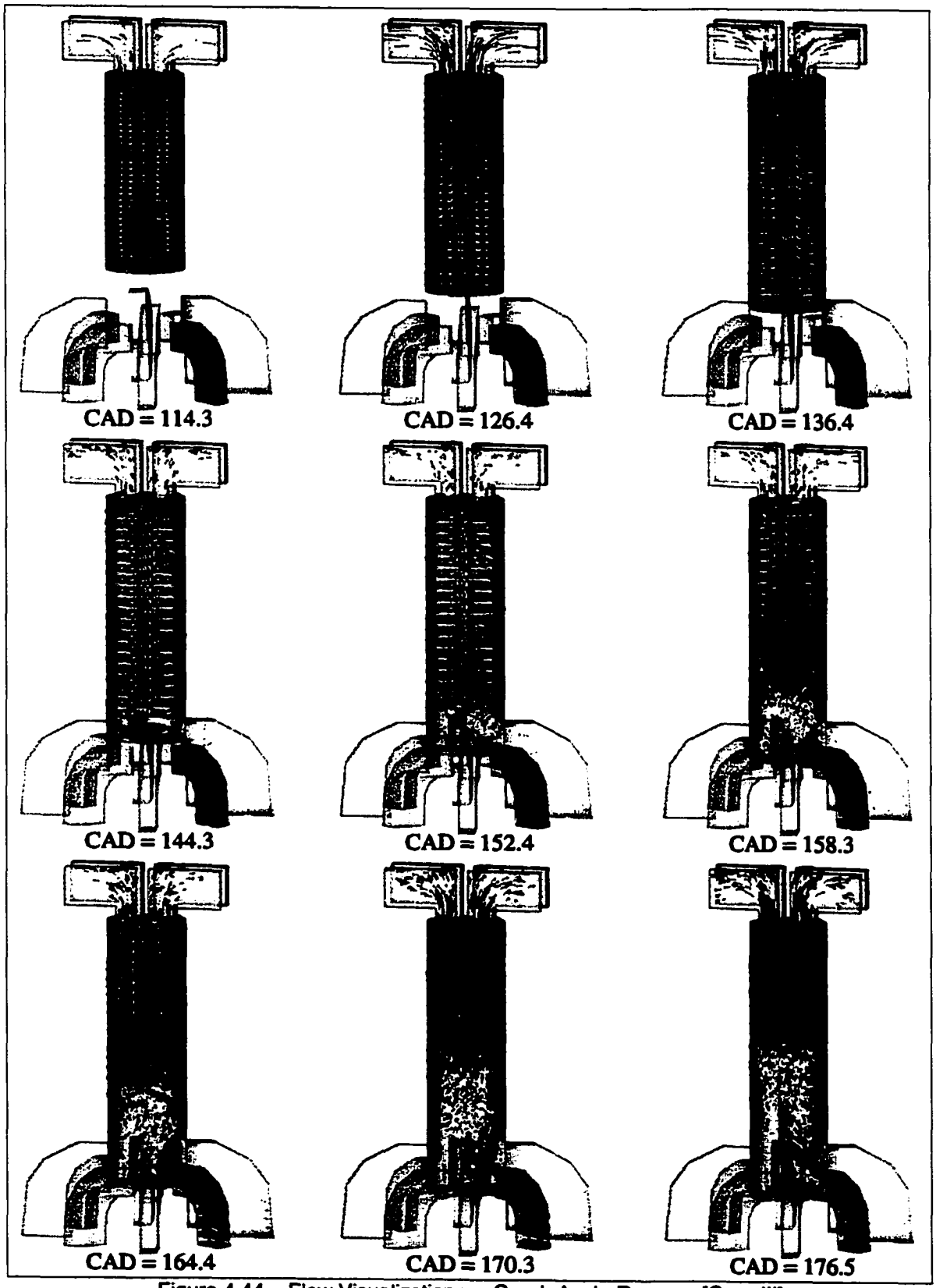

Figure 4.44 – Flow Visualization vs. Crank Angle Degree [Case III]

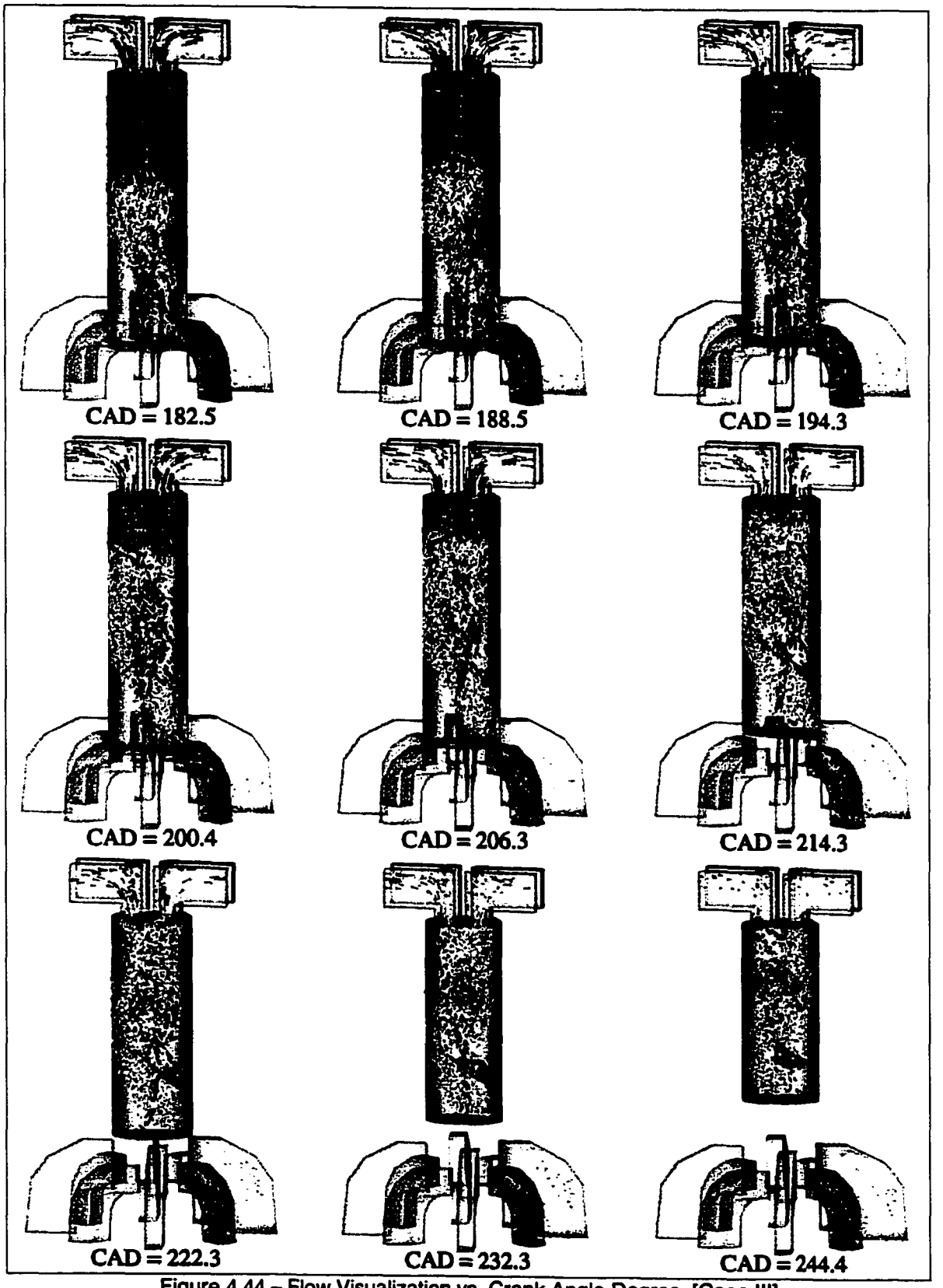

Figure 4.44 – Flow Visualization vs. Crank Angle Degree [Case III]

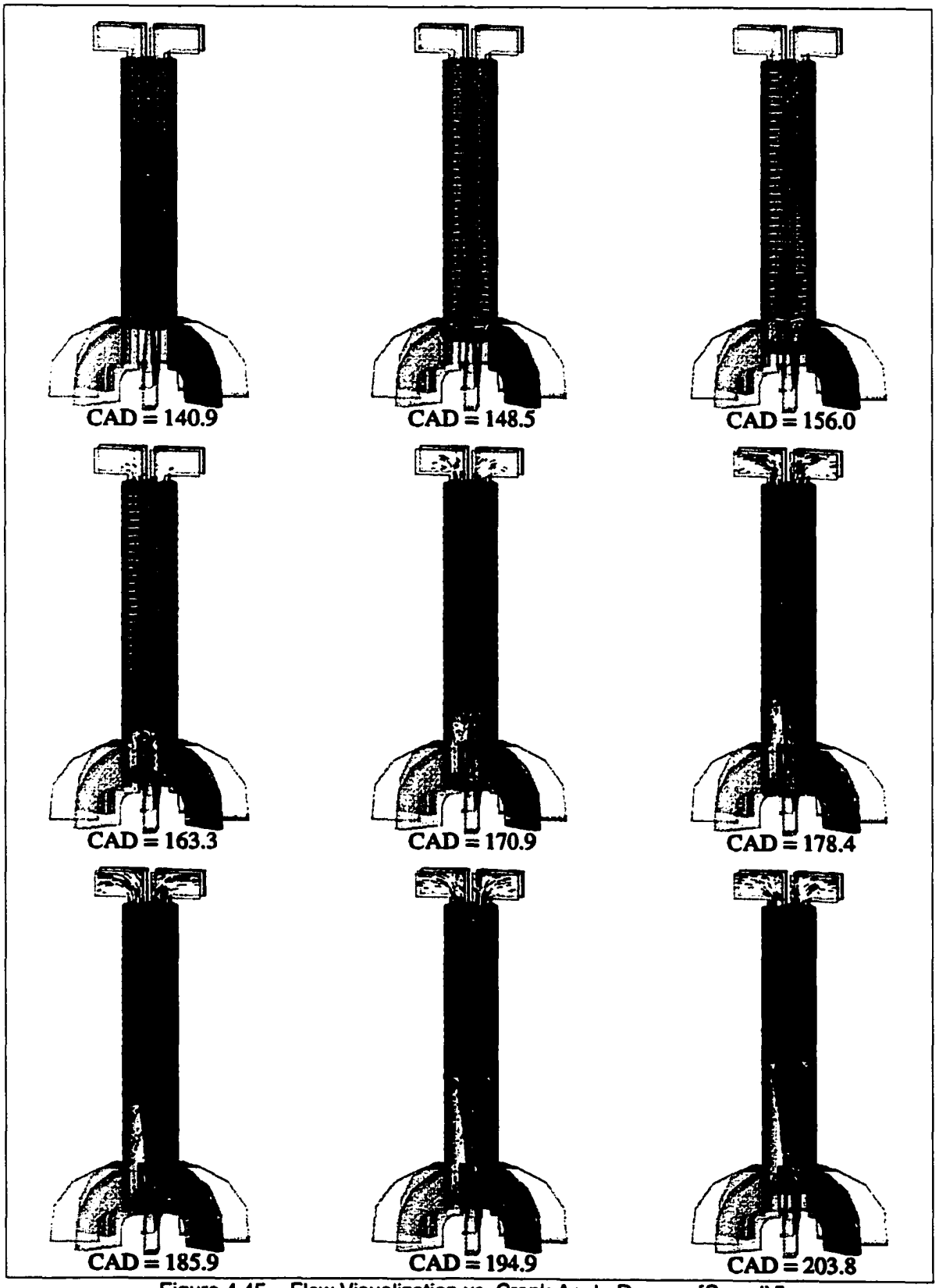

Figure 4.45 – Flow Visualization vs. Crank Angle Degree [Case IV]

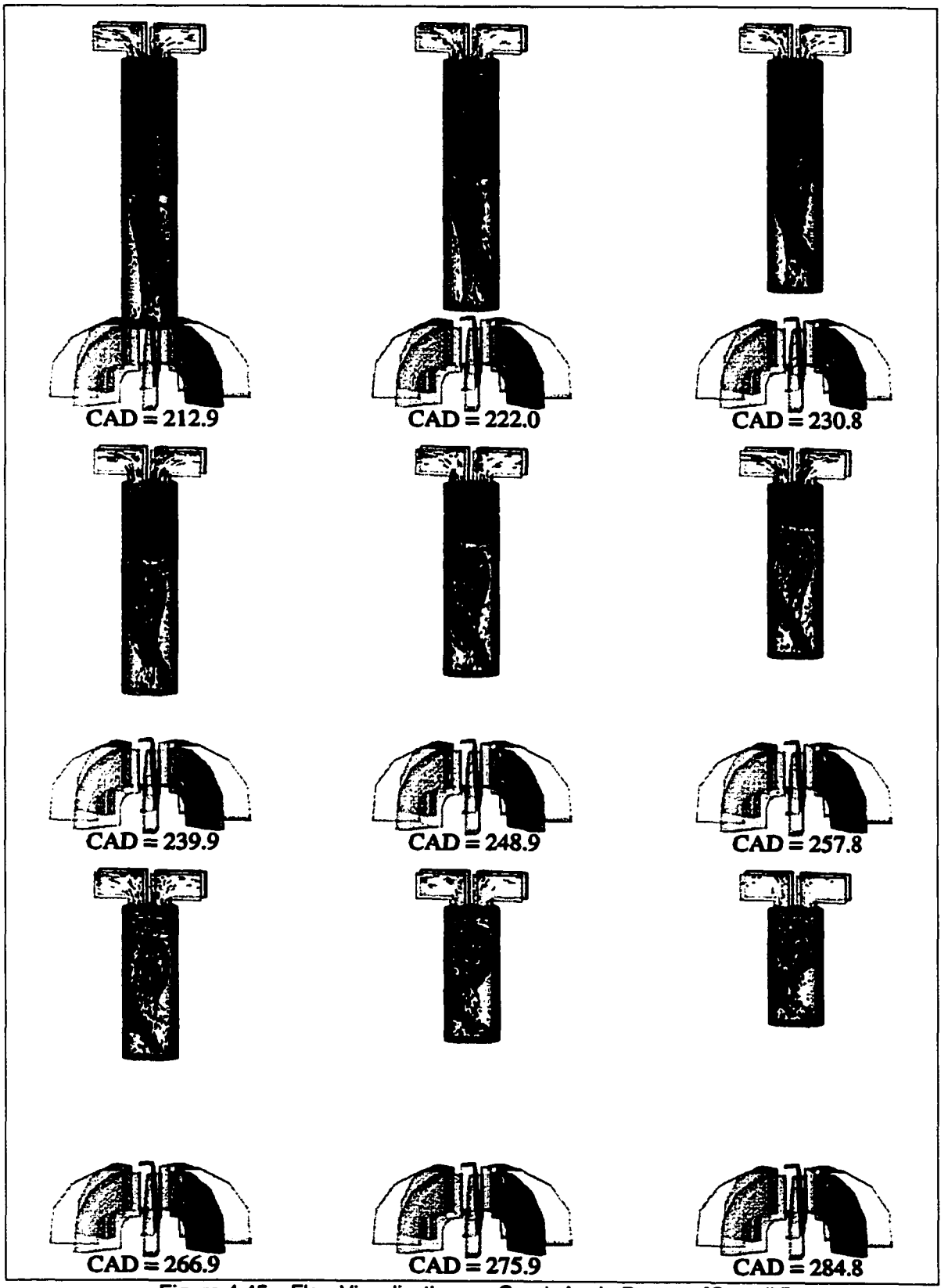

Figure 4.45 – Flow Visualization vs. Crank Angle Degree [Case IV]

A more significant outcome of the tall-port geometry is that the in-cylinder bulk motion becomes less intense, with decreased mixing and lower swirl resulting. [The swirl ratio (SR) drops from 2.9 for Case I to 1.9 for Case II, 2.7 for Case III and 1.7 for Case IV.] This decrease in bulk motion intensity affects both the short-circuiting and NO emissions for these runs.

In terms of short-circuiting, the decrease in in-cylinder bulk motion and associated mixing allows a greater amount of fuel rich gas to penetrate to the exhaust valve region and escape. In terms of NO emissions, the decrease in flow intensity allows greater temperature stratification during the scavenging and compression processes, with this leading to early auto-ignition in parts of the cylinder. This earlier onset of HCCI combustion was noted in Figure 4.40.

Figure 4.46 illustrates the pre-ignition problem by plotting the maximum cylinder temperature versus the instantaneous compression ratio over the engine's cycle. (For this plot the hottest temperature in the cylinder is used. This means that the region (KIVA-3V cells) of maximum temperature is not necessarily located at a single point in the cylinder (say, near the valves), but can move depending on the cylinder conditions throughout the cycle (e.g. if a fuel rich region combusts). However, for these simulations, this region is generally in the cylinder core, near the valves.)

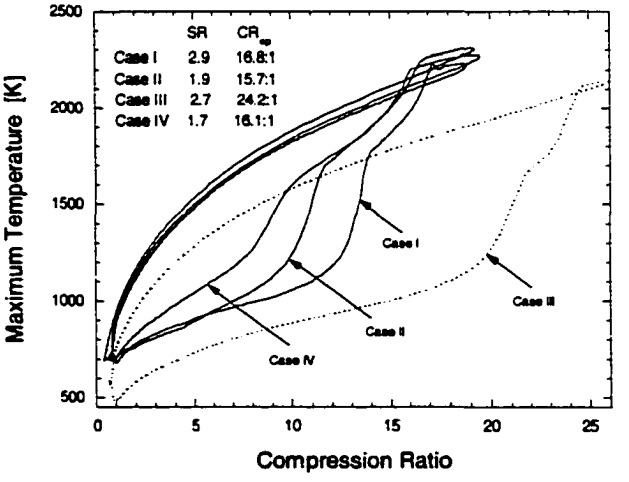

Figure 4.46 – Maximum Cylinder Temperature vs. Compression Ratio

What can be seen in this figure is that, due to the decreased in-cylinder mixing, some parts of the cylinder autoignite before the bulk of the cylinder charge. For Case I the earliest ignition point is at CR=14:1, for Case II this decreases to CR=11:1, and for Case IV this is closer to CR=9:1. For these three arrangements the bulk of the cylinder combusts, as determined by the maximum rate of pressure change, near CR=16.2:1. [Case III is included in this plot for reference, where the bulk combustion occurs at 24.2:1. The reduction in maximum temperature, along with the reduced time spent at high compression ratio, relative to the standard case, accounts for the reduced NO emissions for this case.]

Although the pre-ignition problem has only a slight impact on the cycle efficiency for these runs, the NO production increases substantially since the hotter regions auto-ignite and then are over-compressed. This is most significant for Case II where the piston's velocity is slower and therefore the over-compression is sustained for a longer period of time.

COMPRESSOR WORK – The effects of the compressor and friction work on the overall cycle efficiencies are discussed next. Table 4.8 above shows that the compressor work fraction decreases for Case II (-25%) while it increases for Case III (+37%). This was expected due to the lower charging pressure and higher delivery ratio, respectively. However, with respect to η_{TH} these changes are offset by changes in the thermodynamic cycle. For Case II the conversion efficiency is decreased due to early ignition problems, while for Case III it is higher due to the higher compression ratio achieved.

FRICTION WORK – Regarding the friction work, it can be seen that the only significant change occurs with the over-compression configuration (+200%). This is due to the increased piston velocity used with this arrangement. However, this increased friction work is offset by an increase in the conversion efficiency, in this case due to the additional charge expansion.

Design 'Robustness'

In an attempt to assess the 'robustness' of these four configurations, several simulations were run, slightly varying the input conditions of equivalence ratio and piston frequency (±10%). The objective of these runs was to determine how the engine's performance is affected by slight changes in the operating conditions – a useful analysis for actual engine operation.

The details of these results can be found in Appendix E, however a summary is presented in Table 4.9. Comparing the operating schemes with regard to this final simulation series, it can be seen that the changes in emissions are more significant for Case II, relative to Case I. The thermal efficiency for Case II, however, seems to be slightly more stable for these variations. For Case III the thermal efficiency is also stable, while the changes in emissions are comparable to the standard configuration.

		$\downarrow f$	$\uparrow f$	$\downarrow \phi$	$\uparrow \phi$
CASE I	η_{TH}	+5.5%	-7.9	-1.6	-4.1
	C_3H_8	+217 ppm	-52	-13	+28
	NO	+52 ppm	-8	-224	+447
CASE II	η_{TH}	+2.4	-3.3	+1	-0.8
	C_3H_8	+409	-119	-50	+44
	NO	+85	-37	-531	+1538
CASE III	η_{TH}	+1.4	-1.8	-0.6	+0.8
	C_3H_8	+277	-94	-36	+17
	NO	+103	-39	-67	+243
CASE IV	η_{TH}	NA	NA	-1.5	NA
	C_3H_8			0	
	NO			-383	

Table 4.9 – Change in Operating Results

An important result of this simulation series was that the over-expanded configuration (as designed here) is extremely sensitive to some types of fluctuations in the operating conditions. For three of the small changes investigated the operating cycle became unstable, with large cycle-to-cycle variations in delivery ratio and power output. A plot of the delivery ratio over seven computational cycles for the high ϕ run is presented in Figure 4.47 to illustrate this point.

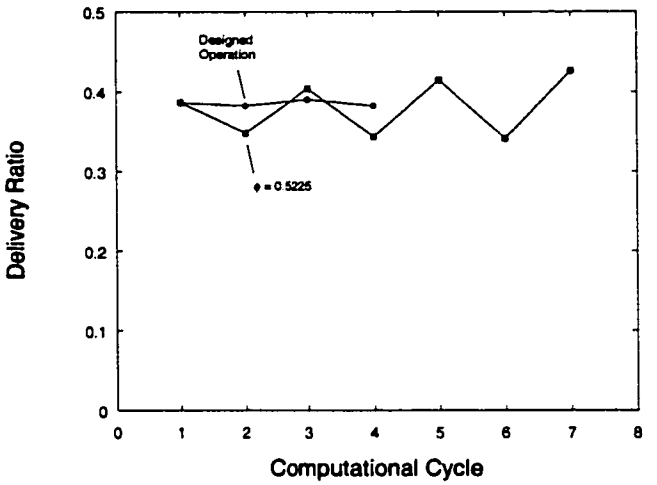

Figure 4.47 – Delivery Ratio vs. Computational Cycle

Similar inconsistent behavior has been observed in actual Atkinson-cycle engine operation [85,86], however, the degree of variation was not as severe as with the KIVA-3V calculations. This may simply be a numerical problem with the problem setup, or due to the configuration utilized for this study where there was absolutely no blowdown into the exhaust port, and the cylinder was over-expanded just to the intake charging pressure (for the designed condition). The experimental investigations cited did not use such an extreme expansion ratio, and this may account for the differences. Nonetheless, rigorous control of the input conditions would be required for effective, and stable operation with the over-expansion scheme.

As an additional point, it can be seen in the table above that the increases in emissions can be substantial for some of the operating variations. This may be important in actual engine operation.

Summary of Final Simulations

The final simulations examined the influence of the scavenging process on the efficiency and emissions performance for four different operating schemes (a standard uniflow

arrangement, a low charging pressure / low frequency option, a stratified scavenging configuration, and an over-expansion geometry). Based on the operating conditions investigated it seems that a stratified scavenging configuration can most effectively maximize the engine's thermal efficiency while sufficiently controlling the short-circuiting and NO emissions. The operating compression ratio is substantially increased with this configuration, with the improvements in thermal efficiency overcoming the increased pumping power. The maximum temperature is effectively reduced since the cylinder is better flushed, with less hot residual remaining throughout the cylinder, and that left more diluted with cool fresh gas. It seems that the rich fuel-air charge can be adequately mixed after EVC to ensure rapid, TDC HCCI combustion.

The KIVA-3V calculations also suggested that the engine's exhaust emissions can be significantly affected by the in-cylinder flow in terms of fuel penetration to the exhaust valve region, and inadequate mixing through the scavenging process and subsequent compression stroke, which can result in substantial temperature stratification, generally in the core region near the valves.

In addition, the simulations suggested that in the premixed operating mode, with low ϕ and moderate η_{sc}, the production of NO is more dependent on hot residual initiated pre-ignition and subsequent over-compression, than on the HCCI combustion of fuel-rich regions within the cylinder.

Finally, the over-expanded design was calculated to be very sensitive to slight changes in the operating conditions with this leading to large cycle-to-cycle variations, and poor performance. Rigorous control of the operating conditions would be required for effective, and stable operation of this scheme.

CHAPTER V SUMMARY AND CONCLUSIONS

The free piston IC engine-generator described in Chapter I represents a significant advancement in the thermal efficiency and exhaust emissions potential of electric power generators. However, the two-stroke scavenging process used to recharge the engine is key to realizing the efficiency and emissions goals of the device. Inadequate charge preparation can degrade the HCCI combustion and cause high NOx levels, while insufficient trapping can lead to excessive short-circuiting emissions. These issues must be resolved through the design.

The free piston engine's unique operating characteristics, including single speed operation and the use of high CR, HCCI combustion allow the design process to be approached from a unconventional perspective. Consideration for speed variation issues, such as changing delivery ratios and exhaust/intake wave characteristics, are reduced, while concerns for adequate spark ignition and flame propagation, or spray formation and fuel diffusion are not relevant. The main drivers for the design are the requirements of high thermal efficiency and low exhaust emissions.

To ensure that the engine's performance goals can be achieved, the scavenging system was configured using a computational approach. CFD, 0D and 1D modeling were employed to describe critical engine processes, and single step parametric variations were used to narrow the design possibilities. KIVA-3V calculated the gas flow through the engine, while the fresh charge pressurization, and piston-ring friction processes were computed using 0D and 1D formulations, respectively. The post-processing software, Ensight, allowed the in-cylinder and port dynamics to be visualized, and more thoroughly understood. Using these tools, a comprehensive study of the scavenging design was undertaken and the preliminary steps to achieving an optimal configuration were completed.

During the course of this study a wide range of design options were investigated including the use of loop, hybrid-loop and uniflow scavenging methods, different charge delivery options, and various operating schemes. Parameters such as the intake/exhaust port arrangement, valve lift/timing, charging pressure and piston frequency were varied. A host of initial simulations gave way to computations with a few select operating schemes. Operating arrangements including a standard uniflow configuration, a low charging pressure / low frequency option, a stratified scavenging geometry, and an over-expansion (Atkinson) cycle were studied, with an optimal configuration concluded from these simulations. A summary of the computational results is presented next, with an outline for the optimal configuration given after that.

Summary of Computational Results

Scavenging Methods

The loop scavenging design represented a mechanically simple means of recharging the engine. However, the long stroke-to-bore ratio utilized for the engine (2:1) dramatically lengthened the path that the scavenging gases must travel, while the in-cylinder dynamics were complicated by a helical motion generated by the opposing, incoming gases. These features degraded the process with a significant amount of residual gas becoming entrained within the fresh charge.

To improve the performance of this arrangement, variations in the intake charge pressure, intake ϕ, exhaust/intake port area/timing, and piston frequency were investigated. The computations revealed that only the charging pressure and piston frequency could significantly improve the flushing capabilities; however, as the scavenging efficiency was sufficiently increased the trapping losses became unacceptable. The cylinder could not be adequately recharged without the significant loss of unburned fuel.

The hybrid-loop design also represented a mechanically simple arrangement, with the possibility of improving the trapping characteristics relative to the loop geometry since the exhaust ports close before the intake ports. However, with this configuration backflow into the intake

manifold was significant, while flow oscillations across the exhaust port altered the incoming flow patterns preventing the desired scavenging loop from forming. Burned charge at the top and in the core of the cylinder was not flushed from the engine.

To improve the flow behavior, variations in the number of intake/exhaust ports, the intake charge pressure, exhaust port area/timing, and piston frequency were investigated. The computations revealed that only a decrease in piston frequency could significantly alter the in-cylinder dynamics. However, this was at the cost of substantial trapping losses. In none of the simulations attempted could the swirling-loop be created, while the resulting charge was extremely stratified at TDC, with the fresh charge concentrated near the walls.

The uniflow scavenging design represented a final option attempted to achieve acceptable scavenging performance without the employment of a complicated fuel delivery system. With this geometry scavenging could be more effective since exhaust valves are located in the cylinder head, therefore ensuring better flushing of the top of the cylinder. The intake ports could be configured to generate plug flow, thereby minimizing burned/unburned charge interaction and the short-circuiting losses associated with this. However, concerns remained regarding the ability to simultaneously flush the cylinder core while sweeping the burned charge from the walls, as well as the uniformity of the trapped charge at TDC.

To address these issues, and to maximize the scavenging and trapping potential for the uniflow design, simulations were run investigating the effects of exhaust valve lift/timing, intake port arrangement (incoming angles, number of ports, area/timing), piston frequency and piston travel past the intake port bottom. The computations revealed the high scavenging and trapping efficiency goals of the engine can be met, and that the process can be optimized under the following conditions: the exhaust/intake timings are matched so that the cylinder pressure blows down to the charging pressure by IPO; the intake ports have sufficient flow area to recharge the cylinder; the ports are oriented with uniform swirl angles of about 15°; and the piston frequency is adjusted to allow adequate discharge of the burned gases.

Charge Delivery

The charge delivery system was investigated to determine the influence of the compressor/tank configuration on the pumping power consumption, and the in-cylinder dynamics that result. The computations revealed that the compressor inlet/outlet flow areas, and the tank size and temperature are significant parameters in the design. The delivery process can be maximized by utilizing a large, cooled tank with sufficient flow area allowed through the internal compressor system.

Operating Schemes

Three operating schemes investigated in this study (low charging pressure, stratified scavenging, over-expansion cycle) represented various means of improving the engine's overall efficiency relative to a standard configuration (by decreasing the pumping power, increasing the operating compression ratio, and decreasing the blowdown losses, respectively). However, the different geometries employed led to changes in the in-cylinder flows thereby affecting the overall engine cycle and the exhaust emissions.

The most significant change was a decrease in the bulk flow intensity, and swirl due to the taller intake ports used on the three non-standard configurations. Because of this change, the mixing throughout the scavenging and compression processes decreased. As a result, the cylinder charges were more thermally stratified, while the fuel more easily escaped through the exhaust valves. Increased thermal stratification led to auto-ignition of the charge before TDC, which resulted in decreased conversion efficiency, and increased NO as the combusted gases were over-compressed.

For the low pressure case, the improved pumping characteristics were negated by the pre-ignition problem, and the emissions were increased relative to the standard configuration. For the stratified scavenging case the improved flushing counteracted the decreased bulk flow intensity, ensuring a significantly higher operating compression ratio. The efficiency of the cycle was improved, even after accounting for the increased pumping power. The emissions were similar to the standard case, while mixing of the rich fuel-air charge seemed sufficient for uniform,

TDC HCCI combustion. For the over-expansion case the early ignition problem, and increased friction work slightly degraded the gains made by over-expanding the charge; however, the efficiency was still better than the standard case. On the other hand, both the NO and short-circuiting emissions were increased for this configuration, again due to the mixing problems.

The low pressure, and stratified scavenging designs responded better (than the standard geometry) to small fluctuations in the operating conditions, achieving consistent performance over the range of parameters studied. The over-expansion design however, was poorly equipped to handle such fluctuations, leading to large cycle-to-cycle variation in delivery ratio and power output. The use of this operating scheme seems limited.

Optimal Configuration

The computational results indicated that the optimal configuration for the engine's scavenging system utilizes a uniflow geometry in combination with a large delivery tank to supply a stable, low temperature (~300K) charge. A stratified scavenging scheme should ensure the highest possible thermal efficiency (through increased compression ratio operation), however, the control of trapping losses, and thus unburned fuel emissions, through small variations in the engine's operating frequency may prove challenging. Conversely, this arrangement should be capable of providing adequate mixing during compression to enable rapid TDC HCCI combustion, while responding well to slight changes in the operating conditions.

Design Concerns

Based on the KIVA-3V calculations, two areas of concern have been highlighted. For premixed, low f operation, the predominant formation of NO is through early auto-ignition in a thermally stratified cylinder, followed by subsequent over-compression. It seems that this path can be more important than combustion in fuel rich regions. In-cylinder flows are important for NO generation and as such, control of the mixing after EVC is expected to be essential for NO emissions management.

With respect to short-circuiting emissions, the stratified scavenging arrangement was calculated to be susceptible to large increases in unburned fuel emissions as the engine's frequency changes, this due to the use of fuel-rich stratified charges. Without adequate control, these charges could easily escape through the exhaust valves before EVC. One option to limit this may be to utilize low pressure, port injection, late in the scavenging cycle, in combination with a uniform intake manifold geometry (i.e. identical ports). The injection timing and duration could be adjusted depending on the operating conditions, and as a result short-circuiting emissions may be better managed.

Future Work

The results of the computational investigation are promising, however, continued development of the scavenging design should proceed towards verifying the simulated output using experimental techniques. Though many aspects of KIVA's two-stroke cycle capabilities have been confirmed through previous studies, additional research would be beneficial, especially for this constant speed/power operating regime. A single-cycle experiment could provide useful information regarding KIVA-3V's accuracy and limitations. Mixing and combustion issues however, can only be assessed during actual operation.

In addition, analyses should be undertaken to investigate the effect of intake/exhaust manifold configurations, and the propagation of pressure waves through the system, on the multi-dimensional computational results. This could validate some of the simplifications assumed in this dissertation.

Finally, two options not investigated here were port fuel injection and turbocharging. The benefits of fuel injection have been discussed. Turbocharging could significantly improve the power density of the engine-generator (especially important due to the engine's low ϕ operation) and possibly improve its operating efficiency, and therefore it should be explored.

REFERENCES

1. Van Blarigan, P., Paradiso, N. and Goldsborough, S. "Homogeneous Charge Compression Ignition with a Free Piston: A New Approach to Ideal Otto Cycle Performance," SAE Paper 982484, 1998.

2. Heywood, J. and Sher, E., The Two-Stroke Cycle Engine: Its Development, Operation, and Design, Taylor & Francis, 1999.

3. Taylor, C. F., The Internal Combustion Engine in Theory and Practice, The M.I.T. Press, 1994.

4. Nagao, F. and Shimamoto, Y., "The Effect of Crankcase Volume and the Inlet System on the Delivery Ratio of Two-Stroke Cycle Engines," SAE Paper 670030, 1967.

5. Dabadie, J., Perotti, M. and Keribin, Ph., "Prediction of Two-Stroke Engine Performance by Unsteady Gas Dynamic Calculations," A New Generation of Two-Stroke Engines for the Future? P. Duret (ed.), Editions Technip, 1993.

6. Blair, G., "The Correlation of Theory and Experiment for Scavenging Flow in Two-Stroke Cycle Engines," SAE Paper 881265, 1988.

7. Nomura, K., Hirano, S., Gotoh, T. and Motoyama, Y., "Improvement of Fuel Consumption with Variable Exhaust Port Timing in a Two-Stroke Gasoline Engine," SAE Paper 850183, 1985.

8. Negurescu, N., Pana, C., Popa, M. and Racovitza, A., "Variable valve – Control systems for spark ignition engine," SAE Paper 2001-01-0671, 2001.

9. Ceccarani, M. and Rebottini, C., "Optimization of volumetric efficiency by the management of gas dynamic phenomena for a high performance V12 engine," SAE Paper 95A168, 1995.

10. Tsuchiya, K., Hirano, S., Okamura, M. and Gotoh, T., "Emission Control of Two-Stroke Motorcycle Engines by the Butterfly Exhaust Valve," SAE Paper 800973, 1980.

11. Sher, E., Hacohen, Y., Refael, S. and Harai, R., "Minimizing Short-Circuiting Losses in 2-S Engines by Throttling the Exhaust Pipe," SAE Paper 901665, 1990.

12. Saxena, M., Mathur, H. and Radzimirski, S., "A Stratified Charging Two-Stroke Engine for Reduction of Scavenged-Through Losses," SAE Paper 891805, 1989.

13. Carson, C., Kee, R., Kenny, R. and Blair, G., "The Reduction of Exhaust Emissions from Two-Stroke Engines," SAE Paper 934035, 1993.

14. Zahn, W., Rosskamp, H., Raffenber, M. and Klimmek, A., "Analysis of a Stratified Charging Concept for High-Performance Two-Stroke Engines," SAE Paper 2000-01-0900, 2000.

15. Stan, C. and Lefebvre, J., "Development of a Direct Injection Concept for Two Wheelers Equipped with Two Stroke Engines," SAE Paper 1999-01-1248, 1999.

16. Gold, M., Stokes, J., Morgan, R., Heikal, M., de Sercey, G. and Begg, S., "Air-Fuel Mixing in a Homogeneous Charge DI Gasoline Engine," SAE Paper 2001-01-0968, 2001.

17. Corcione, F., Rotondi, R., Gentili, R. and Migliaccio, M., "Modeling the Mixture Formation in a Small Direct-Injected Two-Stroke Spark-Ignition Engine," SAE Paper 970364, 1997.

18. Moriyoshi, Y., Mori, K., Morikawa, K. and Takimoto, H., "Mixture Formation Analysis of a Schnurle-Type Two-Stroke Gasoline DI Engine," SAE Paper 2001-01-1091, 2001.

19. Ishibashi, Y. and Asai, M., "A Low Pressure Pneumatic Direct Injection Two-Stroke Engine by Activated Radical Combustion Concept," SAE Paper 980757, 1998.

20. Gentili, R., Frigo, S., Tognotti, L., Habert, P. and Lavy, J., "Experimental Study on ATAC (Active Thermo-Atmosphere Combustion) in a Two-Stroke Gasoline Engine," SAE Paper 970363, 1997.

21. Stanglmaier, R. and Roberts, C., "Homogeneous Charge Compression Ignition (HCCI): Benefits, Compromises, and Future Engine Applications," SAE Paper 1999-01-3682, 1999.

22. Blair, G. P., The Basic Design of Two-Stroke Engines, Society of Automotive Engineers, 1993.

23. Jante, A., "Scavenging and Other Problems of Two-Stroke Cycle Spark-Ignition Engines," SAE Paper 680468, 1968.

24. Montville, D. and Jawad, B., "An Extended Jante Test Procedure for Two-Stroke Piston-Ported Engine Development," SAE Paper 941679, 1994.

25. Wang, Z., "Flow Visualization and Analyses of Two-Stroke Loop Scavenging Diesel," SAE Paper 972739, 1997.

26. Sammons, H., "A Single-cycle Test Apparatus for Studying 'Loop Scavenging' in a Two-stroke Engine," Proceedings of the Institution of Mechanical Engineers, 161, 233-246, 1966.

27. Sher, E., "Investigating the Gas Exchange Process of a Two-Stroke Cycle Engine with a Flow Visualization Rig," Israel Journal of Technology, 20, 127-136, 1982.

28. Sanborn, D. S. and Roeder, W. M., "Single Cycle Simulation Simplifies Scavenging Study," SAE Paper 850175, 1985.

29. Asanuma, T. and Yanagihara, S., "Gas Sampling Valve for Measuring Scavenging Efficiency in High-Speed Two-Stroke Engines," SAE Paper 620540, 1962.

30. Nuti, M. and Martorano, L., "Short-Circuit Ratio Evaluation in the Scavenging of Two-Stroke S.I. Engines," SAE Paper 850177, 1985.

31. Hashimoto, E., Tottori, T. and Terata, S., "Scavenging Performance Measurements of High speed Two-Stroke Engines," SAE Paper 850182, 1985.

32. Hilbert, H. and Falco, R., "Measurements of Flows During Scavenging in a Two-Stroke Engine," SAE Paper 910671, 1991.

33. Bopp, S., Cousyn, B., Green, R. and Witze, P., "Experimental Study of the Scavenging and Combustion Processes in a Two-Stroke Cycle Research Engine," SAE Paper 920183, 1992.

34. McKinley, N., Fleck, R. and Kenny, R., "LDV Measurement of Transfer Port Efflux Velocities in a Motored Two-Stroke Cycle Engine," SAE Paper 921694, 1992.

35. Miles, P., Green, R., and Witze, P., "In-Cylinder Gas Velocity Measurements Comparing Crankcase and Blow Scavenging in a Fired Two-Stroke Cycle Engine," SAE Paper 940401, 1994.

36. Andersson, Ö., Juhlin, G., Ekenbert, M., Johansson, B, and Aldén, M., "Crank Angle Resolved HC-Detection Using LIF in the Exhausts of Small Two-Stroke Engines Running at High Engine Speed," SAE Paper 961927, 1996.

37. Wagner, V., Ipp, W., Wensing, M. and Leipertz, A., "Fuel Distribution and Mixture Formation Inside a Direct-Injection SI Engine Investigated by 2D Mie and LIEF techniques," SAE Paper 1999-01-3659, 1999.

38. Benson, R., "A New Gas Dyamic Model for the Gas Exchange Process in Two Stroke Loop and Cross Scavenged Engines," *International Journal of Mechanical Engineering Science*, **19**, 693-711, 1977.

39. Gupta, C. and Mehta, P., "Assessment of Scavenging Models for Small Two Stroke Cycle Engines," SAE Paper 911249, 1991.

40. Merker, G. and Gertle, M., "Evaluation on Two Stroke Engines Scavenging Models," SAE Paper 970358, 1997.

41. Desantes, J., Boada, F. and Corberán, J., "Exhaust Pipe Design Method for the Optimization of the Scavenging Process," SAE Paper 850083, 1985.

42. Thornhill, D. and Fleck, R., "A Generic Engine Simulation Program Applied to the Development of a V6 Automotive Two-Stroke Engine," SAE Paper 940396, 1994.

43. Kong, S., Ayoub, N. and Reitz, R., "Modeling Combustion in Compression Ignition Homogeneous Charge Engines," SAE Paper 920512, 1992.

44. Haworth, D., Huebler, M., El Tahry, S., and Matthes, W., " Multidimensional Calculations for a Two-Stroke-Cycle Engine: A Detailed Scavenging Model Validation," SAE Paper 932712, 1993.

45. Widener, S., Freitas, C. and McDermomtt, M., "Analysis of a Novel Two-Stroke Engine Scavenging Arrangement: The Neutron Engine," SAE Paper 952140, 1995.

46. Kang, K., Lee, J., Jeong, Y., Huh, K. and Jeong, H., "The Characteristics of Scavenging Flow in a Poppet-Valve Type 2-Stroke Diesel Engine by Using RSSV System," SAE Paper 960368, 1996.

47. McLandress, A., Emerson, R., McDowell, P. and Rutland, C., "Intake and In-Cylinder Flow Modeling Characterization of Mixing and Comparison with Flow Bench Results," SAE Paper 960635, 1996.

48. Delhaye, B. and Cousyn, B., "Computation of Flow and Combustion in Spark Ignition Engine and Comparison with Experiment," SAE Paper 961960, 1996.

49. Raghunathan, B. and Kenny, R., "CFD Simulation and Validation of the Flow within a Motored Two-Stroke Engine," SAE Paper 970359, 1997.

50. Laimböck, F., Meister, G. and Grilc, S., "CFD Application in Compact Engine Development," SAE Paper 982016, 1998.

51. Yang, X., Okajima, A., Takamoto, Y., and Obokata, T., "Numerical Study of Scavenging Flow in Poppet-Valved Two-Stroke Engines," SAE Paper 1999-01-1250, 1999.

52. Mc Elligott, S., Douglas, R., Kenny, R. and Glover, S., "An Assessment of a Stratified Scavenging Process Applied to a Loop Scavenged Two-Stroke Engine," SAE Paper 1999-01-3272, 1999.

53. Sinclair, R., Strauss, T. and Schindler, P., "Code Coupling, a New Approach to Enhance CFD Analysis of Engines," SAE Paper 2000-01-0660, 2000.

54. Hori, H., "Scavenging Flow Optimization of Two-Stroke Diesel Engine by Use of CFD," SAE Paper 2000-01-0903, 2000.

55. Mugele, M., Tribulowski, J., Peters, H, Spicher, U. and Rosskamp, H., "Numerical Analysis of Gas Exchange and Combustion Process in a Small Two-Stroke Gasoline Engine," SAE Paper 2001-01-3602, 2001.

56. Kong, S., Marriott, C., Rutland, C. and Reitz, R., "Experiments and CFD Modeling of Direct Injection Gasoline HCCI Engine Combustion," SAE Paper 2002-01-1925, 2002.

57. Andrews, M. and Bracco, F., "The Use of Intake and Exhaust Measurements with Computer Simulations to Investigate the Evolution of the Internal Flow Field In a Ported Engine," SAE Paper 910262, 1991.

58. Epstein, P., Reitz, R. and Foster, D., "Computations of a Two-Stroke Engine Cylinder and Port Scavenging Flows," SAE Paper 910672, 1991.

59. Kuo, T. and Reitz, R., "Three-Dimensional Computations of Combustion in Premixed-Charge and Direct-Injected Two-Stroke Engines," SAE Paper 920425, 1992.

60. Zhu, Y., Savonen, C., Johnson, N. and Amsden, A., "Three-Dimensional Computations of the Scavenging Process in an Opposed-Piston Engine," SAE Paper 941899, 1994.

61. Stephenson, P. and Rutland, C., "Modeling the Effects of Intake Flow Characteristics on Diesel Engine Combustion," SAE Paper 950282, 1995.

62. Huh, K, Choi, C. and Kim, J., "Flow Analysis of the Helical Intake Port and Cylinder of a Direct Injection Diesel Engine," SAE Paper 952069, 1995.

63. Han, Z., Reitz, R., Claybaker, P., Rutland, C., Yang, J. and Anderson, R., "Modeling the Effects of Intake Flow Structures on Fuel/Air Mixing in a Direct-Injected Spark-Ignition Engine," SAE Paper 961192.

64. Corcione, F., Rotondi, R., Gentili, R. and Migliaccio, M., "Modeling the Mixture Formation in a Small Direct-Injected Two-Stroke Spark-Ignition Engine," SAE Paper 970364, 1997.

65. Senecal, P., Uludogan, A. and Reitz, R., "Development of Novel Direct-Injection Diesel Engine Combustion Chamber Designs Using Computational Fluid Dynamics," SAE Paper 971594, 1997.

66. Ouellette, P., Mtui, P. and Hill, P., "Numerical Simulations of Directly Injected Natural Gas and Pilot Diesel Fuel in a Two-Stroke Compression Ignition Engine," SAE Paper 981400, 1998.

67. Suh, E. and Rutland, C., "Numerical Study of Fuel/Air Mixture Preparation in a GDI Engine," SAE Paper 1999-01-3657, 1999.

68. Rodatz, P., Weisser, G. and Tanner, F., "Assessment of CFD Methods for Large Diesel Engines Equipped with a Common Rail Injection System," SAE Paper 2000-01-0948, 2000.

69. Fan, L. and Reitz, R., "Multi-Dimensional Modeling of Mixing and Combustion of a Two-Stroke Direct-Injection Spark Ignition Engine," SAE Paper 2001-01-1228, 2001.

70. Amsden, A., O'Rourke, P. and Butler, T., "KIVA-II: A Computer Program for Chemically Reactive Flows with Sprays," Los Alamos Report LA-11560-MS, 1989.

71. Amsden, A., "KIVA-3: A KIVA Program with Block-Structured Mesh for Complex Geometries," Los Alamos Report LA-12503-MS, 1993.

72. Amsden, A., "KIVA-3V: A Block-Structured KIVA Program for Engines with Vertical or Canted Valves," Los Alamos Report LA-13313-MS, 1997.

73. Amsden, A., "KIVA-3V, Release 2, Improvements to KIVA-3V," Los Alamos Report LA-13608-MS, 1999.

74. Berlardini, P., Bertoli, C., Corcione, F. and Valentino, G., "In-Cylinder Flow Measurements by LDA and Numerical Simulation By KIVA-II Code," SAE Paper 920155, 1992.

75. Amsden, A., O'Rourke, P., Butler, D., Meintjes, K. and Fansler, T., "Comparisons of Computed and Measured Three-Dimensional Velocity Fields in a Motored Two-Stroke Engine," SAE Paper 920418, 1992.

76. Auriemma, M., Corcione, F., Macchioni, R. and Valentino, G., "Assessment of k-ε Turbulence Model in KIVA-II by In-Cylinder LDV Measurements," SAE Paper 952385, 1995.

77. Delhaye, B. and Cousyn, B., "Computation of Flow and Combustion in Spark Ignition Engine and Comparison with Experiment," SAE Paper 961960, 1996.

78. Kong, S. and Hong, C., "Multidimensional Intake Flow Modeling of a Four-Stroke Engine and Comparisons to Flow Velocity Measurements," SAE Paper 970883, 1997.

79. Fan, L., Reitz, R. and Trigui, N., "Intake Flow Simulation and Comparison with PTV Measurements," SAE Paper 1999-01-0176, 1999.

80. Woschni, G., "A Universally Applicable Equation for the Instantaneous Heat Transfer Coefficient in the Internal Combustion Engine," SAE Paper 670931, 1967.

81. Annand, W. and Roe, G., Gas Flow in the Internal Combustion Engine, G. T. Foulis & Co. Ltd., Sparkford, 1974.

82. Stanley, R., Taraza, D., Henein, N. and Bryzik, W., "A Simplified Friction Model of the Piston Ring Assembly," SAE Paper 1999-01-0974, 1999.

83. R. Raul, K. Parthasarathy, and J. Wozniak, "Numerical Simulation of Natural Gas Powered Internal Combustion Engine," Johns Hopkins APL Technical Digest Vol.17, No. 2, 1996.

84. Goldsborough, S. and Van Blarigan, P., "A Numerical Study of a Free Piston IC Engine Operating on Homogeneous Charge Compression Ignition Combustion," SAE Paper 1999-01-0619, 1999.

85. O'Flynn, G., Saunders, R. and Ma T., "Combustion characteristics of an Otto-Atkinson engine using late inlet valve closing and multi-point electric fuel injection," SAE Paper 925107, 1992.

86. Raynes, S., "An Atkinson cycle engine for low pollution," SAE Paper 984064, 1998.

APPENDICES

APPENDIX A – LOOP SCAVENGING SIMULATIONS

The purpose of this appendix is to more thoroughly describe the parametric simulations with the loop scavenging configuration. A summary of these computations is presented in Chapter IV. Here more detail is given regarding the cases investigated, as well as the results of the simulations.

Intake Charge Pressure

Table A.1 lists the geometric and operating parameters for this simulation series. The mesh for these runs was illustrated in Figure 4.2. Charging pressures between 1.1 and 1.8bar were used, with the exhaust pressure fixed at 1.0bar.

Bore [cm]	7.62	7.62	7.62	7.62	7.62	7.62
Stroke [cm]	18.03	18.03	18.03	18.03	18.03	18.03
Compression Ratio	18:1	18:1	18:1	18:1	18:1	18:1
EPO [CAD]	131	131	131	131	131	131
IPO [CAD]	144	144	144	144	144	144
IPC [CAD]	210	210	210	210	210	210
EPC [CAD]	222	222	222	222	222	222
Ex Port Width [cm]	3.81	3.81	3.81	3.81	3.81	3.81
Ex Port Height [cm]	3.50	3.50	3.50	3.50	3.50	3.50
In Port Width [cm]	3.04	3.04	3.04	3.04	3.04	3.04
In Port Height [cm]	2.25	2.25	2.25	2.25	2.25	2.25
In Incline Angle	40°	40°	40°	40°	40°	40°
In Off-Axis Angle (rear)	72°	72°	72°	72°	72°	72°
In Off-Axis Angle (front)	45°	45°	45°	45°	45°	45°
Frequency [Hz]	50	50	50	50	50	50
Intake Pressure [bar]	1.10	1.20	1.35	1.50	1.65	1.80
Exhaust Pressure [bar]	1.00	1.00	1.00	1.00	1.00	1.00
Intake ϕ	0.78	0.78	0.78	0.78	0.78	0.78

Table A.1 – Geometric and Operating Parameters

Some of the results for this scavenging series are presented in Figures A.1 and A.2. A plot of the overall scavenging performance with respect to intake charge pressure was given in Figure 4.5. In Figs. A.1 and A.2 the cylinder pressure and incoming fresh charge flow rates are plotted over the scavenging period (EPO to EPC). Labeled in these two figures are the port timings for reference.

It is clear in Fig. A.1 that the intake ports open before the cylinder pressure has dropped to the intake charging pressure. This leads to backflow of the combusted gases into the intake manifold and delays the delivery of the fresh charge into the cylinder. (This was noted in the flow visualization presented in Fig. 4.2.)

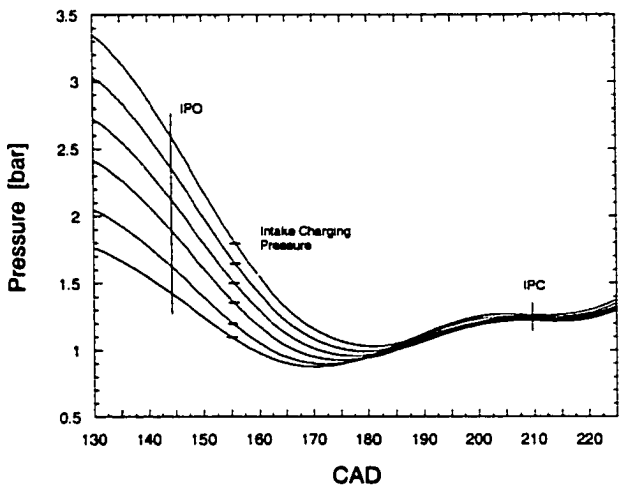

Figure A.1 – Cylinder Pressure vs. CAD

As would be expected from these runs, the rates of fresh charge into the cylinder increase with the increasing charging pressure. The higher flow rates improve the penetration of the fresh charge to the top of the cylinder, though not as much as was hoped. In addition, the in-cylinder mixing, and the entrainment of the burned charge, is intensified. The helical motion generated by the opposing intake ports is also more pronounced.

The changes in the flow behavior are illustrated in Figures A.3 and A.4 where the manifold and in-cylinder flow patterns are depicted (using Ensight's particle tracing method, similar to Figure 4.3), and the average and maximum dilution ratios are plotted over the

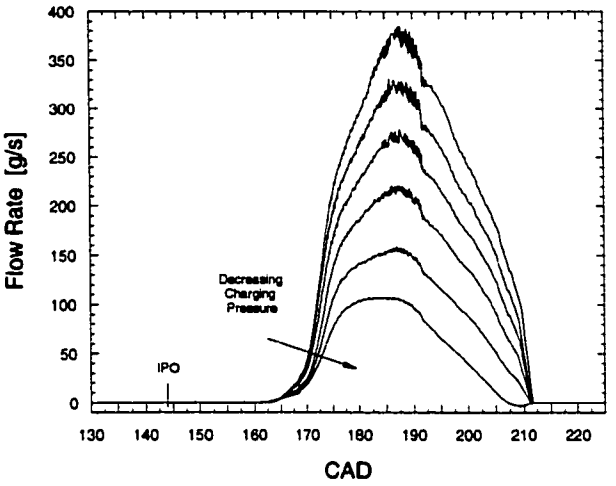

Figure A.2 – Fresh Charge Flow Rates vs. CAD

scavenging and compression processes. (The dilution ratio graph indicates how effectively the fuel becomes distributed throughout the combustion chamber. Differences between the average and maximum values indicate fuel rich regions.)

Through these figures two it can be seen that increased mixing during and after scavenging due to the higher charging pressures, leads to a more uniform charge by the time

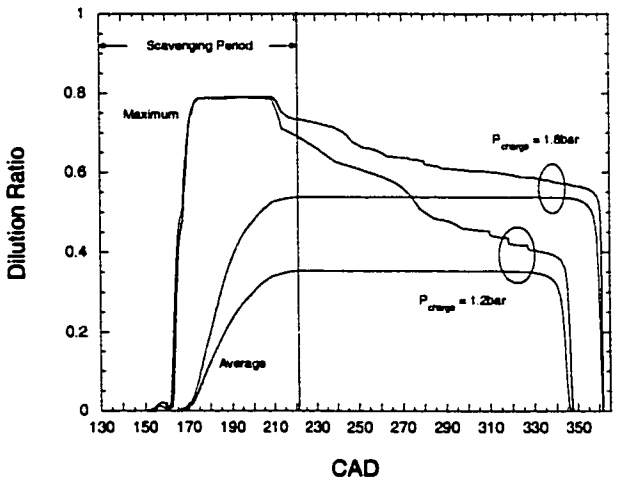

Figure A.3 – Average and Maximum Dilution Ratios vs. CAD

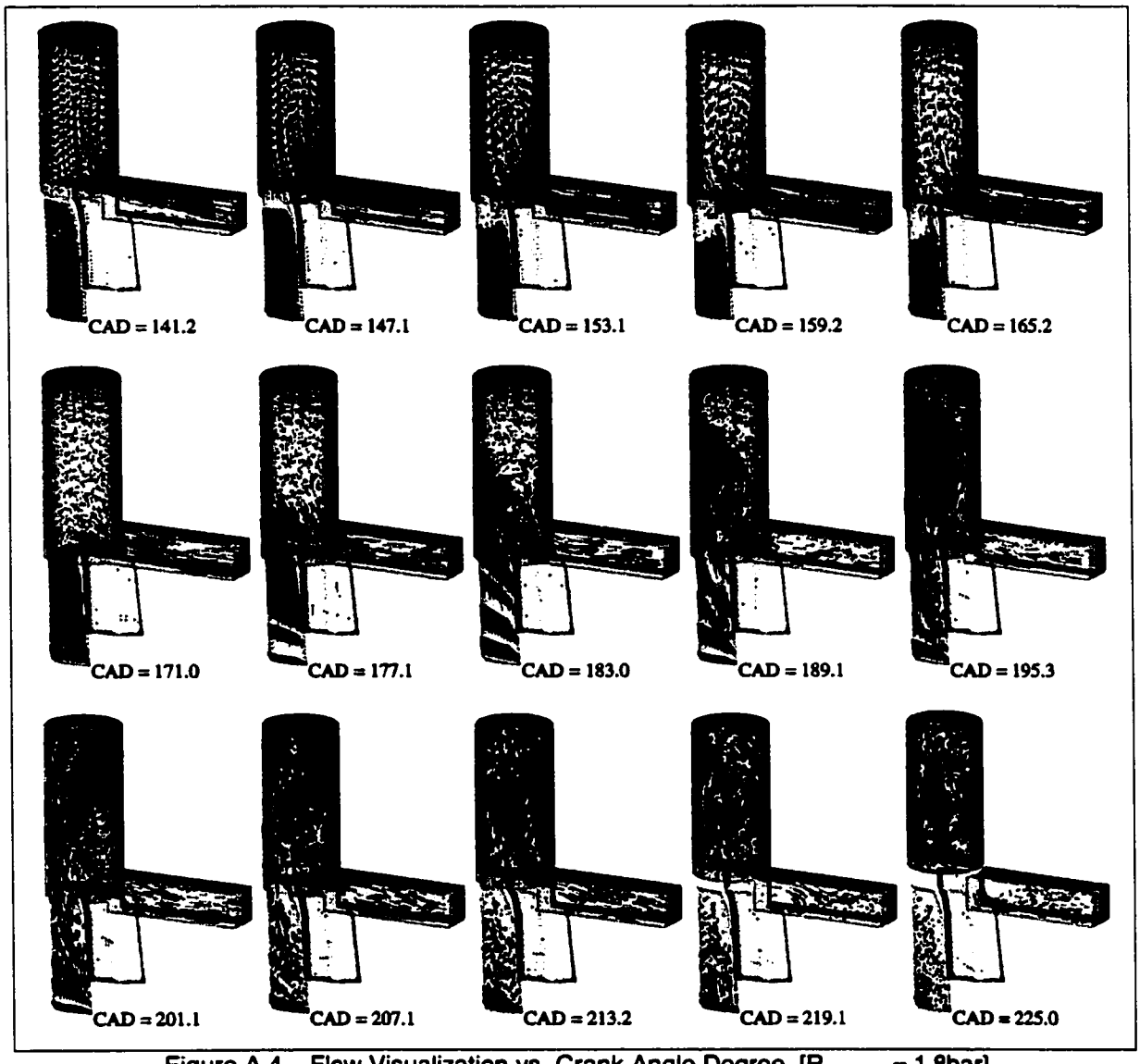

Figure A.4 – Flow Visualization vs. Crank Angle Degree [$P_{charging}$ = 1.8bar]

combustion initiates. (The shifted ignition points is due to the higher scavenging efficiency for the $P_{charging}$ = 1.8bar case.)

Another important feature noted through these simulations is the change in blowdown effectiveness as the charging pressure is increased. The higher pressures at EPO allow the burned gases to discharge more quickly through the exhaust port and a greater fraction of the

burned charge can be removed from the cylinder before the fresh charge enters. This decreases the need for the fresh charge to 'push' the combusted charge from the engine.

Figure A.5 illustrates this where the residual fractions (mass of residual gas in the cylinder to the mass of trapped charge at EPC) are plotted over the scavenging period. Here it is apparent that the effectiveness of the blowdown process can be a significant factor in the resulting scavenging efficiency.

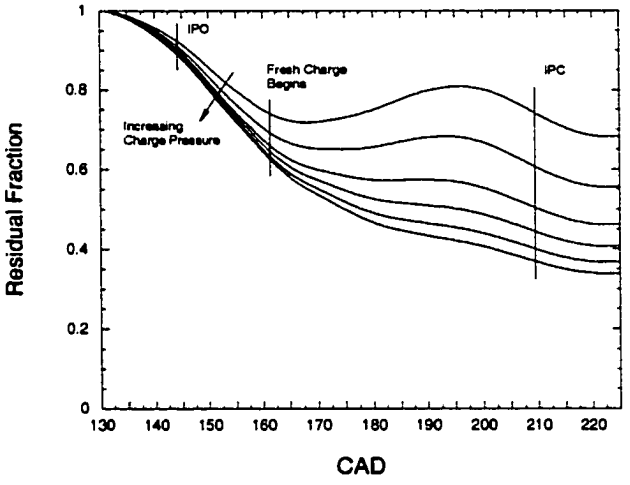

Figure A.5 – Residual Fraction vs. CAD

Intake Equivalence Ratio

Table A.2 lists the geometric and operating parameters for this simulation series. Intake equivalence ratios of 0.50, 0.78 and 0.95 were used, with the intake pressure set to 1.35bar.

Some of the results for this scavenging series are presented in Figures A.6 and A.7. A plot of the overall scavenging performance with respect to intake equivalence ratio was given in Figure 4.6. In Figs. A.6 and A.7 the residual fractions and incoming fresh charge flow rates are plotted over the scavenging period. Labeled in these two figures are the port timings for reference.

Bore [cm]	7.62	7.62	7.62
Stroke [cm]	18.03	18.03	18.03
Compression Ratio	18:1	18:1	18:1
EPO [CAD]	131	131	131
IPO [CAD]	144	144	144
IPC [CAD]	210	210	210
EPC [CAD]	222	222	222
Ex Port Width [cm]	3.81	3.81	3.81
Ex Port Height [cm]	3.50	3.50	3.50
In Port Width [cm]	3.04	3.04	3.04
In Port Height [cm]	2.25	2.25	2.25
In Incline Angle	40°	40°	40°
In Off-Axis Angle (rear)	72°	72°	72°
In Off-Axis Angle (front)	45°	45°	45°
Frequency [Hz]	50	50	50
Intake Pressure [bar]	1.35	1.35	1.35
Exhaust Pressure [bar]	1.00	1.00	1.00
Intake ϕ	0.50	0.78	0.95

Table A.2 – Geometric and Operating Parameters

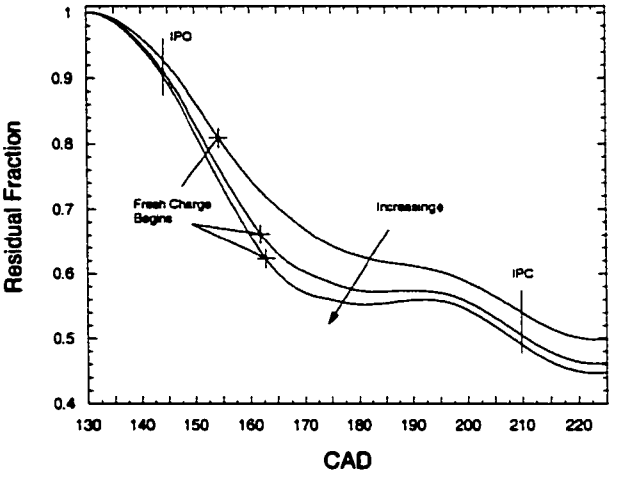

Figure A.6 – Residual Fraction vs. CAD

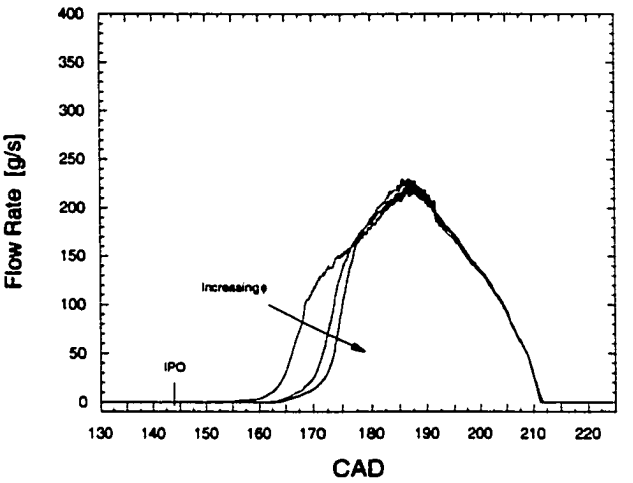

Figure A.7 – Fresh Charge Flow Rates vs. CAD

Again, it can be seen in Fig. A.6 that the increase in scavenging efficiency is due mainly to the improvement of the blowdown process. The difference in residual fraction remains fairly stable after the fresh charge begins to enter the cylinder.

The plot of the incoming flow rates reveals that the overall rates are similar, however, the delay time for fresh charge introduction increases with ϕ. The delayed introduction is due to the greater degree of backflow into the intake manifold caused by the higher combustion pressures. This delay time accounts for the change in trapping efficiency as described next.

Figures A.8 and A.9 illustrate the flow behavior for the low and high ϕ cases. The earlier delivery of fresh charge for the low ϕ case (~165CAD) results in mixing of the initial fresh gas and the cylinder's burned charge. This leads to some of the fresh charge short-circuiting through the exhaust port. The initial incoming gas does not have the momentum to carry it towards the top of the cylinder and away from the exhaust port.

In the high ϕ case the direction of the incoming gas flow seems to be better established (up along the back wall of the cylinder) by the time the fuel/air mixture enters the cylinder (~177CAD). It may be inferred that some blowdown into the intake manifold might be beneficial in the loop scavenging configuration.

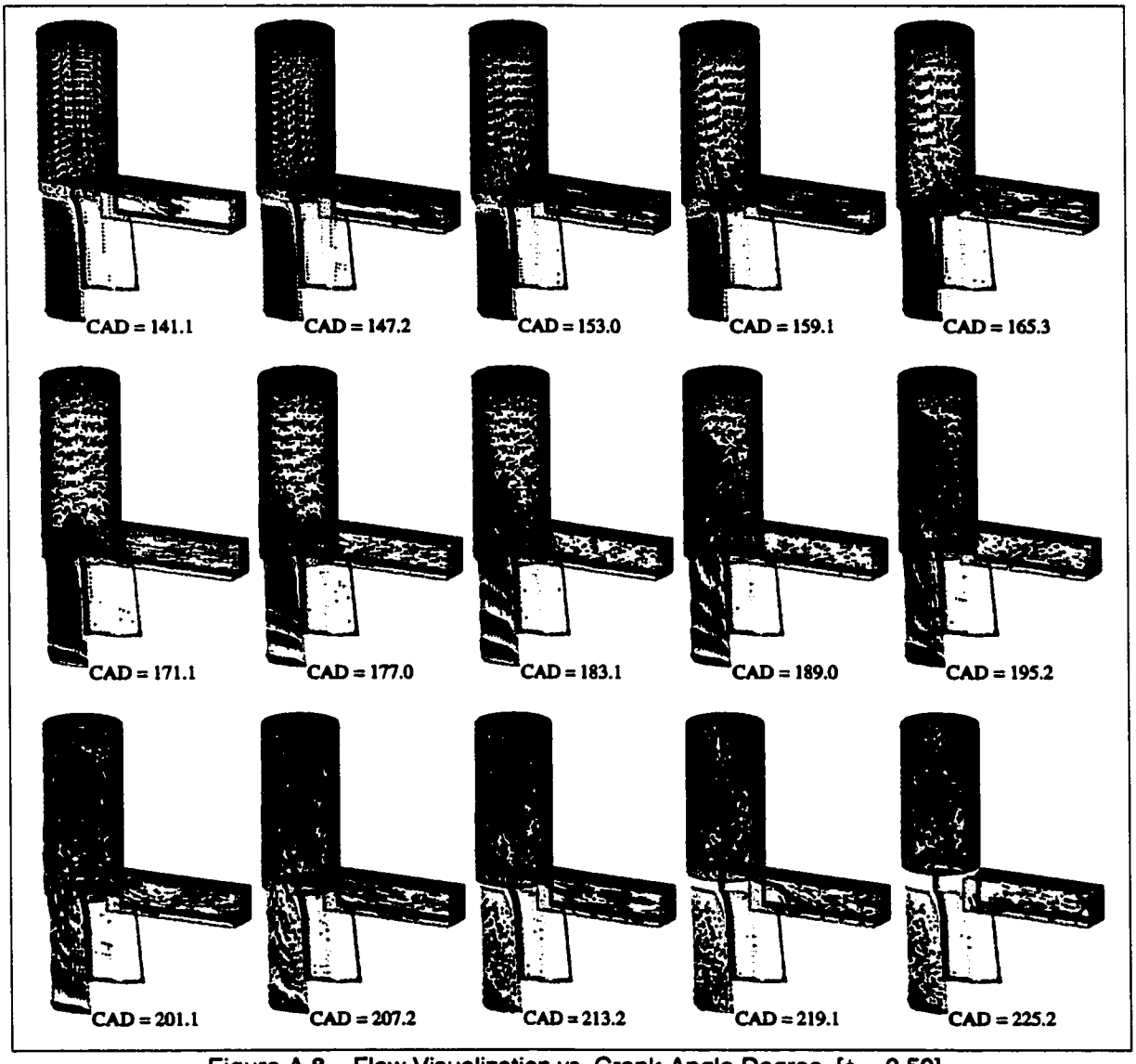

Figure A.8 – Flow Visualization vs. Crank Angle Degree [$\phi = 0.50$]

Exhaust Port Area / Timing

Table A.3 lists the geometric and operating parameters for this simulation series. Here the exhaust port widths and heights were varied with the piston frequency adjusted slightly to keep the intake port open time constant for the exhaust port height modifications.

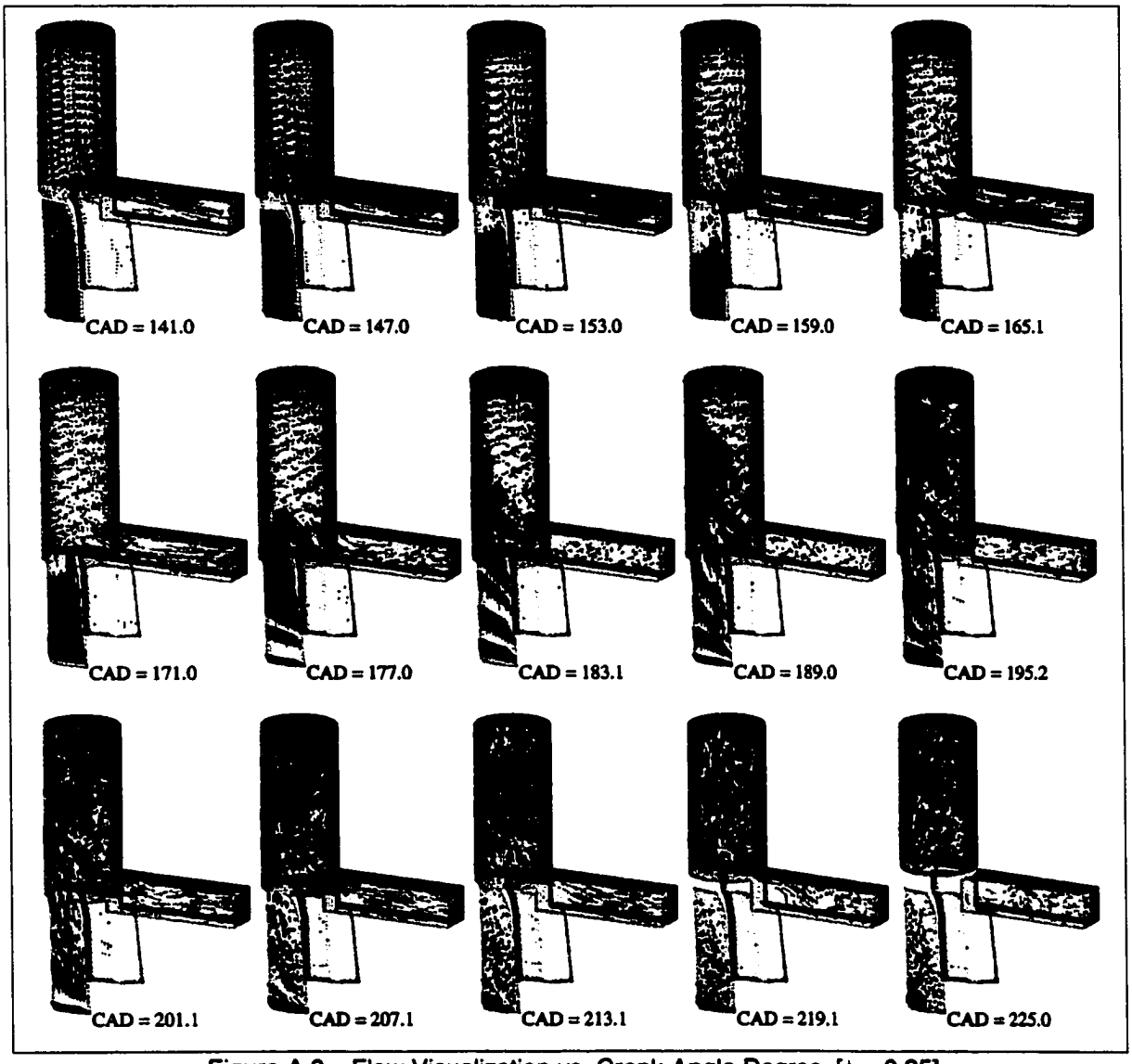

Figure A.9 – Flow Visualization vs. Crank Angle Degree [ϕ = 0.95]

Some of the results for this scavenging series are presented in Figures A.10 and A.11. A plot of the overall scavenging performance with respect to exhaust port area was given in Figure 4.7. In Figs. A.10 and A.11 the residual fractions for the width and height modifications are plotted over the normalized scavenging period. Labeled in these two figures are the port timings for reference.

Bore [cm]	7.62	7.62	7.62	7.62	7.62	7.62
Stroke [cm]	18.03	18.03	18.03	18.53	19.03	19.53
Compression Ratio	18:1	18:1	18:1	18:1	18:1	18:1
EPO [CAD]	131	131	131	126	123	120
IPO [CAD]	144	144	144	145	146	146
IPC [CAD]	210	208	208	209	209	208
EPC [CAD]	222	222	222	225	228	230
Ex Port Width [cm]	3.81	4.35	4.90	3.81	3.81	3.81
Ex Port Height [cm]	3.50	3.50	3.50	4.0	4.50	5.00
In Port Width [cm]	3.04	3.04	3.04	3.04	3.04	3.04
In Port Height [cm]	2.25	2.25	2.25	2.25	2.25	2.25
In Off-Horizontal Angle	40°	40°	40°	40°	40°	40°
In Off-Axis Angle (rear)	72°	72°	72°	72°	72°	72°
In Off-Axis Angle (front)	45°	45°	45°	45°	45°	45°
Operating Frequency [Hz]	50	50	50	49.5	48	47
Intake Pressure [bar]	1.20	1.20	1.20	1.20	1.20	1.20
Exhaust Pressure [bar]	1.00	1.00	1.00	1.00	1.00	1.00
Intake ϕ	0.78	0.77	0.74	0.72	0.67	0.70

Table A.3 – Geometric and Operating Parameters

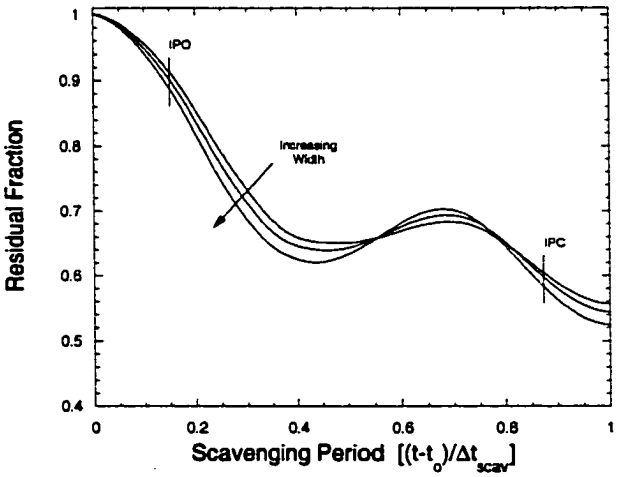

Figure A.10 – Residual Fraction vs. Normalized Scavenging Period

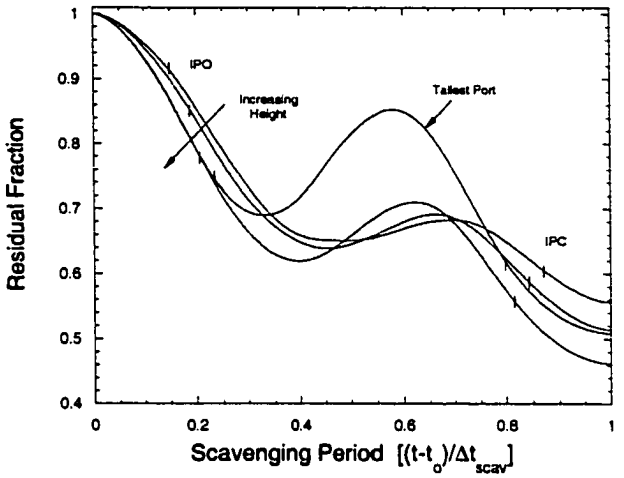

Figure A.11 – Residual Fraction vs. Normalized Scavenging Period

As can be seen again, a significant cause of the improvement in scavenging efficiency is more effective blowdown of the burned charge. However, as the exhaust port becomes too large, or the timing too early the exhaust flow tends to oscillate across the port, initially discharging quickly and then reentering the cylinder. As the fresh charge is delivered, the burned gases are then 'pushed' from the cylinder.

The behavior causes a drop in trapping efficiency as the reentering burned gases mix more with the fresh charge and disrupt the looping flow pattern.

Intake Port Area / Timing

Table A.4 lists the geometric and operating parameters for this simulation series. Here the intake port width and heights were varied. For the port width modifications, the area of the port was increased toward the 'front' of the cylinder, with the 'rear' port wall location fixed. The incoming angles (incline, and rear off-axis) were also fixed.

For the port height modifications, the area was increased toward the top of the cylinder, with the bottom of the port fixed. The incoming angles were again held constant; the lengths of the manifolds were increased to 'capture' the additional blowdown. The intake equivalence ratios were modified so that the overall dilution ratio was fixed at about 0.35.

Bore [cm]	7.62	7.62	7.62	7.62	7.62	7.62
Stroke [cm]	18.03	18.03	18.03	18.03	18.03	18.03
Compression Ratio	18:1	18:1	18:1	18:1	18:1	18:1
EPO [CAD]	131	131	131	131	131	131
IPO [CAD]	144	144	144	138	134	131
IPC [CAD]	208	208	208	215	218	222
EPC [CAD]	222	222	222	222	222	222
Ex Port Width [cm]	3.81	3.81	3.81	3.81	3.81	3.81
Ex Port Height [cm]	3.50	3.50	3.50	3.50	3.50	3.50
In Port Width [cm]	3.56	4.6	4.54	3.04	3.04	3.04
In Port Height [cm]	2.25	2.25	2.25	2.67	3.08	3.50
In Off-Horizontal Angle	40°	40°	40°	40°	40°	40°
In Off-Axis Angle (rear)	72°	72°	72°	72°	72°	72°
In Off-Axis Angle (front)	36°	28°	19°	45°	45°	45°
Operating Frequency [Hz]	50	50	50	50	50	50
Intake Pressure [bar]	1.20	1.20	1.20	1.20	1.20	1.20
Exhaust Pressure [bar]	1.00	1.00	1.00	1.00	1.00	1.00
Intake ϕ	0.74	0.72	0.70	0.86	0.87	0.95

Table A.4 – Geometric and Operating Parameters

Figures A.12 and A.13 present some of the results for the simulations. The improvement in scavenging performance was noted in Figure 4.8. Figure A.12 plots the change in intake mass flow rate for the port width modifications. As would be expected the rates of mass flow increase for increasing port width with the overall delivered charge increased (+26, +43, and +61%, respectively).

This increase in delivery ratio increases the pressure at EPC, and therefore at EPO. The blowdown process becomes more effective, as seen in the residual fraction plot presented in Figure A.13, and this contributes to the increase in scavenging efficiency.

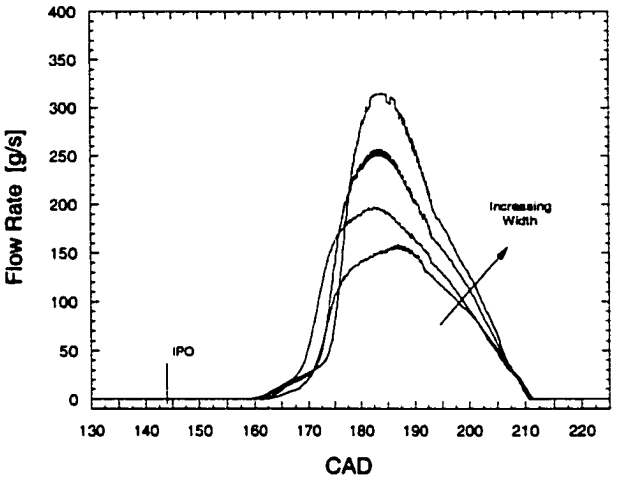

Figure A.12 – Fresh Charge Flow Rates vs. CAD

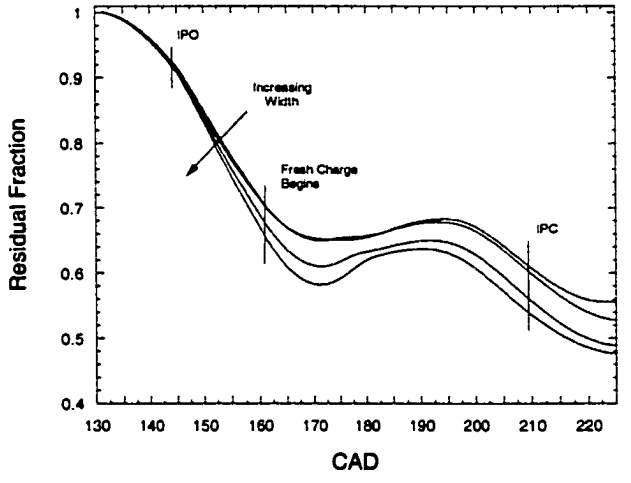

Figure A.13 – Residual Fraction vs. CAD

However, as the port becomes too wide the incoming fresh charge, which enters over a wider fraction of the cylinder's circumference tends to interfere with the discharge of the burned gases at the top of the cylinder. Some of the burned gas becomes trapped in the cylinder.. A shorter scavenging loop is created by the incoming gas and more of the fresh charge is short-circuited. This can be seen in Figure A.14 where the flow behavior for the widest port is illustrated. This change in flow pattern explains change in scavenging performance for the wider ports, and the limitation of improvement for this parameter.

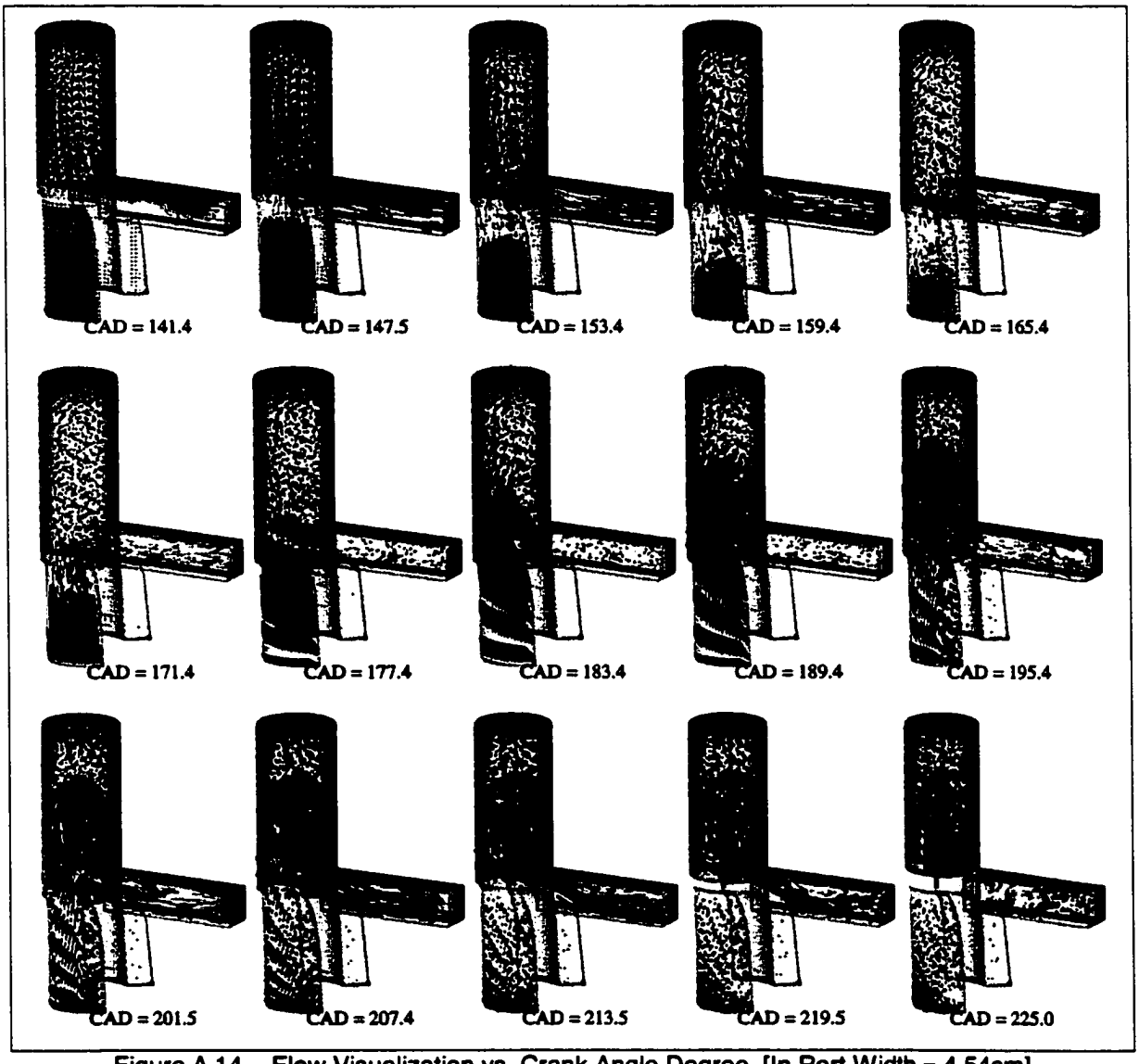

Figure A.14 – Flow Visualization vs. Crank Angle Degree [In Port Width = 4.54cm]

Figure A.15 plots the change in intake mass flow rate for the port height modifications. Here, it can be seen that the incoming flow is delayed increasingly as the intake port height increases, this due to the greater amount of backflow into the intake manifold. This delay leads to a drop in the amount of fresh charge delivered (-10, -18, and -19%, respectively), and a drop in the scavenging efficiency.

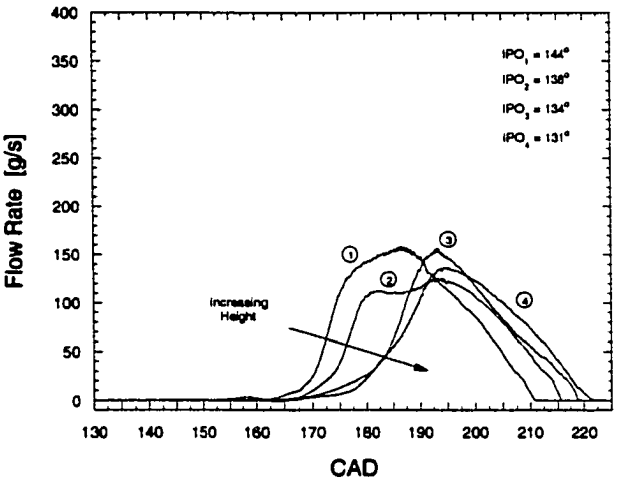

Figure A.15 – Fresh Charge Flow Rates vs. CAD

Piston Dynamics

The influence of the piston dynamics on the scavenging process was investigated, first by varying the piston frequency, and then by using a crankshaft-driven piston profile (KIVA-3V's standard slider-crank formula).

Piston Frequency

For this first simulation series the piston frequency was varied (66.7, 33.3 and 16.7Hz) using the geometry presented in Table A.1. For these runs the intake pressure was set at 1.20bar and the exhaust pressure at 1.0bar. An intake equivalence ratio of 0.78 was used. Scavenging times of 15.0, 7.6 and 3.8ms resulted.

The change in scavenging performance was presented in Figure 4.9; as the time available for scavenging is increased the cylinder can be more thoroughly flushed, however the trapping efficiency suffers. Figures A.16, A.17 and A.18 illustrate the change in in-cylinder flow behavior for these runs.

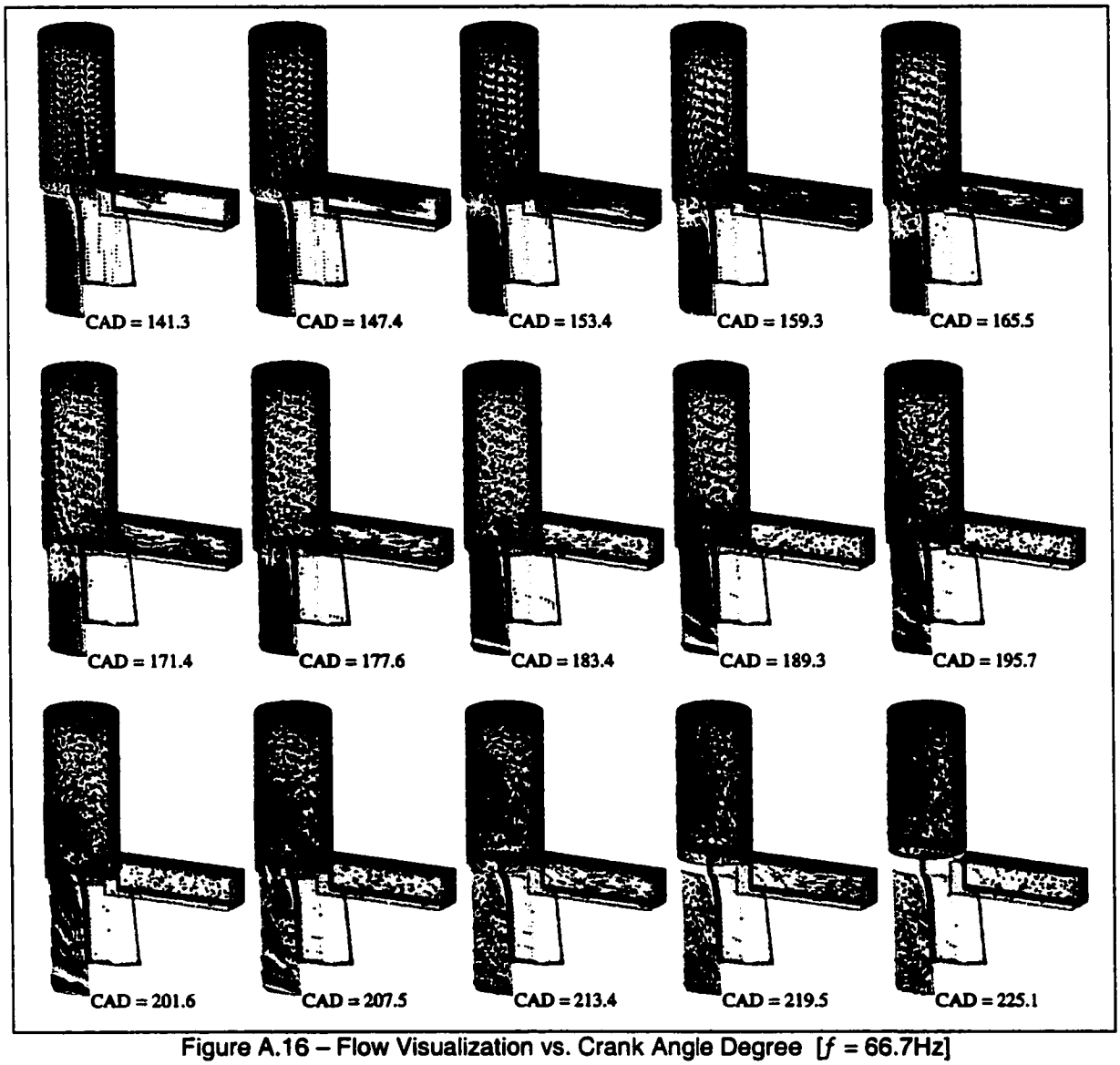

Figure A.16 – Flow Visualization vs. Crank Angle Degree [f = 66.7Hz]

To summarize these figures, it can be seen that with less time for scavenging the blowdown process significantly delays the introduction of fresh charge (~183CAD, compared to ~159CAD for the 66.7, and 16.7Hz cases, respectively), and limits the amount of gas delivered, as well as its penetration to the top of the cylinder. Mixing is also reduced for the faster piston case, so that the charge is not as uniform at TDC. This change can be seen in Figure A.20 where the average and maximum dilution ratios are plotted for the fastest and slowest piston cases.

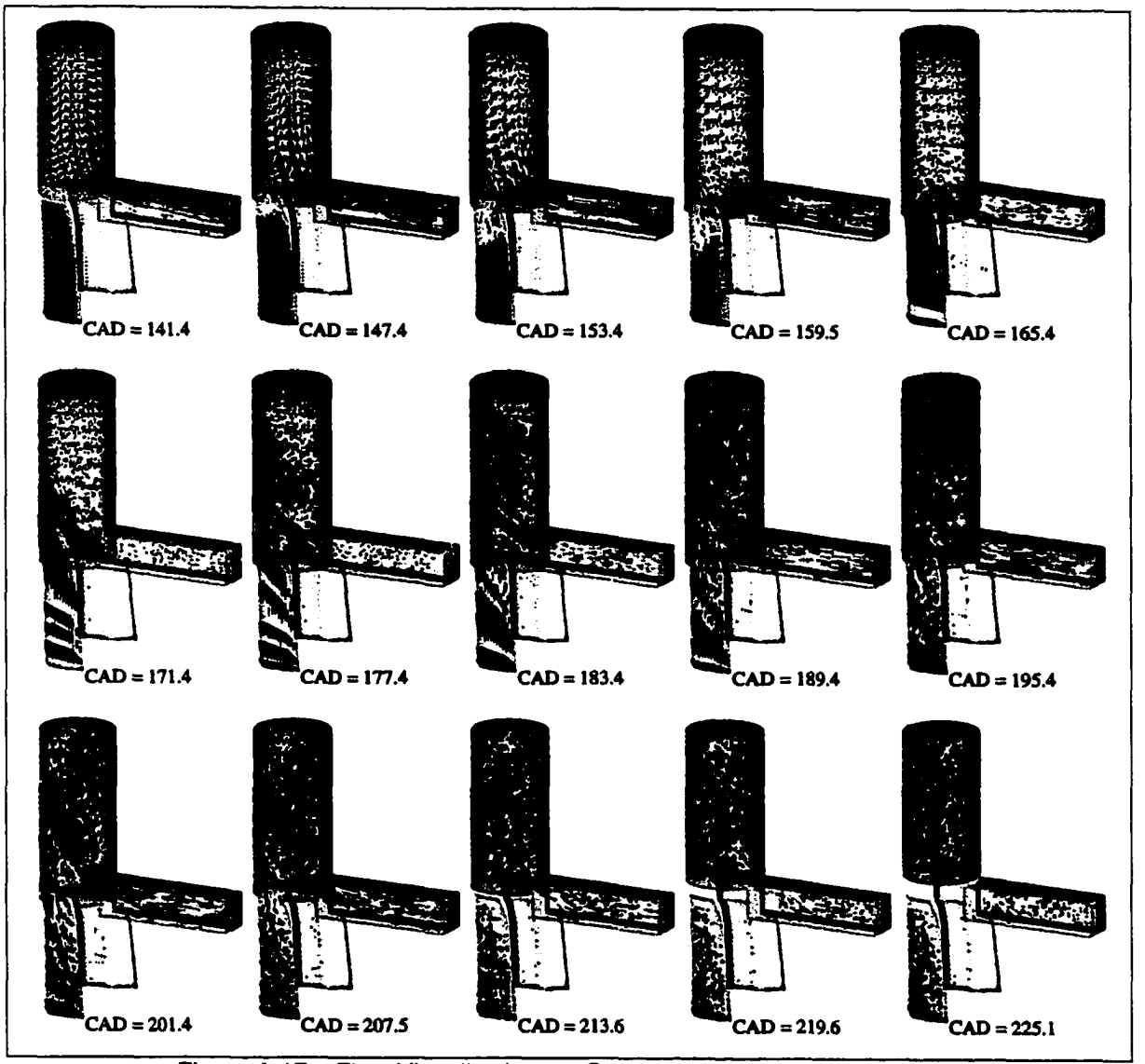

Figure A.17 – Flow Visualization vs. Crank Angle Degree [f = 33.3Hz]

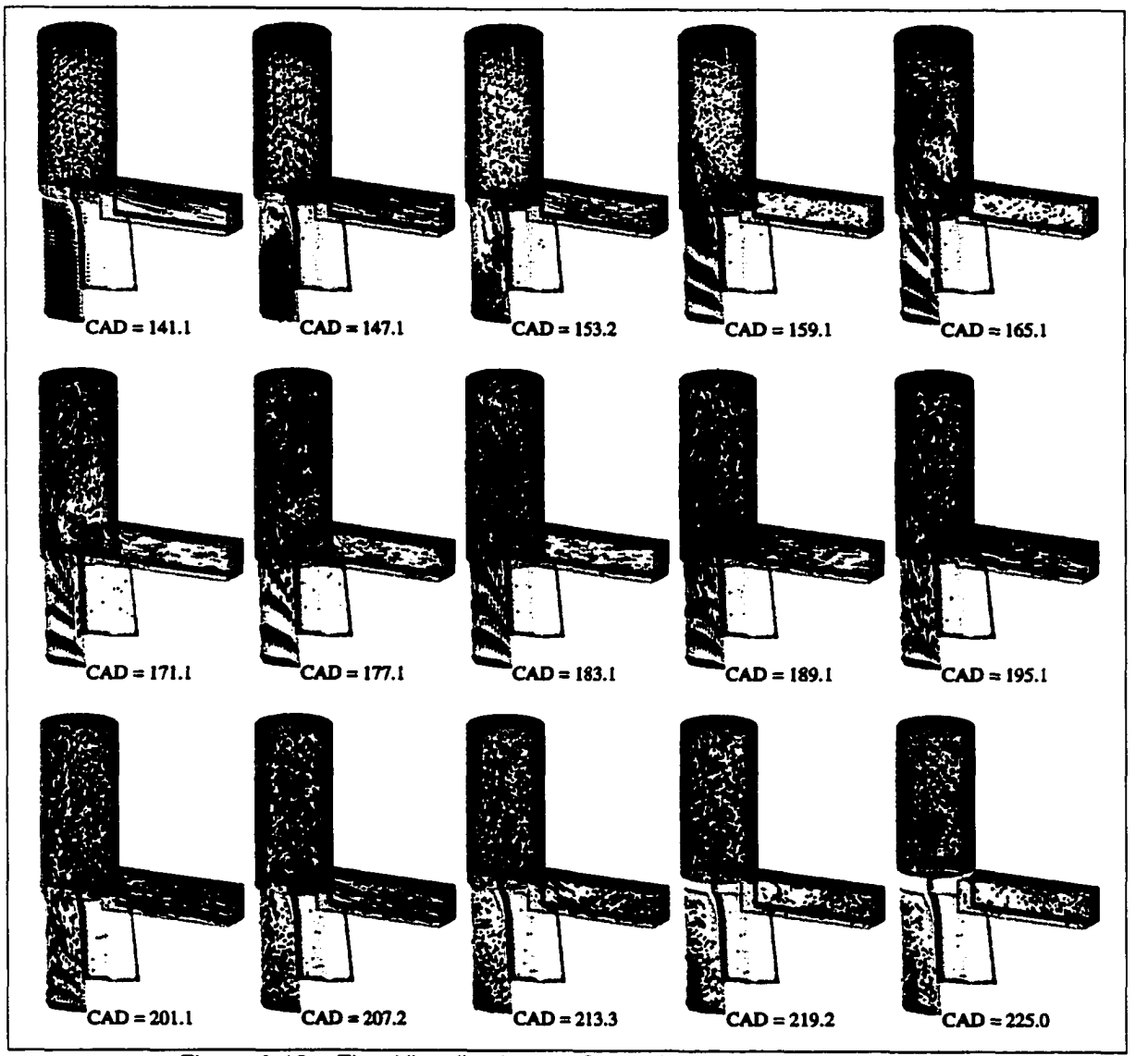

Figure A.18 – Flow Visualization vs. Crank Angle Degree [f = 16.7Hz]

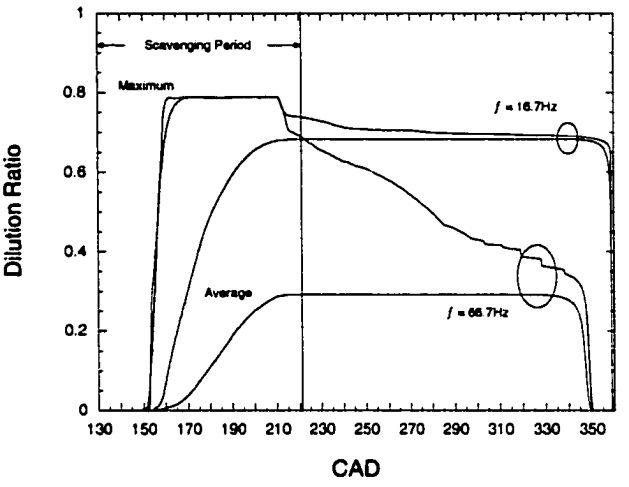

Figure A.19 – Average and Maximum Dilution Ratios vs. CAD

Crankshaft-driven Piston

For the next set of runs the geometric configuration given in Table A.1 was used again. The performance of the scavenging cycle using a free piston (f = 50Hz, V_{max} = 2700cm/s, Δt_{scav} = 5ms) was compared to the performance using a crankshaft-driven profile, with three standards for comparison - similar frequency, similar maximum velocity, and similar scavenging time. Figure A.20 shows the difference in piston dynamics for the four cases where the piston velocity is plotted versus the piston position. The port timings are labeled for these runs.

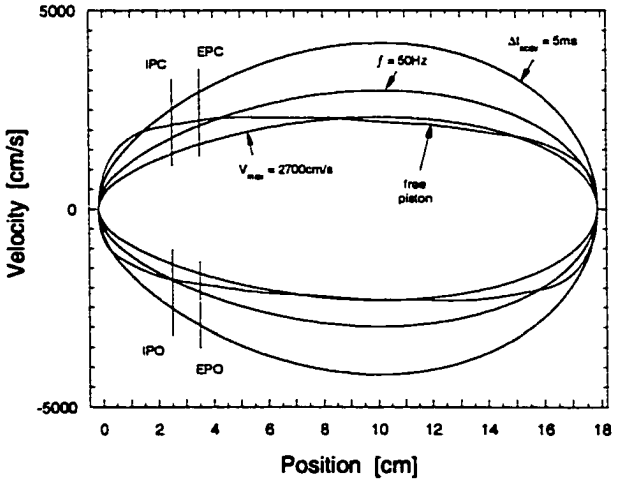

Figure A.20 – Piston Velocity vs. Piston Position

The results of the KIVA-3V simulations suggested that the piston dynamics, based on any of the metrics, can have little effect on the overall scavenging process. Figure A.21 plots the scavenging and trapping efficiencies versus overall scavenging time, with the frequency variation results from Figure 4.9 included for reference. The main determinant seemed to be the amount of time available for scavenging. However, the free piston may provide some advantage because a lower maximum velocity is required to achieve longer scavenging times for the same configuration, and this may have practical applications.

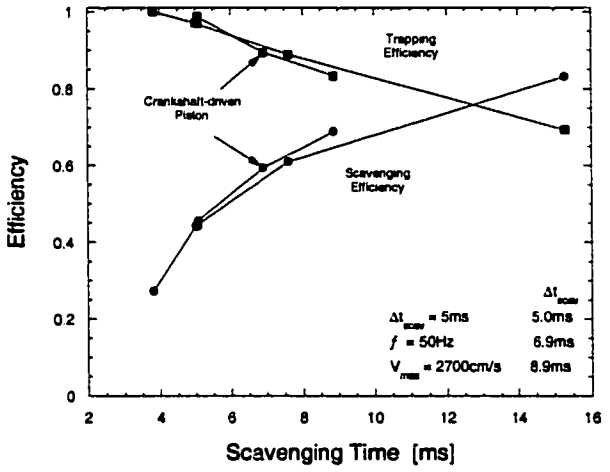

Figure A.21 – Scavenging and Trapping Efficiencies vs. Scavenging Time

Integrate Port Areas

The geometry in Figure A.22 / Table A.5 represented an attempt to achieve the high scavenging efficiency capability of the 16.7Hz case from before (Δt_{scav} = 15.0ms), while maintaining a reasonably high oscillation rate (44Hz). This was undertaken as a means of improving the scavenging efficiency while maintaining adequate power output. In this geometry the intake and exhaust port heights were increased so that the integrated port open area-times were similar to the low *f* case. (Again, as presented in Ch. IV, the integrated area-time is defined as $\int_0^{\Delta t_{scav}} A_{port}\, dt$.) The maximum piston velocity for this trial was fixed at 2500cm/s.

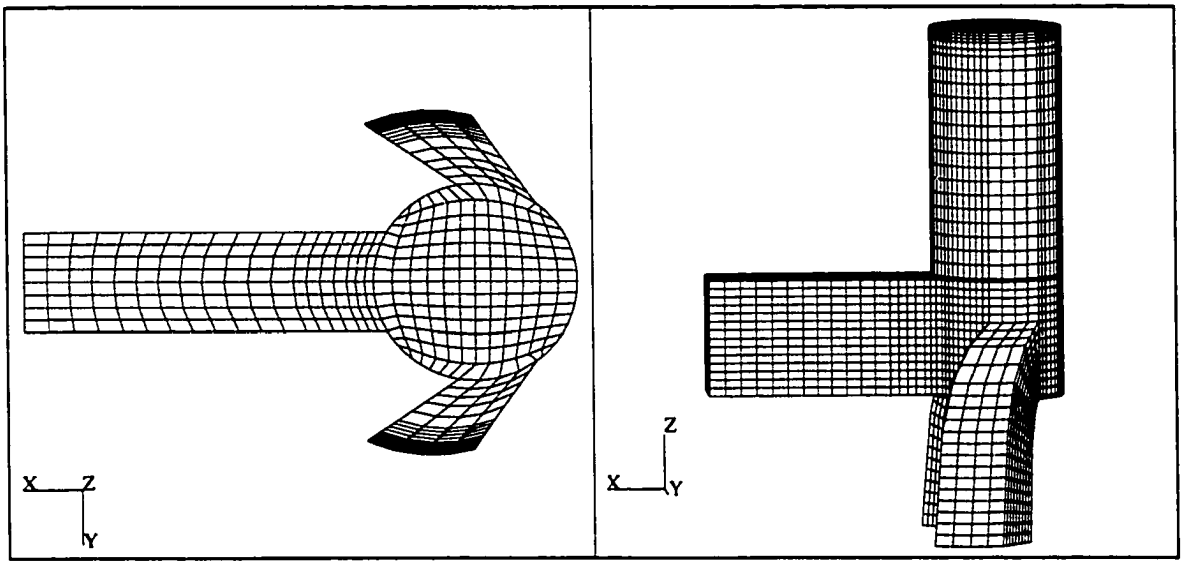

Figure A.22 – Loop Scavenging Mesh [Tall Ports]

Bore [cm]	7.62
Stroke [cm]	21.78
Compression Ratio	18:1
IPO [CAD]	110
EPO [CAD]	130
EPC [CAD]	222
IPC [CAD]	240
Ex Port Width [cm]	3.81
Ex Port Height [cm]	7.00
In Port Width [cm]	3.04
In Port Height [cm]	4.50
In Off-Horizontal Angle	40°
In Off-Axis Angle (rear)	72°
In Off-Axis Angle (front)	45°
Operating Frequency [Hz]	44
Intake Pressure [bar]	1.20
Exhaust Pressure	1.00
Intake ϕ	0.79

Table A.5 – Geometric and Operating Parameters

The results of this run indicated that the scavenging efficiency could be improved by increasing the integrated area-times, however the gain was not quite as good as with the slow piston (16.7Hz) (η_{sc}~0.70), while the trapping losses were just as poor (η_{tr}~0.69). Figure A.23 shows the particle tracing results for this run where the changes in in-cylinder flow behavior due to the altered port configuration are apparent. Indeed the fresh charge still has difficulty flushing the top of the cylinder without losing a lot of fresh charge to short-circuiting.

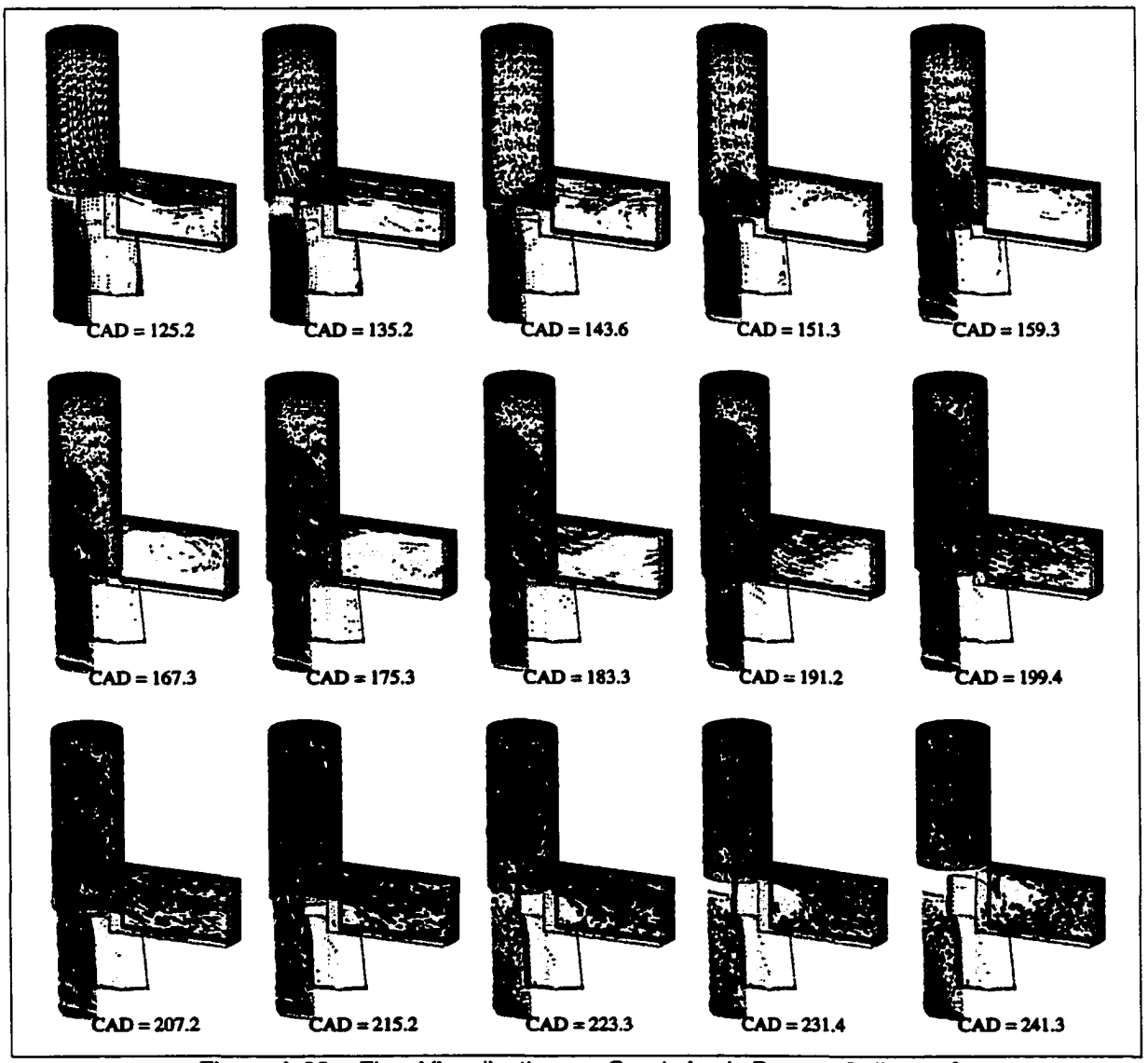

Figure A.23 – Flow Visualization vs. Crank Angle Degree [tall ports]

Summary

Various parametric investigations were conducted using the KIVA-3V code in an effort to maximize the performance of the loop scavenging arrangement, with respect to the design goals (η_{sc}~0.90, η_{tr}~0.99). A summary of the results of these simulations is presented in Figure A.24 where the trapping efficiencies are plotted against the achieved scavenging efficiencies. From this figure it is clear that the loop scavenging method cannot be used to meet the goals of the engine.

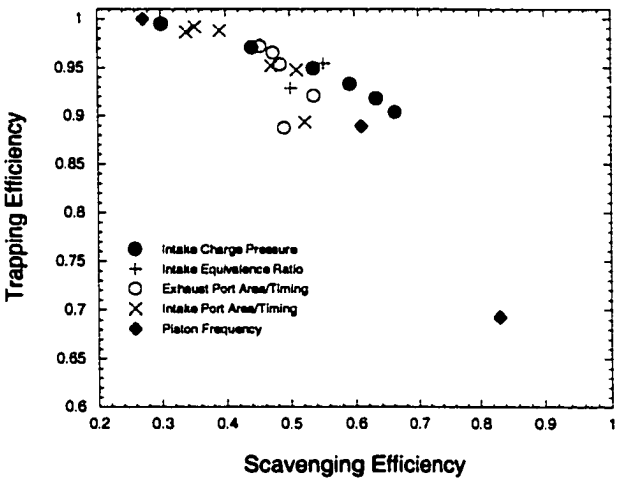

Figure A.24 – Trapping Efficiency vs. Scavenging Efficiency

APPENDIX B – HYBRID-LOOP SCAVENGING SIMULATIONS

The purpose of this appendix is to more thoroughly describe the parametric simulations with the hybrid-loop scavenging configuration. A summary of these computations is presented in Chapter IV. Here more detail is given regarding the cases investigated, as well as the results of the simulations.

Number of Intake / Exhaust Ports

Table B.1 lists the geometric and operating parameters for this simulation series. The mesh for the 5-port arrangement was illustrated in Figure 4.10. The meshes for the 8- and 10-port configurations are presented in Figures B.1 and B.2, respectively.

Number of Ports	5	8	10
Bore [cm]	7.62	7.62	7.62
Stroke [cm]	20.58	20.58	20.58
Compression Ratio	25:1	25:1	25:1
IPO [CAD]	115	114	115
EPO [CAD]	141	141	141
EPC [CAD]	213	213	213
IPC [CAD]	235	236	235
Ex Port Width [cm]	4.20	4.20	4.20
Ex Port Height [cm]	3.00	3.00	3.00
In Port Width [cm]	2.92	2.29	1.49
In Port Height [cm]	1.25	1.50	1.25
Ex Decline Angle	65°	65°	65°
In Incline Angle	35°	50°	55°
In Swirl Angle	57.5°	62.5°	68.75°
Operating Frequency [Hz]	50	50	50
Intake Pressure [bar]	1.50	1.50	1.50
Exhaust Pressure [bar]	1.00	1.00	1.00
Intake ϕ	0.60	0.60	0.60

Table B.1 – Geometric and Operating Parameters

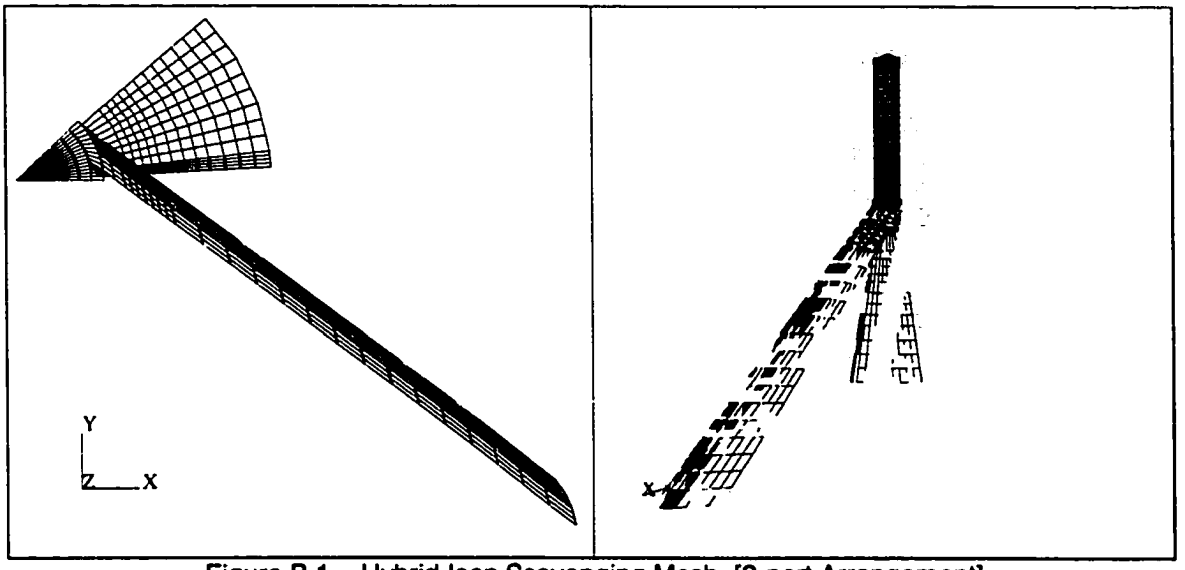

Figure B.1 – Hybrid-loop Scavenging Mesh [8-port Arrangement]

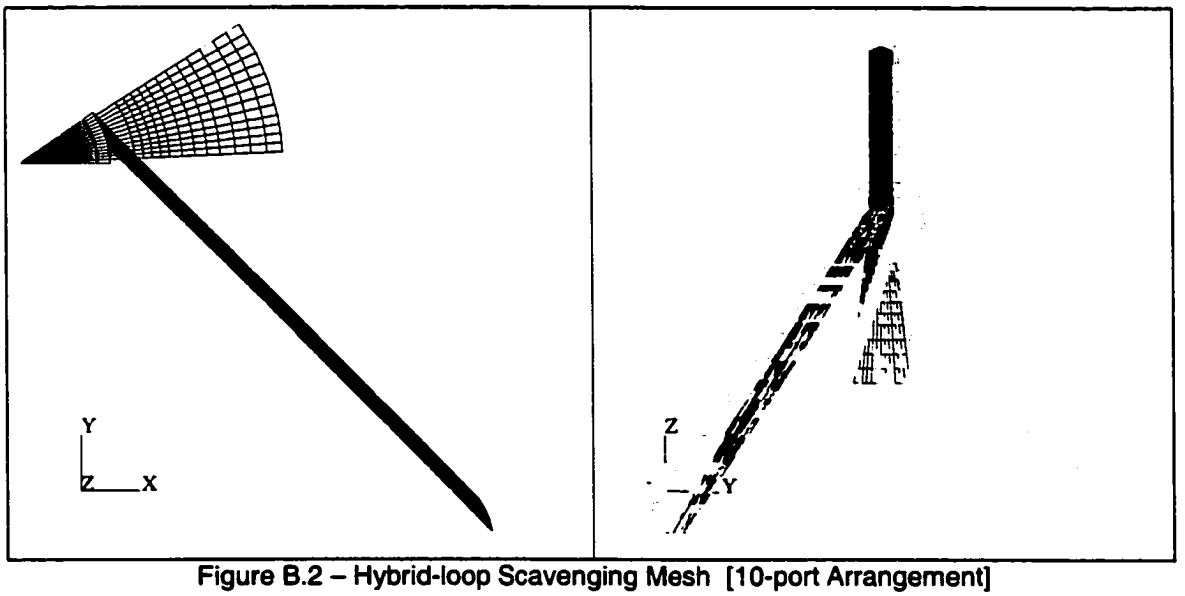

Figure B.2 – Hybrid-loop Scavenging Mesh [10-port Arrangement]

Some of the results from these simulations are presented in Figures B.3-06. Here the cylinder pressures, incoming and exhausting flow rates, and average intake manifold pressures are plotted over the scavenging cycle. The overall scavenging performance was illustrated in Figure 4.15.

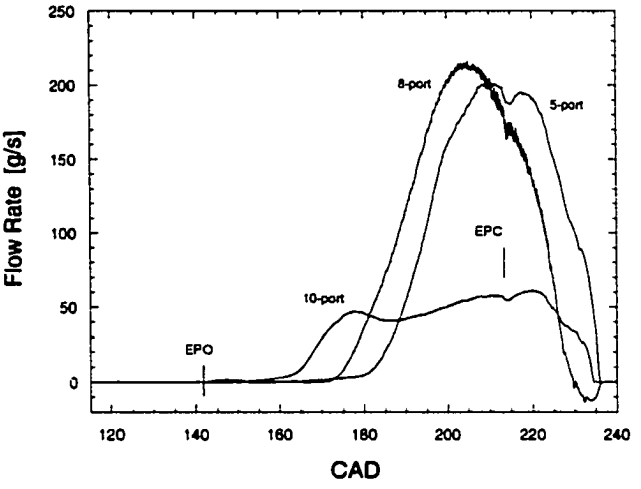

Figure B.3 – Fresh Charge Flow Rates vs. CAD

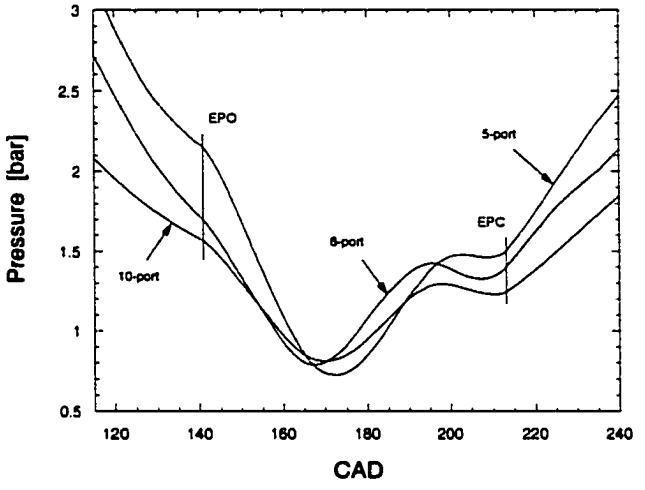

Figure B.4 – Cylinder Pressure vs. CAD

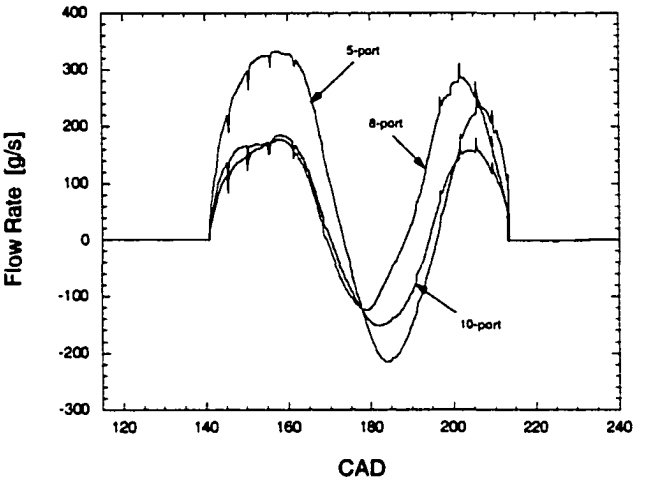

Figure B.5 – Exhaust Port Flow Rate vs. CAD

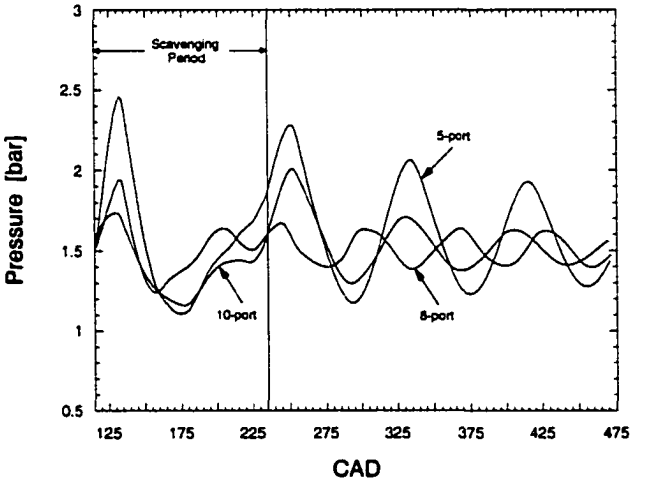

Figure B.6 – Average Intake Manifold Pressures vs. CAD

In Figure B.3 the drop in the fresh charge flow rate for the 10-port configuration is apparent; this was discussed earlier in Chapter IV. Through the rest of the figures however, it can be seen that the dynamics of the process are very similar for the three geometries investigated with the oscillating flow across the exhaust port, and the pressure fluctuations in the intake manifolds dominating the scavenging process.

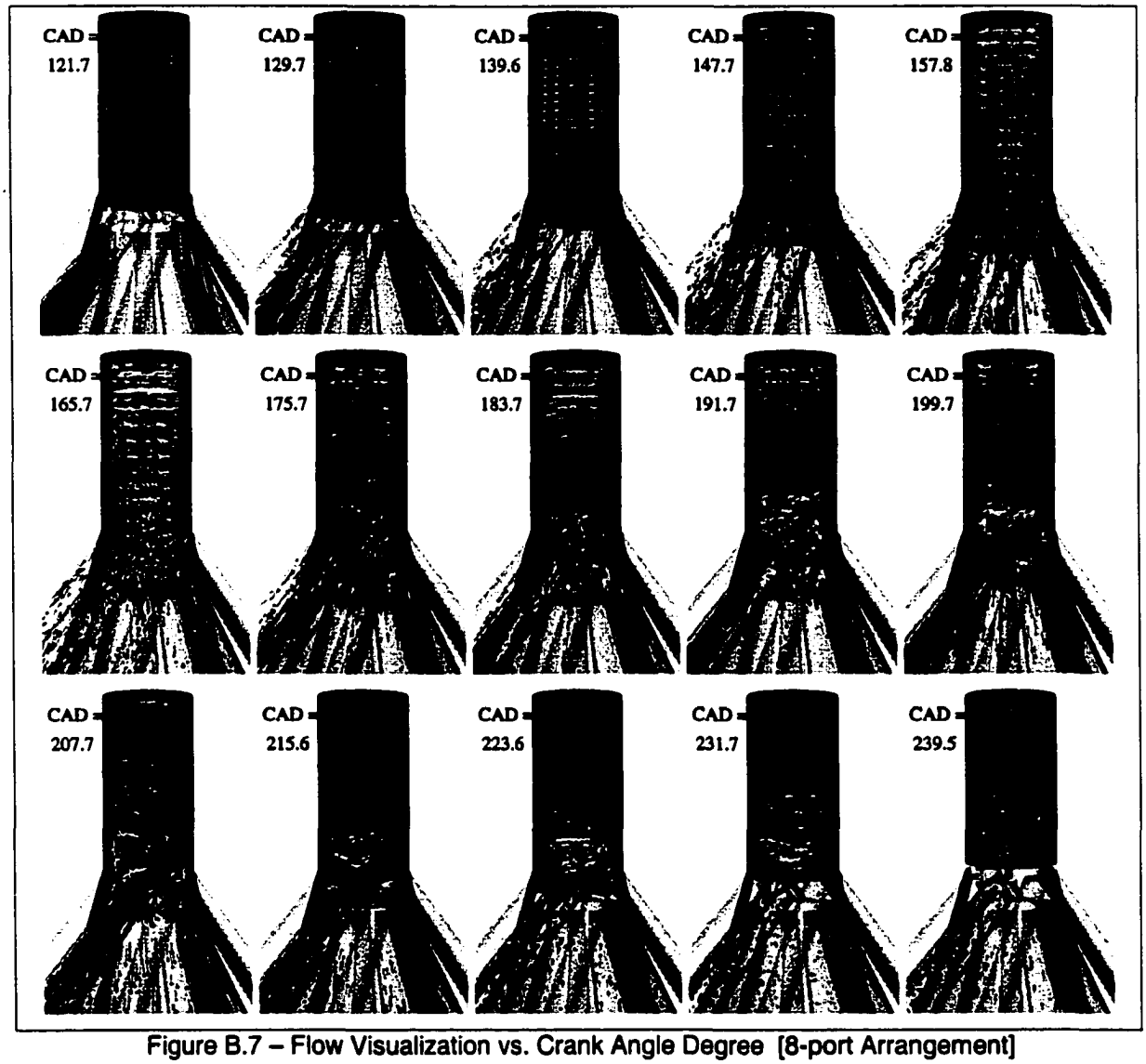

Figure B.7 – Flow Visualization vs. Crank Angle Degree [8-port Arrangement]

The in-cylinder and manifold flows for the 8- and 10-port configuration are presented in Figures B.7 and B.8 for reference. Again, Ensight's particle training method was used, with the from only one intake port shown.

These figures are similar to the Figure 4.11 where the flow for the 5-port geometry was presented. Here it can be seen that there is more blowdown into the intake manifold for the 8-port geometry (21% of the burned charge compared to 2% for the 10-port, and 10% for the 5-port cases) and thus later introduction of fresh charge into the cylinder. In these configurations the

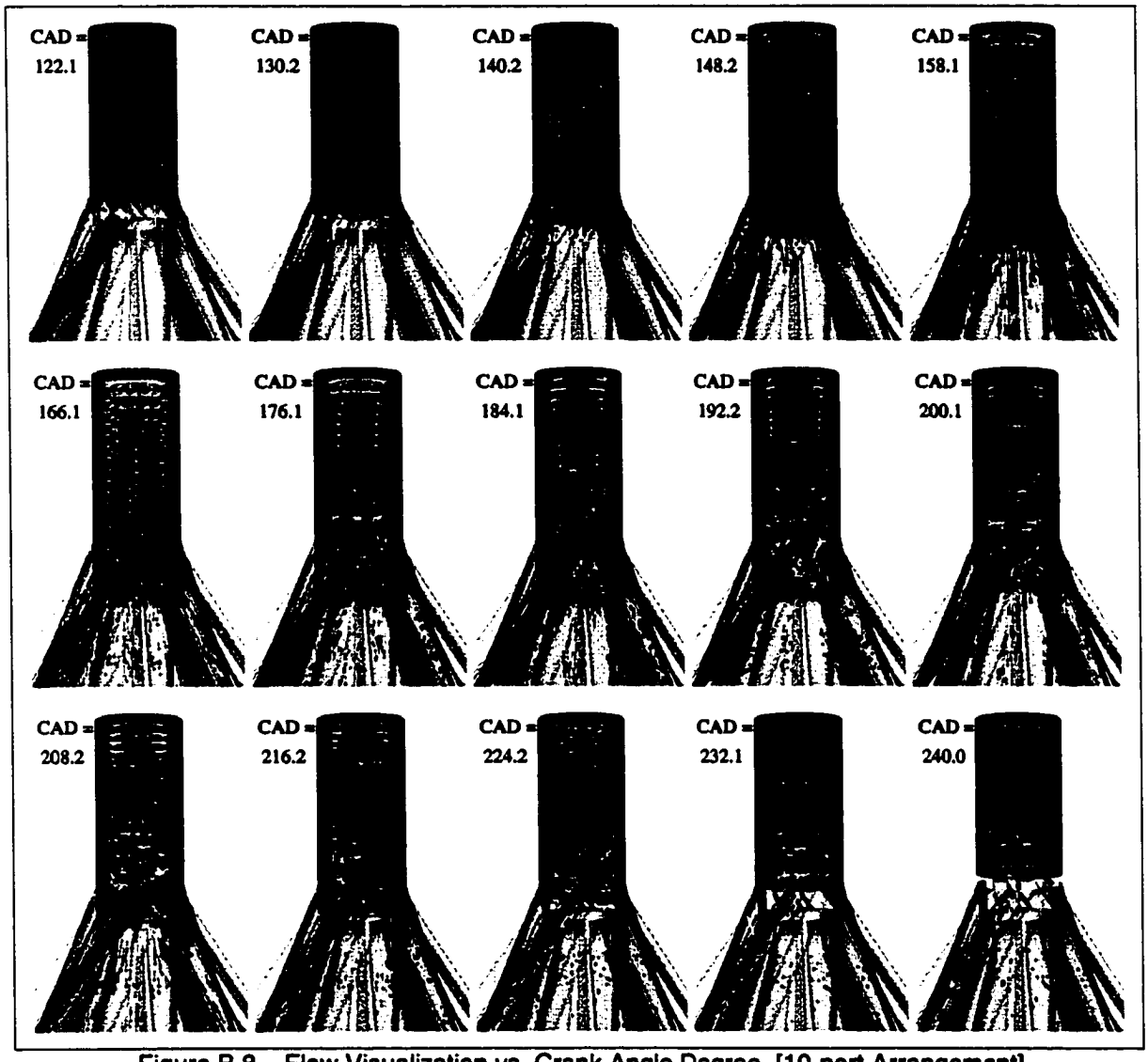

Figure B.8 – Flow Visualization vs. Crank Angle Degree [10-port Arrangement]

initial incoming charges are directed higher than in the 5-port case, due to the steeper incline angles, but again the flow is altered by the residual charge oscillation across the exhaust port. The desired swirling-loop never forms and the resulting charges are quite stratified at TDC.

Figure B.9 plots the average and maximum dilution ratios over the scavenging and compression processes to illustrate the lack of adequate mixing after IPC.

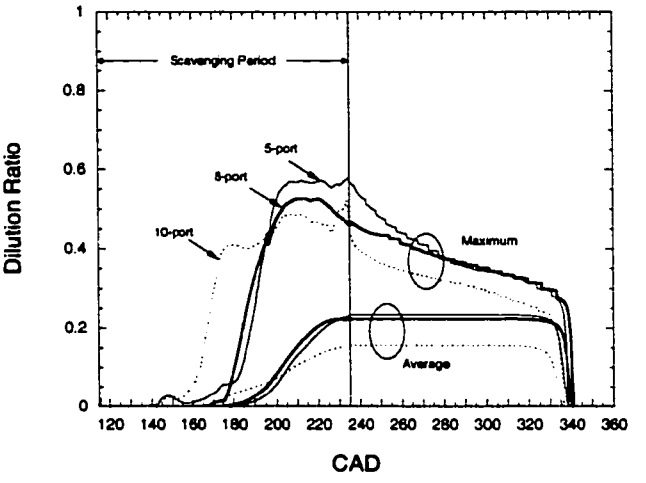

Figure B.9 – Average and Maximum Dilution Ratios vs. CAD

Intake Charge Pressure

Table B.2 lists the geometric and operating parameters for this simulation series. Here the 8- and 10-port arrangements were used with intake charge pressures ranging from 1.5 to 2.1bar. The exhaust boundary pressure was fixed at 1.0bar.\

Figures B.10-B.13 plot the results for the 8-port geometry; the 10-port arrangement exhibited similar behavior. The overall change in scavenging performance was illustrated in Figure 4.16. In Figure B.10 the average intake manifold pressures are displayed for the three pressure cases. It can be seen that the only change for these runs is the offset of the oscillations; the amplitudes were only slightly altered. The higher cylinder pressure at IPO counteracts the effect of the higher boundary pressure, and as a result more burned charge is actually blown into the intake manifold (23% for the 1.8bar case, and 26% for the 2.1bar case).

In Figure B.11 the plot of the intake flow rates shows that the fresh charge enters the cylinder at the same time, with the higher charge pressures leading to higher delivery ratios.

Number of Ports	8	8	8	10	10	10
Bore [cm]	7.62	7.62	7.62	7.62	7.62	7.62
Stroke [cm]	20.58	20.58	20.58	20.58	20.58	20.58
Compression Ratio	25:1	25:1	25:1	25:1	25:1	25:1
IPO [CAD]	114	114	114	115	115	115
EPO [CAD]	141	141	141	141	141	141
EPC [CAD]	213	213	213	213	213	213
IPC [CAD]	236	236	236	235	235	235
Ex Port Width [cm]	4.20	4.20	4.20	4.20	4.20	4.20
Ex Port Height [cm]	3.00	3.00	3.00	3.00	3.00	3.00
In Port Width [cm]	2.29	2.29	2.29	1.49	1.49	1.49
In Port Height [cm]	1.50	1.50	1.50	1.25	1.25	1.25
Ex Decline Angle	65°	65°	65°	65°	65°	65°
In Incline Angle	50°	50°	50°	55°	55°	55°
In Swirl Angle	62.5°	62.5°	62.5°	68.75°	68.75°	68.75°
Operating Frequency [Hz]	50	50	50	50	50	50
Intake Pressure [bar]	1.50	1.80	2.10	1.50	1.80	2.10
Exhaust Pressure [bar]	1.00	1.00	1.00	1.00	1.00	1.00
Intake ϕ	0.60	0.60	0.60	0.60	0.60	0.60

Table B.2 – Geometric and Operating Parameters

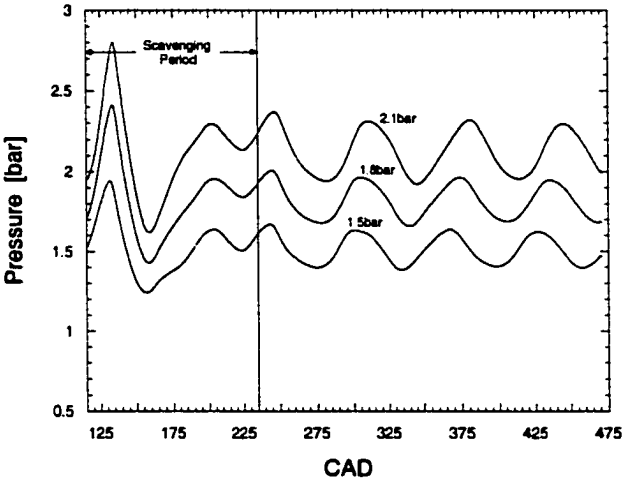

Figure B.10 – Average Intake Manifold Pressures vs. CAD

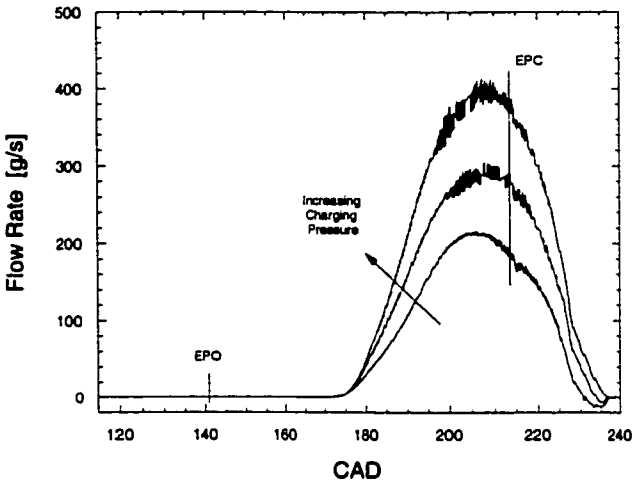

Figure B.11 – Fresh Charge Flow Rate vs. CAD

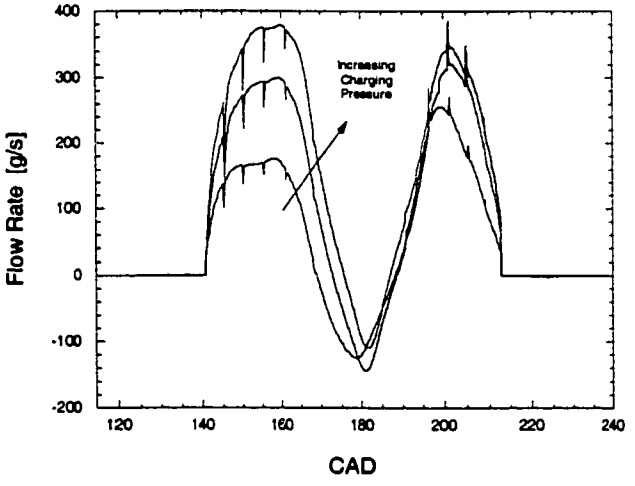

Figure B.12 – Exhaust Port Flow Rate vs. CAD

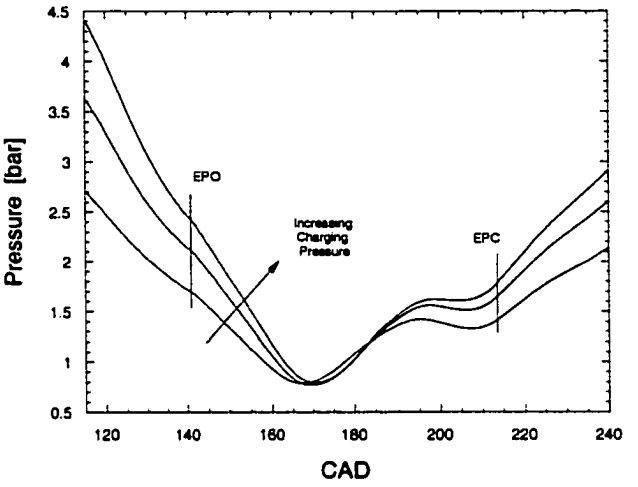

Figure B.13 – Cylinder Pressure vs. CAD

Figure B.12 shows that the initial flow through the exhaust port is greater for the higher charge pressures, but the effect of the flow oscillation is basically the same with reverse flow preventing adequate scavenging and leading to high trapping losses. In Figure B.13 it can be seen that the cylinder pressure curves are similar, leading to the conclusion that the dynamics of the scavenging process are changed little by the increase in charging pressure.

Exhaust Port Timing / Area

Table B.3 lists the geometric and operating parameters for this simulation series. Here the 10-port arrangement was used with a charging pressure of 1.80bar and an exhaust pressure of 1.0bar. The frequencies were adjusted slightly to keep the time between IPO and EPO constant to allow similar backflow into the intake manifold.

Figures B.14 and B.15 plot some of the results for these runs; the overall performance was presented in Figure 4.17. From an examination of the exhaust flow rates (these are plotted versus the actual time, starting at IPO) it can be seen that as the scavenging time increases the flow oscillations tend to dampen near the end of the gas transfer period. However, the overall effect on the in-cylinder flows is detrimental with alterations in the fresh charge flow patterns, and leading to significant trapping losses.

Number of Ports	10	10	10	10	10
Bore [cm]	7.62	7.62	7.62	7.62	7.62
Stroke [cm]	20.58	21.18	21.78	22.38	22.98
Compression Ratio	25:1	25:1	25:1	25:1	25:1
IPO [CAD]	115	113	110	107	104
EPO [CAD]	141	137	132	129	125
EPC [CAD]	213	216	220	223	226
IPC [CAD]	235	236	240	242	246
Ex Port Width [cm]	4.20	4.20	4.20	4.20	4.20
Ex Port Height [cm]	3.00	3.60	4.20	4.80	5.40
In Port Width [cm]	1.49	1.49	1.49	1.49	1.49
In Port Height [cm]	1.25	1.25	1.25	1.25	1.25
Ex Decline Angle	65°	65°	65°	65°	65°
In Incline Angle	55°	55°	55°	55°	55°
In Swirl Angle	68.75°	68.75°	68.75°	68.75°	68.75°
Operating Frequency [Hz]	50	48	46	44	42
Intake Pressure [bar]	1.80	1.80	1.80	1.80	1.80
Exhaust Pressure [bar]	1.00	1.00	1.00	1.00	1.00
Intake ϕ	0.60	0.60	0.60	0.60	0.60

Table B.3 – Geometric and Operating Parameters

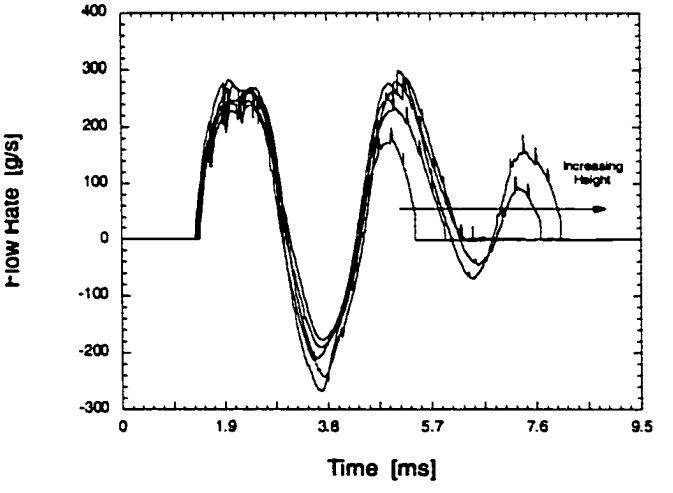

Figure B.14 – Exhaust Port Flow Rate vs. Time

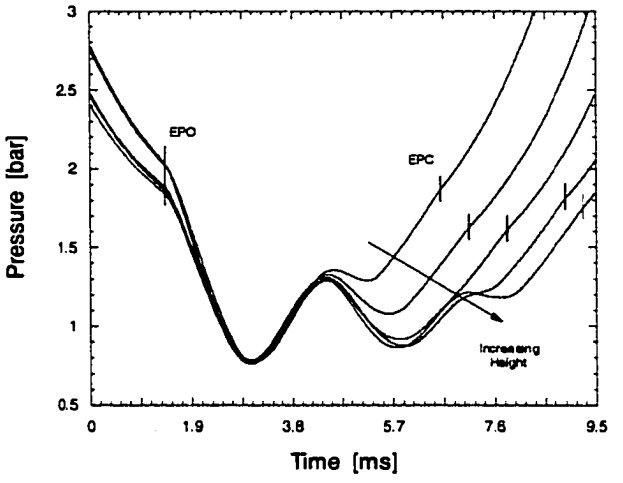

Figure B.15 – Cylinder Pressure vs. Time

Figure B.15 plots the average cylinder pressure during the scavenging period for these runs (again plotted versus actual time, starting at IPO). It can be seen that as the scavenging time increases the pressure oscillations tend to dampen, however this is not enough for the forward charging pressure to dominate. As a result, the basic in-cylinder flow patterns are unchanged with the swirling-loop not formed, and the cylinder charge highly stratified at TDC.

This can be seen in Figures B.16 and B.17 where the in-cylinder flows for the tallest exhaust port case are illustrated, and the average and maximum dilution ratios plotted. The flow visualization clearly illustrates the detrimental effect of the exhaust flow oscillation on the incoming charge direction, as well as the stratification problems.

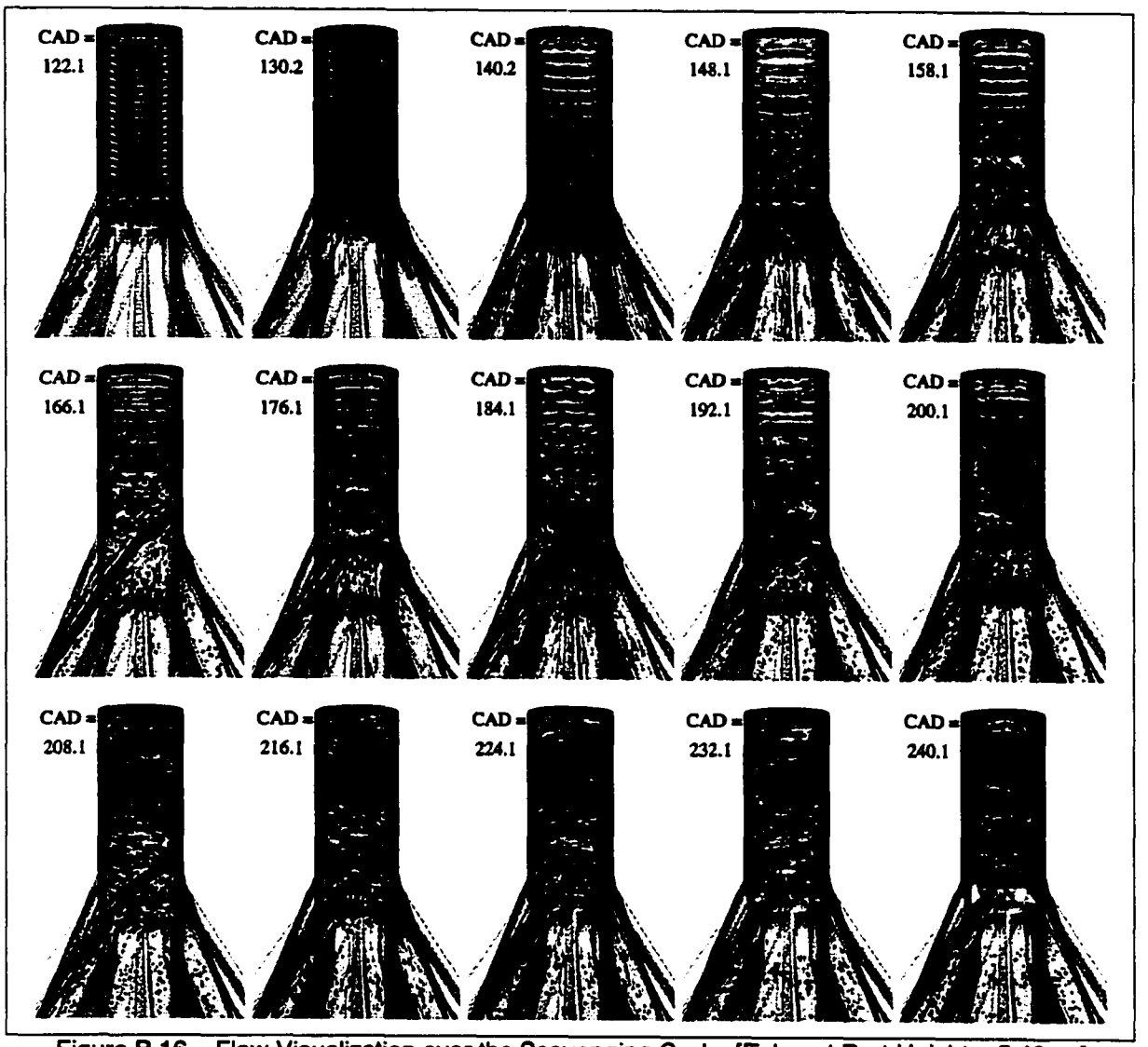

Figure B.16 – Flow Visualization over the Scavenging Cycle [Exhaust Port Height = 5.40cm]

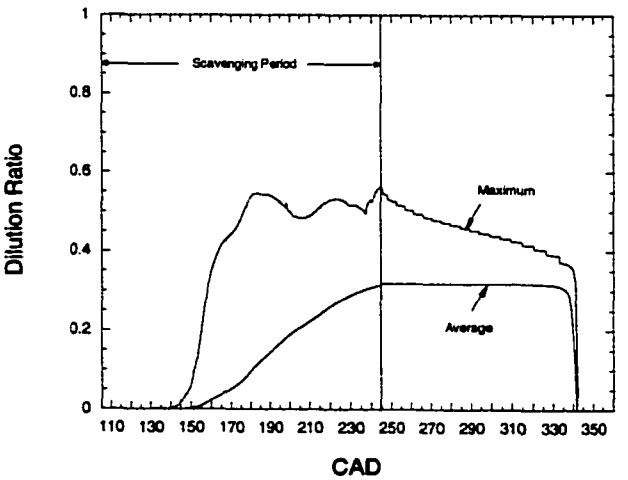

Figure B.17 – Average and Maximum Dilution Ratios vs. CAD [Exhaust Port Height = 5.40cm]

Piston Frequency

Table B.1 listed the geometric and operating parameters used for this simulation series. For this run the 5-port geometry was used with the piston frequency set to 16.7Hz - the overall scavenging time increased to 19.1ms.

Some of the scavenging results were presented in Figures 4.18 and 4.19. Figure B.18 below illustrates the flow patterns for the slower moving piston where the paths of a few select points from within the intake manifold are depicted for four different 'starting' times (as in Fig. 4.4). Again, flat 'ribbons' indicate twisting, or rotational motion as the gas moves through the cylinder. (Problems were encountered with the Ensight software for this case regarding its ability to accurately calculate the particle traces. The slower moving piston, in combination with the sector mesh and its resolution led to these problems. The calculated animations indicated that as the incoming particles swirl toward the top of the cylinder they exit the wall and disappear. Obviously this does not occur in reality, and the CFD calculations did not predict this loss. On the other hand however, the computed visualizations can show the general behavior of the fresh charge flow, and indicate how it is different from the higher frequency case.)

In Fig. B.18, it is obvious that the exhaust flow oscillations do not affect the fresh charge motion, with the incoming flow consistently directed toward the top of the cylinder. However, much of the charge still finds its way to the exhaust port. Even in this low f case however, the desired swirling-loop cannot be generated and the fresh charge cannot displace the burned gas at the top and in the core of the cylinder. A low scavenging efficiency (0.65) results, while a good deal of unburned gas is lost to short-circuiting (35%). Additionally, the resulting charge remains stratified through the compression and combustion processes. This can be seen in the plot of the dilution ratio over the scavenging and compression stroke presented in Figure B.19.

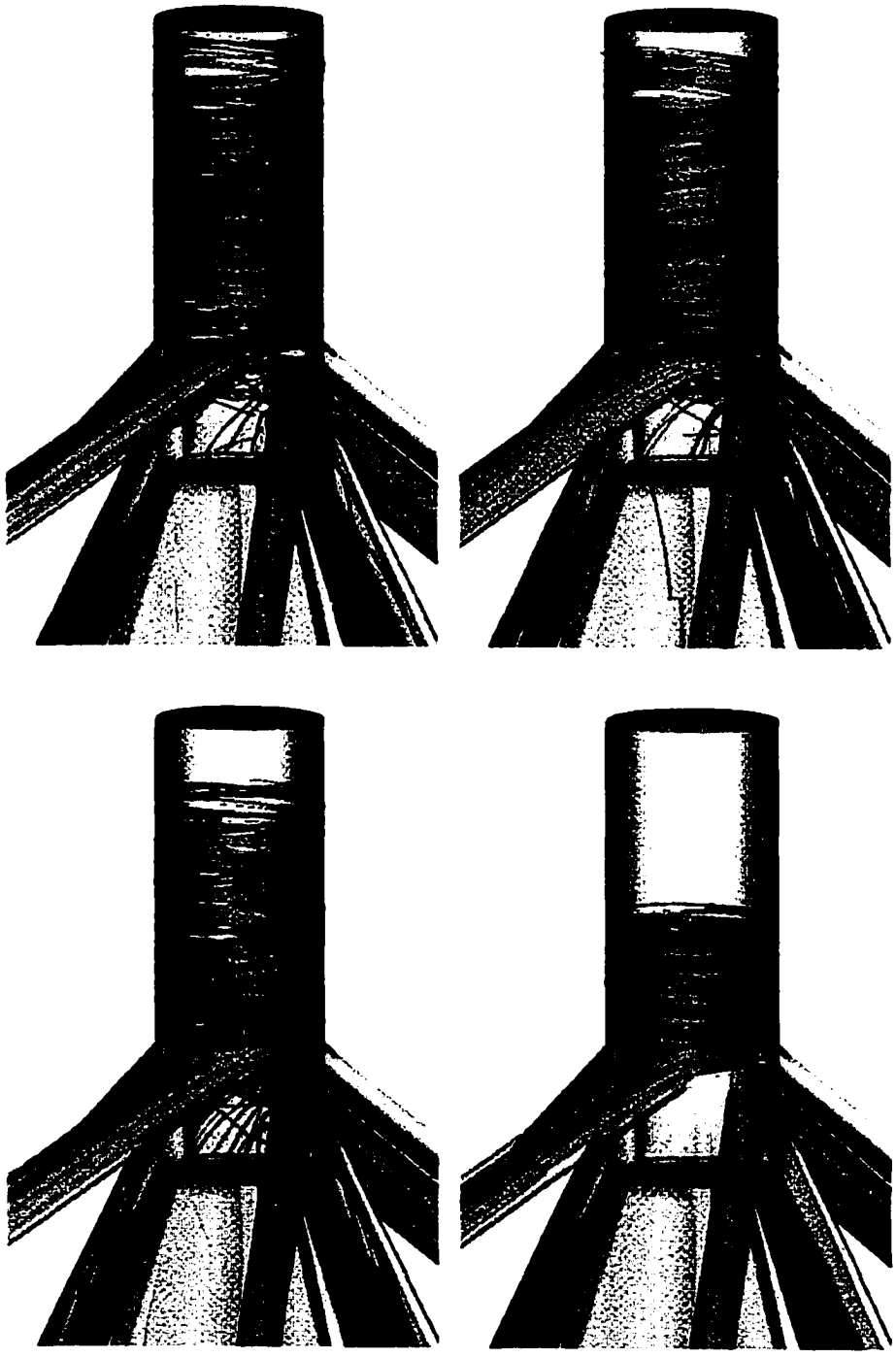

Figure B.18 – Hybrid-Loop Scavenging Flow Visualization Illustrating Path Lines from Select Points within the Intake Manifold [f = 16.7Hz]

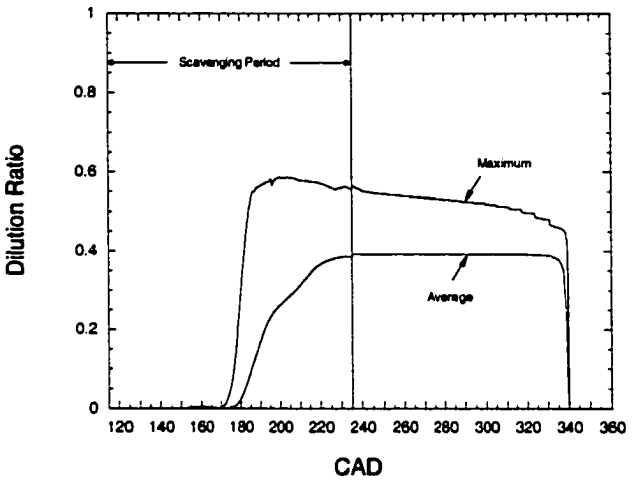

Figure B.19 – Average and Maximum Dilution Ratios vs. CAD [f = 16.7Hz]

Summary

Various parametric investigations were conducted using the KIVA-3V code in an effort to optimize the in-cylinder flow behavior, and the resulting scavenging performance of the hybrid-loop scavenging arrangement, with respect to the design goals (η_{sc}~0.90, η_{tr}~0.99). A summary of these results is presented in Figure B.20 where the trapping efficiencies are plotted against the achieved scavenging efficiencies. From this figure and the preceding presentation, it is clear that the hybrid-loop scavenging method represents a poor means of recharging the engine, and certainly cannot be used to meet the goals of the design.

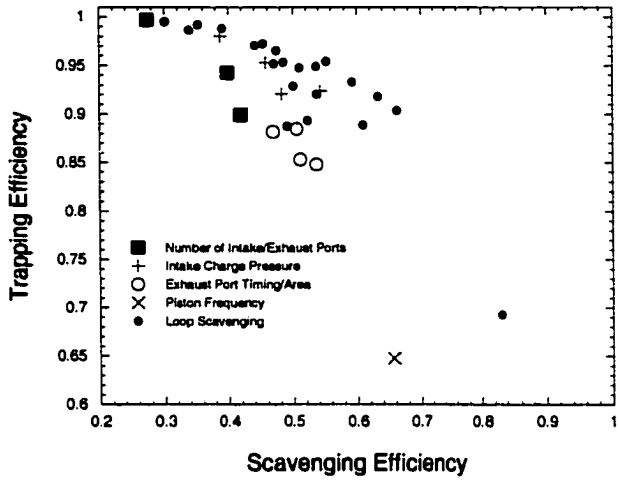

Figure B.20 – Trapping Efficiency vs. Scavenging Efficiency

APPENDIX C – UNIFLOW SCAVENGING SIMULATIONS

The purpose of this appendix is to more thoroughly describe the parametric simulations with the uniflow scavenging configuration. A summary of these computations is presented in Chapter IV. Here more detail is given regarding the cases investigated, as well as the results of the simulations.

Valve Specifications

The valve profile used for this study is given in Figure C.1. This was input to the mesh generator, K3PREP. The mesh resolution used however, provided only a crude approximation of this geometry, as can be seen in this figure.

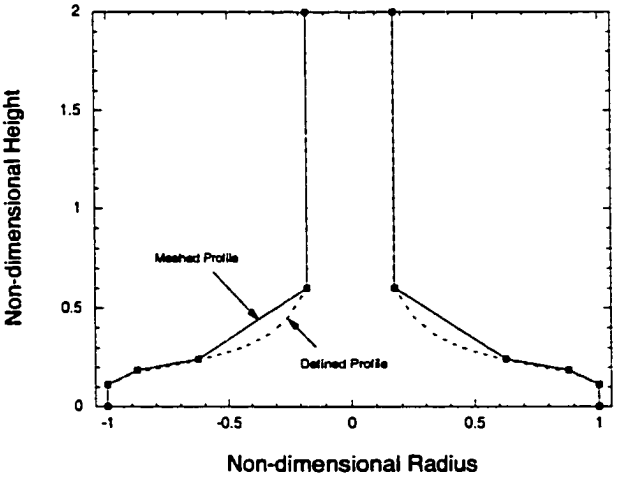

Figure C.1 – Non-dimensional Valve Profile

The valve lift history is presented in Figure C.2. For this study it was assumed that an electro-hydraulic actuator could be used to control the valve motion. The only adjustable parameters were the maximum lift and the duration of valve opening. The valve lift was centered

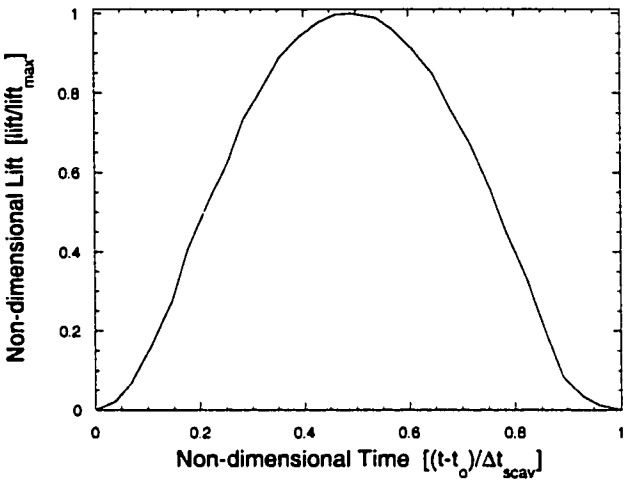

Figure C.2 – Non-dimensional Valve Lift History

at 175CAD to account for the non-symmetrical behavior of the piston about BDC (as seen in Fig. A.20, and Fig. C.29 below). This ensured that the exhaust valve opening (EVO) and exhaust valve closing (EVC) would occur at about the same point along the piston's trajectory.

Exhaust Valve Lift/Timing

Table C.1 lists the geometric and operating parameters for this simulation series. A sample mesh for this geometry was illustrated in Figure 4.20. Lifts ranging from 0.70 to 1.0cm were used with the lift duration ranging from 139 to 99CAD. The integrated valve area-times remained constant with these combinations. The intake port heights were adjusted as well to keep the integrated port area-times constant between the runs.

Some of the results for this scavenging series are presented in Figures C.3-C.5. A plot of the overall scavenging performance with respect to valve lift was given in Figure 4.22. (To review from Ch. IV, the 0.85cm lift/timing combination maximized the scavenging efficiency for these simulations.) In these figures the cylinder pressures, incoming fresh charge and exhausting flow rates for three cases are plotted over the non-dimensional scavenging period. The three cases illustrated represent the maximum and minimum valve lifts, and the optimal lift/timing configuration for this series. Indicated here are the IPO points, as well as the average intake

Bore [cm]	7.62	7.62	7.62	7.62	7.62	7.62
Stroke [cm]	26.13	24.46	23.24	22.26	21.35	20.12
Compression Ratio	45:1	45:1	45:1	45:1	45:1	45:1
EVO [CAD]	104	108	112	116	119	124
IPO [CAD]	147	145	145	144	144	143
IPC [CAD]	208	209	209	210	210	211
EVC [CAD]	243	238	234	232	230	223
Valve Diameter [cm]	2.54	2.54	2.54	2.54	2.54	2.54
Valve Lift [cm]	0.70	0.75	0.80	0.85	0.90	1.0
Number of Ports	8	8	8	8	8	8
Port Width [cm]	2.00	2.00	2.00	2.00	2.00	2.00
Port Height [cm]	2.77	2.70	2.65	2.60	2.56	2.50
Incline Angle	0°	0°	0°	0°	0°	0°
Swirl Angle	0°	0°	0°	0°	0°	0°
Operating Frequency [Hz]	50	50	50	50	50	50
Intake Pressure [bar]	1.20	1.20	1.20	1.20	1.20	1.20
Exhaust Pressure [bar]	1.00	1.00	1.00	1.00	1.00	1.00
Intake ϕ	0.42	0.42	0.42	0.42	0.42	0.42

Table C.1 – Geometric and Operating Parameters

manifold pressure for the optimal configuration (similar manifold pressures were seen with the other two cases).

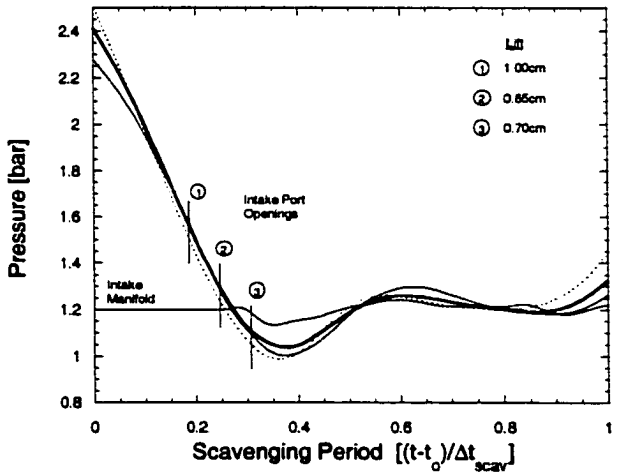

Figure C.3 – Average Cylinder Pressures vs. Scavenging Period

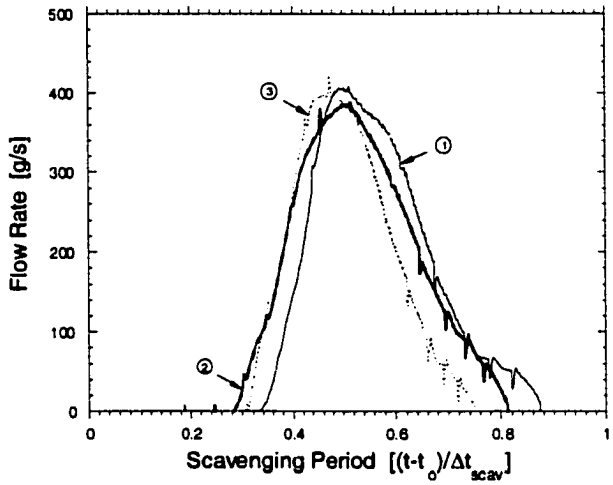

Figure C.4 – Fresh Charge Flow Rates vs. Scavenging Period

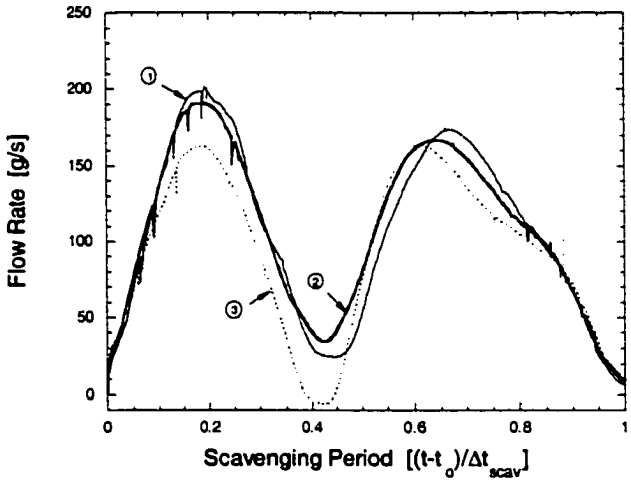

Figure C.5 – Exhaust Valve Flow Rates vs. Scavenging Period

From Figure C.3 it can be seen that the pressures histories were similar for this series; however, there is a significant difference between the three cases. For the maximum η_{sc} case, the intake ports open just when the cylinder pressure has blown down to the intake manifold pressure. In this arrangement the fresh charge enters the cylinder just as the ports are uncovered, allowing the cylinder to be recharged to the greatest degree possible.

Uniform Swirl Angles

Table C.2 lists the geometric and operating parameters for this simulation series. Swirl angles of 0°, 10°, 20° and 40° were used with the intake port widths adjusted to maintain the total intake cross-sectional area constant. For these runs a 12-port configuration was used.

Bore [cm]	7.62	7.62	7.62	7.62
Stroke [cm]	22.26	22.26	22.26	22.26
Compression Ratio	45:1	45:1	45:1	45:1
EVO [CAD]	116	116	116	116
IPO [CAD]	144	144	144	144
IPC [CAD]	210	210	210	210
EVC [CAD]	232	232	232	232
Valve Diameter [cm]	2.54	2.54	2.54	2.54
Valve Lift [cm]	0.85	0.85	0.85	0.85
Number of Ports	12	12	12	12
Port Width [cm]	1.33	1.35	1.42	1.75
Port Height [cm]	2.60	2.60	2.60	2.60
Incline Angle	0°	0°	0°	0°
Swirl Angle	0°	10°	20°	40°
Operating Frequency [Hz]	50	50	50	50
Intake Pressure [bar]	1.20	1.20	1.20	1.20
Exhaust Pressure [bar]	1.00	1.00	1.00	1.00
Intake ϕ	0.42	0.42	0.42	0.42

Table C.2 – Geometric and Operating Parameters

The differences in flow behavior and resulting scavenging performance for this series were adequately detailed in Ch. IV. However, for reference here, the lack of significant mixing after EVC is illustrated. The results for the 20° case are presented.

In Figure C.6 the average and maximum dilution ratios are plotted over the scavenging and compression processes. It can be seen that this behavior is quite different than that seen with the conventional loop arrangement, and this may be significant with regard to mixture uniformity at TDC.

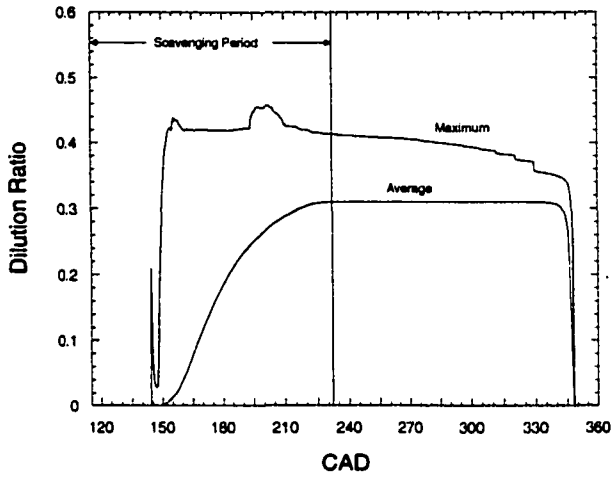

Figure C.6 – Average and Maximum Dilution Ratios vs. CAD [20° swirl]

Non-Uniform Swirl Angles

Table C.3 lists the various swirl angles used for this series; the angle designations are based on Fig. 4.27 which is reprinted here for reference. All other geometric and operating parameters are the same as from the uniform swirl angle series.

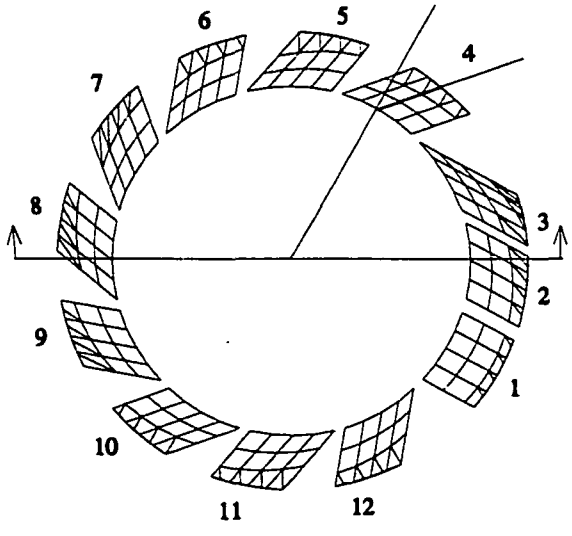

Figure 4.27 – Intake Port Arrangement [CASE 1]

	CASE 1	CASE 2	CASE 3	CASE 4	CASE 5
Angle 1	0.00	0.00	0.00	0.00	0.00
Angle 2	30.00	30.00	4.9	1.82	20.00
Angle 3	60.00	60.00	8.18	3.64	18.18
Angle 4	40.00	40.00	12.27	5.45	16.36
Angle 5	40.00	40.00	16.36	7.27	14.55
Angle 6	40.00	40.00	20.45	9.09	12.73
Angle 7	40.00	40.00	24.54	10.91	10.91
Angle 8	40.00	40.00	28.64	12.73	9.09
Angle 9	40.00	40.00	32.73	14.55	7.27
Angle 10	40.00	40.00	36.82	16.36	5.45
Angle 11	40.00	40.00	40.91	18.18	3.64
Angle 12	40.00	-30.00	45.00	20.00	1.82

Table C.3 – Swirl Angles

Some of the results for these runs are presented in Figures C.7-C.10 (CASE 4 was detailed in Ch. IV). Again, the characteristics of the in-cylinder flows are illustrated by plotting two iso-surfaces through the scavenging period. These surfaces represent residual fractions of 0.76 and 0.08, from the top of the cylinder, respectively, and indicate how the cylinder is flushed by the incoming fresh charge.

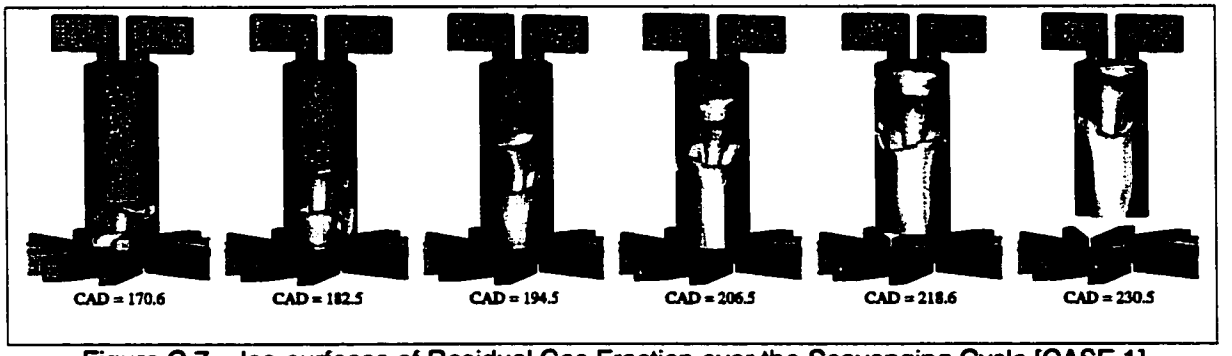

Figure C.7 – Iso-surfaces of Residual Gas Fraction over the Scavenging Cycle [CASE 1]

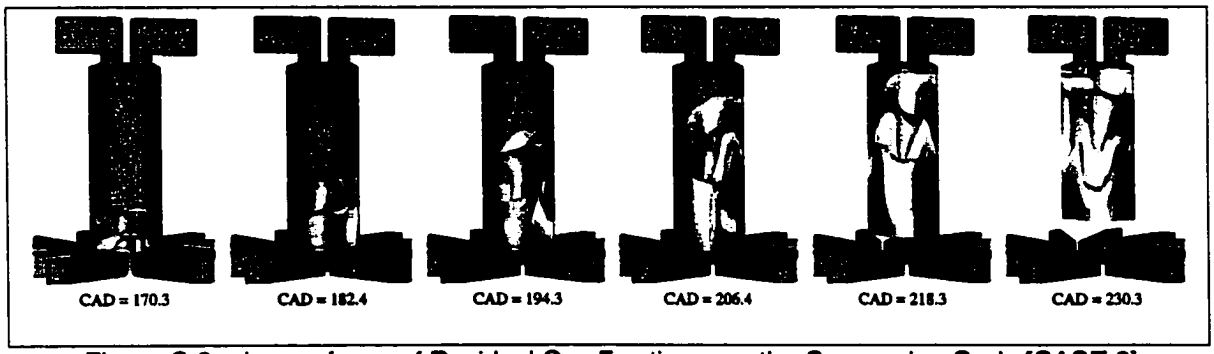

Figure C.8 – Iso-surfaces of Residual Gas Fraction over the Scavenging Cycle [CASE 2]

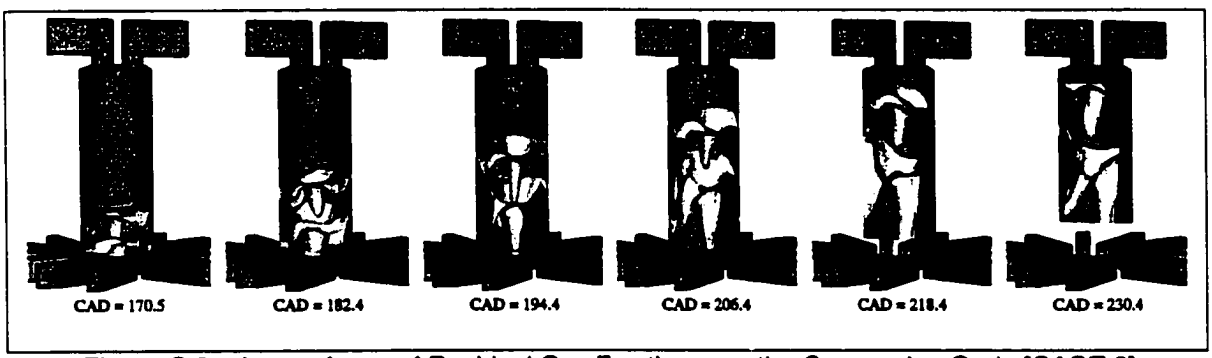

Figure C.9 – Iso-surfaces of Residual Gas Fraction over the Scavenging Cycle [CASE 3]

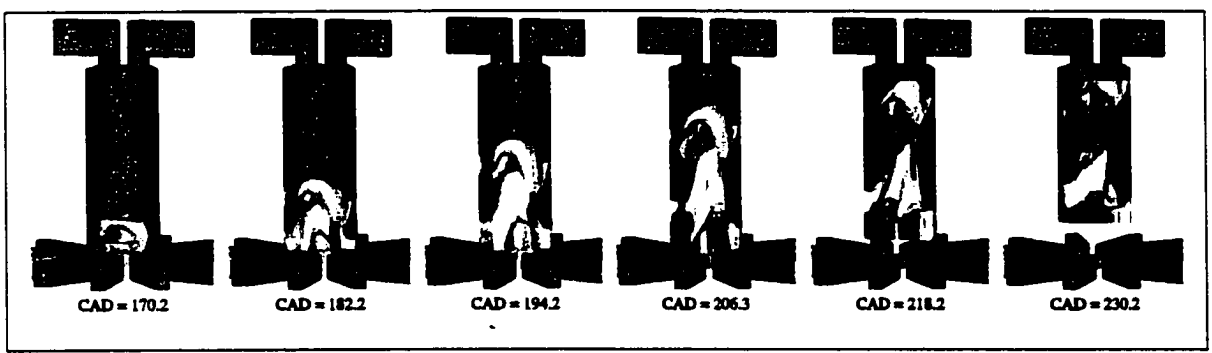

Figure C.10 – Iso-surfaces of Residual Gas Fraction over the Scavenging Cycle [CASE 5]

While each case represented here reveals an interesting flow pattern, the goal of simultaneous core flushing and wall sweeping was not achieved in any configuration. These figures illustrate the non-uniform flow that results from non-uniform swirl angle arrangements. Clearly, plug flow is not generated in any of the configurations, and there is an increased chance of short-circuiting, relative to either the 10° or 20° uniform cases.

Number of Intake Ports

Table C.4 lists the geometric and operating parameters for this simulation series. Here 8-port configurations were constructed to compare the scavenging performance to the 12-port geometries used previously (Table C.2).

Bore [cm]	7.62	7.62
Stroke [cm]	22.26	22.26
Compression Ratio	45:1	45:1
EVO [CAD]	116	116
IPO [CAD]	144	144
IPC [CAD]	210	210
EVC [CAD]	232	232
Valve Diameter [cm]	2.54	2.54
Valve Lift [cm]	0.85	0.85
Number of Ports	8	8
Port Width [cm]	2.00	2.63
Port Height [cm]	2.60	2.60
Incline Angle	0°	0°
Swirl Angle	0°	40°
Operating Frequency [Hz]	50	50
Intake Pressure [bar]	1.20	1.20
Exhaust Pressure [bar]	1.00	1.00
Intake ϕ	0.42	0.42

Table C.4 – Geometric and Operating Parameters

Some of the results from these simulations are presented in Figures C.11 and C.12. The cylinder pressures and fresh charge flow rates are plotted over the scavenging period with the results from the 12-port simulations included for reference. The overall scavenging performance for the two geometries was identical to the 12-port cases.

In Fig. C.11 it can be seen that in the 0° swirl case there is no difference in pressure for the 8- and 12-port geometries. In addition, the pressures for the 40° swirl case are quite similar, with the differences due to the change in the incoming flow rates. Flow through the 8 intake port

geometry is initially more rapid than the 12-port flow, but this drops to below the rate of the 12-port flow as the scavenging process progresses.

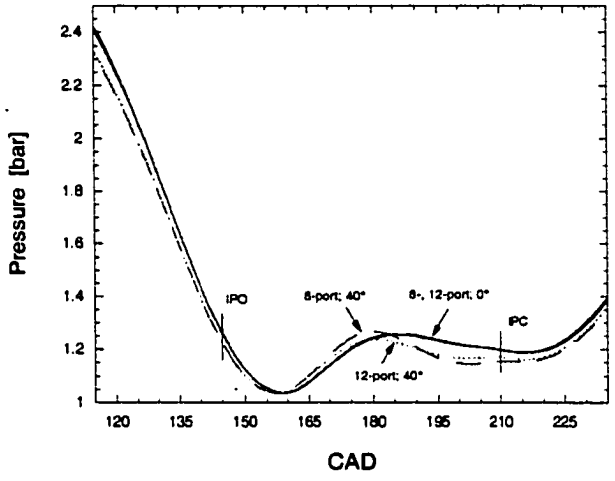

Figure C.11 – Cylinder Pressures vs. CAD

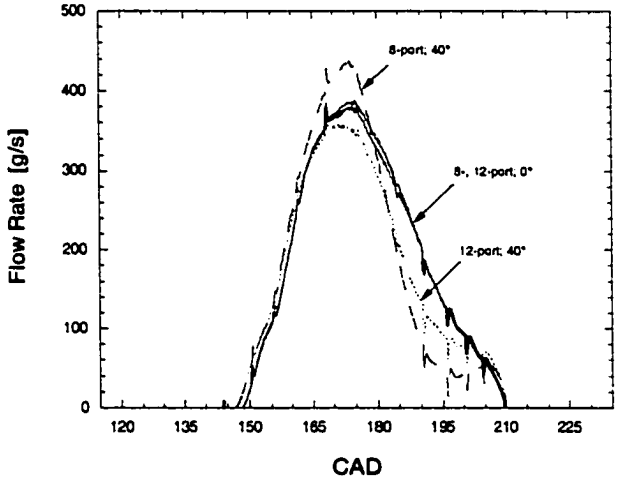

Figure C.12 – Fresh Charge Flow Rates vs. CAD

The in-cylinder flow patterns for the 8-port geometries are presented in Figures C.13 and C.14. Again, as in Figures 4.23-4.26, the flow is visualized through contour plots of the residual gas fraction, presented at various points in the scavenging cycle. The contours are plotted on a plane parallel to the cylinder's axis with fractions of 0.76, 0.69, 0.61, 0.53, 0.46, 0.38, 0.31, 0.23,

0.15, 0.08, respectively from the top of the cylinder shown. These patterns are not different from those seen previously with the 12-port design.

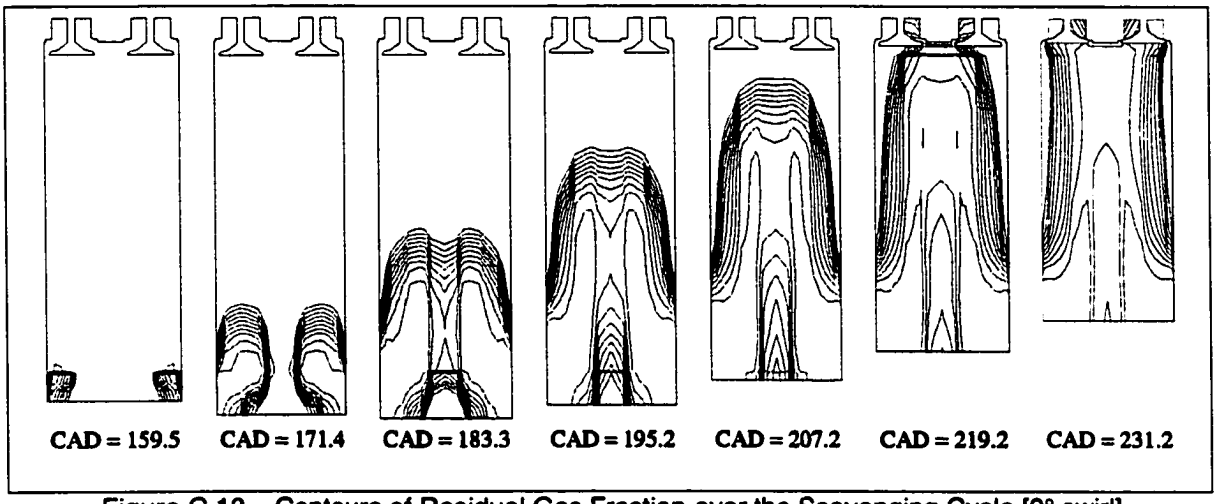

Figure C.13 – Contours of Residual Gas Fraction over the Scavenging Cycle [0° swirl]

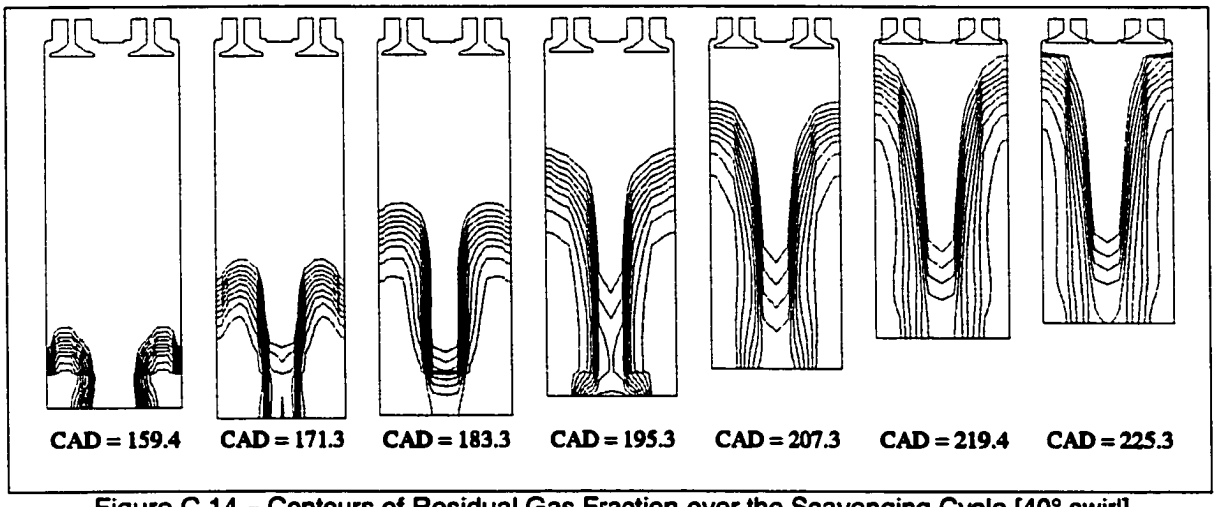

Figure C.14 – Contours of Residual Gas Fraction over the Scavenging Cycle [40° swirl]

Intake Port Area

Table C.5 lists the geometric and operating parameters for this simulation series. The intake port heights were varied from 3.0 to 4.5cm while the widths remained constant. The blowdown time (EVO-IPO) was set constant at 1.9ms, with the integrated valve area-time fixed

for the four runs (the valve lifts were varied to achieve this). A charging pressure of 1.2bar was used with the exhaust pressure set at 1.0bar.

Bore [cm]	7.62	7.62	7.62	7.62
Stroke [cm]	22.99	23.77	24.60	25.50
Compression Ratio	45:1	45:1	45:1	45:1
EVO [CAD]	113	110	108	105
IPO [CAD]	142	139	136	134
IPC [CAD]	212	214	217	219
EVC [CAD]	233	236	238	241
Valve Diameter [cm]	2.54	2.54	2.54	2.54
Valve Lift [cm]	0.80	0.78	0.74	0.72
Number of Ports	8	8	8	8
Port Width [cm]	2.00	2.00	2.00	2.00
Port Height [cm]	3.00	3.50	4.0	4.50
Incline Angle	0°	0°	0°	0°
Swirl Angle	15°	15°	15°	15°
Operating Frequency [Hz]	50	50	50	50
Intake Pressure [bar]	1.20	1.20	1.20	1.20
Exhaust Pressure [bar]	1.00	1.00	1.00	1.00
Intake ϕ	0.42	0.42	0.42	0.42

Table C.5 – Geometric and Operating Parameters

Figures C.15-C.17 illustrate some of the results from these runs; a summary of the scavenging performance was presented in Chapter IV. In the following figures the cylinder pressures, intake and exhaust flow rates are plotted over the normalized scavenging period. The plot of the cylinder pressure shows the timing issue encountered in this series, with the pressure at IPO increased for the taller intake ports. Also evident in this figure is that the cylinder pressure closely follows the intake manifold pressure after about halfway through the scavenging period, indicating that the valves represent the major flow restriction in this configuration.

Figures C.16 and C.17 show the changes in mass flow rate with the port size; the total delivered mass is listed for reference. Here it can be seen that there is not too much difference for the four cases analyzed.

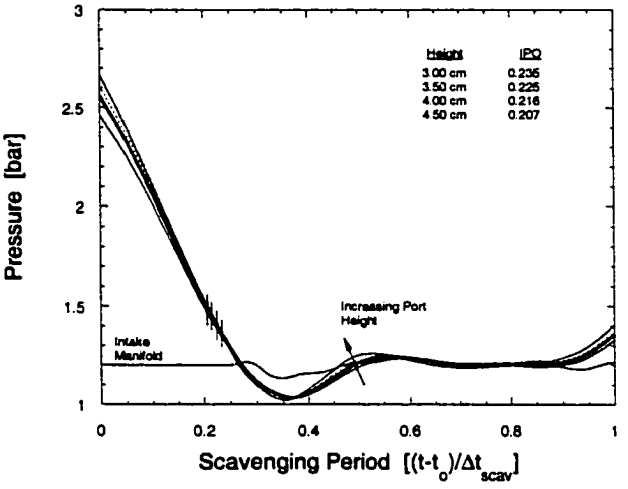

Figure C.15 – Cylinder Pressures vs. Normalized Scavenging Period

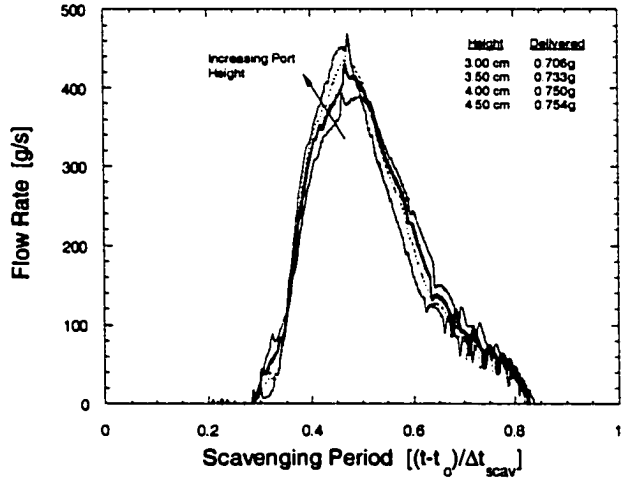

Figure C.16 – Fresh Charge Flow Rates vs. Normalized Scavenging Period

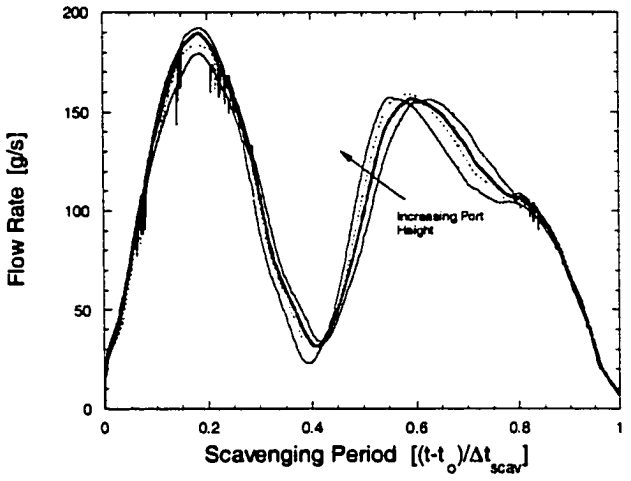

Figure C.17 – Exhaust Valve Flow Rates vs. Normalized Scavenging Period

Piston Frequency

Table C.6 lists the geometric and operating parameters for this simulation series. Frequencies ranging from 50 to 30Hz were used with the blowdown time fixed at 2.03ms. To set this time the valve timing was adjusted with the valve lift fixed at 0.925cm.

Some of the results from this series are presented in Figures C.18-C.21. The overall scavenging performance was illustrated in Fig. 4.30. In Figure C.18 the cylinder pressures are plotted versus the time past EVO, with the IPO and EVC points noted. The average intake manifold pressure for the 50Hz case is included for reference. Here it can be seen again that the cylinder pressures closely follow the intake manifold pressure for a good portion of the scavenging period, especially for the low f case, indicating that the major flow restriction is through the valves.

The integrated exhaust flow is presented in Figure C.19; this is also plotted over the time past EVO. It is evident that the initial blowdown period yields similar flow rates, but as the scavenging process progresses, more flow is able to discharge through the valves as the scavenging time increases.

Bore [cm]	7.62	7.62	7.62	7.62
Stroke [cm]	25.81	24.60	23.24	22.26
Compression Ratio	45:1	45:1	45:1	45:1
EVO [CAD]	104	107	112	116
IPO [CAD]	141	140	138	137
IPC [CAD]	213	213	215	216
EVC [CAD]	243	240	235	232
Valve Diameter [cm]	2.54	2.54	2.54	2.54
Valve Lift [cm]	0.925	0.925	0.925	0.925
Number of Ports	8	8	8	8
Port Width [cm]	2.00	2.00	2.00	2.00
Port Height [cm]	3.50	3.50	3.50	3.50
Incline Angle	0°	0°	0°	0°
Swirl Angle	15°	15°	15°	15°
Operating Frequency [Hz]	50	43.3	36.7	30
Intake Pressure [bar]	1.20	1.20	1.20	1.20
Exhaust Pressure [bar]	1.00	1.00	1.00	1.00
Intake ϕ	0.42	0.42	0.42	0.42

Table C.6 – Geometric and Operating Parameters

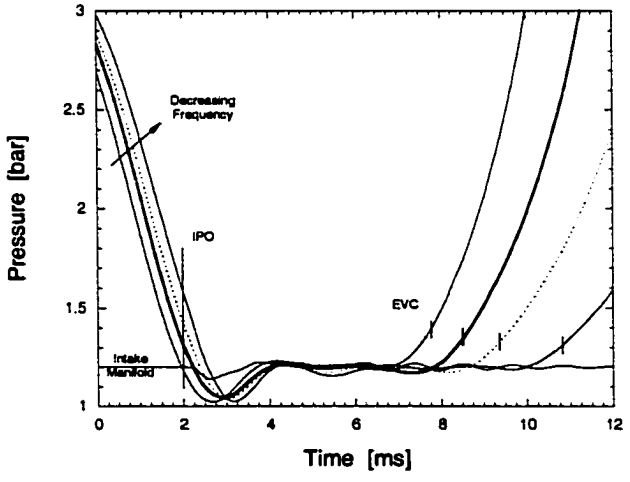

Figure C.18 – Cylinder Pressure vs. Time after EVO

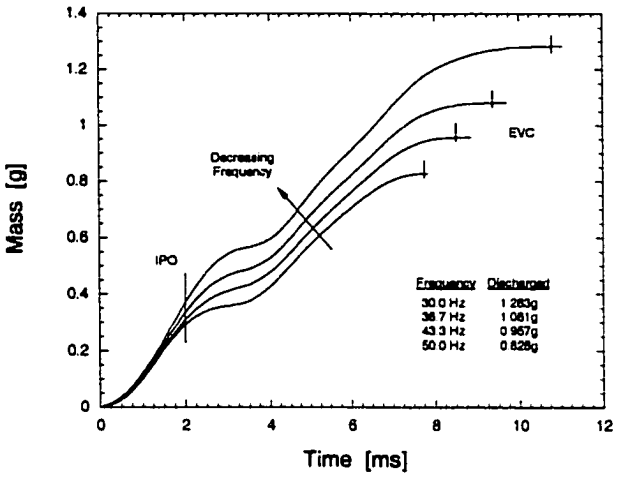

Figure C.19 – Integrated Exhaust Valve Flow vs. Time after EVO

Figures C.20 and C.21 are presented to illustrate the changes in in-cylinder flow behavior as the piston frequency decreases; the 50Hz case is given in Figure C.20, while Figure C.21 shows the flows for the 30Hz case. Here Ensight's particle tracing routine was used again.

Indeed there is greater penetration of the fresh charge to the top of the cylinder for the 50Hz case, and the cylinder is more completely scavenged. However, the basic swirling flow patterns seem similar.

Figure C.22 is presented next to illustrate the mixing behavior of the charges after EVC. The average and maximum dilution ratios are plotted over the scavenging and compression processes for the 50 and 30Hz cases. As can be seen there is little change in the uniformity of the charge through the compression stroke, however, the low f case (with the longest scavenging time) allows the charge to become quite uniform before EVC.

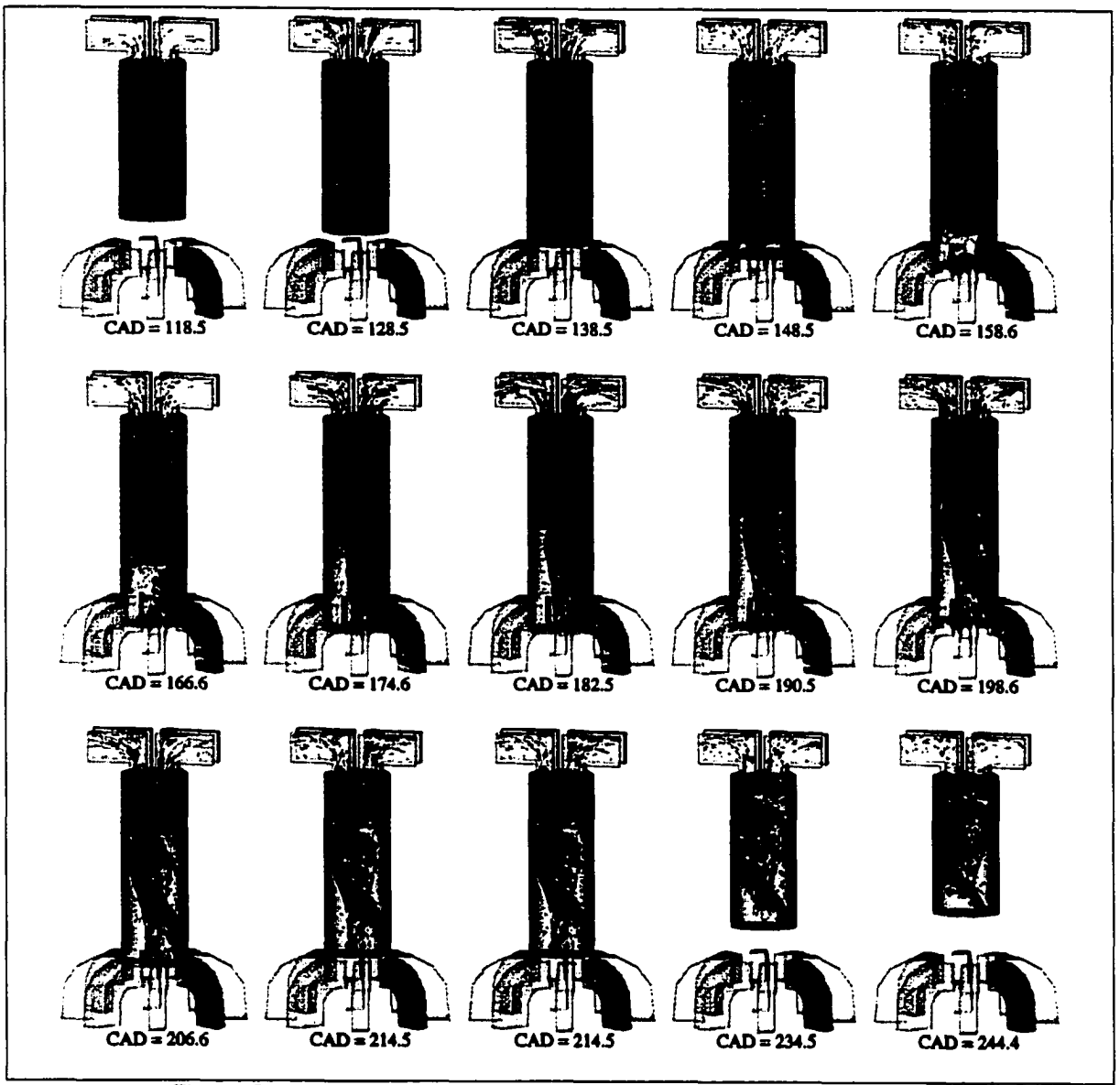

Figure C.20 – Flow Visualization over the Scavenging Cycle [f = 50Hz]

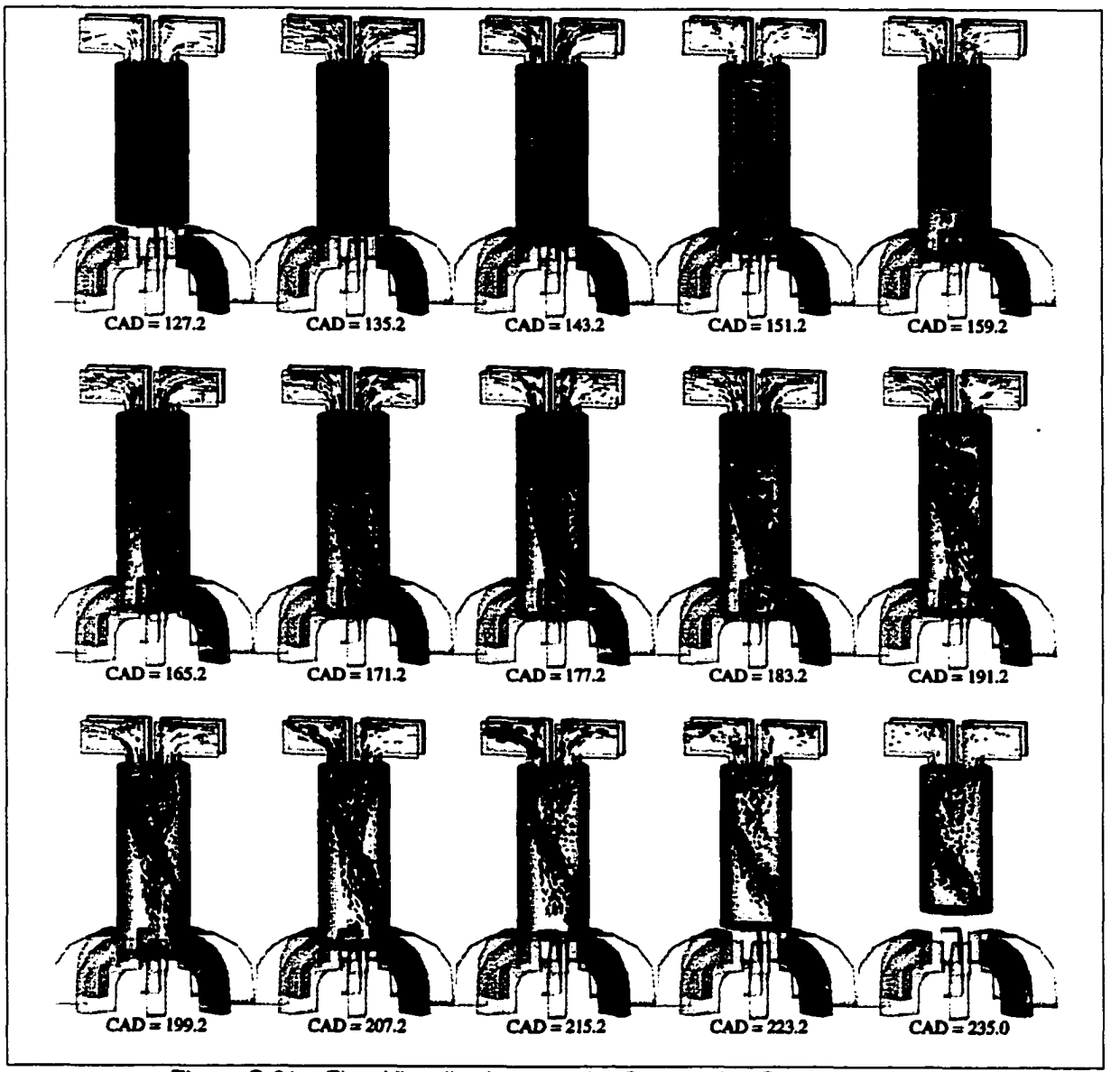

Figure C.21 – Flow Visualization over the Scavenging Cycle [f = 30Hz]

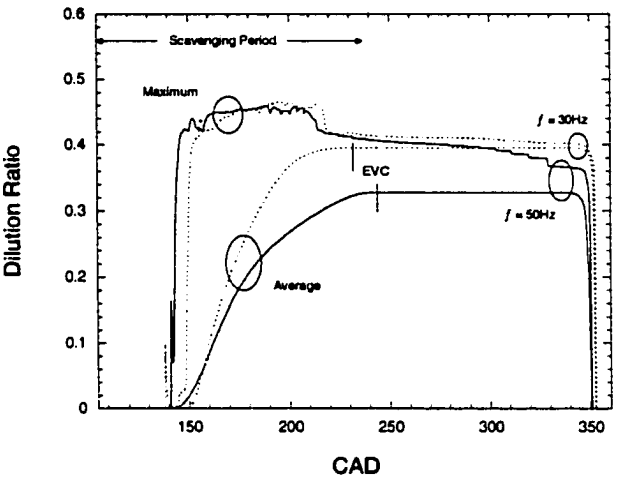

Figure C.22 – Average and Maximum Dilution Ratios vs. CAD

Piston Travel Past Port Bottom

Table C.7 lists the geometric and operating parameters for this simulation series. Piston travel past the intake port bottom was set at 1.65 and 4.0cm with the frequency fixed at 50Hz. Intake port heights of 3.5cm were utilized with the valve timing adjusted so that the time from EVO to IPO was maintained at 2.03ms.

Some of the results of these simulations are presented in Figures C.23-C.26. The overall performance of the scavenging cycle was illustrated in Figure 4.31. Figures C.23 and C.24 plot the fresh charge and exhaust flow rates versus CAD for the three geometries simulated. The changes in flow rates are apparent with more charge delivered for the longest stroke case (4.cm additional travel). However, the curves are quite similar.

Figures C.25 and C.26 illustrate the change in in-cylinder flow behavior for the two cases simulated here. Again, Ensight's particle tracing function was utilized. These illustrations can be compared to Figure C.20, which depicts the flow patterns for the case of no additional piston travel. The significant features for these two configurations were described earlier in Chapter IV.

Bore [cm]	7.62	7.62
Stroke [cm]	28.23	32.53
Compression Ratio	45:1	45:1
EVO [CAD]	97	88
IPO [CAD]	134	125
IPC [CAD]	219	227
EVC [CAD]	250	258
Valve Diameter [cm]	2.54	2.54
Valve Lift [cm]	0.925	0.925
Number of Ports	8	8
Port Width [cm]	2.00	2.00
Port Height [cm]	3.50	3.50
Incline Angle	0°	0°
Swirl Angle	15°	15°
Operating Frequency [Hz]	50	50
Intake Pressure [bar]	1.20	1.20
Exhaust Pressure [bar]	1.00	1.00
Intake ϕ	0.42	0.42

Table C.7 – Geometric and Operating Parameters

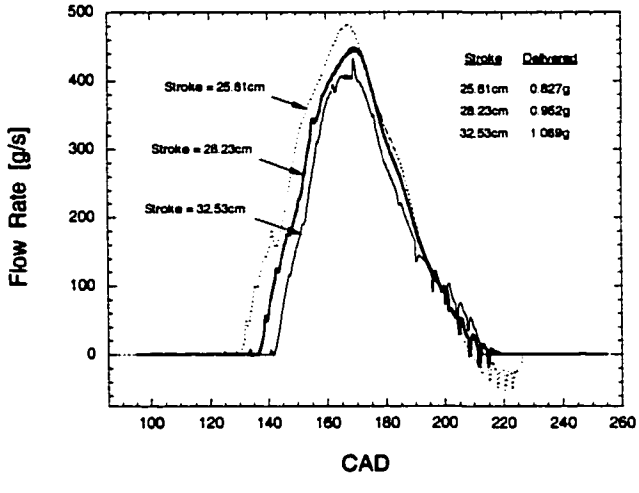

Figure C.23 – Fresh Charge Flow Rates vs. CAD

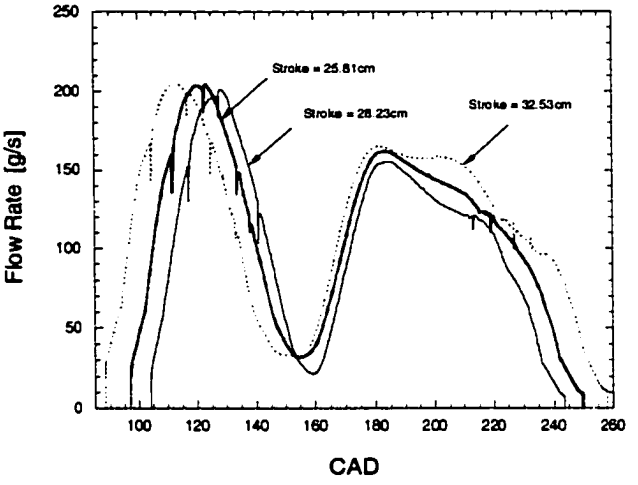

Figure C.24 – Exhaust Valve Flow Rates vs. CAD

Figure C.27 plots the piston velocity versus the piston's position for the three cases investigated here. Apparent are the changes in the piston dynamics, required to maintain the operating frequency for the longer stroke cases. The substantial increase in piston velocity will certainly affect the piston ring friction for these designs, however, the extent to which this is significant was not determined for these runs.

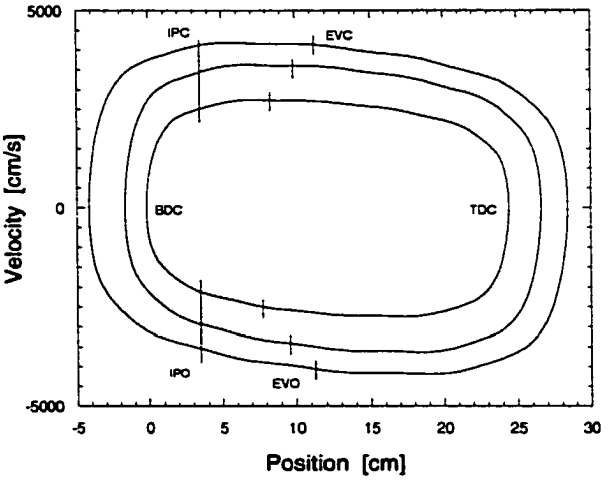

Figure C.27– Piston Position vs. Position

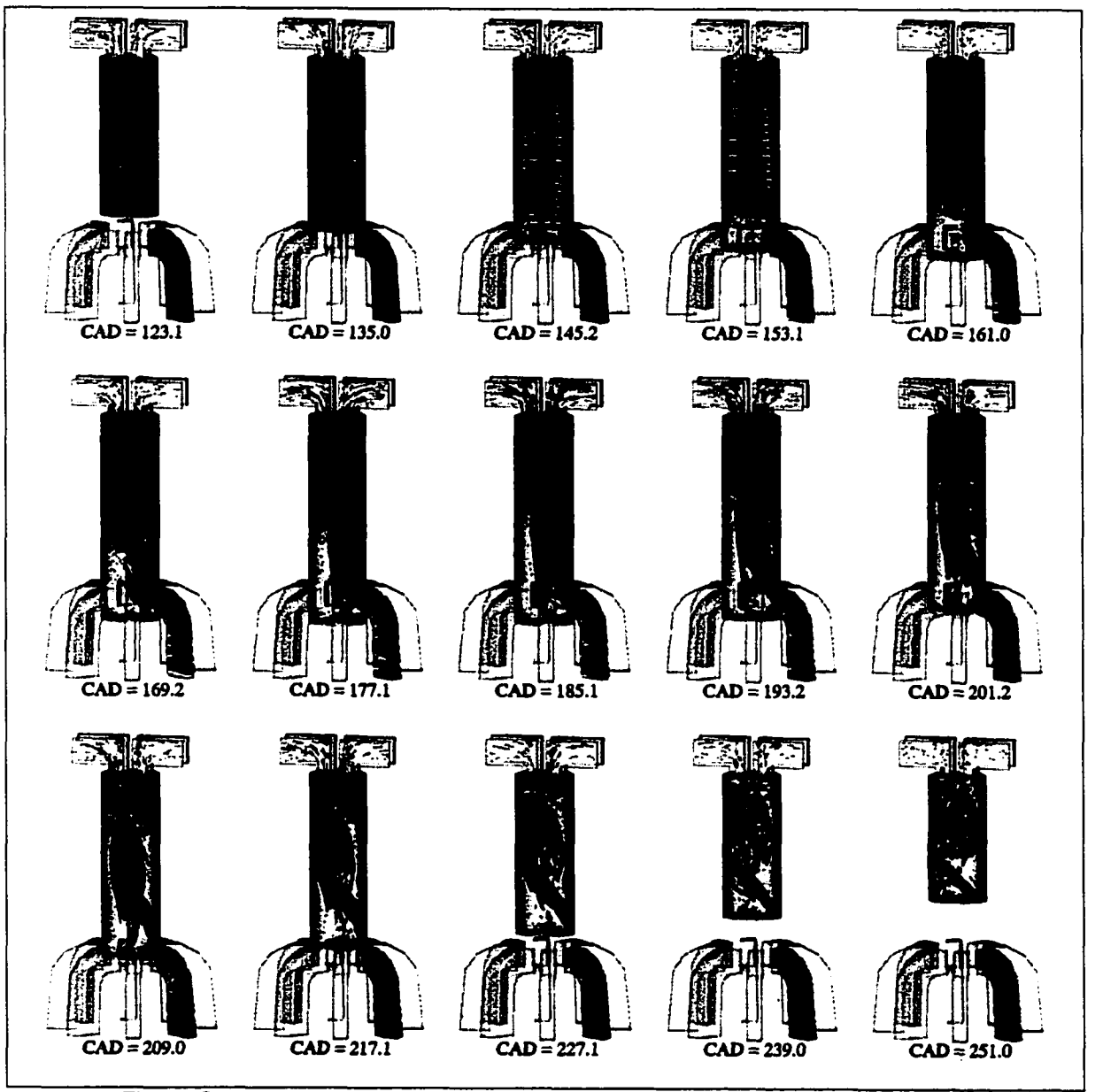

Figure C.25 – Flow Visualization over the Scavenging Cycle [Stroke =28.23cm]

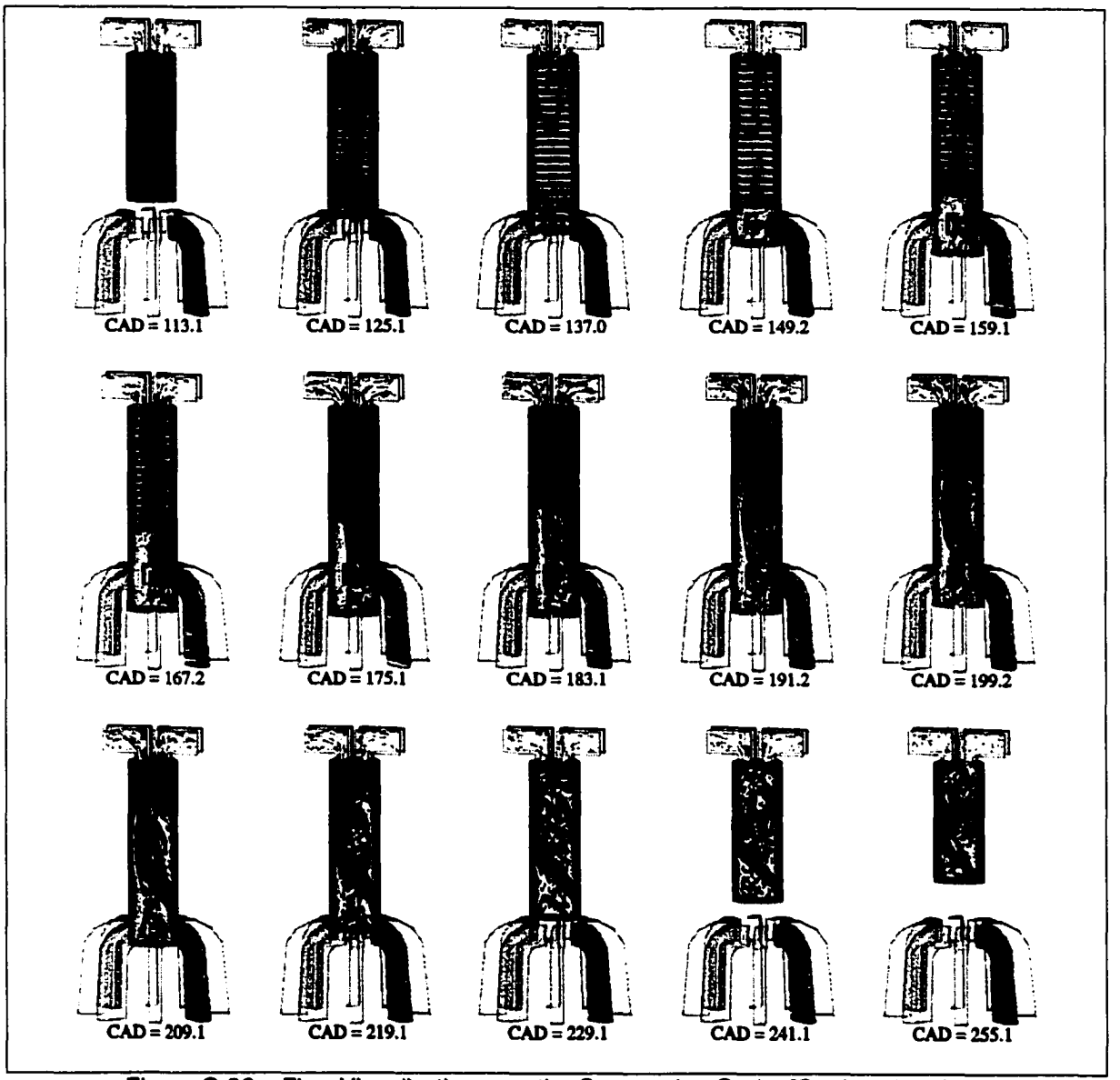

Figure C.26 – Flow Visualization over the Scavenging Cycle [Stroke =32.53cm]

Summary

Various parametric investigations were conducted using the KIVA-3V code in order to maximize the performance of the uniflow scavenging arrangement, with respect to the design goals (η_{sc}~0.90, η_{tr}~0.99). A summary of the results of these simulations is presented in Figure C.28 where the trapping efficiencies are plotted against the achieved scavenging efficiencies. This figure shows that the uniflow scavenging system, unlike the conventional loop, or hybrid-loop configurations, can be arranged to nearly achieve the goals of the engine.

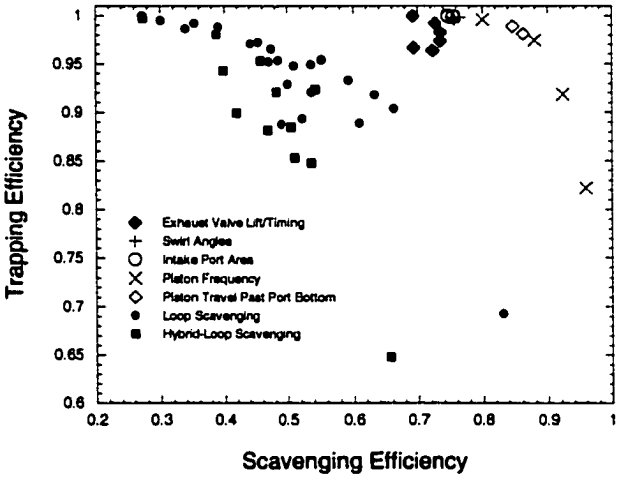

Figure C.28 – Trapping Efficiency vs. Scavenging Efficiency

APPENDIX D – CHARGE DELIVERY SIMULATIONS

The purpose of this appendix is to more thoroughly describe the parametric simulations with the charge delivery system. A summary of these computations is presented in Chapter IV. Here more detail is given regarding the cases investigated, as well as the results of the simulations.

Engine Specifications

Table D.1 lists the geometric and operating parameters of the engine used for these simulations. The 43.3Hz case from Table C.06 was chosen for these runs.

Bore [cm]	7.62
Stroke [cm]	24.60
Compression Ratio	45:1
EVO [CAD]	107
IPO [CAD]	140
IPC [CAD]	213
EVC [CAD]	240
Valve Diameter [cm]	2.54
Valve Lift [cm]	0.925
Number of Ports	8
Port Width [cm]	2.00
Port Height [cm]	3.50
Incline Angle	0°
Swirl Angle	15°
Operating Frequency [Hz]	43.3
Intake Pressure [bar]	1.20
Exhaust Pressure [bar]	1.00
Intake ϕ	0.42

Table D.1 – Geometric and Operating Parameters

Compression Ratio

Table D.2 lists the parameters for the charge delivery model used for these runs. Compressor compression ratios of 3.5:1 and 30:1 were investigated, with the volume of the compressor configured so that similar delivery ratios were achieved.

Inner Bore [cm]	8.00	8.00
Outer Bore [cm]	13.0	10.9
Compression Ratio	3.5:1	30.0:1
Inlet Flow Area [cm^2]	4.50	4.50
Outlet Flow Area [cm^2]	4.50	4.50
Tank Volume [cm^3]	20000	20000
Tank Temperature [K]	300	300

Table D.2 – Delivery System Parameters

Figure D.1 presents some of the results from these simulations; where the compressor's pressure is plotted over the compressor volume. The differences in pressure history are apparent, however the maximum pressures are similar, as is the power consumption for these two arrangements. With regard to the scavenging cycle, little difference was seen between these two runs.

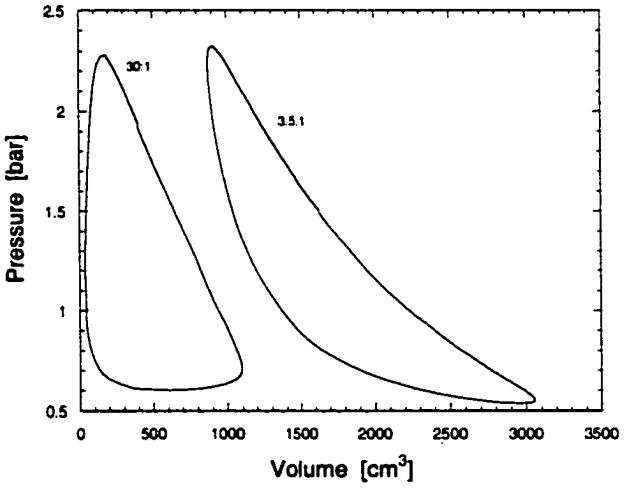

Figure D.1 – Compressor Pressure vs. Compressor Volume

Tank Volume

Table D.3 lists the parameters for the charge delivery model used for these simulations. Delivery tank volumes of 20 and 0.1L were utilized.

Inner Bore [cm]	8.00	8.00
Outer Bore [cm]	10.9	10.9
Compression Ratio	30.0:1	30.0:1
Inlet Flow Area [cm^2]	4.50	4.50
Outlet Flow Area [cm^2]	4.50	4.50
Tank Volume [cm^3]	20000	100
Tank Temperature [K]	300	300

Table D.3 – Delivery System Parameters

Figures D.2-D.5 illustrate some of the results from this simulation series; the tank pressure histories were presented in Figure 4.33. In Fig. D.2 the change in compressor pressure history is evident, with this due to the higher tank pressure to which the fresh charge must be delivered.

In Figure D.3 the cylinder pressures are plotted over the scavenging cycle, with the tank pressures included for reference. The port openings are also noted in this figure. The differences in cylinder pressure after IPO are apparent, though both cases follow the tank pressure closely after about 175CAD (as seen earlier in Appendix C).

The intake and exhaust flow rates are presented in Figures D.4 and D.5. It is evident how the flow rates change with the crankcase-type delivery pressure. The initial incoming charge enters at a high velocity but then drops to near zero for almost ⅓ of the intake port open time. The effect of this on the exhaust flow rate is significant.

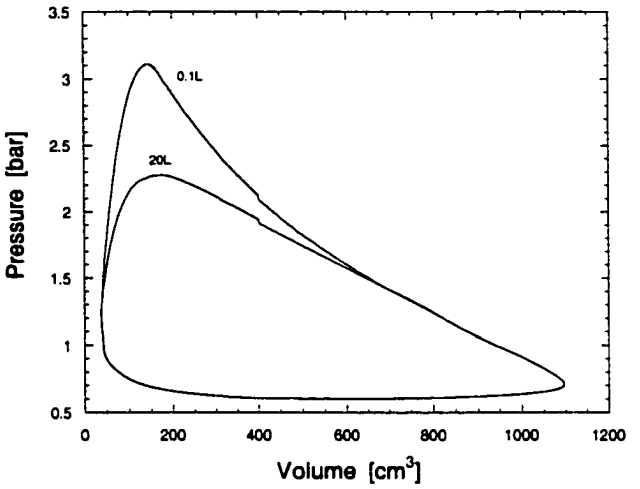

Figure D.2 – Compressor Pressure vs. Compressor Volume

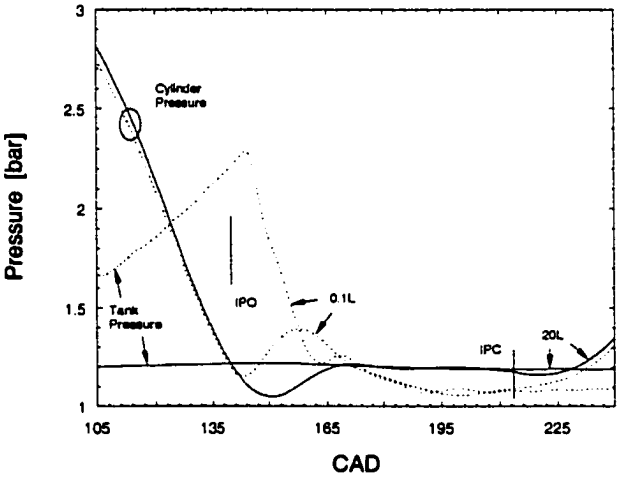

Figure D.3 – Cylinder Pressure vs. CAD

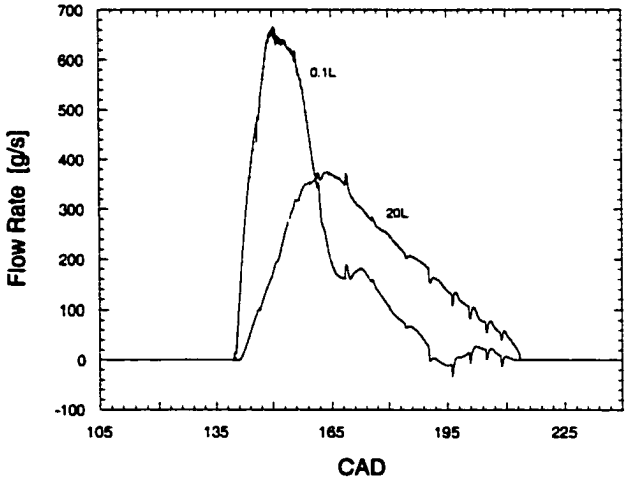

Figure D.4 – Intake Flow Rates vs. CAD

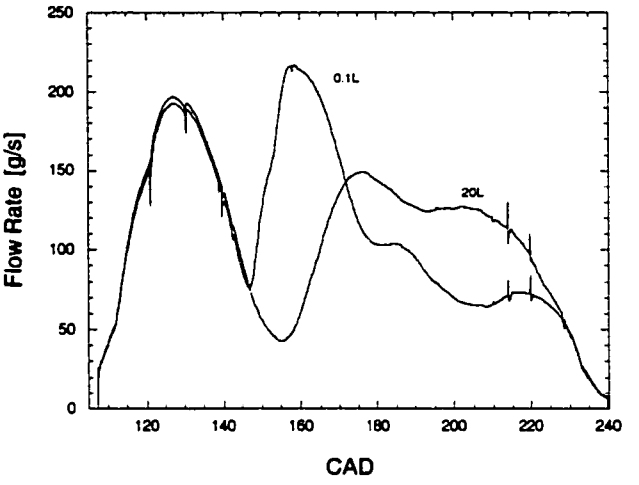

Figure D.5 – Exhaust Valve Flow Rates vs. CAD

Figure D.6 is presented to illustrate the change in-cylinder flow behavior for the small tank case; the large tank flows are similar to those presented in Figure C.20 (for the steady intake boundary simulations). Again, Ensight's particle tracing method was used to generate this figure.

In this figure the earlier fresh charge introduction is noticeable with greater penetration of the fuel-air mixture to the valve region leading to the increased trapping losses. In addition, it can be seen that there is a greater degree of charge swirl due to the higher initial incoming flow rates.

Figure D.7 illustrates the average and maximum dilution ratios plotted over the scavenging and compression processes for the two cases investigated. The degree of mixing after EVC can be inferred from this plot. It can be seen however, that even with the higher initial flow rates, the in-cylinder dynamics are similar and the charge sees little change in dilution after the valves close.

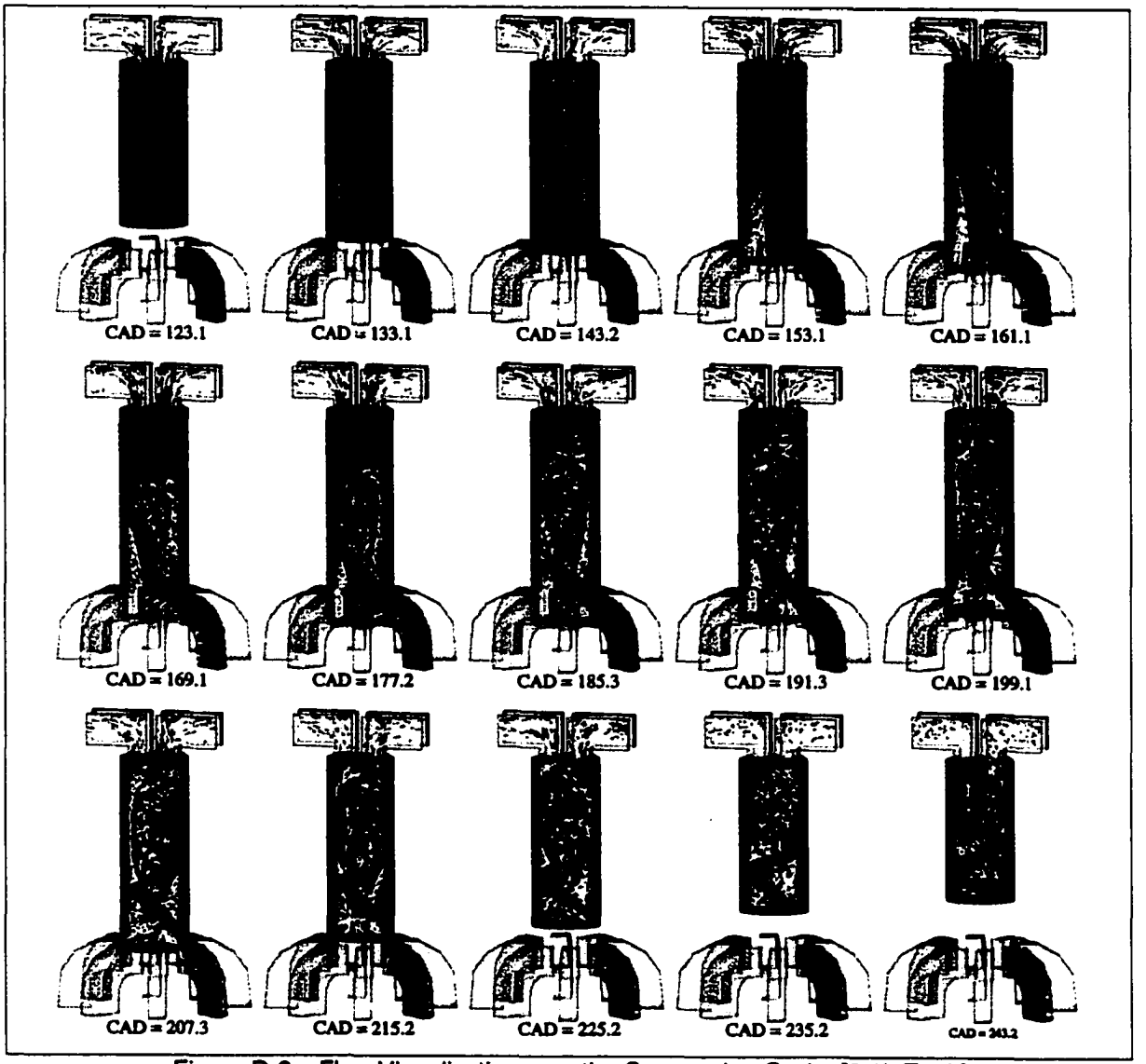

Figure D.6 – Flow Visualization over the Scavenging Cycle [0.1L Tank]

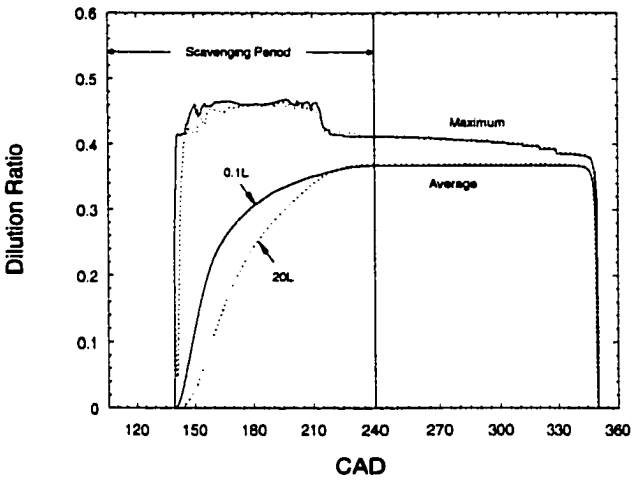

Figure D.7 – Average and Maximum Dilution Ratios vs. CAD

Inlet/Outlet Flow Areas

Table D.4 lists the delivery system parameters used for these simulations. Flow areas of 4.5 and 8.0cm^2 (compressor inlet and outlet) were utilized.

Inner Bore [cm]	8.00	8.00
Outer Bore [cm]	10.9	10.9
Compression Ratio	30.0:1	30.0:1
Inlet Flow Area [cm^2]	4.50	8.00
Outlet Flow Area [cm^2]	4.50	8.00
Tank Volume [cm^3]	20000	20000
Tank Temperature [K]	300	300

Table D.4 – Delivery System Parameters

The results for this series were adequately described in Chapter IV however, and no more detail will be given here.

Adiabatic Tank

Table D.5 lists the delivery system parameters used for these runs. An isothermal tank (300K) was compared to an adiabatic tank, both of which were 20L in volume.

Inner Bore [cm]	8.00	8.00
Outer Bore [cm]	10.9	10.9
Compression Ratio	30.0:1	30.0:1
Inlet Flow Area [cm^2]	4.50	4.50
Outlet Flow Area [cm^2]	4.50	4.50
Tank Volume [cm^3]	20000	20000
Tank Temperature [K]	300	Adiabatic

Table D.5 – Delivery System Parameters

For the adiabatic tank case, the tank stabilized to about 400K, with only slight variation through the engine cycle. In Figure D.8 it can be seen that the higher tank temperature dramatically affects the cylinder charge, with the higher scavenged temperature (cylinder temperature at EVC) leading to earlier HCCI combustion, and thus reduced efficiency potential.

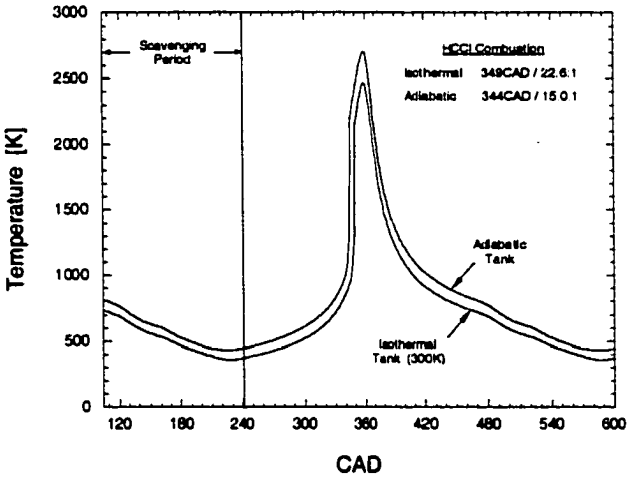

Figure D.10 – Average Cylinder Temperature vs. CAD

The exhaust flow rates are presented in Figure D.11, where the changes in blowdown and short-circuited flow are clearly illustrated. The higher emissions and reduced power output problems resulting from increased fuel loss were detailed in Ch. IV.

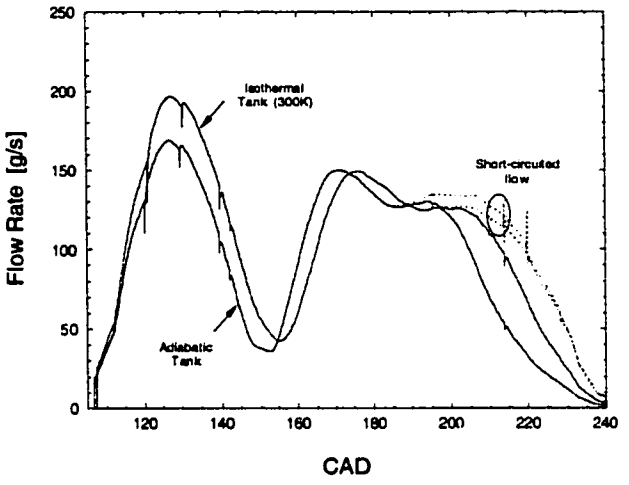

Figure D.11 – Exhaust Valve Flow Rates vs. CAD

Summary

Various parametric investigations were conducted using the KIVA-3V code and a 0D representation of the compressor / tank system in an effort to minimize the power consumption of the charge delivery system, while reducing the detrimental effects on the in-cylinder flow behavior and HCCI process. A summary of these simulations is presented in Table D.6 where the scavenging and trapping efficiencies, compressor work fraction (W_{comp}/W_{cycle}), and operating compression ratio (CR_{op}) are listed. The base case employs a compressor compression ratio (CR_{comp}) of 30:1, inlet and outlet flow areas of 4.5cm^2, a tank volume of 20L and a constant tank temperature of 300K, with the engine specifications listed in Table D.1.

	η_{sc}	η_{tr}	W_{comp}/W_{cycle}	CR_{op}
Base Case	0.900	0.956	0.207	23:1
Low CR_{comp} (30:1)	0.897	0.961	0.212	23:1
Small Tank (0.1L)	0.894	0.936	0.243	24:1
Large Flow Areas (8.0cm^2)	0.900	0.965	0.124	23:1
Adiabatic Tank (~400K)	0.947	0.877	0.353	15:1

Table D.6 – Charge Delivery Simulation Results

From this table it can be concluded that an arrangement utilizing a large, cooled tank with sufficient compressor flow area will maximize the performance of the scavenging system.

APPENDIX E – FINAL SIMULATIONS

The purpose of this appendix is to provide some additional information regarding the final simulations with the optimal configuration. A summary of these computations is presented in Chapter IV. Here more detail is given regarding the fuel distribution during scavenging and through the compression stroke, as well as the simulations investigating 'design robustness'.

Fuel Dilution

Figures E.1-E.4 plot the average and maximum dilution ratios over the scavenging and compression processes for the four cases investigated. From these figures it can be inferred that the in-cylinder mixing and fuel dilution processes after EVC are quite similar for each of the configurations, even for the stratified scavenging arrangement where the intake equivalence ratio is 2.7. This is important in ensuring that there are no fuel-rich regions at the time of HCCI combustion.

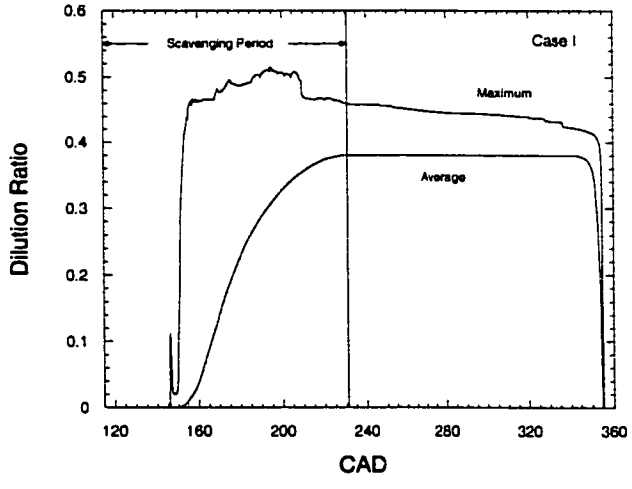

Figure E.1 – Average and Maximum Dilution Ratios vs. CAD [Case I]

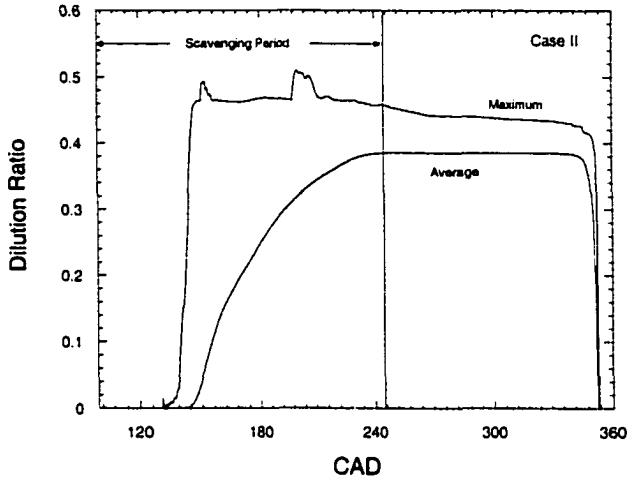

Figure E.2 – Average and Maximum Dilution Ratios vs. CAD [Case II]

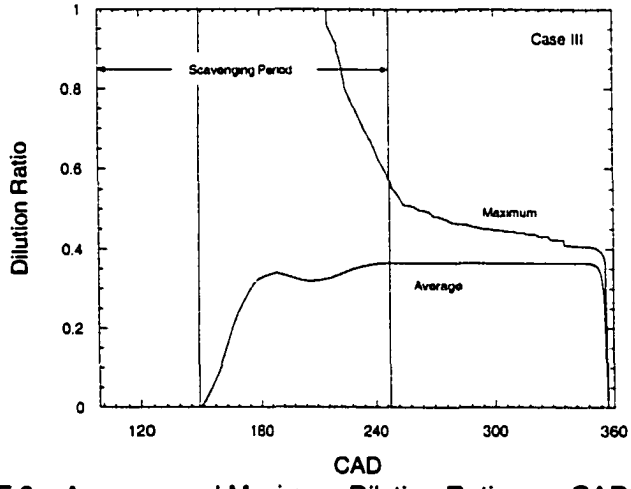

Figure E.3 – Average and Maximum Dilution Ratios vs. CAD [Case III]

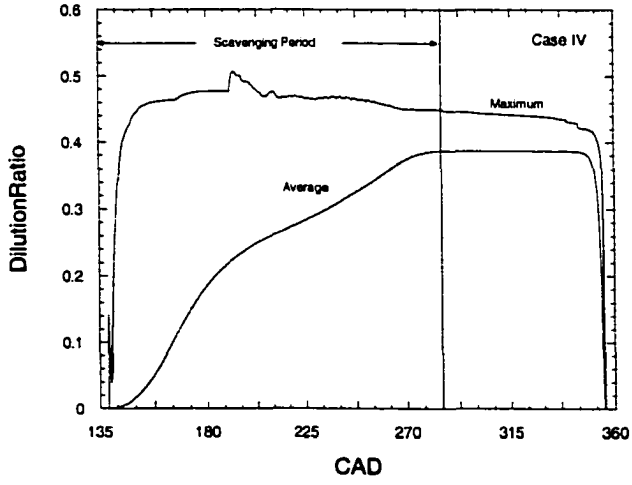

Figure E.4 – Average and Maximum Dilution Ratios vs. CAD [Case IV]

Design Robustness

Tables E.1-E.4 list the results from the input variation simulations. That there is only one condition for Case IV is discussed in Chapter IV.

CASE I	η_{sc}	η_{tr}	m_{del} [g]	W_{cycle} [J]	W_{comp} [J]	W_{fric} [J]	η_{th}	C_3H_8 [ppm]	NO [ppm]	Power [kW]
f = 40Hz	0.87	0.985	0.76	556	21.0	17.8	0.501	285	333	19.7
f = 50Hz	0.78	0.999	0.63	420	28.9	20.6	0.437	15	273	17.6
ϕ =0.4275	0.82	0.997	0.69	429	24.6	19.2	0.467	55	57	16.5
ϕ =0.5225	0.83	0.997	0.68	512	24.7	19.2	0.455	95	729	20.0

Table E.1 – Operating Results [CASE I – Input Variations]

CASE II	η_{sc}	η_{tr}	m_{del} [g]	W_{cycle} [J]	W_{comp} [J]	W_{fric} [J]	η_{th}	C_3H_8 [ppm]	NO [ppm]	Power [kW]
f = 40Hz	0.87	0.972	1.27	872	25.5	24.3	0.486	542	793	23.1
f = 50Hz	0.79	1.000	1.06	713	35.1	28.2	0.460	14	671	22.8
ϕ =0.4275	0.83	0.997	1.15	716	29.5	26.4	0.480	83	176	20.9
ϕ =0.5225	0.83	0.993	1.13	843	30.1	26.3	0.471	177	2245	24.9

Table E.2 – Operating Results [CASE II – Input Variations]

CASE III	η_{sc}	η_{tr}	m_{del} [g]	W_{cycle} [J]	W_{comp} [J]	W_{fric} [J]	η_{th}	C_3H_8 [ppm]	NO [ppm]	Power [kW]
f = 40Hz	0.96	0.870 (A) 0.969 (F/A)	1.15 0.18	710	38.2	22.5	0.532	483	197	24.7
f = 50Hz	0.91	0.963 (A) 0.994 (F/A)	0.98 0.15	635	53.3	26.0	0.516	112	55	26.4
ϕ = 2.43	0.93	0.922 (A) 0.989 (F/A)	1.05 0.16	600	4630	24.3	0.522	170	27	22.7
ϕ = 2.97	0.94	0.924 (A) 0.981 (F/A)	1.06 0.16	716	46.0	24.2	0.529	223	337	27.6

Table E.3 – Operating Results [CASE III – Input Variations]

CASE IV	η_{sc}	η_{tr}	m_{del} [g]	W_{cycle} [J]	W_{comp} [J]	W_{fric} [J]	η_{th}	C_3H_8 [ppm]	NO [ppm]	Power [kW]
ϕ =0.4275	0.84	0.993	0.94	636	35.5	54.6	0.488	136	177	23.1

Table E.4 – Operating Results [CASE IV – Input Variations]

Summarizing these tables, it can be seen that:

1. As the frequency is decreased the cylinder is more completely scavenged and therefore operates on a higher dilution ratio. This leads to greater NO production, while the increased scavenging time leads to higher short-circuiting. Overall the thermal efficiency is increased slightly due to the higher operating CR and lower compressor work. The compressor work decreases due to the effective decrease in flow restriction.
2. As the frequency is increased the scavenging is not as complete and thus the engine operates on a lower dilution ratio. As such the NO is decreased, while the shorter scavenging time leads to lower short-circuiting emissions. The overall efficiency is decreased slightly as the operating CR is decreased and the compressor work increased. The compressor work increases due to the effective increase in flow restriction.
3. As the equivalence ratio drops both the NO and short-circuiting emissions are reduced. The short-circuiting decreases due to the decline in blowdown effectiveness and resulting scavenging efficiency. The decrease in ϕ has little impact on the thermal efficiency.
4. As the equivalence ratio increases the NO and short-circuiting increase. This is due to the hotter charge temperature and better blowdown effectiveness. Again, the thermal efficiency is only slightly affected.